CRANFIELD UNIVERSITY LIBRARY

CRANFIELD UNIVERSITY

SCHOOL OF INDUSTRIAL AND
MANUFACTURING SCIENCE

PhD Thesis

Academic Year 1997-1998

GARY ANTHONY FISHER

# THE OPTIMISATION OF BONDCOAT OXIDES FOR IMPROVED THERMAL BARRIER COATING ADHESION

Supervisors: Prof. J. R. Nicholls
Dr D. S. Rickerby

March 1998

In collaboration with Rolls-Royce plc &
Chromalloy UK Ltd

ProQuest Number: 10832285

All rights reserved

INFORMATION TO ALL USERS
The quality of this reproduction is dependent upon the quality of the copy submitted.

In the unlikely event that the author did not send a complete manuscript
and there are missing pages, these will be noted. Also, if material had to be removed,
a note will indicate the deletion.

ProQuest 10832285

Published by ProQuest LLC (2018). Copyright of the Dissertation is held by Cranfield University.

All rights reserved.
This work is protected against unauthorized copying under Title 17, United States Code
Microform Edition © ProQuest LLC.

ProQuest LLC.
789 East Eisenhower Parkway
P.O. Box 1346
Ann Arbor, MI 48106 – 1346

CRANFIELD UNIVERSITY
LIBRARY

## Abstract

Superalloys used for the critical hot sections of modern aero-gas turbines are designed primarily to exhibit good creep and fatigue resistance, coupled with toughness and microstructural stability. However, an optimum level of these properties can only be attained with a decrease in the oxidation and corrosion resistance of the alloy. This had led to the adoption of surface coatings to protect turbine blades against the corrosive environments in which they operate.

The use of Thermal Barrier Coatings (TBCs) enables the design of more efficient and powerful gas turbines whilst still providing environmental protection for the blade. A TBC is a duplex coating system, combining a ceramic topcoat with a metallic bondcoat. The ceramic layer thermally insulates the turbine blade whilst the bondcoat protects the substrate from oxidation and corrosive attack. Central to the performance of a TBC is the integrity and adherence of the alumina scale promoted by the bondcoat. The scale acts to both bond the ceramic topcoat and to act as a barrier against environmental attack. This study aimed to optimise the oxide formed by the bondcoat and so increase the life of the TBC.

This was achieved by investigating the effects of bondcoat pre-treatments and by the design and development of coatings to be used specifically as bondcoats. The performance of the systems was assessed using hot oxidation isothermal and cyclic tests and the coatings were analysed using a variety of techniques, including optical microscopy, SEM, XRD and the modified scratch test.

The investigation of the effects of pre-treatments revealed that the pre-oxidation of bondcoats could help promote an initial alumina scale. However, any potential

benefits were overshadowed by the degradation mechanisms inherent within the coating systems. This highlighted the importance of the composition and chemistry of the bondcoat in determining the properties of the alumina scale, the relevance of which was demonstrated in the bondcoat design element of the study. Both a platinum aluminide bondcoat and a novel diffusion-type bondcoat were developed and optimised. The performances of the systems were assessed and their degradation modes analysed, resulting in a range of bondcoats which outperform those currently available, making them ideal for the design of modern Thermal Barrier Coating systems.

Acknowledgements

I wish to express my thanks and appreciation to Professor J. R. Nicholls of the School of Industrial and Manufacturing Science, Cranfield University and Dr D. S. Rickerby of the Surface Treatment and Coatings Technology Group, Rolls-Royce plc, for their supervision and encouragement provided throughout the course of my study.

I am also appreciative of the help and advice given by Mr R. Jones, Mr A. Johnstone and Mr J. Higgins of the Surface Treatment and Coatings Technology Group, Rolls-Royce plc, Mr R. Wing of Chromalloy UK Ltd and Mr F. Cullen and Mr J. Fairchild of AEA Technology, Harwell.

Finally, I thank Rachel, my parents, friends and family for their support and encouragement.

This thesis was produced in collaboration with Rolls-Royce plc and Chromalloy UK Ltd

The copy of this thesis has been supplied on condition that anyone who consults it is understood to recognise that its copyright rests with the Cranfield University and Rolls-Royce plc. No quotation from the thesis and no information derived from it may be published without due reference and without written consent For full written consent, contact;

Prof. J. R. Nicholls

SIMS

Cranfield University

Cranfield, MK43 0AL

UK

Contents


| | Page |
|---|---|
| **Chapter 1** - Introduction | 1 |
| **Chapter 2** - Literature review: Turbine components and the need for surface coatings | 5 |
| 2.1- The metallurgy of superalloys | 5 |
| 2.2- Turbine blade production | 9 |
| 2.3- Diffusion coatings | 11 |
| 2.4- Overlay coatings | 12 |
| 2.5- Thermal barrier coatings | 12 |
| **Chapter 3** - Literature review: Oxide chemistry and the degradation of TBCs | 17 |
| 3.1- Introduction | 17 |
| 3.2- The principles of oxidation | 17 |
| 3.3- The nature of bonding at the bondcoat/ceramic interface | 19 |
| 3.4- Alumina | 21 |
| 3.5- Degradation of an 'ideal' system | 24 |
| 3.6- Degradation of an 'actual' system | 24 |
| 3.7- Hot corrosion | 25 |
| 3.8- The effect of sulphur | 27 |
| 3.9- Erosion | 28 |
| 3.10- Oxidation | 28 |
| **Chapter 4** - Literature review: Pre-treatments and diffusion coatings | 37 |
| 4.1- Introduction | 37 |
| 4.2- Pre-treatments for bondcoats | 37 |

Page

4.3- Diffusion coatings 39

4.3.1- Production of aluminide coatings 39

4.3.2- Growth mechanisms 40

4.3.2.1- High aluminium activity 40

4.3.2.2- Low aluminium activity 40

4.3.3- Limitations of aluminide coatings 41

4.3.4- The benefits of platinum 41

4.3.4.1- Platinum as an alloy addition 41

4.3.4.2- Platinum aluminide coatings 42

4.3.5- The manufacture of platinum aluminide coatings 43

4.3.6- The degradation of aluminide coatings 44

**Chapter 5** - Scope of the research programme 52

**Chapter 6** - Experimental technique 54

6.1- Introduction 54

6.2- Samples 54

6.3- Pre-oxidation 54

6.4- Ageing treatments 55

6.4.1- Isothermal ageing treatments 55

6.4.2- Thermal cycling 55

6.5- Sample preparation 56

6.5.1- For examination of the surface 56

6.5.2- For examination in section 56

6.6- Analysis 57

Page

6.6.1- Scratch testing 57

6.6.2- β-depletion measurements 58

6.6.10- Other techniques 58

**Chapter 7** - Results: The effects of pre-oxidation and gritting on oxide chemistry 64

7.1- Introduction 64

7.2- Research plan 64

7.3- Analysis of results 64

7.3.1- β depletion measurements 64

7.3.2- SEM examination of the surface 65

7.3.3- SEM examination of spalled areas 66

7.3.4- XRD analysis 66

7.4- Summary 67

**Chapter 8** - Results: The effect of bondcoat composition on the chemistry of the oxide chemistry 81

8.1- Introduction 81

8.2- Research plan 81

8.3- Analysis 81

8.3.1- The effects of aluminium content 82

8.3.2- The effects of platinum 83

8.3.3- The effects of hafnium and silicon 86

8.3.4- The effects of a ceramic topcoat 87

8.4- Overall summary 88

**Chapter 9** - Results: Assessment of in-situ and ex-situ pre-oxidation treatments 104

Page

9.1- Introduction 104

9.2- Research plan 104

9.2.1- Ex-situ pre-oxidation 104

9.2.2- In-situ pre-oxidation 104

9.3- Results 106

9.3.1- Ex-situ pre-oxidation 106

9.3.2- In-situ pre-oxidation 107

9.4- Overall summary of the assessment of pre-oxidation treatments 108

**Chapter 10** - Results: The optimisation of an out-of-pack platinum aluminide for Thermal Barrier Coating systems 115

10.1- Introduction 115

10.2- Research plan 115

10.3- Analysis 116

10.3.1- Modified scratch test results 116

10.3.2- XRD analysis 116

10.3.3- Optical analysis in section 116

10.3.4- XPS analysis 117

10.3.5- SEM examination of the surface 117

10.3.6- Image analysis 117

10.3.7- SEM analysis in section 118

10.4- Summary 118

**Chapter** 11 - Results: The design and optimisation of a platinum enriched CMSX-4 bondcoat for TBC systems 130

11.1- Introduction 130

Page

11.2- Experimental 130

11.3- Analysis 131

11.3.1- Thermal cycling of the superalloy/ceramic systems 131

11.3.2- Optical analysis of the platinum/CMSX-4 systems 131

11.3.3- Probe analysis 131

11.3.4- XRD analysis 132

11.3.5- Modified scratch test results 133

11.3.6- Analysis of the isothermally aged samples 133

11.3.7- Thermal cycling 133

11.4- Assessment of double-layer platinum systems 135

11.5- Summary 136

**Chapter 12** - Discussion 149

12.1- Introduction 149

12.2- The effects of pre-oxidation 149

12.3- The effect of gritting as a surface preparation 155

12.4- The effect of bondcoat composition on the chemistry of an oxide scale 156

12.5- The effects of aluminium content 156

12.6- The effects of platinum 157

12.7- The effects of hafnium and silicon additions 160

12.8- The effect of a ceramic topcoat 160

12.9- Summary of the pre-treatment studies 161

12.10- The optimisation of an out-of-pack platinum aluminide bondcoat 162

Page

12.11- The development and optimisation of a platinum/ CMSX-4 bondcoat system 167

**Chapter 13** - Conclusions 173

13.1- The effects of pre-oxidation on the oxide 173

13.2- The effect of gritting as a surface preparation 174

13.3- The effect of bondcoat composition on the chemistry of an oxide scale 174

13.4- The effects of aluminium content 174

13.5- The effects of platinum 174

13.6- The effects of hafnium and silicon additions 174

13.7- The effect of a ceramic topcoat 174

13.8- Assessment of in-situ and ex-situ pre-oxidation treatments 175

13.9- The optimisation of an out-of-pack platinum aluminide bondcoat 175

13.10- The development and optimisation of a platinum/ CMSX-4 bondcoat system 176

13.11- Overall conclusions 176

**Chapter 14** - Future work 178

14.1- Introduction 178

14.2- Hot corrosion 178

14.3- The addition of active elements 178

14.4- Noble metal aluminide bondcoats 179

14.5- Co-Pt/CMSX-4 bondcoat systems 179

Page

**References** 182

Tables


| | Page |
|---|---|
| **6.1** - Composition of superalloys | 59 |
| **6.2** - Coating composition and deposition techniques | 59 |
| **6.3** - Polishing procedure for bondcoats | 60 |
| **6.4** - Polishing procedure for ceramics | 60 |
| **6.5** - Etch compositions and procedures | 60 |
| **10.1** - Matrix of the platinum aluminide coatings | 120 |
| **11.1** - Matrix of the platinum/CMSX-4 coatings | 137 |
| **11.2** - Coating thickness, in the as-processed condition | 137 |
| **11.3** - Representative compositions of the phases present in the platinum/CMSX-4 coatings, in the as-processed condition | 137 |
| **11.4** - Phase composition of coating C after isothermal soaks | 138 |
| **11.5** - Phase composition of coating C after thermal cycling at 1135°C | 138 |

## Figures


| | | Page |
|---|---|---|
| **1.1-** | The increase in operational temperature of turbine components due to alloy and TBC development | 3 |
| **1.2-** | Diagram of a Thermal Barrier Coating | 3 |
| **1.3-** | Schematic diagram of the research programme | 4 |
| **2.1-** | Micrograph of a typical $\gamma/\gamma'$ structure | 14 |
| **2.2-** | Diagram showing the relative solubilities of elements in $\gamma'$ at 1100°C | 14 |
| **2.3-** | Schematic representation of the major alloying elements in in a superalloy | 15 |
| **2.4-** | Micrograph of a typical diffusion coating (RT22LT high activity platinum aluminide), in section | 15 |
| **2.5-** | Micrograph of a typical overlay coating (RT122, applied by LPPS) in section | 16 |
| **2.6-** | Micrograph of a typical EB-PVD thermal barrier coating, in section | 16 |
| **3.1-** | Schematic cross section of an alloy A-B, with a low concentration of A | 32 |
| **3.2-** | Schematic cross section of an alloy A-B, with a critical concentration of B | 32 |
| **3.3-** | The linear relationship between the work of adhesion of the liquid metals on alumina and the electron density of the corresponding metals | 33 |
| **3.4-** | The work of adhesion of solid transition metals on sapphire as a functio of electron density of the corresponding metal | 33 |
| **3.5-** | The adhesive properties of a number of metal/ceramic diffusion bonds | 34 |
| **3.6-** | The tensile strength of interfaces formed by solid metals with alumina as a function of the electron densities of the corresponding metals | 34 |
| **3.7-** | Micrograph of the surface of a β-phased diffusion coating, aged for 25h at 1100°C | 35 |

Page

**3.8-** Schematic diagram of the oxidation of a MCrAlX coating at temperatures less than 1000°C 35

**3.9-** Schematic diagram of the oxidation of a MCrAlX coating at temperatures of 1100°C and above 36

**4.1-** Schematic of Chang and co-workers investigations of pre-treatments 48

**4.2-** Schematic diagram of a pack cementation process 48

**4.3-** Schematic diagram of an 'out-of-pack' process 49

**4.4-** Schematic diagram of a CVD process 49

**4.5-** Microstructure of a high aluminum activity aluminide 50

**4.6-** Microstructure of a low aluminium activity aluminide 50

**4.7-** Microstructure of a low temperature-high activity platinum aluminide 51

**4.8-** Microstructure of a high temperature-low activity platinum aluminide 51

**5.1-** Scope of the research programme 53

**6.1-** Ellingham diagram for the pre-oxidation atmospheres 61

**6.2-** The CSEM scratch test rig 61

**6.3-** 'Scratch track' produced by the conventional scratch test 62

**6.4-** Schematic diagram of the modified scratch test 62

**6.5-** Schematic of a crack length versus load plot produced by the modified scratch test 63

**6.6-** Micrograph showing the β-depletion level of an MCrAlX coating 63

**7.1-** Research plan 68

**7.2-** β-depletion measurments 68

**7.3-** Ar-20%$O_2$ pre-oxidation, ungritted, aged for 1h at 1150°C 69

**7.4-** $H_2$-10%$H_2O$ pre-oxidation, ungritted, aged for 1h at 1150°C 69

Page

**7.5-** $H_2$-10%$H_2O$ pre-oxidation, gritted, aged for 1h at 1150°C 70

**7.6-** $H_2$-10%$H_2O$ pre-oxidation, gritted, aged for 1h at 1150°C 70

**7.7-** Ar-20%$O_2$ pre-oxidation, ungritted, as-processed 71

**7.8-** Ar-20%$O_2$ pre-oxidation, gritted, as-processed 71

**7.9-** $H_2$-10%$H_2O$ pre-oxidation, ungritted, as-processed 72

**7.10-** Ar-20%$O_2$ pre-oxidation, gritted, 1h at 1150°C 72

**7.11-** $H_2$-10%$H_2O$ pre-oxidation gritted, 1h at 1150°C 73

**7.12-** $H_2$-10%$H_2O$ pre-oxidation, ungritted, 1h at 1150°C 73

**7.13-** $H_2$-10%$H_2O$ pre-oxidation, gritted, aged for 100h at 1100°C. The chromia is marked (A) 74

**7.14-** Ar-20%$O_2$ pre-oxidation, ungritted, 100h at 1100°C 74

**7.15-** Ar-20%$O_2$ pre-oxidation ,ungritted, 100h at 1100°C 75

**7.16-** Production route for the RT122 bondcoat 75

**7.17-** Zirconia debris at the oxide/metal interface. $H_2$-10%$H_2O$ pre-oxidation, ungritted, 100h at 1150°C 76

**7.18-** Spallation associated with Cr-oxide. $H_2$-10%$H_2O$ pre-oxidation gritted, aged for 100h at 1100°C 77

**7.19-** Cohesive failure within alumina. Ar-20%$O_2$ pre-oxidation, aged for 100h at 1100°C 77

**7.20-** XRD traces for Ar-20%$O_2$ pre-oxidation, gritted RT122 78

**7.21-** XRD traces for $H_2$-10%$H_2O$ pre-oxidation, gritted RT122 79

**7.22-** XRD traces for $H_2$-10%$H_2O$ pre-oxidation, ungritted RT122 80

**8.1-** Work plan 89

**8.2-** Coating A, as-processed 89

**8.3-** RT122, as-processed 90

Page

**8.4-** Coating A, aged for 100h at 1050°C 90

**8.5-** RT122, aged for 100h at 1050°C 91

**8.6-** Spallation of the oxide formed on RT122, aged for 100h at 1150°C 92

**8.7-** Surface of RT122, aged for 100h at 1050°C 93

**8.8-** Surface of Coating A, aged for 100h at 1050°C 93

**8.9 -** XRD analysis of RT122 and Coating A 94

**8.10-** RPS320, as-processed 95

**8.11-** RPS320, aged for 100h at 1050°C 95

**8.12-** RT122, as-processed 96

**8.13-** RT122LT, aged for 100h at 1050°C 96

**8.14-** Spallation of the oxide scale. RPS320, aged for 100h at 1150°C 97

**8.15-** Catastrophic failure of the oxide. RPS320, aged for 100h at 1150°C 98

**8.16-** XRD analysis of RPS320 99

**8.17-** XRD analysis of RT22LT 100

**8.18-** Coating B, as-processed 101

**8.19-** XRD analysis of RT122 to determine the effect of a ceramic topcoat 102

**8.20-** XRD analysis of RT22LT to determine the effect of a ceramic topcoat 103

**9.1-** Ex-situ pre-oxidised RT122, as-processed, in section 110

**9.2-** Untreated RT122, as-processed, in section 110

**9.3-** Ex-situ pre-oxidised RT122, aged for 100h at 1100°C, in section 111

**9.4-** Ex-situ pre-oxidised RT22LT, as-processed, in section 111

**9.5-** Untreated RT22LT, as-processed, in section 112

**9.6-** Ex-situ pre-oxidised RT22LT, aged for 100h at 1100°C, in section 112

Page

**9.7-** Scratch test results for the ex-situ pre-oxidised systems 113

**9.8-** Scratch test results for the in-situ pre-oxidised systems 114

**10.1-** Modified scratch test results 120

**10.2-** Modified scratch test results 121

**10.3-** Modified scratch test results 121

**10.4-** XRD analysis of coating C, in the as-processed condition 122

**10.5-** Coating C, in section, etched, as-processed 122

**10.6-** Coating C, in section, etched, aged for 25h at 1210°C 123

**10.7-** Grain size measurments of the development coatings in the as-processed condition 123

**10.8-** Oxide thickness measurments 124

**10.9-** Oxide thickness measurments 124

**10.10-** XPS analysis of coating C, isothermally soaked for 25h at 1190°C 125

**10.11-** XPS analysis of coating Z, isothermally soaked for 25h at 1190°C 126

**10.12-** Coating E, aged for 25h at 1170°C. Micrographs show the formation of pits at the TGO/coating interface 127

**10.13-** Coating C, aged for 25h at 1170°C, deep etched. Micrographs show the outward diffusion along grain boundaries 128

**10.14-** Coating C, aged for 25h at 1170°C, deep etched. Micrographs of the interdiffusion diffusion 129

**11.1-** Cyclic life of the superalloy/ceramic systems 139

**11.2-** Coating A, as-processed, in section 139

**11.3-** Coating B, as-processed, in section 140

**11.4-** Coating C, as-processed, in section 140

**11.5-** Coating D, as-processed, in section 141

**11.6-** XRD analysis of coating C, as-processed 141

Page

**11.7-** XRD analysis of coating D, as-processed 142

**11.8-** Schematic diagram of coating structures 143

**11.9-** Scratch test results for the Pt/CMSX-4 systems 143

**11.10-** Coating C, aged for 25h at 1150°C 145

**11.11-** Oxide thickness measurments 145

**11.12-** Coating C, aged for 25h at 1190°C, in section 146

**11.13-** Cyclic life of coating C at 1135°C 146

**11.14-** Coating C, 236 cycles at 1135°C 147

**11.15-** Coating C, 586 cycles, spalled area 147

**11.16-** Coating C, 586 cycles, ceramic attached 148

**11.17-** Scratch test results for the double layer systems 148

**12.1-** Schematic diagram of the failure mechanism of the platinum aluminide/TBC systems 172

**14.1-** Specific weight gains of NiCrAlY and CoCrAlY coatings, thermally cycled at 1050°C 181

**14.2-** Processing route for the Co-Pt/CMSX-4 coatings 181

**14.3-** Scratch test results for the Co-Pt/CMSX-4 systems 182

# INTRODUCTION

Chapter 1

# Introduction

The constant drive for increased aero-gas turbine efficiency has led to the development of several generations of superalloys, which have permitted increased turbine inlet temperatures and higher engine performance. Superalloys are required to maintain mechanical and surface integrity for, typically, between five and ten thousand hours under very high stresses in aggressively corrosive environments [1, 2, 3]. To prolong the life of the blade , compressor discharge air is injected through the blade to cool the component. However, to gain further increases in the efficiency of the engine, it is necessary to decrease the amount of air used for cooling. This, combined with increased environmental attack (due to higher operating temperatures) has led to the adoption of Thermal Barrier Coatings (TBCs) to provide thermal and environmental protection [4, 5].

Coatings technology was first used in the 1960's with the application of metallic coatings for the protection of turbine blades from the environment [2]. However, simple environmental coatings could not keep pace with the needs of increased engine efficiency and turbine blade protection, so by the 1980's Thermal Barrier Coatings were adopted (Figure 1.1). A TBC is a duplex coating, comprising an yttria stabilised zirconia top layer (approximately 0.3 to 0.4 mm thick), which is deposited onto a bondcoat. Bondcoats were initially adapted from metallic environmental coatings. By the formation of an alumina scale they provide corrosion protection for the blade and aided the adhesion between the substrate and the ceramic, accommodating the stresses that arise from the thermal and mechanical fluctuations of the blade and the difference in Young's

Modulus and thermal expansion coefficients between the superalloy and the ceramic [5, 6]. The insulating properties of the ceramic layer allows for a temperature reduction across the coating of, up to, 170 °C (Figure 1.2) [7]. This large temperature reduction can be utilised by increasing in the operating temperature of the turbine blade and/or reducing the degree of component cooling [8]. Therefore, by the application of a Thermal Barrier Coating, the benefits equivalent of two to three generations of superalloy development can be achieved, with a possible decrease in fuel consumption of 0.25% [9].

Currently, TBCs are used to extend the service life of existing components, i.e. to make a turbine blade, which has adequate performance without a coating and extend its life by a factor of three or four times using a TBC [10]. However, by producing a turbine blade with a 'designed-in' TBC, it is thought possible to increase the performance of the coated blade and the efficiency of the engine.

This study formed part of a 'Joint Development Programme' between Rolls-Royce plc and Chromalloy UK Ltd,(which also included Cranfield University, Sheffield Hallam University and AEA Technology), to produce 'designed-in' EB-PVD Thermal Barrier Coating systems. Critical to the performance of such a coating is the adherence and oxidation resistance of the oxide scale promoted by the bondcoat. This study aimed to optimise the properties of the bondcoat oxide. A review of the current state of the technologies is presented and, with the aid of innovative analysis tools, such as the modified scratch test, studies of either the use of pre-treatments of the bondcoat or the design and development of novel diffusion coatings to be used specifically for bondcoats in TBC systems were undertaken (Figure 1.3).

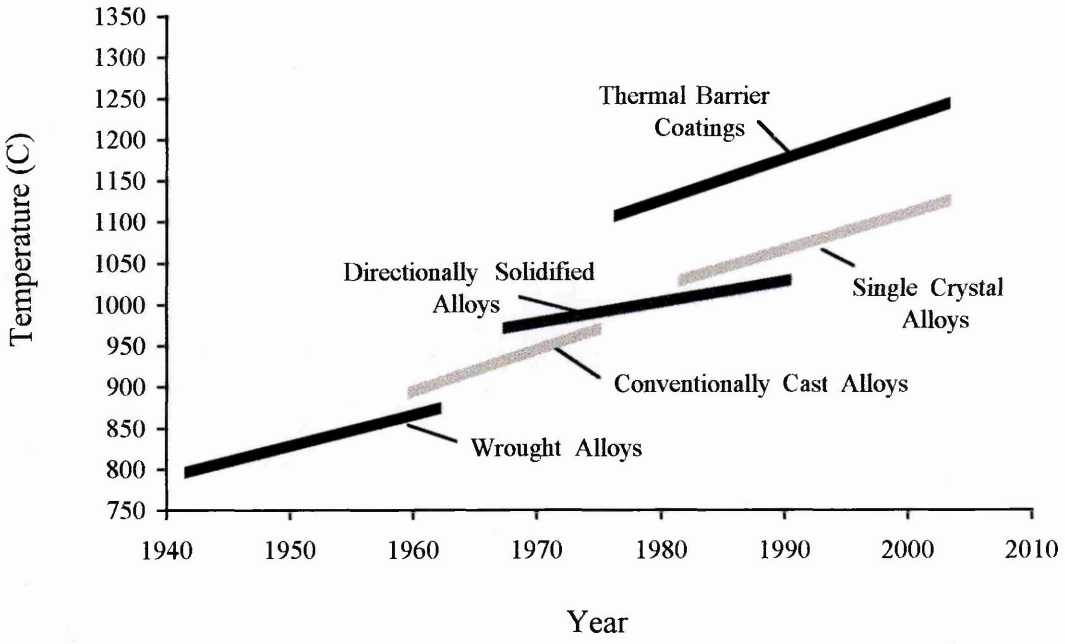


Figure 1.1- The increase in operational temperature of turbine components due to alloy and TBC development.

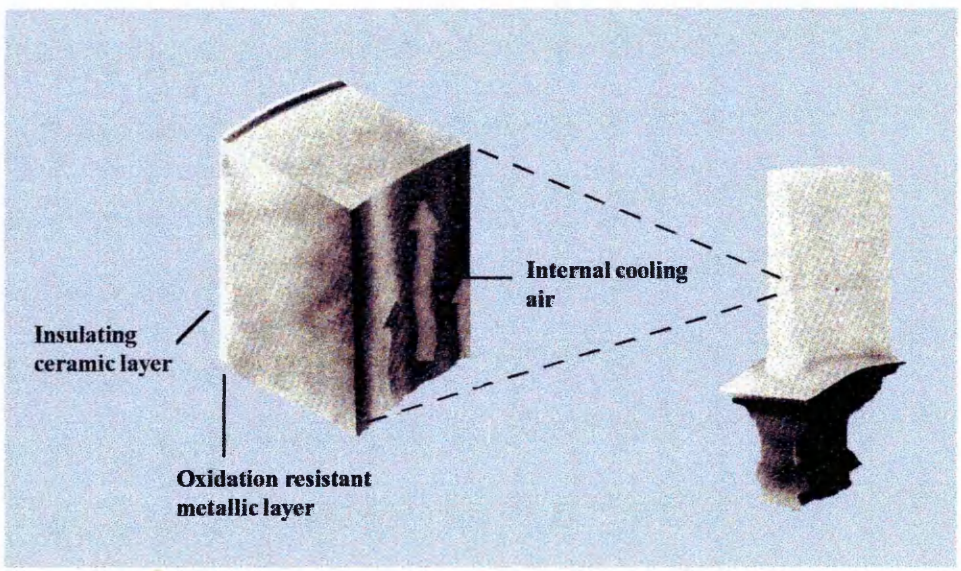


Figure 1.2- Diagram of a Thermal Barrier Coating

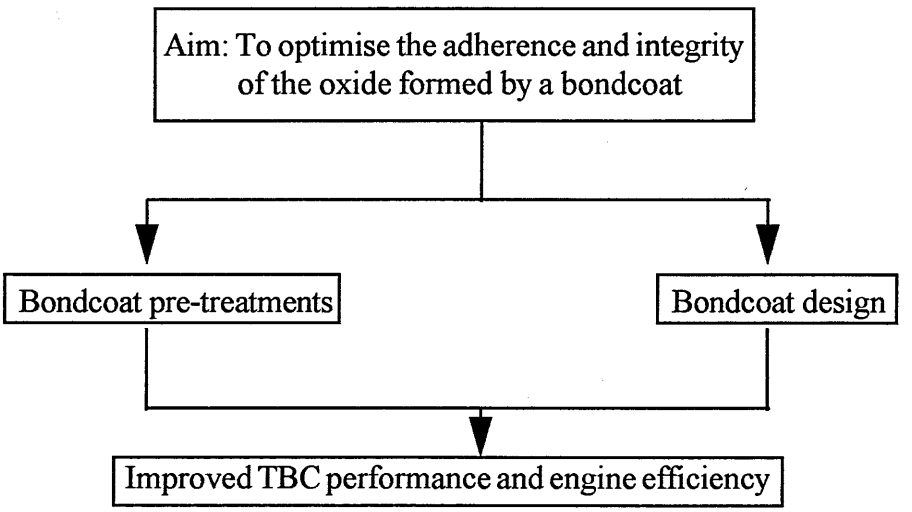


Figure 1.3- Schematic diagram of the Research Programme

# LITERATURE REVIEW

Chapter 2- Literature Review

## Turbine Components and the need for Surface Coatings

### 2.1 The Metallurgy of Superalloys

Within the aero-industry, a need for high temperature alloys arose in the 1930's, from the development of both aircraft superchargers and gas turbine engines. Initially, modified austenitic stainless steels were adopted, their f.c.c. structure being tougher and more ductile than ferritic alloys. Ni and Co additions were made to these alloys to stabilise the f.c.c. structure and increases creep and oxidation resistance. The gradual increase in Ni additions led to the adoption of Ni based superalloys in the 1940's [11, 12].

Ni based superalloys were developed from a Ni·20%Cr alloy used for electrical resistance applications [13]. Microstructurally, they have the desired austenitic f.c.c. $\gamma$ phase matrix. To further strengthen the alloys, additions are made to act as either precipitation or solid solution strengtheners. Additions of principally Al and Ti will produce the precipitation strengthening phase $\gamma'$ (Figure 2.1). This is an ordered fcc phase based on an $A_3B$ composition. 'A' represents either Ni, Co or Fe. Both Co or Fe can partition to either the $\gamma$ or the $\gamma'$ phases, but have a preference for $\gamma'$. Co additions were first made to the alloy 'Nimonic 90', where 20%Co was substituted for Ni. The Co acts to increase the solubility temperature for $\gamma'$ and so increases the maximum operating temperature of the alloy. 'B' represents either Al, Ti Ta or Nb. Whilst most alloys rely on a combination of both Al and Ti, a number rely solely on the addititon of Ti to form the $Ni_3Ti$ $\gamma'$ phase [11]. Alternatively, Nb is present in a number of alloys to form the bct $Ni_3Nb$ $\gamma''$precipitate, which is similar in nature and function to $\gamma'$ [14]. The relative

solubilities of elements in γ′ is shown in Figure 2.2. Precipitation hardeners act to increase creep resistance by impeding dislocation movement. Dislocations are forced to either bow around or cut through the precipitate. The optimum distribution of precipitates is a fine dispersion with a small interparticle spacing. This is achieved due to a high level of coherency between the precipitate and the matrix, resulting from a low level of mismatch between the γ and γ' ( for $Ni_3Al$ the mismatch is approximately 0.05% and for $Ni_3Ti$ it is slightly higher). The shape of the γ' also depends on γ's mismatch with the lattice. A mismatch of less than 0.4% will produce a spherical γ', a mismatch greater than 0.4% but less than 1% will produce a cube, whilst a level of greater than 1% will result in a plate-like morphology. Whether the γ' is spherical or a cube does not affect the alloy's mechanical properties, however plate-like γ' is considered detrimental [15, 16].

Elements, such as Mo, W, Cr and Re have a relatively low solubility in γ′ and so partition to the γ phase. As these elements have a larger atomic diameter than Ni by 1 to 13%, they act as solid solution strengtheners due to the resultant lattice expansion [11, 17, 18]. Cr levels were traditionally between 16 and 25wt% and gave an acceptable performance, both from a mechanical and corrosion point of view, when operating temperatures were around 700°C. As temperature requirements increased the amount of Cr was decreased to as low as 10wt% to allow for increased Al to aid mechanical properties. Problems arose during the 1960's as blades suffered from hot corrosion attack (see Chapter 4). As Cr gives some protection from this, a balance has been sought between the required levels of Al and Cr [17]. The major alloying elements which may be present in a superalloy are shown in Figure 2.3, the height of the element blocks give an indication as to relative amounts present.

Ti, Hf, Nb, Cr and Ta also act as strong carbide formers. Carbides will stabilise the alloys microstructure at high temperature by forming networks at grain boundaries. These inhibit grain boundary motion and therefore increase creep and rupture properties [16].

The M-C type carbide is the most stable, where M represents the carbide forming elements. In wrought alloys, the carbide will form as a large sphere or cube. In cast alloys, its morphology is affected by cooling rate. Rapid cooling produces small particles, whilst a slow cooling rate will produce a dendritic shape. These dendrites are undesirable as their tips act as high stress concentrations which can lead to crack nucleation. The preferential order of formation of the carbide is HfC, TaC, NbC and TiC. However, elements can substitute for each other (e.g (Ti,Nb)C) or the carbides can be formed by less reactive elements such as W or Mo. An important aspect of the M-C carbide is that, with time at temperature, it will decompose to form either the $M_{23}C_6$ carbide and $\gamma'$ or the $M_6C$ and $\gamma'$ [18].

$$\text{M-C} + \gamma \rightarrow M_{23}C_6 + \gamma'$$

$$\text{e.g } (Ti,Mo)C + (Ni,Cr,Al,Ti) \rightarrow Cr_{21}Mo_2C_6 + Ni_3(Al,Ti)$$

$$MC + \gamma \rightarrow M_6C + \gamma'$$

$$\text{e.g } (Ti,Mo)C + (Ni,Co,Al,Ti) \rightarrow Mo_3(Ni,Co)_3C + Ni_3(Al,Ti)$$

Thus $M_{23}C_6$ and $M_6C$ carbides will form at grain boundaries and then be enveloped by the $\gamma'$ [16,19]. $M_{23}C_6$ carbides are formed on cooling in cast alloys and are found as discrete particles on grain boundaries. In $M_{23}C_6$ 'M' usually represents Cr, but other alloying elements are possible, which may act to replace part of the Cr content (e.g.

$Cr_{21}Mo_2C_6$). Due to its position on the grain boundaries, the carbide will increases the alloys creep resistance and ductility [16, 19]. The $M_6C$ carbide (e.g. $(Ni,Co)_4(Mo,W)_2C$) is formed in alloys with a moderate to high Mo and W concentrations and is more stable than $M_{23}C_6$, but less so than M-C. The carbides morphology is either as discrete particles on the grain boundaries, or as plates nucleated at grain boundaries growing into the matrix [16]. Extreme carbide formation can produce a network of carbides that can allow rapid crack propagation. Extenssive boundery concentrations of $M_{23}C$ and $M_6C$ are reduced by Hf which will react with the carbon freed by the MC breakdown to form a stable HfC precipitate [18].

Alloying additions which act in a similar fashion to the $M_{23}C_6$ carbide as grain boundary strengtheners by increasing the alloys rupture strength are Zr and B. However, these were phased out with the advent of Directionally Solidified and Single Crystal alloys [13, 16].

During the 1950's, the requirement for higher operating temperatures was met by increasing the concentrations of precipitation and solid solution strengthening additions. The $\gamma'$ content in the alloys rose to as high as 60% ($\gamma'$ has an optimum level of 70%, after which it begins to coarsen, decreasing its beneficial properties) [19]. This high level of alloying additions produced metastable alloys, whose structure changed with time at temperature and resulted in detrimental phases, such as lower $\sigma$ and $\eta$ [16, 17]. These phases form as plates or rods, and in excessive amounts will decrease the alloys mechanical properties. Instead of regressing chemically to produce simpler alloys, these problems were overcome by improving production technology, namely improved casting techniques and better blade design.

## 2.2 Turbine Blade Production

Up untill the 1940's, blades were either cast or wrought. Wrought alloys had a high yield strength up to moderate temperatures and a high fracture toughness and were in wide usage, whilst cast alloys although offering a superior creep resistance, had a limited fracture toughness [11, 17].

As explained in the previous section, to strengthen the alloys, additions of Al and Ti were made to promote the formation of $\gamma'$. However fabrication problems arose when higher concentrations of Al and Ti were needed to meet the desire for increased levels of $\gamma'$, due to the reactivity of these elements. This was overcome by the adoption of vacuum melting techniques in the 1950's. This allowed for even higher levels of Al and Ti (resulting in $\gamma'$ levels of between 60 and 70%) and the inclusion of solid solution strengtheners such as Mo [17, 19].

To keep pace with the continued need to increase fuel inlet temperatures (and so increase thrust), both blade design and casting techniques were improved. In the 1960's, internally air cooled blades were introduced. Initially, these were forged from a drilled preform. However more complex and efficient cooling designs can be produced in cast blades. The latest designs feature 'film cooling', where air exhausts from small holes in the blade to form a film of relatively cool air on the components surface [19].

In the mid-1960's, oxide dispersion strengthened (ODS) alloys were introduced. Metal powders are ground together with dispersoids (e.g. yttria) in a ball mill. This produced a fine, uniform dispersion of oxide in the powder acting to increase the overall strength of the alloy. When compared to cast alloys, ODS alloys offer improved fatigue life and fewer cast defects [12, 17, 20].

Creep damage within a turbine blade initiates at grain boundaries normal to the major direction of the stress. By eliminating these transverse grains, the creep properties of the blade could be improved. Directional solidification (DS), promotes columnar grain growth from the blade root to tip by creating a steep temperature gradient in the mould, so that the grains grow in the direction of heat flow. This process was developed by Pratt and Witney Aircraft in the late 1960's with the alloy MarM002. DS blades were introduced into military engines in 1969, and commercial engines in 1974 [16, 17, 19, 21]. Single crystal alloys were developed from DS techniques by PWA in the early 1970's. Single crystal blades are formed by either incorporating a geometrical constriction in the mould such that only one grain continues to grow, or by using a 'seed crystal' that nucleates one grain that grows in a similar orientation to the seed crystal. The alignment or elimination of grain bounderies normal to the stress axis increased the high temperature properties of the alloys and removed the need for grain boundary strengtheners such as Zr and B. This allowed for higher solution heat treatments, which decreased chemical segregation and produced a more uniform distribution of $\gamma'$, and so improved the properties of the alloys [17, 19, 21].

Advances in superalloy metallurgy permit their operation at up to $0.9T_m$ [18]. The possibility of achieving further development of nickel superalloys, which are already operating at temperatures within 300°C of their incipient melting temperature is somewhat limited [22]. Even improved blade design with, for example, internal cooling, cannot provide the nescessary protection. This is due to the surface temperature being higher than the average metal temperature and that the temperatute distribution within a cooled blade is divergent, with the leading edge of the blade subjected to as much as 25% of the heat transfer, whilst the remaining heat is distributed across the blade [23].

This, combined with the need to further increase blade tip speed and reduce degradation problems such as hot corrosion, has led to the adoption of surface engineering and coatings. Coatings are designed to provide improved corrosion and oxidation resistance or reduced metal surface temperatures. There are three types of coatings for turbine applications: diffusion, overlay and thermal barrier coatings, each of these will be reviewed in turn.

## 2.3 Diffusion Coatings

These were the first coatings widely used for the protection of superalloy turbine components. Generally, they tend to be aluminides, where the surface of the alloy is enriched with aluminium by pack cementation or CVD techniques. Two types of process can be employed: 'low activity', where the aluminide coating is formed by outward diffusion of nickel or cobalt from the substrate, or 'high activity', where the coating is formed by the inward diffusion of aluminium (Figure 2.4) [24, 25].

Aluminide coatings offer only limited protection at temperatures greater than 1100°C or in severe corrosive environments, have poor mechanical properties, and their effectiveness can also be dependent on the composition of the base alloy [26]. Their performance can be improved by the addition of platinum. Platinum modified aluminides offer superior corrosion and oxidation resistance. (They have been reported to have twice the lifetime of a standard aluminide [27]). Diffusion coatings will be discussed in greater depth in chapter 4.

## 2.4 Overlay Coatings

Overlay coatings have the advantage over diffusion coatings that their composition can be tailored to suit and, are not reliant on the composition of the base alloy. An overlay composition is based on M-CrAl-X, where M represents nickel and/or cobalt, and X represents an active element such as hafnium or yttria, which act to improve oxidation resistance [6]. They have a two phase microstructure, with a fine dispersion of Co or Ni aluminide (β) in a Cr rich matrix [28] (Figure 2.5).

Each overlay coating is designed to meet the demands of a particular application, offering balanced oxidation and corrosion resistance as well as good mechanical properties. For example, CoCrAlY coatings tend to be favoured for corrosion protection due to their high chromium contents (~25%), whilst nickel or nickel/cobalt containing MCrAlX's will have superior mechanical properties. (The presence of nickel will decrease the coatings' ductile/brittle transition temperature due to the higher DBTT of β-CoAl compared with β -NiAl [26]). Overlay coatings will not be considered further in this study, other than as bondcoats to thermal barrier coatings.

Overlays were originally deposited using EB-PVD techniques. However, in the early 1980's, low pressure plasma spraying (LPPS) techniques were developed, offering a cost effective alternative that produced coatings of comparable quality [26]. A detailed review of the design and application of overlay coatings is given in references [26] and [28].

## 2.5 Thermal Barrier Coatings

Thermal barrier coatings (TBCs) are duplex coating systems (Figure2.6). The ceramic coating achieves compatibility with the superalloy substrate by first applying a

bondcoat layer. The bondcoat can be either a diffusion or an overlay coating and are traditionally unmodified versions of environmental/corrosion protection coatings.

Zirconia is the preferred choice of ceramic due to it's low thermal conductivity and relatively high thermal expansion coefficient for a ceramic. However, small additions of either yttrium or magnesium are made to the ceramic to prevent phase transformations occurring during thermal cycling [6, 26].

Due to the combination of a thick ceramic layer and an oxidation/corrosion resistance bondcoat, TBCs offer superior protection to the component. On cooled components, the insulating properties of the ceramic (the temperature drop between the outer surface of the TBC and the substrate interface can be as high as 150°C), help to reduce the components metal surface temperature giving improved performance due to the increased creep and fatigue properties at these lower metal temperatures. [6, 26, 29].

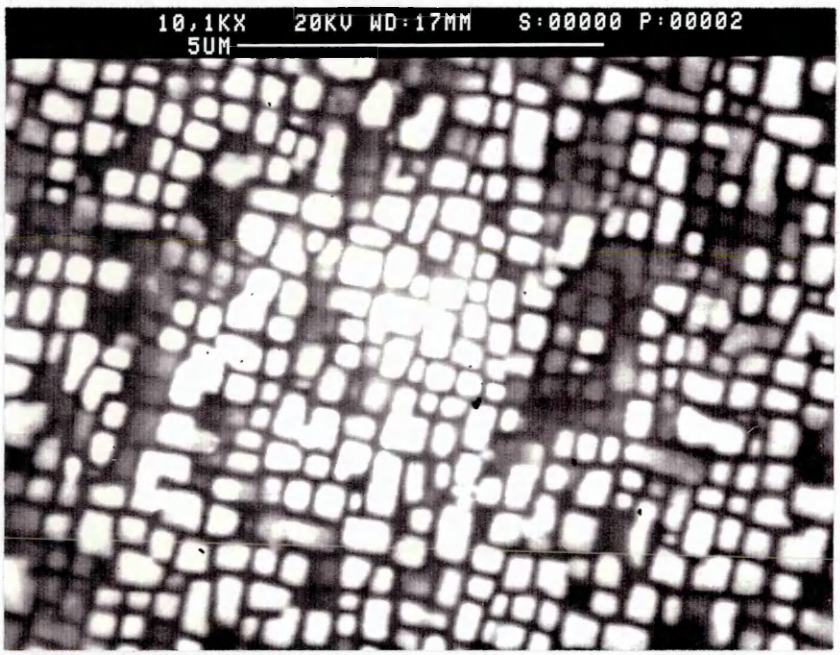


Figure 2.1- Micrograph of a typical γ/γ′ structure

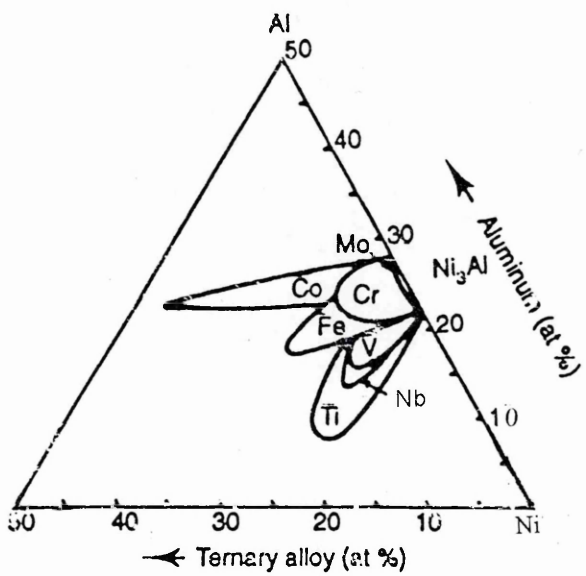


Figure 2.2- Diagram showing the relative solubilities of elements in γ′ at 1100°C [16]

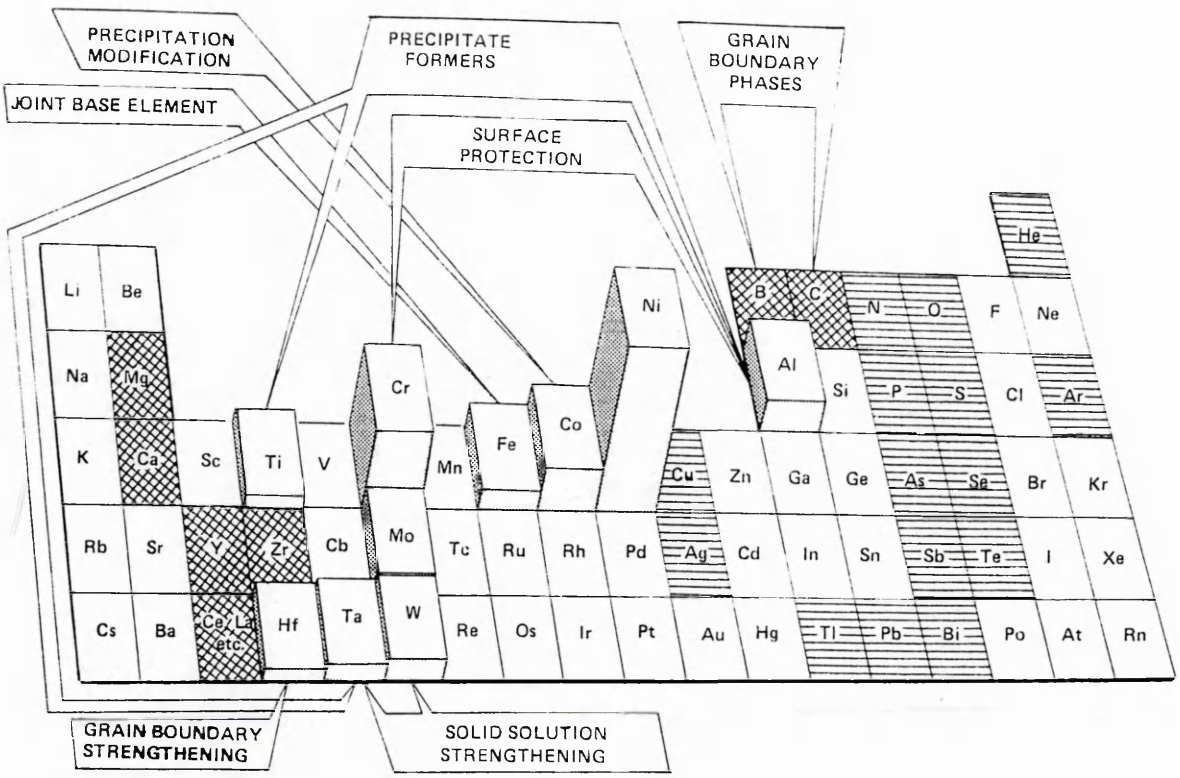


Figure 2.3- Schematic representation of the major alloying elements in a superalloy [17]

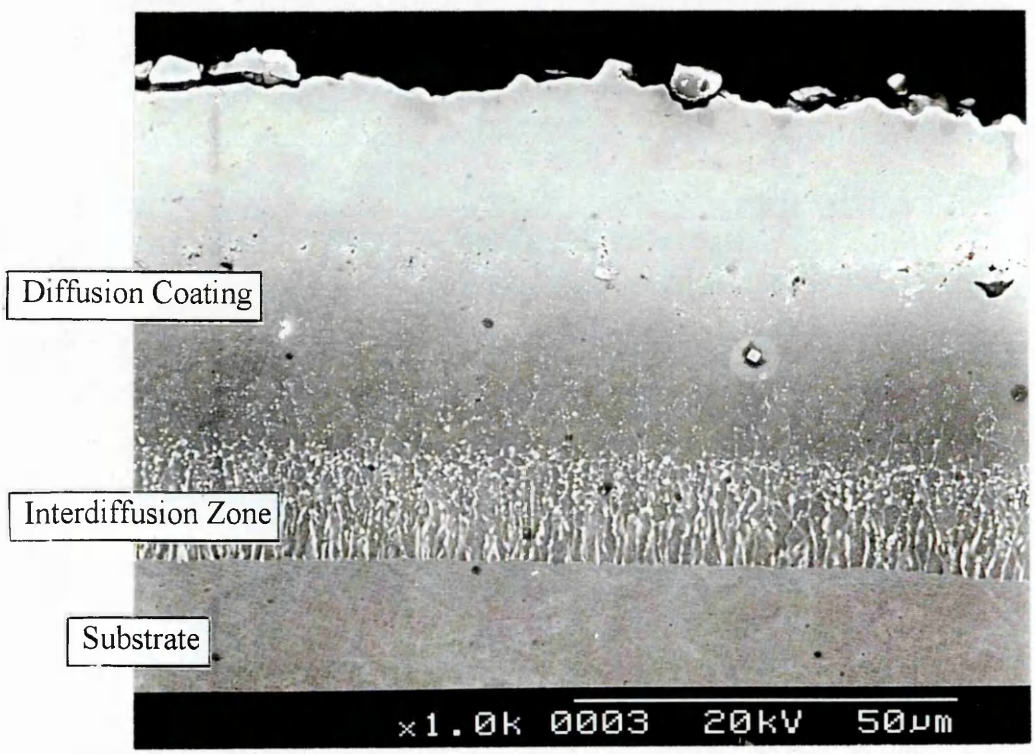


Figure 2.4- Micrograph of a typical diffusion coating (RT22LT high activity platinum aluminide), in section

Figure 2.5- Micrograph of a typical overlay coating (RT122, applied by LPPS), in section

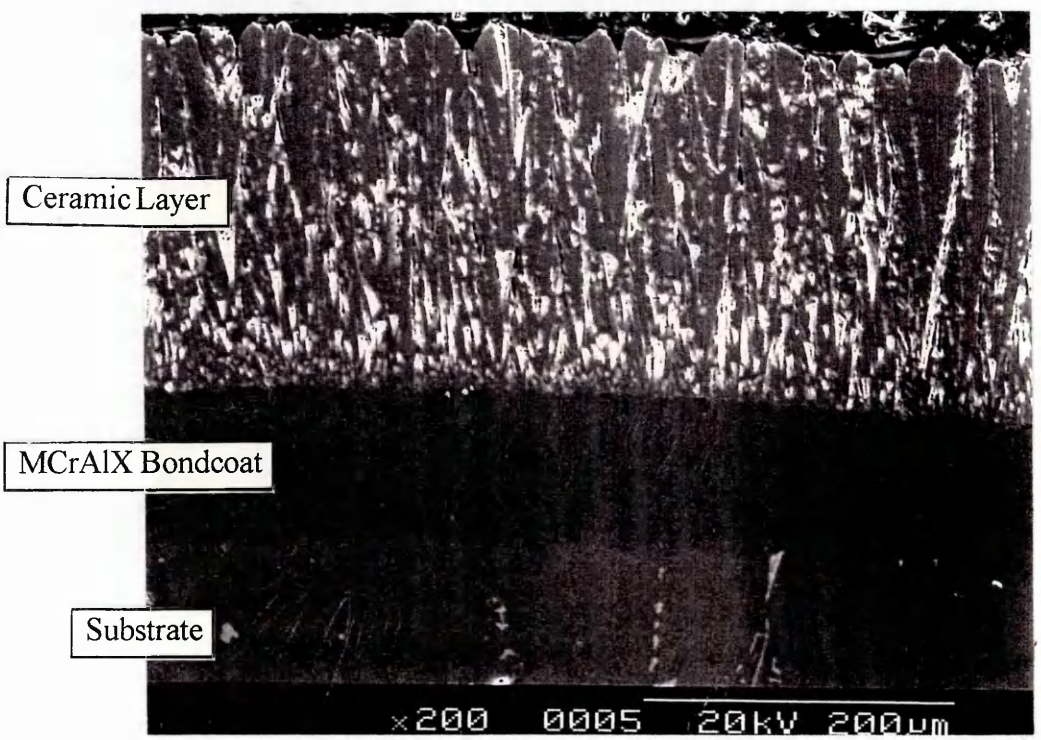


Figure 2.6- Micrograph of a typical EB-PVD thermal barrier coating, in section

Chapter 3: Literature Review

## Oxide Chemistry and the Degradation of TBCs

### 3.1 Introduction

Central to the performance of both environmental coatings (i.e. diffusion and overlay coatings) and TBCs is the scale grown at the metallic coating surface. The oxide will act as a barrier between a component and its environment, and in the case of TBCs, will bond the ceramic to the bond coat.

Ideally, within a TBC system, the bondcoat and zirconia layer are adhered by an $\alpha$-alumina oxide scale. As well as providing optimum adhesion between the two layers, the alumina provides protection from environmental attack and mechanical damage. This chapter will explain the properties of alumina, the nature of the bonding at the bondcoat-ceramic interface, and how the oxide scale can be degraded by corrosion and oxidation.

### 3.2 The Principles of Oxidation

The oxide film formed by a metal for protection in an oxidising environment usually grow at a rate that decreases as the thickness of the oxide increases. The common explanation of this is that the growth of the scale is a diffusion controlled process, resulting in the parabolic growth of the oxide [30]. This can be expressed by the equation;

$$x^2 = k_p t$$

Where 'x' represents the film thickness, 't' is time and '$k_p$' is the parabolic rate constant for film growth [30].

Wagner [31] showed how $k_p$ could be explained in terms of the transport properties of the oxide scale, based on a number of assumptions;

1) The oxide layer is a compact, perfectly adherent scale.

2) Migration of the ions or electrons across the scale is the rate controlling process.

3) Thermodynamic equilibrium is established at both the metal-oxide and gas-oxide interface.

4) The oxide shows only small deviations from stiochiometry.

5) Thermodynamic equilibrium is established locally throughout the scale.

6) The scale is thick compared with the distances over which space charge effects occur.

7) Oxygen solubility in the metal may be neglected.

Therefore, $k_p$ may be expressed as;

$$k_p = \frac{1}{RT}\int_{\mu_O^I}^{\mu_O^{II}} \left( D_O + \frac{Z_M D_M}{2} \right) d\mu_O$$

where $D_M$ and $D_O$ are the diffusivities of M and O in the oxide, $Z_M$ is the volume of metal and $\mu'_O$ and $\mu''_O$ are the chemical potentials of O at the metal-oxide and oxide-gas interfaces, respectively. Good agreement has been found between experimental and calculated values for $k_p$. For example, for the system of CoO formed on Co, the discrepancy between theory and experimental is within +/- 10% [30]. However, the majority of data can deviate from the Wagner model as all of the criteria are rarely met [31]. For example, diffusion across the scale may not be the rate controlling step (therefore the growth will not be parabolic), or for certain oxides, such as alumina, the observed growth rate is far greater than that calculated. This is caused

by short circuit diffusion paths and point defect concentrations as a result of impurities doping the oxide [30, 32].

The oxidation of an alloy is more complex than that of a pure metal. For an alloy 'AB', where both A and B are stable but BO is more stable than AO (in superalloys, A= Ni etc., whilst B= Cr or Al ), if the concentration of B is low, an external scale of AO will form and internal oxides of BO will precipitate (Figure 3.1). If the concentration of B is increased to a critical value, an external BO scale i.e. formed (Figure 3.2). The layer of BO will halt the formation of the less stable AO (however, some AO will have formed in the transient oxidation period before BO had formed a continuous layer). The selective oxidation of B results in its depletion in the alloy under the scale. This will eventually lead to the growth of the AO oxide. The time taken before this occurs relies on a number of factors such as temperature, the initial concentration of B and any cracking or mechanical damage to the oxide [31].

## 3.3 The Nature of Bonding at the Bondcoat/Ceramic Interface

The ceramic topcoat is adhered to the bondcoat via an alumina scale. The mismatch in physical properties between the metal and the oxide (i.e. compared to metals, oxides are usually brittle, elastically stiffer, insulating and have less thermal expansion) highlights the importance of the adhesive bond between these two components.

The considered opinion on interfacial bonding has been explained by Jian-Guo Li [33]. The adhesion between a metal and a ceramic may essentially be a covalent bond between the metals outer shell electrons (d-orbitals for aluminium)

and the 2p-orbital electrons of the oxygen anion. It has been indicated that bonding may also be due to the transfer of valence charges. At temperature, electrons from the anions valence band pass into the conduction band by thermal excitation. When a metal approaches the oxides surface, the thermally created holes in the oxides valence band are filled by free electrons from the metal. Enhanced electron transfer will increase adhesion. The intensity of electron transfer depends upon the electron density (i.e. The number of electrons per gram of material) of the metal and the concentration of holes in the oxide valence band. Figure 3.3 shows the work of adhesion of a number of liquid metals on alumina plotted as a function of electron density.

For an ideal crystal, free from impurities and defects, the concentration of holes in the valence band (which is equal to the number of free electrons in the conduction band) is related to the bandgap energy ($E_g$) by the equation;

$$C = C_O \exp(-E_g/2KT)$$

Where C is the concentration of holes in the valence band, K is the Boltzmann's constant, $C_O$ is a constant and T represents temperature in degrees Kelvin. As temperature is increased, so does the concentration of holes in the valence band. The subsequent increased electron transfer will give improved adhesion. Also, as C (and electron transfer) increases, the bandgap energy will decrease, resulting in greater adhesion.

When the work of adhesion values of various transition metals on sapphire surfaces were plotted as a function of electron density, a similar linear relationship is observed (Figure 3.4). This suggests that the nature of bonding in a solid/solid system is similar to that of a solid/liquid. Derby [34] has collated the adhesion data

for a number of metal/ceramic diffusion bonds (Figure 3.5). Of particular interest for TBC systems is the good adherence of the $Pt/Al_2O_3$ system as compared to the $Ni/Al_2O_3$ bond.

The mechanical properties of a solid/solid interface are primarily determined by the adhesion. Therefore, the mechanical strength of different metal/alumina interfaces should be a function of the electron density of the corresponding metals. This is shown in Figure 3.6, in which the tensile strength of interfaces formed by various solid metals with alumina are plotted against the electron density of the corresponding metals. This also predicts that the interfaces mechanical strength will increase as the band gap energy decreases [33].

## 3.4 Alumina

The ideal protective oxide grown by a coating should be highly stable, continuous, slow growing, free from cracks and pores and be both adherent and coherent. The enrichment of the components substrate with aluminium will promote the formation of a protective alumina film, which has many of these properties, as α-alumina will form a complete and compact, slowly grown scale. [35]

α–alumina will grow at approximately 1000°C and above. Below this temperature, transitional aluminas (such as δ and θ) will be formed by the outward diffusion of aluminium. These aluminas have the detrimental effect of transforming to α-alumina at higher temperatures, which gives rise to volume changes and an increase in strain within the scale ( the δ to α transformation occurs with a volume contraction of 13%). [36]

α-alumina has a hcp structure with two thirds of the octahedral sites filled by trivalent cations [37]. The high temperature protection afforded by α-alumina results from the oxide having low concentrations and mobilities of ionic and electronic defects.[35] The slow growth rate of the oxide is related to its highly stoichiometric structure and large bandgap width, which makes electronic conduction difficult. In the main, α-alumina acts as poor ionic and electronic conductor, in which both oxygen and aluminium are mobile.[32, 35, 38]

There appears to be some contention over the growth mechanism of the alumina scale. It has been reported that the columnar structure of α- alumina is indicative of oxide formation at the scale/substrate interface [37, 39]. Tracer studies of the oxide formed by overlay coatings [35] and β-NiAl [40] have confirmed that the alumina grows by the inward diffusion of oxygen. However, measurements of the rate of oxygen diffusion along alumina grain boundaries show that it was too slow to account for the growth rate of the oxide [41]. It has been proposed that the growth of the oxide formed by overlay coatings is controlled by anion transport and that the growth of alumina by diffusion coatings is either exclusively by the outward diffusion of cations or is a combination of anion and cation transport.[30, 42]

Prescott et al [41] report that at 1100°C, the oxide initially formed by NiAl is due to the outward diffusion of aluminium to form transitional aluminas. As the scale matures however, the growth mechanism changes, with both inward and outward growth occurring. The characteristic ridge morphology of the scale results from the transformation of the transitional aluminas to α-alumina. The α-alumina cells nucleate and then grow laterally across the surface, consuming the transient phases, until the cells impinge upon one another. This results in the formation of the

ridges between neighbouring cells (Figure 3.7) [41, 43]. However, Jedlinski et al [44] propose that the ridge morphology observed in the oxide promoted by NiAl is due to the inward diffusion of $O_2$ into cracks in the scale. This results in internal oxidation within the scale, with the ridges being formed by the 'new' oxide. Alternatively, Hindman et al [45] have proposed that the ridge network is a result of the scale being comprised of oriented α-alumina grains bordered by mis-oriented oxide, formed by defects in the oxide and by the influence of the substrate. As oxidation progresses, the mis-oriented areas grow by a combination of $O_2$ and Al diffusion (due to the high defect structure) resulting in ridge formation, whilst the oriented oxide grew by Al diffusion, leading to the formation of faceted voids at the oxide/substrate interface.

Rybicki et al [43] suggest that the different growth mechanisms may result from the microstructure of the coatings. MCrAlX coatings form an inwardly grown oxide due to a short-circuit grain diffusion mechanism, resulting from a fine grain size. β-NiAl has a relatively large grainsize and so, promotes outward diffusion. However, due to the numerous contradictory results, both Atkinson [30] and Huntz [42] agree that the actual growth mechanism for alumina has not been identified with certainty.

The alumina scale can vary in thickness producing a convoluted morphology. This results from the diffusion mechanisms operating within the oxide where the inwardly diffusing oxygen and the outwardly diffusing cations will either, preferentially diffuse along short circuit paths, such as grain boundaries [46], or the cations will diffuse within the lattice and oxygen down the grain boundary [35]. When the oxygen reacts with the outward flux of cations, new oxide is formed

within the scale. This internal growth (resulting in the convoluted scale morphology) creates compressive stresses within the oxide, that can result in the local detachment of the scale.[37, 47, 48]

## 3.5 Degradation of an 'Ideal' System

Even oxides grown under ideal conditions will ultimately lead to the failure of a TBC system due to scale thickening. During thermal cycling , upon cooling, the coating will contract at a greater rate than the oxide and so biaxial compressive stresses are produced within the oxide. As oxidation progresses, both the scale thickness and the level of compressive stress increase. At a critical oxide thickness of approximately 5μm, the stresses within the oxide cannot be compensated for and spallation will occur [29].

## 3.6 Degradation of an 'Actual' System

The proposed degradation mechanism for an ideal system is complicated in actual service by factors such as operational environment, temperature and substrate/bondcoat chemistry. At temperatures below 1000°C the TBC system may undergo corrosive attack from the environment during service. Above 1000°C substrate/bondcoat chemistry plays a key role in oxidation, determining the scale composition and so the lifetime of the TBC system. Each of the main degradation modes that effect TBCs will be explained in turn.

## 3.7 Hot Corrosion

TBC systems are susceptible to degradation from hot corrosive atmospheres. The main aggressive compounds responsible for this are sulphates, formed when NaCl (from a sea environment) is ingested through the engines intake air and reacts with $SO_2$, produced by the fuel burning process.[6, 49]

$$2NaCl + SO_{2(g)} + {}^1/_2O_{2(g)} + H_2O \rightarrow Na_2SO_4 + HCl$$

The sulphate slag deposits onto the turbine blade, fluxes the protective oxide and then attacks the component.

The corrosive attack follows two stages. Firstly, there is an initiation stage. This has a relatively low rate of corrosion as the protective oxide is gradually broken down. Once this is completed, the propagation stage follows, as the substrate is rapidly attacked and consumed. As the initiation period is the slowest stage, it is considered that the criteria for the corrosion resistance of a coating is the duration that the protective scale can be self-repaired, hopefully for the design life of the component.[6, 49]

The protective oxide is dissolved by a process of either basic or acidic fluxing. The formation of an alumina film by the coating will decrease the local $O_2$ activity and increase the sulphur activity. The sulphur will act to penetrate the alumina scale to form sulphides within the coating. The removal of sulphur from the $Na_2SO_4$ deposit increases the activity of the $Na_2O$ component. Alumina will react with the $Na_2O$ enriched slag and so is removed by 'basic fluxing' [50].

$Al_2O_3 \rightarrow$ Sulphide formation $\rightarrow \uparrow$ activity of $Na_2O \rightarrow Al_2O_3 + O^{2-} = 2AlO_2^-$

basic fluxing

Acidic fluxing can occur due to contamination, such as $V_2O_3$ ( from the fuel) which will co-deposit with the $Na_2SO_4$, or due to the reaction of Mo, W or V oxides (from alloy additions) in the turbine. The oxide component (e.g. $V_2O_3$) will act to increase the sulphur potential.

$$V_2O_3 + SO_4^{2-} \rightarrow 2VO_3^- + {}^1/_2O_2 + SO_{2(g)}$$

This allows the alumina to be dissolved by a process of acidic fluxing . [50]

$$Al_2O_3 + SO_2 + {}^3/_2O_2 \rightarrow Al_2(SO_4)_3$$

Two types of hot corrosion have been identified. High temperature (Type I) hot corrosion (HTHC) occurs between 800 and 950°C and low temperature (Type II) hot corrosion (LTHC), between 650 and 800°C. [51] The two forms of corrosion can be distinguished by the metallographic appearance of the attack. During type I hot corrosion, sulphides are formed with a corresponding depletion of reactive components, such as Cr, in the coating/alloy (therefore, alloys/coatings with a high Cr content are preferable as chromium is less susceptible than alumna to fluxing and the depletion of the substrate will not be as rapid [52]). The external corrosion products frequently comprise of oxide precipitates dispersed in the salt film. [51] Type II corrosion is characterised by a non-uniform pitting attack, with

only a slight amount of sulphide formation close to the coating/oxide interface and a minor depletion of Cr or Al in the coating. [51]

Compared with metallic coatings, TBCs offer superior resistance to hot corrosion, as the ceramic layer acts as a barrier between the corrodants and the oxide [53]. However, the penertration of the ceramic can lead to the dissolution of the $Y_2O_2$, which can result in the destabilisation of the ceramic [54].

## 3.8 The Effect of Sulphur

The damaging effect of sulphur will be further explained as it is known to deteriorate the coating through both corrosion and oxidation. Sulphur can be introduced as a contaminant into a coating either during the production process or subsequently from the environment during operation. There is some confusion as to the effect of sulphur contamination. It has been argued that sulphur will segregate to the oxide/metal interface and interfaces within the oxide scale, such as grain boundaries [55, 56, 57, 58]. This segregation will alter the oxidation kinetics of the scale, promoting the outward diffusion of damaging elements [47, 56] and act to embrittle the oxide [55, 59]. Both these factors will decrease the adhesion of the coating.

Alternatively, it has been proposed by Grabke et al [60] that early work on the 'sulphur effect' was inconclusive, as it was either carried out on free metal surfaces (assuming that they were comparable to oxide/metal interfaces) or used equipment that did not have resolutions fine enough to discern that the sulphur had actually segregated to the interface. Also, when sulphur segregates, it becomes negatively charged ($S^{2-}$ ions) and so increases in size. At the oxide/metal interface

there is neither enough free-space nor bonds to allow for sulphur segregation due to the strong interaction between the metal and the oxide. By using sputter profiling and Auger analysis, Grabke et al established that sulphur will preferentially segregate to free surfaces produced by the growth of voids at the oxide/metal interface. The sulphur will promote further detachment by augmenting the effect of thermal and growth stresses, increasing void size and number and so decreasing the adhesion of the interface. It has also been argued however, that once sulphur has segregated to the voids it can play no further part in the degradation of the coating [61, 62]

Any effects of sulphur contamination can be nullified, at least partially, by the addition of 'active elements', such as yttrium, to the coating. These act as 'sulphur getters'(i.e. they form stable sulphur containing compounds) preventing segregation to the proposed degradation sites [57, 60, 63].

## 3.9 Erosion

Erosion, combined with either oxidation or corrosion, is undesirable as the protective oxide scale formed by the coating can be cracked and spalled by the erosion process. The extent of this process is dependent upon a number of factors, such as particle size and velocity, temperature and corrosion/oxidation conditions. The problem of erosion is greater for environmental coatings than TBCs, as the ceramic layer offers protection to the TGO and bondcoat, but may erode itself [22].

## 3.10 Oxidation

Oxidation of the bondcoat is a three stage process. Initially, there is a transient stage involving the simultaneous formation of oxides of all the active

components on the surface of the bondcoat. This is followed by a period of steady growth where a protective alumina film is formed. The duration of this stage is critical , as it determines the lifetime of the component. Ideally the bondcoat should prolong this stage. By drawing on the aluminium rich reserves within the coating, the bondcoat will promote a continuous and self-repairing oxide. Lastly, during the breakaway stage, the attack on the coating will become accelerated and the protective oxide will breakdown, leading to the eventual failure of the component [35, 37]. During the breakaway stage of oxidation, there are several factors that will influence the failure of the scale. These include [62];

1. The extent of contact between the interfaces.
2. The bond strength between the scale and the bondcoat/ceramic.
3. The scale/coating interface configuration, as an irregular surface can increase adhesion.
4. The properties of the scale, such as fracture toughness.

Degradation by oxidation has been described in numerous papers for TBC systems. Sacre et al [64] has given a particularly concise portrayal of the oxidation of MCrAlX coatings. At temperatures below 1000°C, an outwardly grown scale is formed. The aluminium activity beneath the oxide falls until a critical level is reached that initiates the internal oxidation of chromium. When cracking occurs in the brittle outer oxide layer, chromia will grow outwards towards the oxide/ceramic interface. The formation of chromia on $\gamma'$ rich phases in the coating is the rate determining step at temperatures below 1000°C (Figure 3.8). At temperatures below 1100°C, a mixed oxide of chromia and alumina is formed. The alumina is the inwardly grown $\alpha$-type, as opposed to the transitional aluminas grown at lower

temperatures. Above 1100°C, after the initial transient stage, the inward growth of α-alumina takes over as the rate determining/steady-state stage, acting to suppress the growth of chromia. During this period the chromia formed at the transient stage decomposes whilst the cobalt and nickel oxides combine with the alumina to form $(Co,Ni)Al_2O_3$ type compounds. This mixed alumina-based scale has also been observed by Lee et al [65], who noted that the oxide formed by a NiCrAlY, thermally cycled at 1135°C, was a solid solution of $(Al,Cr)_2O_3$ with dissolved NiO. As the oxidation progresses, the aluminium activity in the bondcoat becomes depleted, allowing the growth of nickel and chromia spinels at the oxide coating interface (Figure 3.9). Lee et al [65] observed that, where the local concentration of NiO was above the solubility limit of $(Al,Cr)_2O_3$, the precipitation of NiO and spinels occurred. This is considered a life-limiting factor for TBC systems, as spinels provide easy fracture paths within the oxide, due to the fact that they have a higher growth stress than alumina (the Pilling-Bedworth or $M^{2+}/M$ volume ratio is smaller for alumina than for NiO, 1.28 compared to 1.65), and low adhesion with the scale [64, 65, 66].

Investigations of APS TBC systems [67, 68] have noted outcrops of NiO at the ceramic/oxide interface. These outcrops grow into the pores contained in the ceramic. As the coefficient of thermal expansion of the PYSZ ceramic is larger than that of the oxide, the NiO ingrowths promote stress concentration, leading to failure. This degradation mechanism can be avoided by depositing the ceramic using EB-PVD. The ceramic columns of the EB-PVD produced structure are poorly bonded to the adjacent columns but are chemically bonded to the substrate, as opposed to

APS ceramics which rely heavily on mechanical keying. The resulting structure is highly tolerant of thermal strains [5].

Similarly, diffusion coatings appear to degrade due to the interdiffusion of elements between the substrate and the coating. During oxidation, the aluminium rich outer coating becomes depleted due to the formation of the alumina scale. This depletion leads to the phase composition of the coating degrading from $\beta$ to $\gamma'$ (in the case of platinum aluminides, $PtAl_2$ to $\beta$ to $\gamma'$) [69]. As with MCrAlX coatings, the outward diffusion of transition metals to form spinels within the oxide lowers the interfacial adhesion [70, 71]. The degradation of diffusion coatings, including the effect of the outward diffusion of refractory metals from the interdiffusion zone, will be further explained in chapter 4.

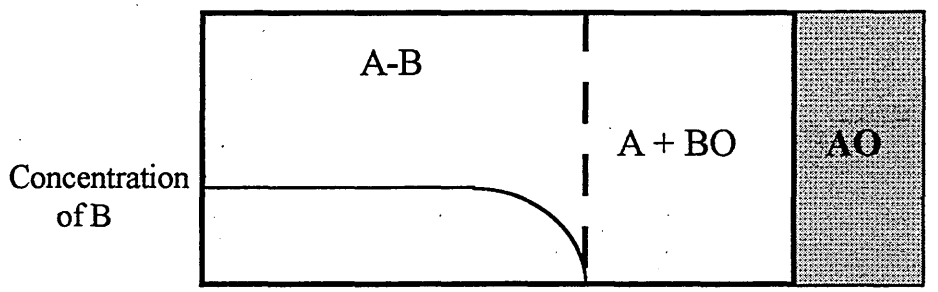


Figure 3.1- Schematic cross section of alloy A-B , with a low concentration of B [31]

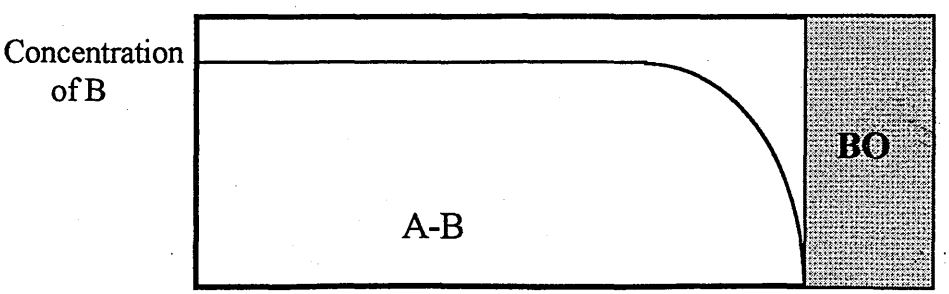


Figure 3.2- Schematic cross section of an alloy A-B, with a critical concentration of B [31]

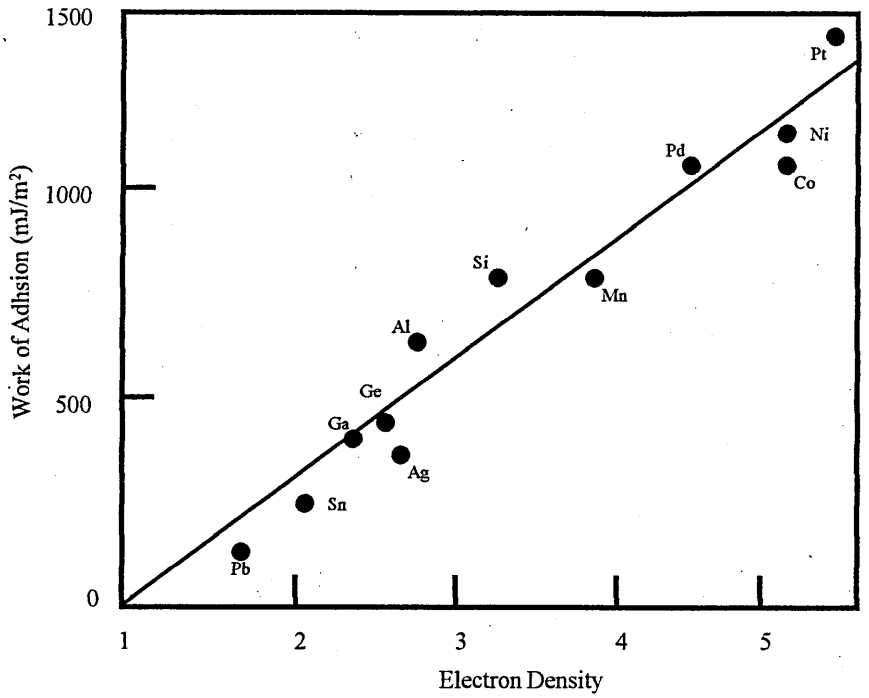


Figure 3.3- The linear relationship between the work of adhesion of the liquid metals on alumina and the electron density of the corresponding metals [33]

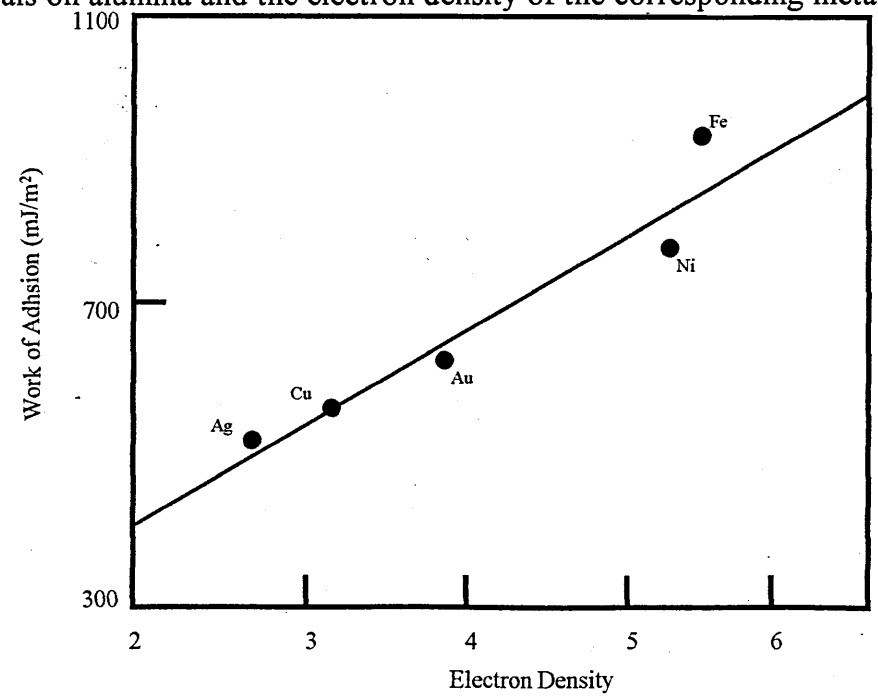


Figure 3.4- The work of adhesion of solid transition metals on sapphire as a function of electron density of the corresponding metals [33]

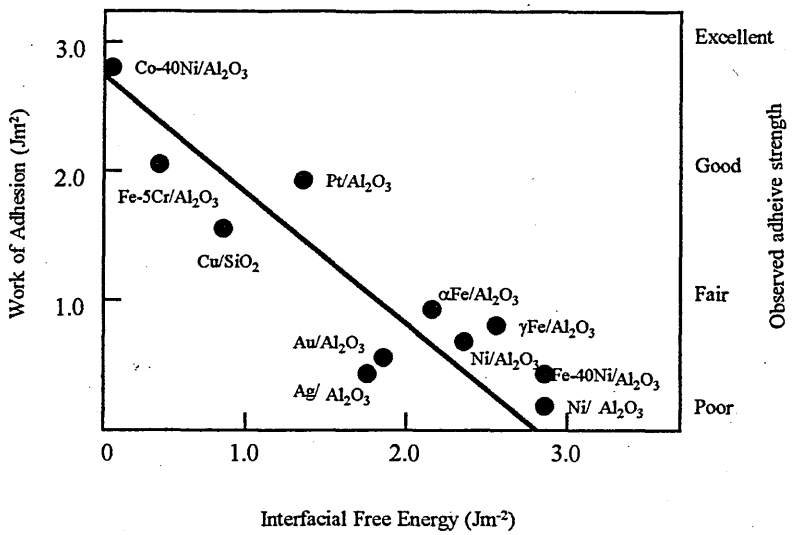


Figure 3.5- The adhesive properties of a number of metal/ceramic diffusion bonds [34]

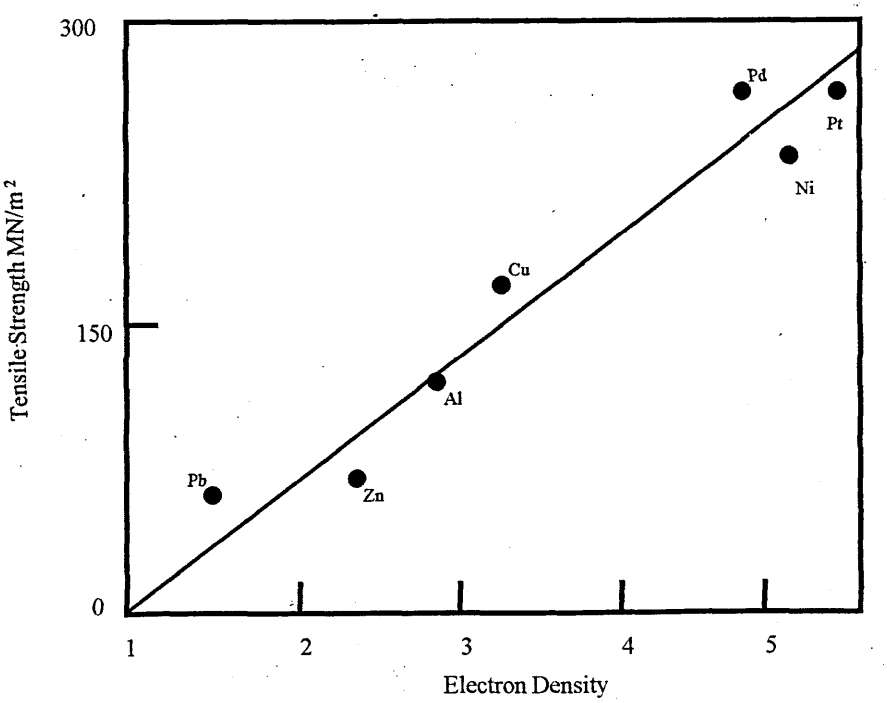


Figure 3.6- The tensile strength of the interfaces formed by solid metals with alumina as a function of the electron densities of the corresponding metals [33]

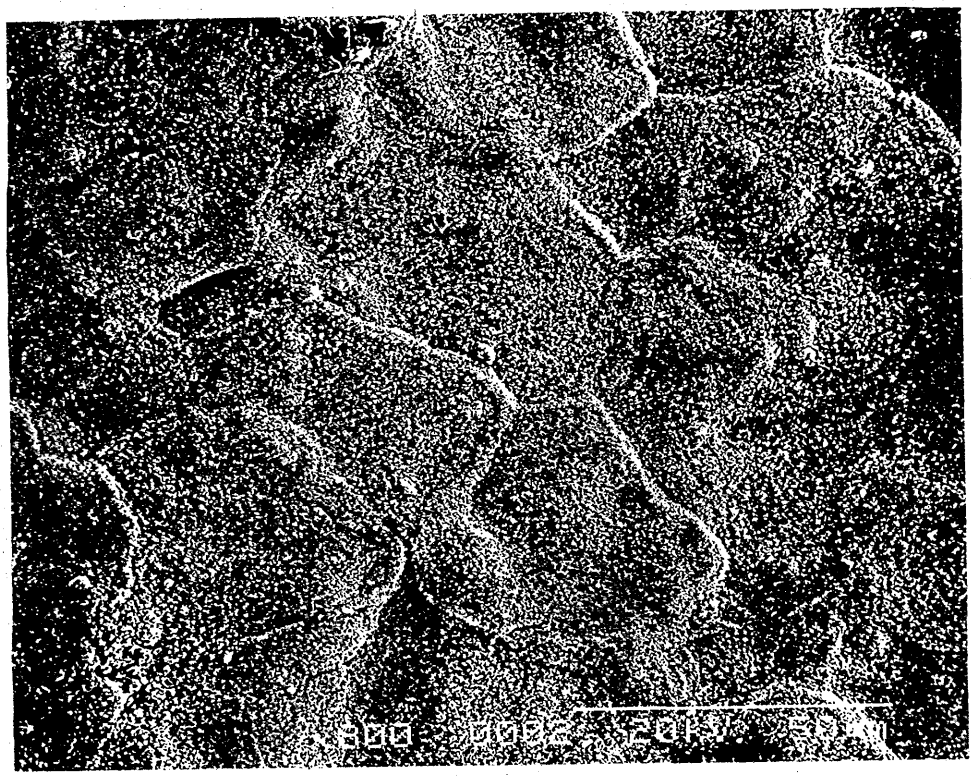

Figure 3.7- Micrograph of the surface of a β-phased coating, aged for 25h at 1100°C

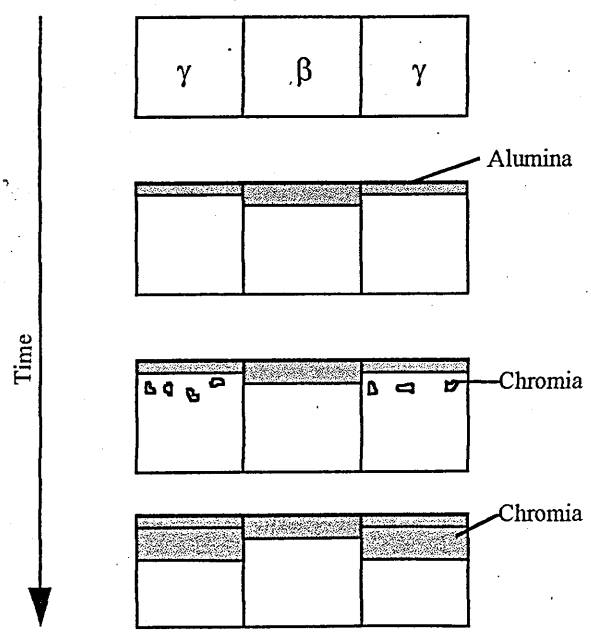


Figure 3.8- Schematic diagram of the oxidation of a MCrAlX coating at temperatures less than 1000°C [64]

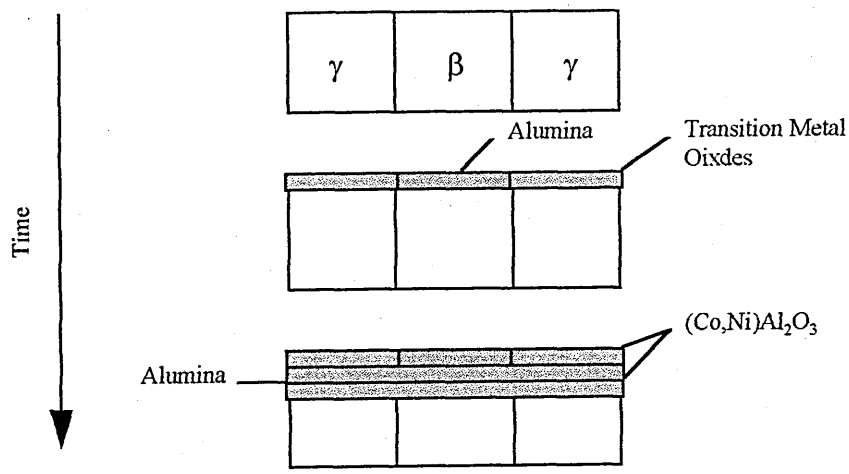


Figure 3.9- Schematic diagram of the oxidation of a MCrAlX coating at temperatures of 1100°C and above [64]

Chapter 4: Literature Review

## Pre-treatments and Diffusion Coatings

### 4.1 Introduction

This chapter reviews the literature that relates to the optimisation of a bondcoat's oxide by using either pre-treatments or by the development of diffusion coatings, which has a direct effect on TBC life.

### 4.2 Pre-treatments for Bondcoats

Published literature has reported that the application of pre-treatments will extend the life of a T.B.C system.

Recent Taiwanese studies [72 → 76] have investigated the effects of various pre-treatments on the life of TBC systems. It was recognised that failure within a T.B.C system was associated with the formation of Ni, Cr and Co based spinels as part of the oxide formed on the bondcoat. These oxides are formed during the initial stages of oxidation, prior to the formation of a continuous alumina and again in the latter stages, when the aluminium activity has decreased to a level where the formation of an inwardly grown alumina cannot be sustained. The presence of these lesser protective spinels lowers the adhesion at the oxide/metal interface and can lead to spallation. It was hoped that by pre-treating the bondcoat to ensure the early and rapid growth of an alumina film and therefore the elimination of the initial Ni,Cr and Co oxides, the lifetime of the T.B.C would be increased.

For their investigations, Chang and co-workers used T.B.C systems on either MarM247 or IN713LC substrates. The bondcoats were deposited using either vacuum

plasma spraying (V.P.S) or low pressure plasma spraying (L.P.P.S), whilst the T.B.C was air plasma sprayed. In these studies, the first pre-treatment to be examined was the pre-oxidation of a NiAlCrY bondcoat in air. The prior formation of an α-alumina film was achieved, and it was reported that this increased the T.B.C's lifetime by a factor of two [72].

Their second approach was to enrich the surface of the bondcoat by aluminising. This proved to be beneficial on a CoCrAlY bondcoat, promoting alumina formation [73, 74]. Similarly, when a 3-5 μm thick alumina layer was deposited by C.V.D on a NiCrAlY bondcoat, the T.B.C lifetime was increased by factors between two and five [75].

Superior results were achieved by combining both the aluminising and air pre-oxidation on a CoCrAlY bondcoat. [76] Under these combined conditions the cyclic life of the coating was increased by six to eight times and bondcoat oxidation was substantially reduced. A summary of these results is plotted in Figure 4.1.

Prior to ceramic deposition, bondcoats are traditionally cold worked as part of the grit blasting procedure. This is primarily to produce a rougher surface, but also as a cleaning aid. Both factors are thought to aid the adherence of the ceramic top coat. Information gathered on $Cr_2O_3$ forming alloys has shown that cold working of the surface increases the dislocation density within the substrate and decreases the grain size of the oxide formed and so aids outward diffusion of cations.[58, 77]

Alumina forming alloys grow transitional aluminas (eg θ, δ etc) at less than 900°C. These are formed by the outward diffusion of aluminium ( as opposed to α-alumina, which grows predominantly by the inward diffusion of $O_2$). At temperatures greater than 1000°C, the transitional alumnas will transform to α-alumina and so aid the

adherence of the ceramic to the bondcoat. As cold working provides further diffusion paths to the metal surface and promotes outward diffusion, such pre-treatments should have a beneficial effect on the early oxide that is formed [77].

## 4.3 Diffusion Coatings

Diffusion coatings were the original, and are still the most cost effective method of protecting superalloy turbine components. They are employed either as an environmental protective coating, or latterly, as a bondcoat for T.B.C's [26].

### *4.3.1 Production of Aluminide Coatings*

The most common type of diffusion coating in service are the aluminides, formed by enriching the components substrate with aluminium. The basic aluminising process is by pack cementation. The component is cleaned and placed in an air tight container with a pack consisting of aluminium powder, a halide activator ($NH_4Cl$, NaCl or $CrF_2$) and an inert powder filler (usually a refractory oxide). The container is heated to promote diffusion for a period of between two and twenty four hours at a temperature ranging from 750 to 1000°C. The halide activator will decompose and the halogen released will react with aluminium to form an aluminium halide which diffuses to the surface of the component where it dissociates. The deposit on the surface diffuses into the substrate, whilst the halide ions react with yet more aluminium and the cycle continues [26, 78, 79]. A schematic of the pack aluminising process is shown in Figure 4.2.

A modification of this technique is the 'Out-of-Pack' process. Here, the component is suspended above the powder, the aluminium halide gas being transported over its surface by a carrier gas (Figure 4.3) [27]. Chemical Vapour Deposition (C.V.D)

is similar to the 'Out-of-Pack' process, in that the components are not in contact with the powder and it uses a gaseous transport agent (Figure 4.4) [26]. The advantages both these processes have over pack cementation are that they enable the coating of intricate shapes and offer the ability to 'mask off' areas which are not required to be coated. Also, the pack is renewable and there is no surface contamination from the pack particles [26, 78, 80]..

*4.3.2 Growth Mechanisms*

There are two main growth mechanisms for aluminides, depending on whether a high or a low activity aluminium activity pack is used.

*4.3.2.1 High Aluminium Actvity-* This process involves the inward diffusion of aluminium to form δ-$Ni_2Al_3$ with a minor phase of β-NiAl. $Ni_2Al_3$ is a brittle phase that decomposes at low temperature, so the coating is heat treated to allow Ni to diffuse out from the substrate to form β-NiAl, a more ductile and oxidation resistant phase. As a result, a three zoned structure is formed (Figure 4.5). The outer zone contains α-Cr and other substrate phases in a β-NiAl matrix, whilst the middle zone has a single phased β structure, with Cr, Ti, Mo and Co in solution. The inner zone is a β matrix containing carbides and σ phases [26, 80, 81].

*4.3.2.2 Low Aluminium Activity-* A two zoned structure is produced by the outward diffusion of nickel from the substrate to react with the aluminium (Figure 4.6). The outer zone is single phased β-NiAl with alloying elements that diffused out alongside nickel

from the substrate. The inner zone contains carbides and/or phases formed by the nickel withdrawal, in a β-NiAl matrix [26, 81, 80].

*4.3.3 Limitations of Aluminide Coatings*

The effectiveness of a coating depends on the maintenance of the alumina film to act as barrier to the environment or to adhere a ceramic topcoat in a T.B.C system. The oxide scale produced by aluminide coatings will degrade with time at temperature due to the outward diffusion of alloying elements from the substrate. These act to dope the alumina, increasing the scales growth rate and ultimately leading to spallation (see section 4.3.2.8). High activity aluminides, being 'inwardly grown', incorporate these elements in the coating and so have a lower resistance to corrosion and oxidation than low activity aluminides, where these damaging elements are excluded from the coating.[27]

Aluminides also suffer from the attack by impurities in the combustion gases caused by engines running on lower grade fuels or operating in harsher environments. [26] This decrease in the effectiveness of standard aluminides has led to the development/modification of aluminide coatings by the addition of platinum.

*4.3.4 The benefits of platinum*

Platinum has been investigated both as an alloy addition to the substrate material and as a platinum aluminide coating.

*4.3.4.1 Platinum as an alloy addition-* Several studies, [82, 83], have analysed platinum additions to a superalloy and its effects on the alloys properties and oxide scale adherence. Microstructurally, platinum was found to preferentially partition to the γ'.

This acted to increase the γ′ lattice parameter by 0.5% and to increase the γ′volume fraction. These effects acted to increase the alloys mechanical properties.

The effect of the platinum additions on scale adherence was assessed using isothermal ageings in air at temperatures between 1100 and 1200°C. The standard superalloys, without platinum additions, had grown a discontinuous alumina scale, damaging elements such as Ti were observed at the interface and internal oxidation was prevalent. The alloys that contained the platinum additions had grown a continuous alumina film (containing small precipitates of platinum) with no internal oxidation observed. It was, therefore, concluded that platinum promoted and maintained a more slowly grown alumina scale [82, 83].

*4.3.4.2 Platinum aluminide coatings-*

It is generally agreed that platinum aluminides outperform conventional aluminides [28, 84, 85]. They have improved oxidation resitance [78] and a greater resistance to Type I hot corrosion (however, there is only a marginal improvement against Type II hot corrosion) [6, 26, 78]. This superior performance is due to the beneficial interaction between platinum and aluminium which produces a number of importent effects.

In the as -processed condition, platinum will be present as either β or $PtAl_2$. Compared with simple aluminides, a platinum aluminide will contain more aluminium than β-NiAl. Work by Schaffer et al [78] has shown that β-NiAl will be formed with the $X_{AL}$ no larger than 0.49, compared to $X_{AL}$ of 0.67 in a platinum aluminide coating. In esscence, the affinity of aluminium for platinum creates an aluminium 'resevoir' in the outer portion of the coating [85].

Platinum promotes the selective oxidation of aluminium. This is due to two reasons. Firstly, no platinum oxide is formed at the operational temperatures of the coatings [86] and secondly, aluminium is very mobile in the platinum phases. Other elements have been shown to competitively diffuse relatively slowly to the oxide scale. The platinum aluminide acts as a physical barrier to these damaging elements, separating them from the oxide/coating interface [78, 87].

For these reasons, platinum promotes a slowly growing, continuous and compact alumina scale. The improved protection afforded by platinum aluminides is due to the coatings ability to grow a coherent scale for longer periods than standard aluminides and so avoids the oxide cracking and spallation that accelerates oxidation rates and corrosive attack.

*4.3.5 The manufacture of platinum aluminides*

The first patents for platinum aluminides were filed in the early 1970's by Deutches Edelstahlwerke (D.E.W). This 'high temperature-high activity' process involved the electroplating of a thin layer of platinum onto a components surface. This was then heat treated at temperatures from 1040 to 1100°C and then pack aluminised to produce an inwardly grown platinum aluminide [84, 88]

The high temperature of these initial processes could potentially damage the base material. This problem was overcome by the 'low temperature-high activity' series of coatings produced by Rolls Royce p.l.c and Johnson Matthey, where the components were heat treated after platinum plating at temperatures between 870 and 980°C. The resultant structure is shown in Figure 4.7. The amount of $PtAl_2$ in the coating depends

on the platinum concentration. High levels of platinum will produce a continuous $PtAl_2$ layer. At lower levels however, β-(Ni,Pt)Al will precipitate in the $PtAl_2$ [78, 89].

High activity platinum aluminides have a number of limitations, being hard and brittle coatings and when subject to thermo-mechanical fatigue cracking is observed and 'rumpling' on oxidation [27]. These problems can be overcome however, by using a 'low activity' processes where, during aluminising, the aluminium moves through the platinum layer, however growth is due to the outward diffusion of nickel (Figure 4.8). For high temperature processes,the outer zone will contain $PtAl_2$ and β or solely β, whilst for low temperature processes the outer zone will have a $PtAl_2$ composition. For low temperature processes the middle layer will be a nickel rich β phase, whilst for high temperature processes the proportion of platinum in the β will increase [78, 87]. Low activity platinum aluminides have an increased resistance to fatigue cracking and high temperature oxidation , are more ductile and are less susceptible to 'rumpling' [27].

*4.3.6 The degradation of aluminide coatings.*

The method in which aluminide coatings degrade differs from that reported for MCrAlX coatings (chapter 3). As opposed to the adhesion of the scale decreasing due to the growth of transition metal spinels, the integrity of the oxide formed on aluminide coatings depends on the growth mechanism of the scale and how that is effected by the outward diffusion of alloying elements from the substrate. A feature of the oxide scale grown on diffusion coatings is the development of smooth, facetted pits on the surface of the coating. They are observed at the interface between the substrate and the T.G.O, or on the exposed surface. This is a widely reported phenomena, having been observed on

superalloys [37, 58], intermetallics [90, 91, 92], aluminides [41] and FeCrAl/FeCrAlY coatings [93 → 96].

There are two schools of thought as to how these pits are formed. Firstly, it has been proposed that the voidage can be attributed to the Kirkendall Effect, due to the preferential consumption of aluminium [90, 91, 96]. It has also been suggested that they maybe a result of preferential growth within the oxide scale. Localised thickening can occur at 'easy diffusion paths' such as grain boundaries. The inwardly diffusing oxygen will react with the outward flux of cations to form an oxide within an oxide. This will lead to a build up of compressive stress within the scale, causing buckling and local detachment [37, 48, 90, 93]. The facetted nature of the pits is thought to be either the grain boundary structure or that the metal has rearranged itself on a free surface to achieve the lowest surface energy. This would be achieved by growth in the low index planes (110) and (100) [91, 96].

In general, the detachment of the oxide from the substrate due to the formation of these pits is thought to be detrimental, leading to spallation. However, work by Hou et al [95] proposed that the formation of pits beneath an oxide does not nescessarily affect the scales adhesion, as they found no correlation between the proportion of pits and the amount of spallation.

During oxidation, the β-NiAl within simple aluminides will degrade to γ'as the aluminium is consumed to form the oxide scale. When platinum aluminides are aged, the platinum containing phases degrade as the platinum diffuses inwards and nickel and cobalt outwards. The $PtAl_2$ phase will be converted to β-(NiPt)-Al and then to γ' [70, 71, 87, 97].

As part of the aging process, alloying elements diffuse outwards from the substrate to the oxide interface. These elements have a detrimental effect on the scale's adhesion [71]. Once at the interface these elements dope the oxide, increasing its growth rate and so fore-shortening the scales lifespan [70, 98]. The relationship between void formation and these damaging elements has not been fully reported in the published literature.

Titanium is the most commonly analysed of these elements, as it has a high diffusion rate in nickel and cobalt based alloys, making it more prevalent in the oxide. However, the exact role of the element and the level at which it is damaging are matters of contention. It has been proposed that up to 1at%Ti within the substrate will not affect the scale and that increased growth rates were only noted at concentrations of 3at% or above [99, 100]. Conversely, Tawancey et al [715] considered 1at%Ti to have a detrimental level, whilst Choi et al [90] regarded a titanium level of 3at% to be beneficial in promoting alumina formation. The dopant effect of Ti on alumina is well documented, as the sintering rates of alumina ceramic components can be significantly increased by the addition of titania [101, 102]. From ceramic studies it has been proposed that;

a) 3 $Ti^{4+}$ ions substitute for 4 $Al^{3+}$ ions with the creation of an aluminium vacancy [A112]; and/or

b) 2 $Ti^{4+}$ ions substitute for 2 $Al^{3+}$ ions, with an extra ion entering a vacant oxygen site. If the number of Schottky defects in the alumina is constant, then the addition of extra oxygen will alter the equilibrium and therefore more pairs of oxygen and aluminium vacancies will have to form. This would lead to an increase in the number of aluminium vaccancies and therfore an increase in aluminium diffusion [103].

The effects of titanium can be decreased by tantalum. The two elements become associated to form carbides, effectively 'tieing-up' the titanium. Even when oxycarbides are observed in the scale, the damaging growth rates are drastically reduced [100]. Tantalum by itself appears to act in a similar fashion to titanium. At a concentration of 1at%, it is considered either benign [100] or beneficial [99] to the alumina adhesion. However, a concentration of 3at% has been found to significantly reduce oxidation resistance [103]. The effects of other alloying elements, such as tungsten and molybdenum, has not been fully reviewed in the published literature, although they are widely recognised as being detrimental to thr corrosion resistance.

Sulphur contamination may increase the detrimental effect of pitting. Auger analysis of Fe-Cr-Al alloys has found sulphur present within voids. The sulphur was thought to have segregated to the free surface, where it acted to augment both thermal and growth stresses, decreasing the adhesion of the scale [94, 104]. However, in the auger analysis carried out by Hou et al [95] sulphur was found to be present in the oxide and voids, indicating no preferential segregation to interfacial voids.

High activity aluminides are more susceptible to the effects of outward element movement. than low activity coatings. as they are inwardly grown. The damaging substrate elements are therefore present in the coating in the as-processed condition [98] and will therefore take less time to reach the critical concentration level at the metal/oxide interface.. The detrimental effect of these elements has been noted on platinum aluminides [69]. However, the blocking effect of the platinum aluminide extends the lifetime of the scale, even in the presense of these elements.

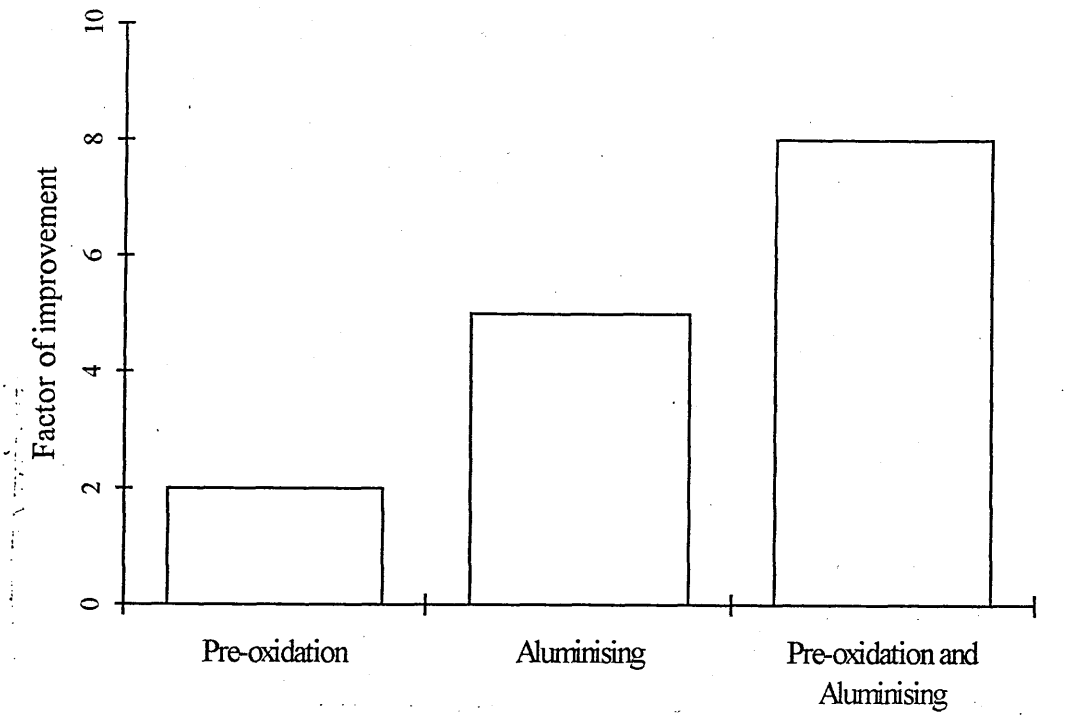


Figure 4.1- Summary of Chang and co-workers investigations of pre-treatments [72 → 76]

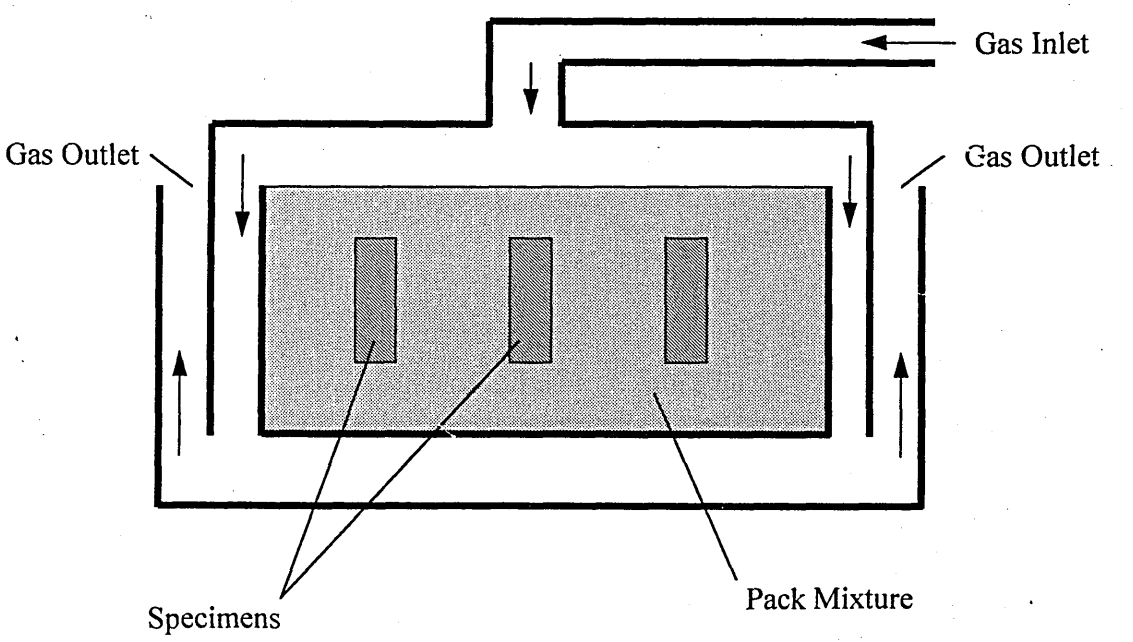


Figure 4.2- Schematic diagram of a pack cementation process [26]

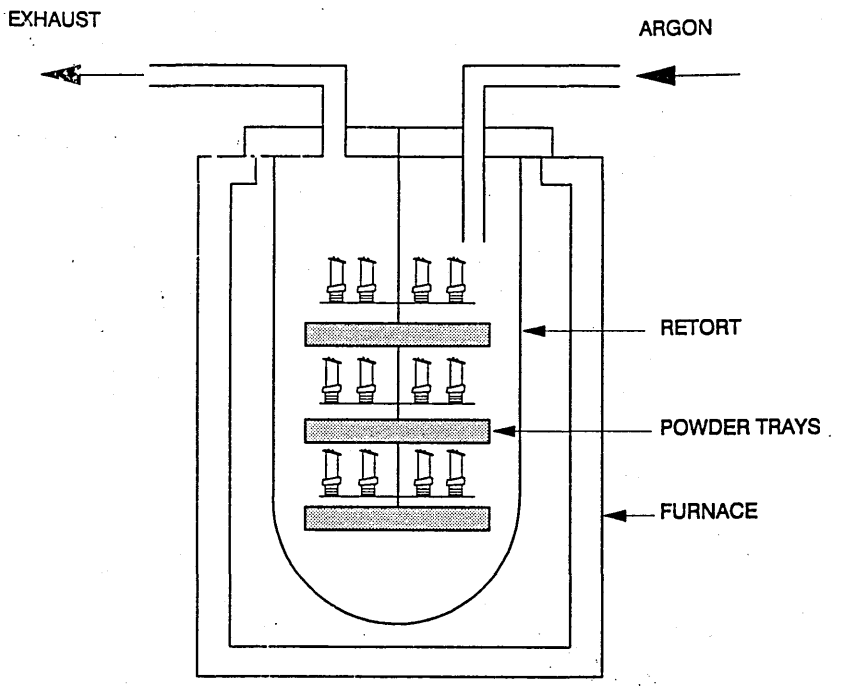


Figure 4.3- Schematic diagram of an 'out-of-pack' process

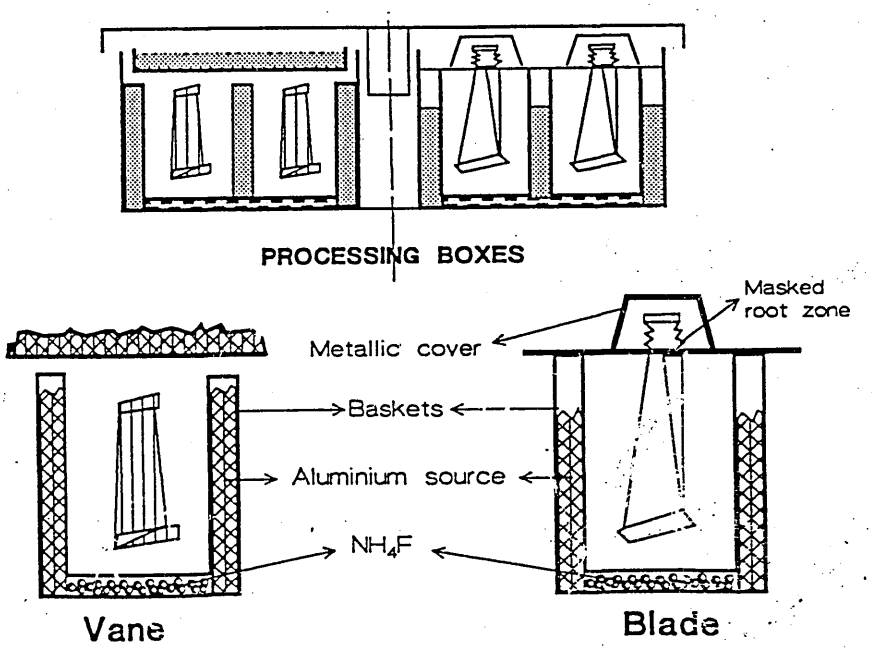


Figure 4.4- Schematic diagram of a CVD process [26]

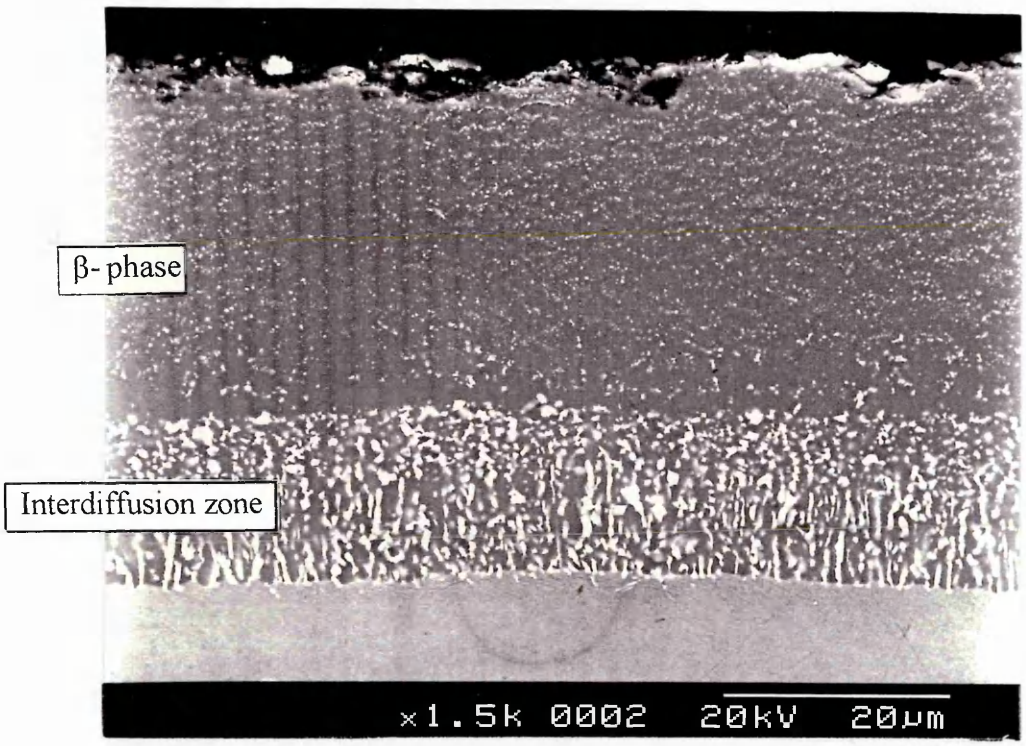


Figure 4.5- Microstructure of a high aluminium activity aluminide

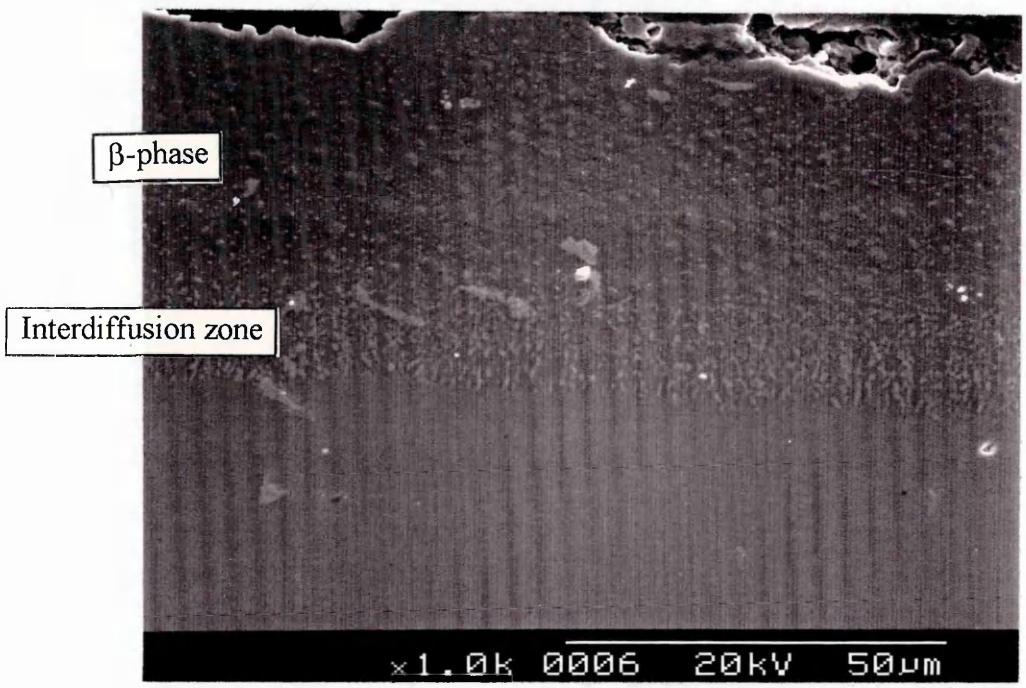


Figure 4.6- Microstructure of a low aluminium activity aluminide

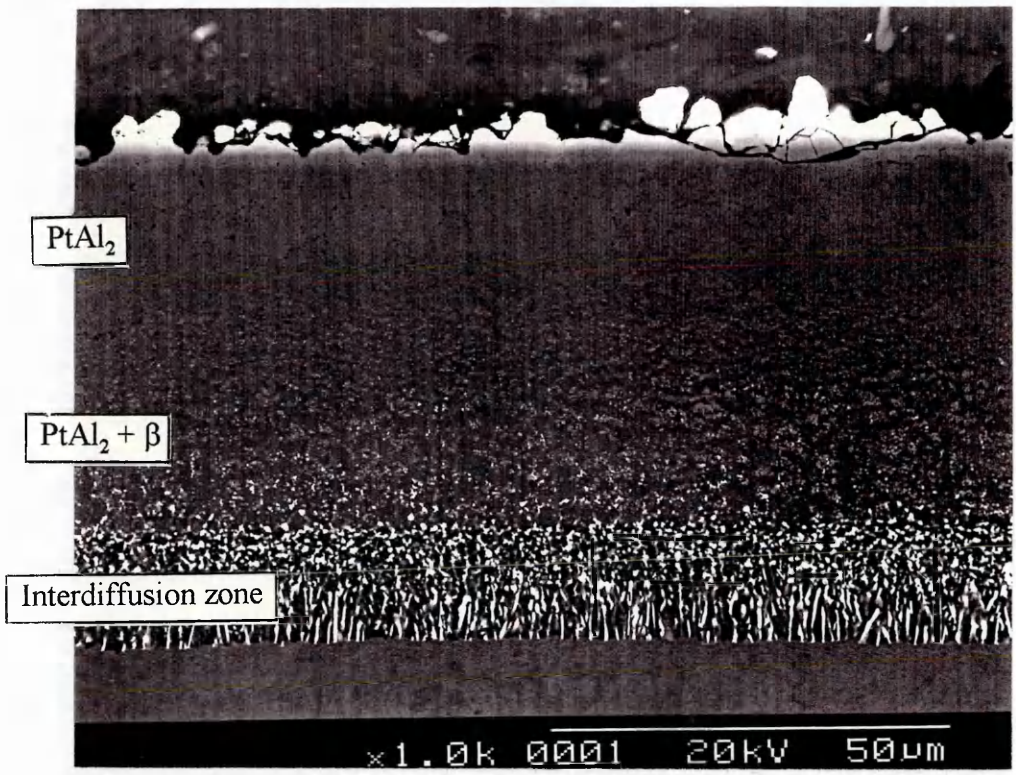


Figure 4.7- Microstructure of a low temperature-high activity platinum aluminide

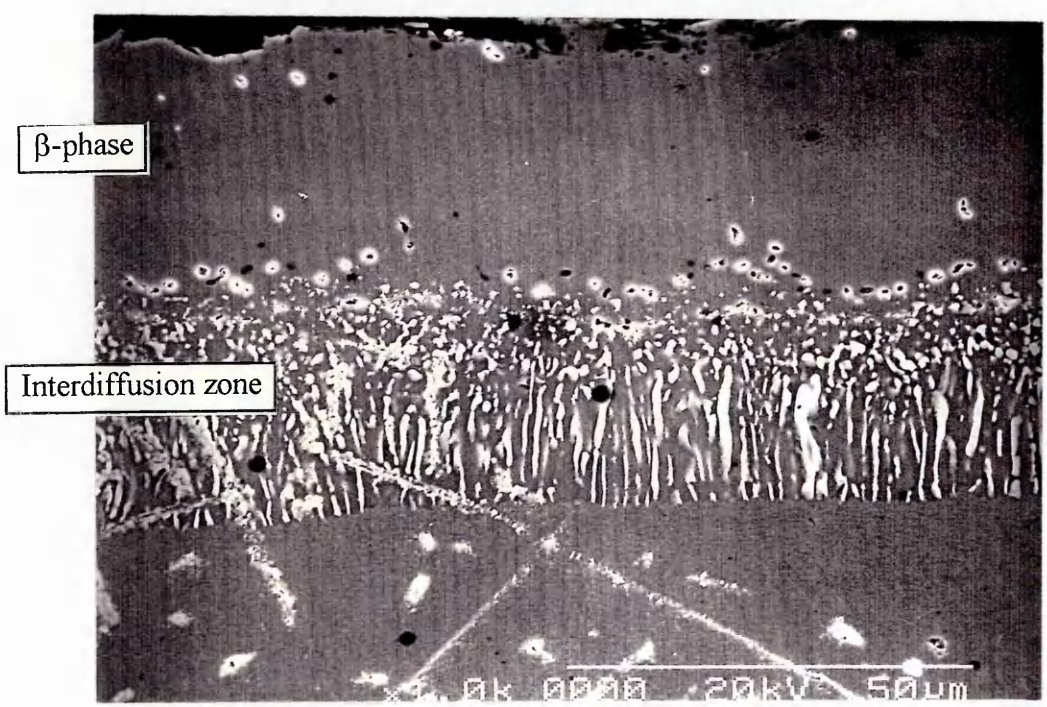


Figure 4.8- Microstructure of a high temperature-low activity platinum aluminide

# SCOPE

Chapter 5

## Scope of the Research Programme

Essential to the performance of a TBC is the quality of the adherence of the oxide scale grown by the bondcoat. As part of the philosophy of a 'designed-in' TBC, this research programme aimed to optimise the adhesion of the alumina scale and so increase the life time of the TBC. This was undertaken by either the use of pre-treatments to the bondcoat or by the design of a new range of bondcoats, developed to meet the needs of a TBC.

The investigations of bondcoat pre-treatments examined the effects of pre-oxidation treatments in either Ar-20%$O_2$ or $H_2$-10%$H_2O$ atmospheres, both in- and ex-situ, and the effects of gritting on the bondcoats ability to grow an adherent alumina scale. The bondcoat design programmes assessed a range of diffusion coatings, designed and optimised to met the specific needs of a TBC. The overall scope of the programme is presented in Figure 5.1.

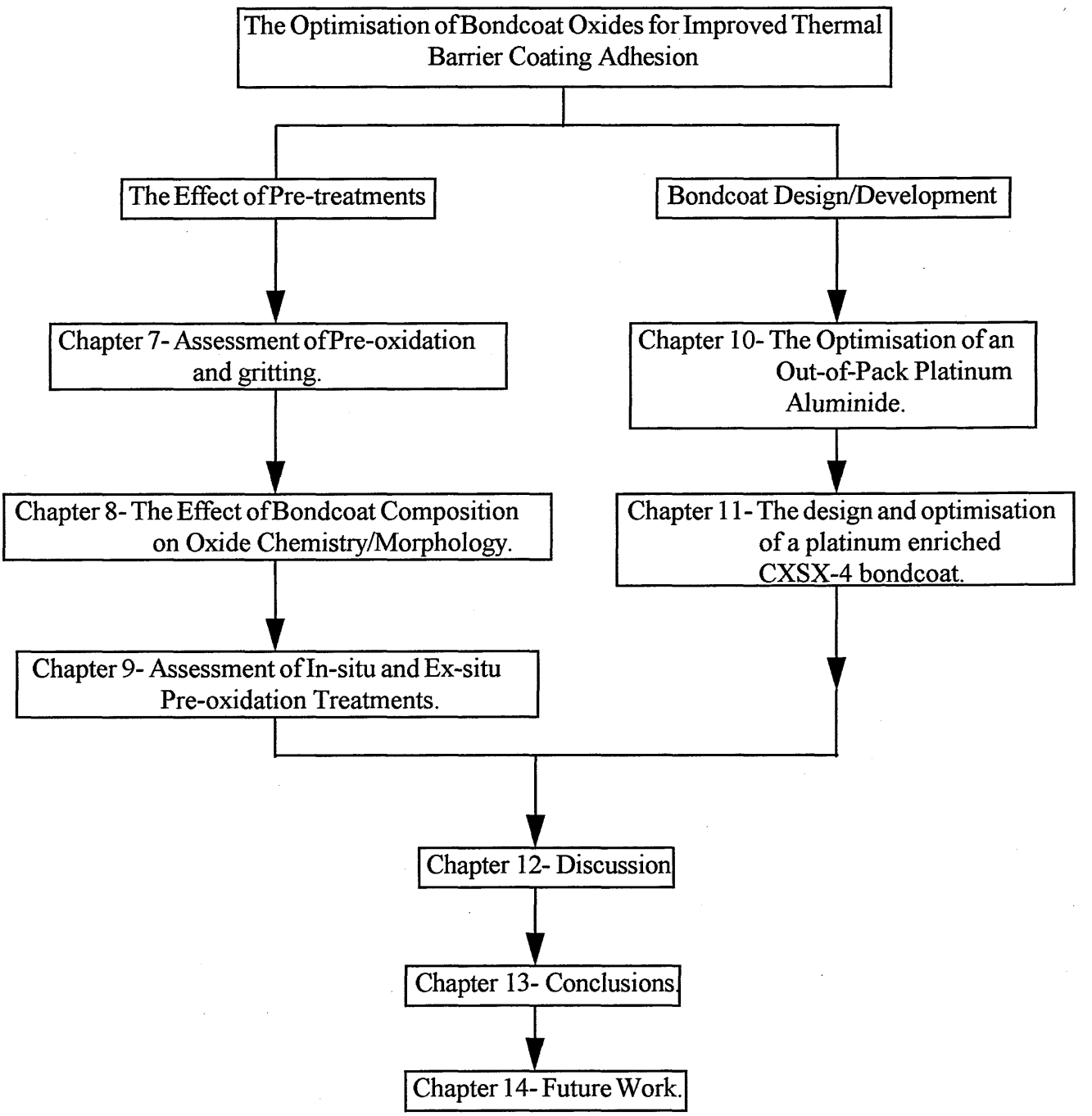


Figure 5.1- Scope of the research programme

# EXPERIMENTAL

Chapter 6

# Experimental Technique

## 6.1 Introduction

The need to gain an understanding of how the integrity of the oxide and the composition of the coating changed after exposure at temperature was central to optimising the adhesion of the TGO. This section details the analytical techniques used for this purpose, including how the modified scratch test can provide a method to rank the adhesion of the systems.

## 6.2 Samples

The superalloy substrates for the TBC systems were supplied as 110mm long, 9mm diameter pins by Rolls Royce p.l.c. A range of alloys were assessed during the programme. Their type and composition are given in Table 6.1.

Bondcoats were deposited onto these superalloy pins by Chromalloy UK Ltd. Initially, five bondcoat systems were investigated; three overlay and two diffusion coatings. The deposition techniques used and the compositions of the initial range of coatings under investigation are given in Table 6.2. The PYSZ topcoat was deposited using EB-PVD at Chromalloy UK Ltd.

## 6.3 Pre-oxidation

To determine the effects of pre-treatment on the adhesion of a TBC system, selected samples (see chapters 7, 8 and 9) were pre-oxidised in either an

Ar-20%$O_2$ or a $H_2$-10%$H_2O$ atmosphere. The Ar-20%$O_2$ atmosphere is an air equivalent, aimed at suppressing the formation of nitride phases, whilst the $H_2$-10%$H_2O$ atmosphere is designed to promote the formation of predominantly alumina and chromia scales as evident from the Ellingham diagram included as Figure 6.1..

The samples were pre-oxidised for one hour at 1000°C in alumina lined furnaces. The pre-treatments were carried out at AEA Technology, Harwell.

## 6.4 Ageing Treatments

Sections (approximately 10mm long for the isothermal soaks and 50mm long for thermal cycling), were cut from the test pins using Struers grinding wheel cut off machines.

### 6.4.1 *Isothermal ageing treatments*

The isothermal ageings were carried out at Rolls Royce p.l.c using Carbolite furnaces. These were assessed regularly for conformance with BS5750 to within +/- 10°C over the range of working temperatures. Samples were contained in low sided high purity alumina crucibles and exposed in still air at atmospheric pressure.

### 6.4.2 *Thermal Cycling*

The thermal cyclic testing was carried out at Rolls Royce p.l.c using a cyclic furnace designed and constructed by Cranfield University.

For each cycle, the samples were held at temperature for one hour, exclusive of a "heat-up" period of fifteen minutes. At the end of the cycle, the samples were

cooled by an air blast for ten minutes, lowering their temperature to approximately 50°C. Once every twenty four hours the samples, after air cooling, underwent a water quench to room temperature.

## 6.5 Sample Preparation

### 6.5.1 *For examination of the surface*

Samples were ultrasonically cleaned in an acetone bath. For SEM analysis, the samples were attached to metal stubs using silver dag and then carbon coated.

### 6.5.2 *For examination in section*

Samples were impregnated with epoxy resin in order to maintain the ceramic structure during metallographic preparation. The impregnated samples were then mounted in Struers cold setting resin, "Triofix", in order to minimise any further stresses being induced during the mounting procedure. The samples were then prepared according to the procedure laid out in Table 6.3 for bondcoat examination or Table 6.4 if a good ceramic structure was required.

Various etchants were used to highlight metallographic features. Marbles and Phophoric etchants were used for structural analysis, whilst a bromine/methanol etch was used to allow investigation of the oxides. The etching procedures are detailed in Table 6.5.

## 6.6 Analysis

### 6.6.1 *Scratch Testing*

The scratch test was used as an aid to investigating the oxide chemistry and as a means of ranking the TBC systems. The analysis was undertaken using a CSEM scratch tester (Figure 6.2).

*The Conventional Scratch Test*

The conventional scratch test was employed to induce spallation in the bondcoats oxide film. A Rockwell "C" diamond indentor was loaded normal to the samples surface until a predetermined load was reached. The sample was then traversed under the indentor, resulting in a scratch track across the surface. The oxide spallation at the edge of this track (Figure 6.3) was analysed using SEM and EDX analysis techniques.

*The Modified Scratch Test*

Due to the thickness of the TBC coating it was impractical to use the conventional scratch test to gauge the coatings adhesion, as the normal load required to place sufficient shear stress at the interface would be prohibitive. Hence, a modified scratch test was used.. Instead of the diamond stylus being driven normal to the plane of the coating/substrate interface, it was driven across the interface , from the substrate to the coating, on a cross-section through a TBC system (Figure 6.4). As the indentor passes from the bondcoat to the TBC, the interfacial oxide becomes stressed. The loading causes debonding to occur and a crack will run along the weakest point of the bond. The length of the crack is related to the normal load

through an inherent bond strength term. By stepwise increases in the normal load, a graph can be plotted of crack extension versus normal load. Ideally, a straight line plot is produced which can be regressed back to zero crack extension (Figure 6.5). This critical load required to cause crack initiation is quoted as a measure of the adhesive strength of the bondcoat/TBC system. The bond strength is affected by both isothermal and cyclic ageing. The modified scratch test can identify these changes and so provides a means of quantifiably ranking the systems.

### 6.6.2 *β-Depletion Measurements*

The β Ni-Al phase in a MCrAlY degrades on ageing as it sources aluminium to the surface to produce the alumina scale. Hence the measurement of the depth of β depletion can be used to rank the longevity of a coating. Samples were prepared in section and optically assessed to determine the amount of β depletion (Figure 6.6).

### 6.6.3 *Other Techniques*

Energy Dispersive X-ray analysis was undertaken using EDAX and Link systems coupled to a Cambridge instruments SEM. Wavelength microprobe analysis was conducted using a Cameca Electron Probe Micro-analyser. XRD analysis was carried out at AEA Technology Harwell, whilst the XPS and Image Analysis was conducted at Cranfield University.

| Alloy | Type | Composition (wt%) | | | | | | | | | | | | | |
|---|---|---|---|---|---|---|---|---|---|---|---|---|---|---|---|
| | | Ni | Cr | Co | Mo | W | Re | Al | Ti | Nb | Ta | Hf | Zr | C | B |
| MarM002 | Directionally Solidified | Bal | 9 | 10 | | 10 | | 5.5 | 1.5 | | 2.5 | 1.5 | 0.06 | 0.15 | 0.015 |
| C1023 | Conventionally Cast | Bal | 15.5 | 9.7 | 8.3 | | | 4.1 | 3.6 | | | | | 0.15 | 0.007 |
| CMSX-4 | Single Crystal | Bal | 6.5 | 9.5 | 0.6 | 6.4 | 3 | 5.6 | 1 | | 6.5 | 0.1 | | 0.006 | |
| Alloy RR | Single Crystal | Bal | 2.2 | 3.3 | 0.04 | 5.5 | 6.3 | 5.75 | 0.23 | 0.1 | 8.3 | 0.03 | | | |

Table 6.1- Compositions of the superalloys (wt%)

| Coating | Deposition Method | MCrAlX Coatings | | | | |
|---|---|---|---|---|---|---|
| | | Ni | Cr | Co | Al | Others |
| RT122 | LPPS | 32.9 | 20.1 | 39.3 | 6.2 | Y |
| Coating A | LPPS | 45.2 | 18.1 | 23.9 | 11.8 | Y |
| Coating B | LPPS | 51.3 | 12.9 | 21 | 14.2 | Y, Hf & Si |
| | | Diffusion coatings | | | | |
| | | Al | Pt | | | |
| RPS320 | High activity pack aluminide | 23.3 | | | | |
| RT22LT | High activity pack platinum aluminide | 20 | 30-60 | | | |

Table 6.2- Coating compositions and deposition techniques (wt%)

| Polishing Media | Type | Time |
|---|---|---|
| SiC Grit Paper | 80 | 1.5 min |
| SiC Grit Paper | 120 | 1.5 min |
| SiC Grit Paper | 180 | 1.5 min |
| SiC Grit Paper | 220 | 1.5 min |
| SiC Grit Paper | 500 | 1.5 min |
| SiC Grit Paper | 1200 | 1.5 min |
| SiC Grit Paper | 2400 | 1 min x2 |
| SiC Grit Paper | 4000 | 1 min x2 |
| Diamond Polish | 1 micron | 1 min |
| O.P.A Solution | | 2 min |

Table 6.3- Polishing procedure for bondcoat examination

| Polishing Media | Type | Time |
|---|---|---|
| SiC Grit Paper | 80 | 1.5 min |
| SiC Grit Paper | 120 | 1.5 min |
| SiC Grit Paper | 180 | 1.5 min |
| SiC Grit Paper | 220 | 1.5 min |
| SiC Grit Paper | 500 | 1.5 min |
| SiC Grit Paper | 1200 | 1.5 min |
| SiC Grit Paper | 2400 | 1 min x2 |
| Diamond Polish | 6 micron | 6 min |
| Diamond Polish | 1 micron | 4 min |
| O.P.A Solution | | 2 min |

Table 6.4- Polishing procedure for ceramic examination

| Type | Composition | Procedure |
|---|---|---|
| Bromine/Methanol | 10% Bromine<br>90% Methanol | Immerse the sample in the etchant for 1.5 min. Clean thoroughly with methanol |
| Marbles | 2g CuCl<br>40ml HCl<br>40ml Methanol | Immerse for 2s. Clean using water |
| Phosphoric | 8g CuCl<br>5ml $H_2SO_4$<br>80ml Phosphoric acid | Elecrochemical etch.<br>Apply 10V for 10s. Clean using water. |

Table 6.5- Etch compositions and procedures

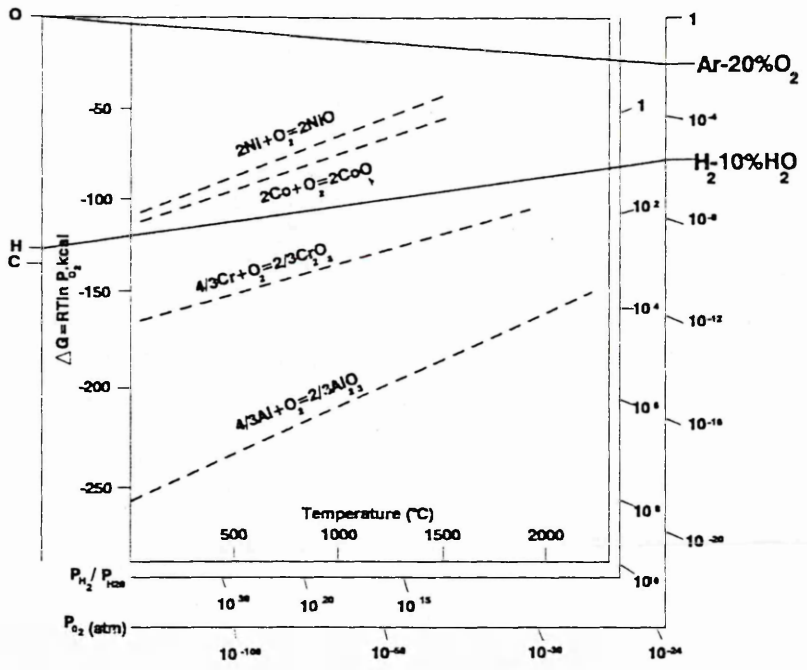


Figure 6.1- Ellingham diagram for the pre-oxidation atmospheres

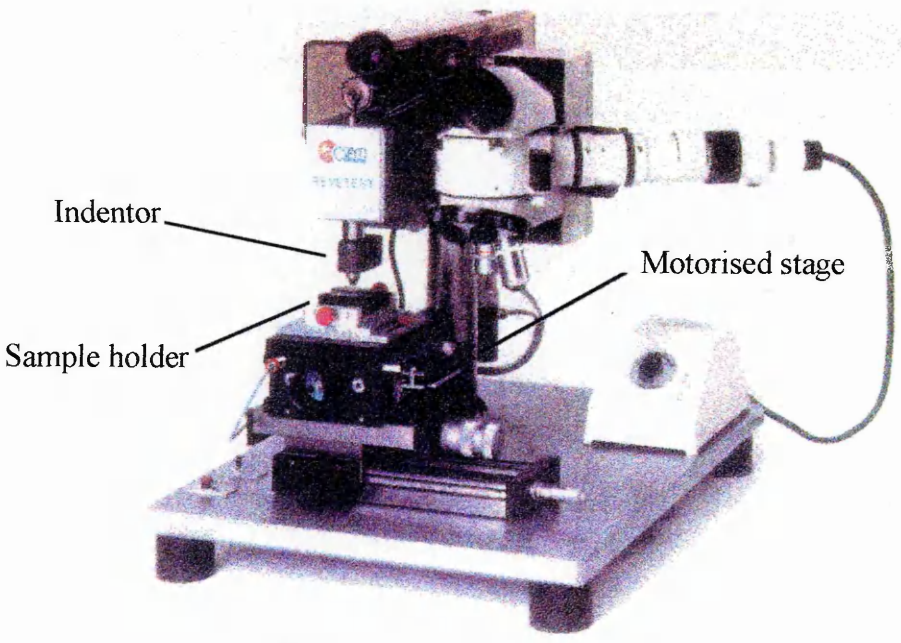


Figure 6.2- The CSEM scratch test rig

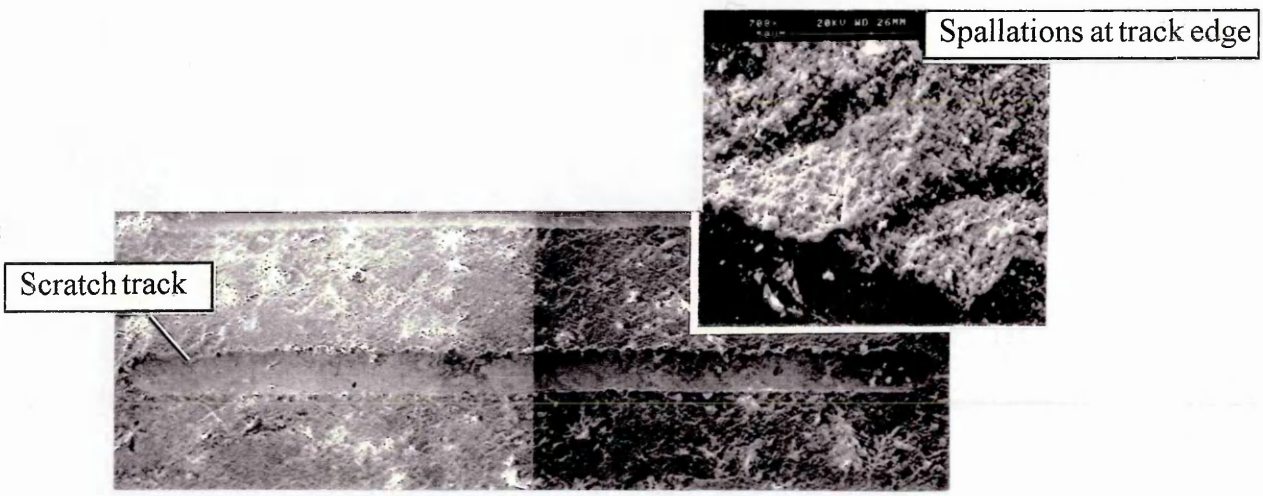


Figure 6.3- 'Scratch track' produced by the conventional scratch test

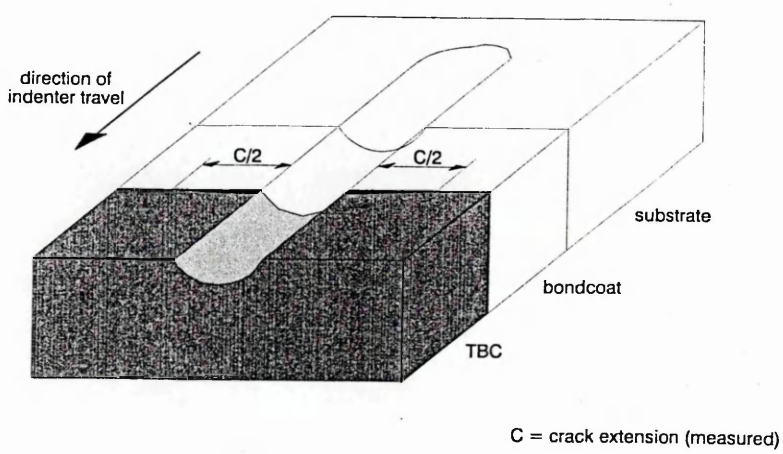


Figure 6.4- Schematic diagram of the modified scratch test

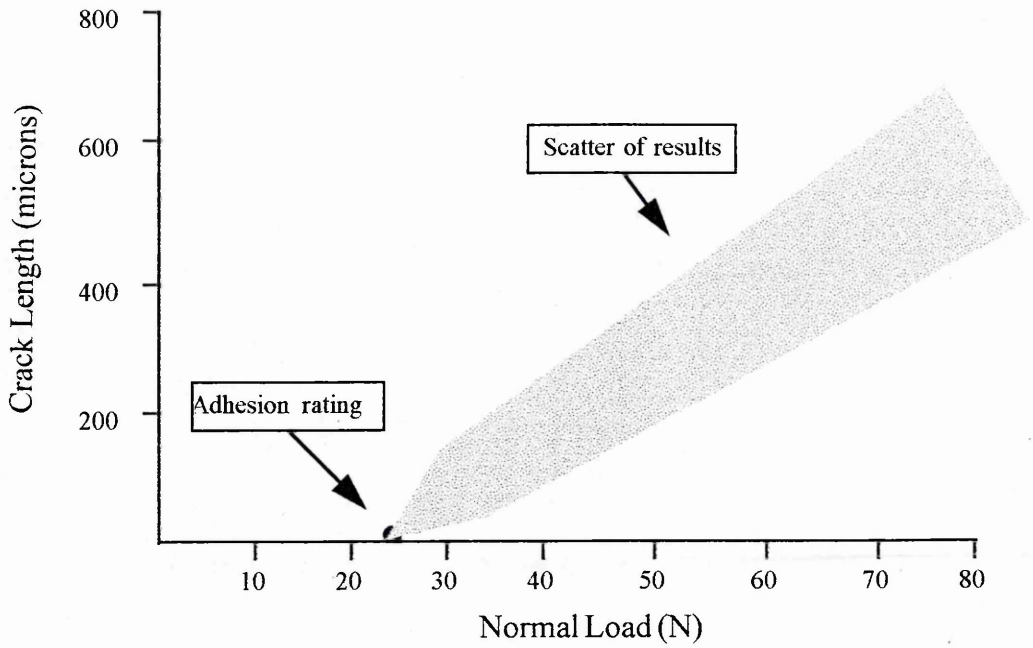


Figure 6.5- Schematic of a crack length versus load plot produced by the modified scratch test

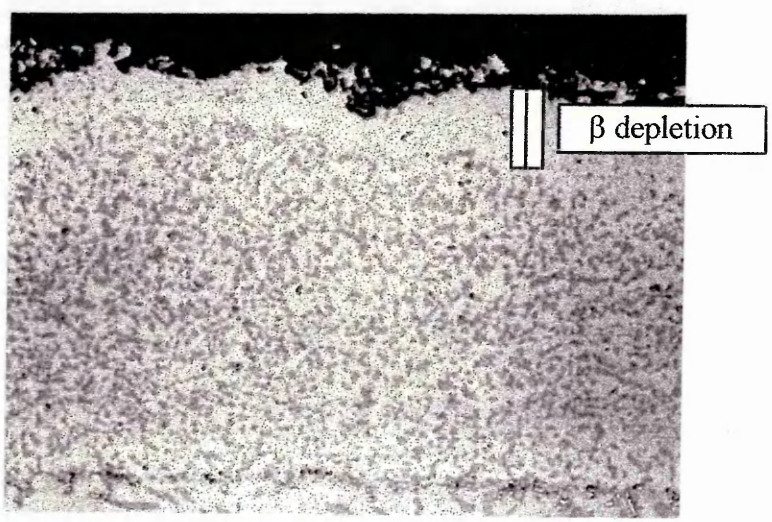


Figure 6.6- Micrograph showing the β depletion level of an MCrAlX coating

# RESULTS

Chapter 7-Results

## The effects of pre-oxidation and gritting on the oxide chemistry

### 7.1 Introduction

It has been reported in the published literature (see chapter 4) that the pre-treatment of a bondcoat to promote the formation of an alumina film prior to ceramic deposition, will extend the lifetime of a thermal barrier coating.

This chapter aimed to determine the effects of both pre-oxidation and gritting on the adherence of the oxide scale and so assess the potential benefits of a pre-treatment to TBC adhesion.

### 7.2 Research Plan

The research plan for this activity is illustrated in Figure 7.1. The pre-treatments were assessed using the MCrAlX coating, RT122, on a MarMOO2 substrate. Half of the samples were gritted with 220 mesh alumina at 2.04 bar, the other half were left ungritted. Samples from each group were then pre-oxidised in either Ar-20%$O_2$ or $H_2$-10%$H_2O$ atmospheres as detailed in the experimental procedure. The samples were aged for 100h at 1050 and 1100°C and for 1, 10 and 100h at 1150°C.

### 7.3 Analysis of Results

#### 7.3.1 *β depletion measurments.*

Sections were taken from samples aged for 100h at 1050 and for 1 and 100h at 1150°C. These were optically assessed to determine the amount of β depletion.

Little difference was noted in the β depletion between either of the pre-oxidation atmospheres or the gritted and ungritted samples. The results of the β depletion measurments are presented in Figure 7.2. Examples of the sections are shown in Figures 7.3 to 7.6.

7.3.2 *S.E.M examination of the surface.*

In the as-processed condition , there appeared to be little difference between the gritted and ungritted Ar-20%$O_2$ pre-oxidised samples, both having produced a mixed alumina/spinel oxide scale (Figures 7.7 and 7.8). However, the $H_2$-10%$H_2O$ pre-oxidised samples were shown to have promoted outwardly grown transitional aluminas (Figure 7.9). The type of transitional alumina (e.g. γ or δ ) could not be identified.

After ageing for 1h at 1150°C, significant outcrops of chromia were observed on the surface of the Ar-20%$O_2$ treated samples (Figure 7.10). Although not as prominent, the $H_2$-10%$H_2O$ atmosphere also produced a mixed scale of alumina and transition metal oxides. Little difference was noted between the oxides of the gritted and ungritted surfaces (Figures 7.11 and 7.12).

After ageing for 100h at 1100°C, the β phase within the coatings was fully depleted, making it impossible to sustain an alumina film. Figure 7.13 shows how in areas where the alumina has spalled, chromia has grown to replace it. Most of the scale has spalled off the Ar-20%$O_2$ pre-oxidised samples, leaving only isolated areas of mixed oxide. No differences were noted between the oxides produced by either the gritted or ungritted samples (Figures 7.14 and 7.15). The scale produced by the $H_2$-10%$H_2O$ pre-oxidation was more adherent, but again, a mixture of alumina and

undesirable Cr and Ni oxides were observed. However, the growth of the alumina on the $H_2$-10%$H_2O$ exposed samples appears to have been modified by zirconia debris from the 10A-Z850 ceramic bead peen treatment (Figure 7.16). This is evident in Figure 7.17 were it can be seen that the zirconia acted to block alumina growth at the metal/oxide interface, as should be expected due to inward oxygen diffusion and instead it promoted the outward growth of chromia in these zirconia doped regions.

### 7.3.3 *S.E.M examination of spalled areas.*

The SEM and EDX analysis were used to analyse areas of spallation induced by the conventional scratch test. Failures were found to be associated with either Cr and Ni oxides or alternatively were cohesive failures within the alumina. No differences in the damage induced by the scratch test were noted between either of the pre-treatments or whether the surface had been gritted or not (Figures 7.18 and 7.19).

### 7.3.4 *X.R.D analysis.*

Both gritted and ungritted $H_2$-10%$H_2O$ pre-oxidised samples and the gritted Ar-20%$O_2$ pre-oxidised samples in the as-processed and aged for 1 and 100h at 1150°C conditions, were X.R.D analysed at A.E.A Technology, Harwell. In the as-processed condition, the Ar-20%$O_2$ pre-treated sample had developed a mixed oxide, containing both alumina and spinels, confirming the observations made using the SEM/EDX. The $H_2$-10%$H_2O$ pre-oxidation appeared to provide some initial benefits by promoting a spinel free alumina film. However, after ageing for 1 and 100h at 1100°C, any benefits were lost as the scale became contaminated with

spinels and was indistinguishable from that produced by the Ar-20%$O_2$ pre-treatment (Figures 7.20 and 7.21).

No differences were noted between the gritted and the ungritted samples, as similar species of oxide were grown on both (Figure 7.22). Zirconia, from the peening treatment was found to be present on the surface of the ungritted, $H_2$-10%$H_2O$ pre-oxidised sample.

## 7.5 Summary

Chapter 4 illustrated how in the literature it has been proposed that pre-treatments will prolong the life of a TBC. This was achieved by promoting the formation of an α-alumina film through pre-oxidation and aluminising techniques and it was shown that the lifetime of the coating could be extended by up to a factor of eight. In addition, gritting of the bondcoats surface was thought to further improve the life and aid the adherence of the ceramic by mechanical keying and the promotion of the early formation of a stable alumina scale. This investigation has shown that in the as-processed condition, the Ar-20%$O_2$ pre-oxidation atmosphere resulted in an oxide scale, containing both alumina and transition metal spinels, while the $H_2$-10%$H_2O$ pre-oxidation atmosphere showed some potential benefits by promoting a pure alumina film. Once aged however, any benefits were lost due to spinel growth in the oxide during the ageing process. The effects from gritting the bondcoat must be considered benign, playing no inherent role in determining the initial chemistry of the oxide scale or influencing its rate of growth. The full analysis of these results and why they differ from investigations of pre-treatments reported in literature is presented and discussed in chapter 12.

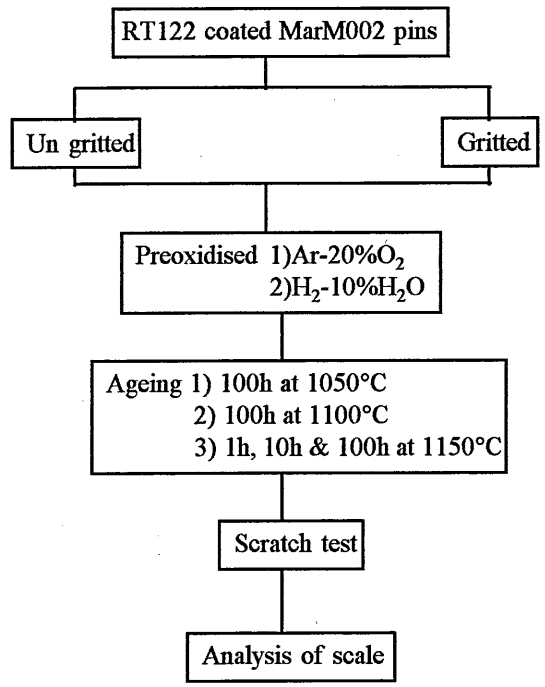


Figure 7.1- Research plan

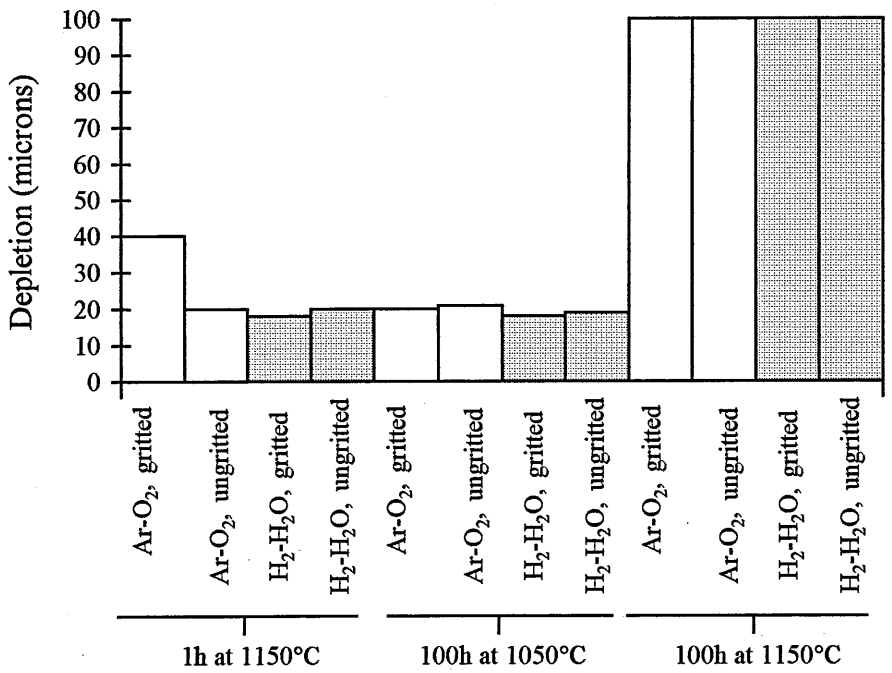


Figure 7.2- β depletion measurments

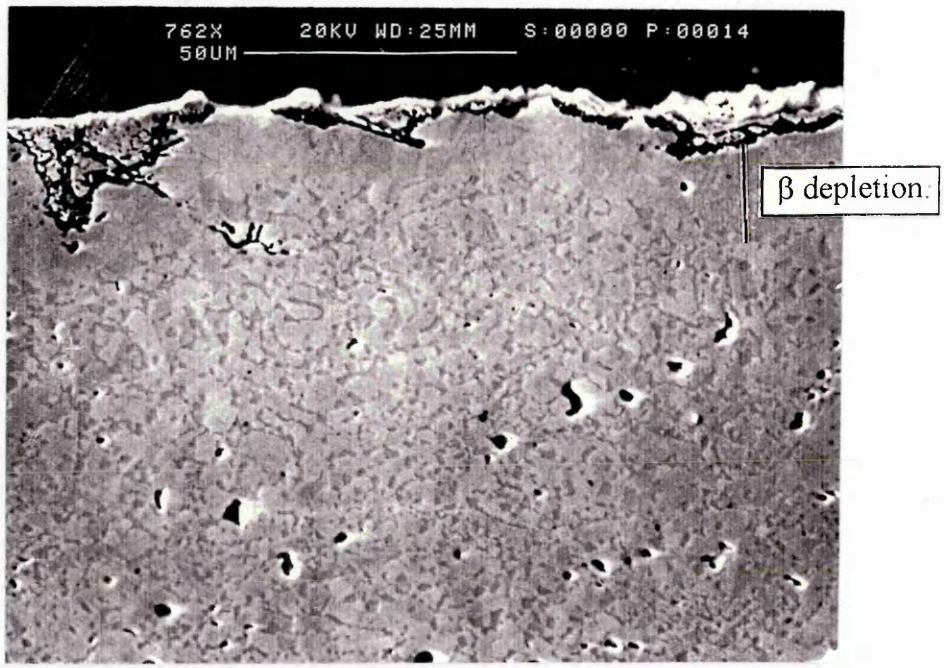


Figure 7.3- Ar-20%$O_2$ pre-oxidation, ungritted, aged for 1h at 1150°C

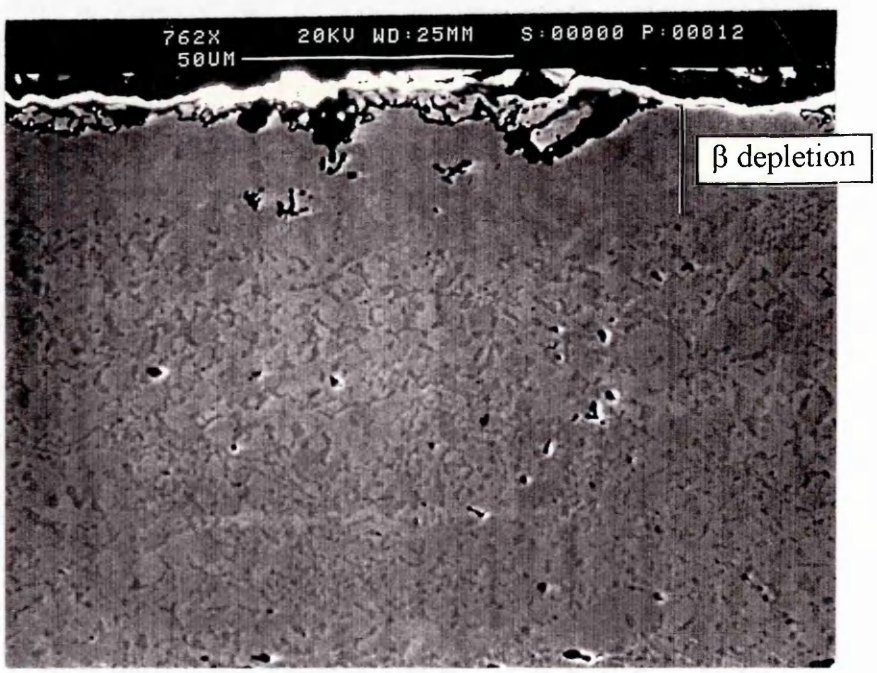


Figure 7.4- $H_2$-10%$H_2O$ pre-oxidation, ungritted, aged for 1h at 1150°C

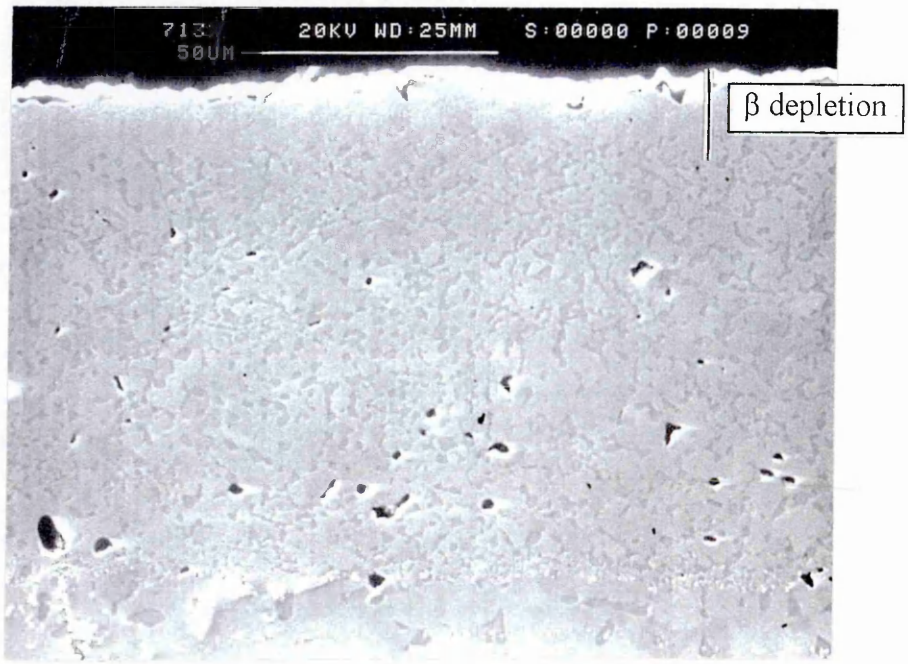


Figure 7.5- $H_2$-10%$H_2O$ pre-oxidation, ungritted, aged for 1h at 1150°C

Figure 7.6- $H_2$-10%$H_2O$ pre-oxidation, gritted, aged for 100h at 1100°C

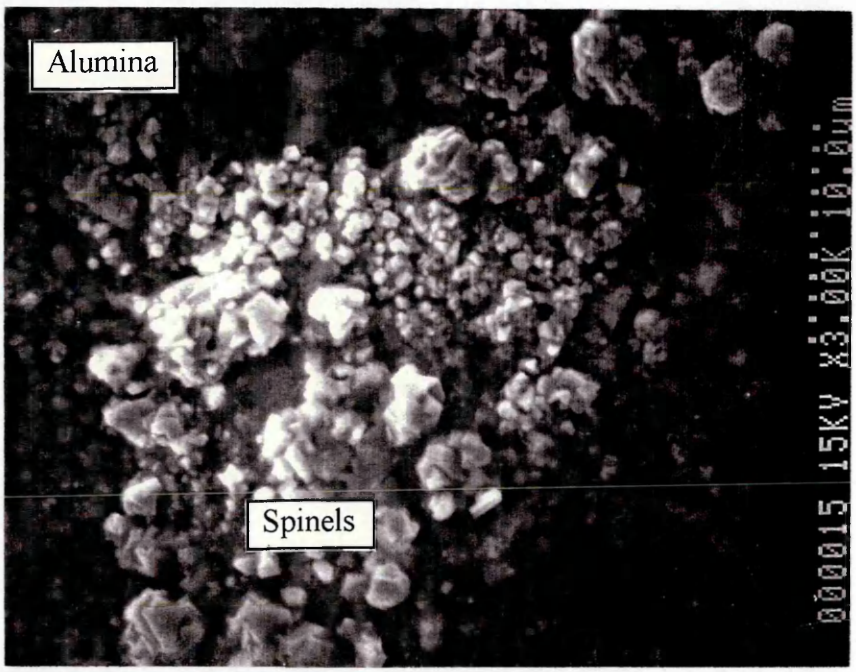


Figure 7.7- Ar-20%$O_2$ pre-oxidation, ungritted, as-processed

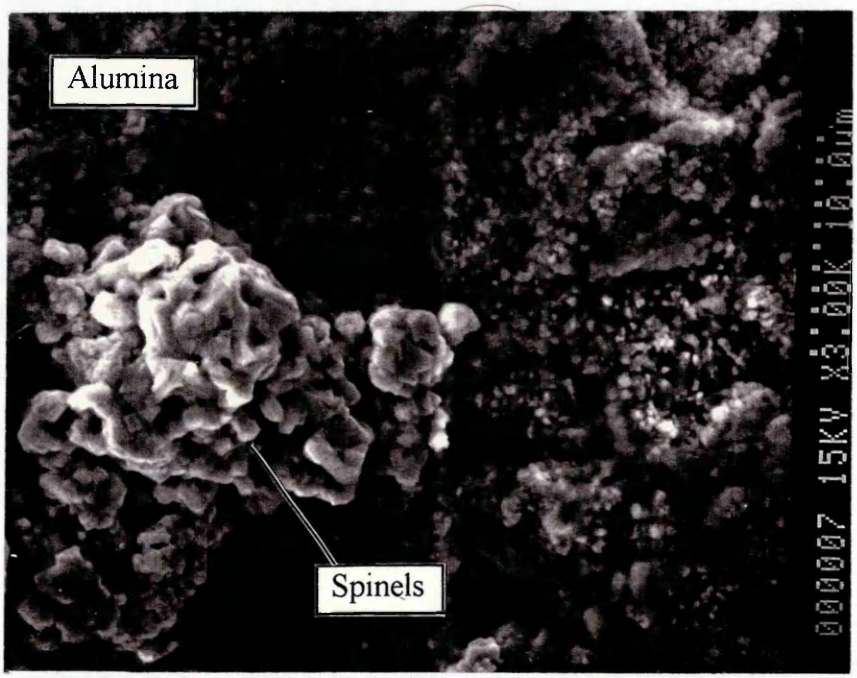


Figure 7.8- Ar-20%$O_2$ pre-oxidation, gritted, as-processed

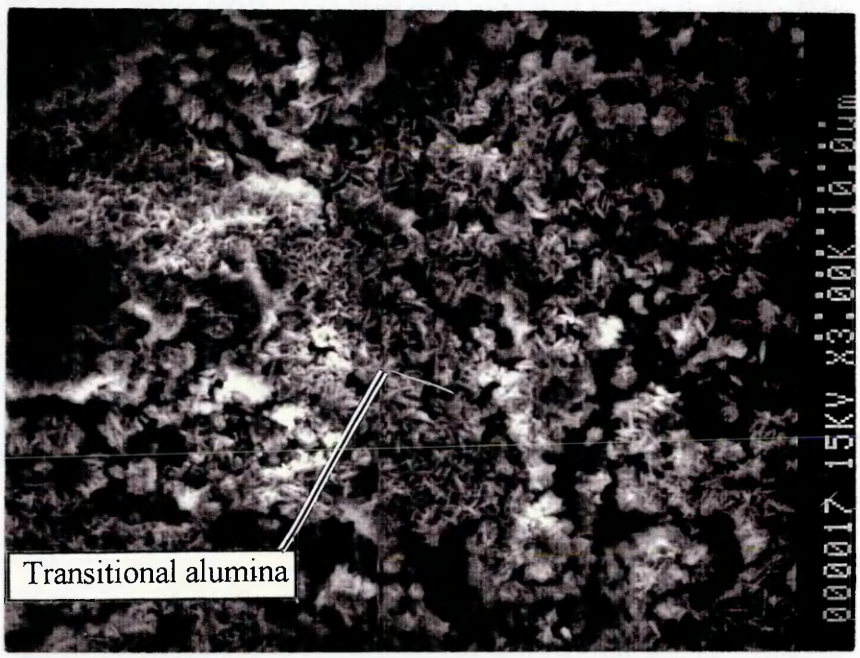


Figure 7.9- $H_2$-10%$H_2O$ pre-oxidation, ungritted, as-processed

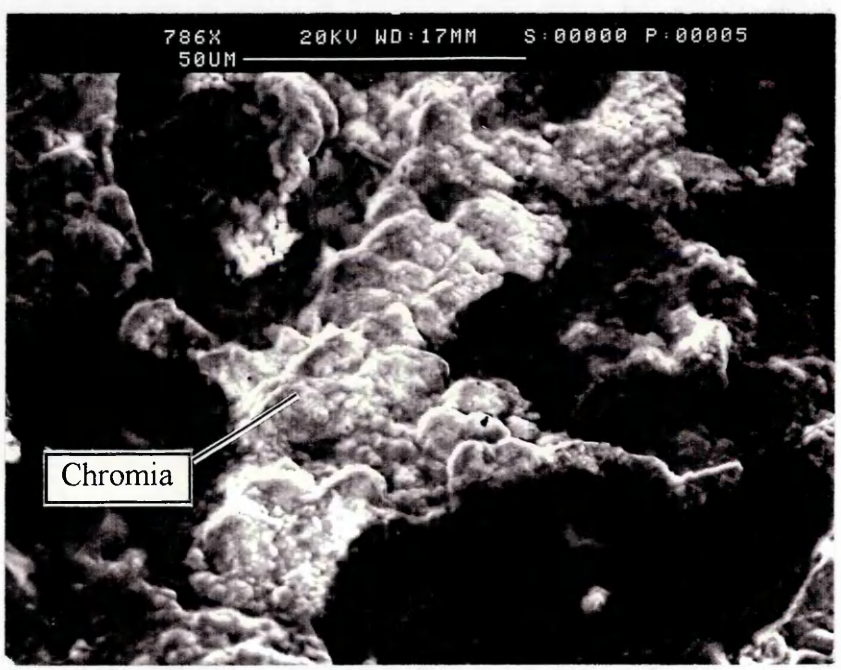


Figure 7.10- Ar-10%$O_2$,, pre-oxidation, gritted, aged for 1h at 1150°C

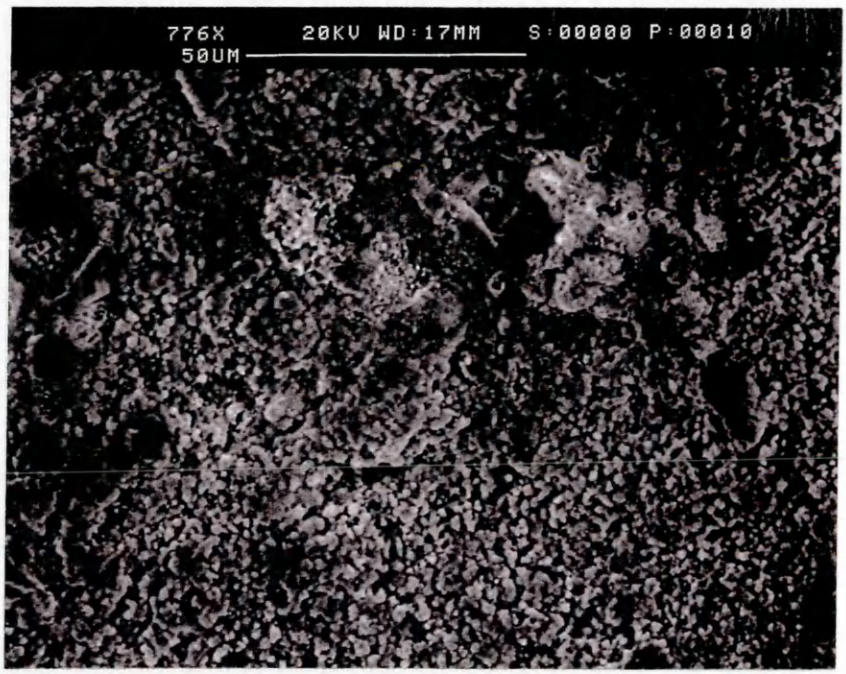


Figure 7.11- $H_2$-10%$H_2O$ pre-oxidation, gritted, aged for 1h at 1150°C

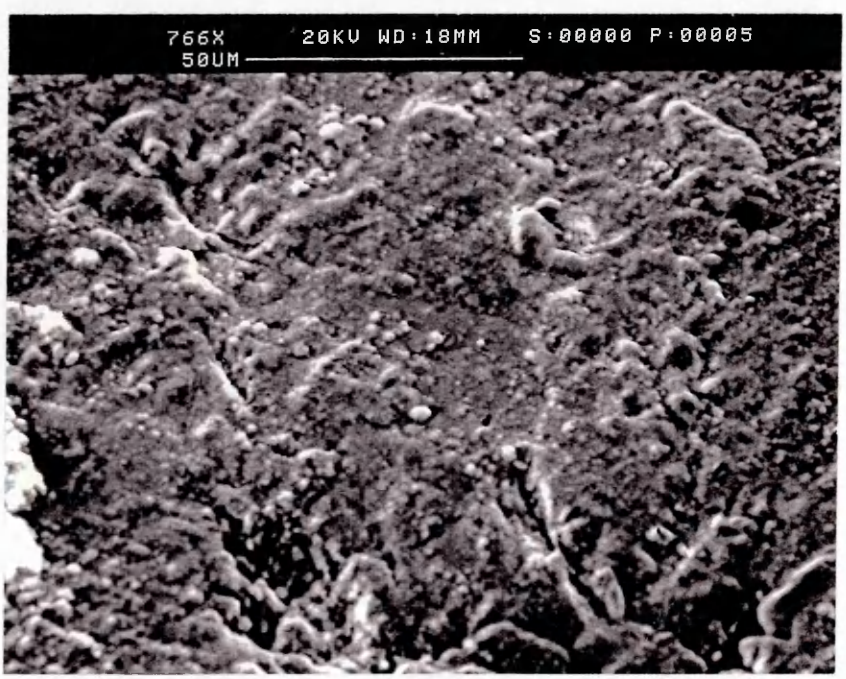


Figure 7.12- $H_2$-10%$H_2O$ pre-oxidation, ungritted, aged for 1h at 1150°C

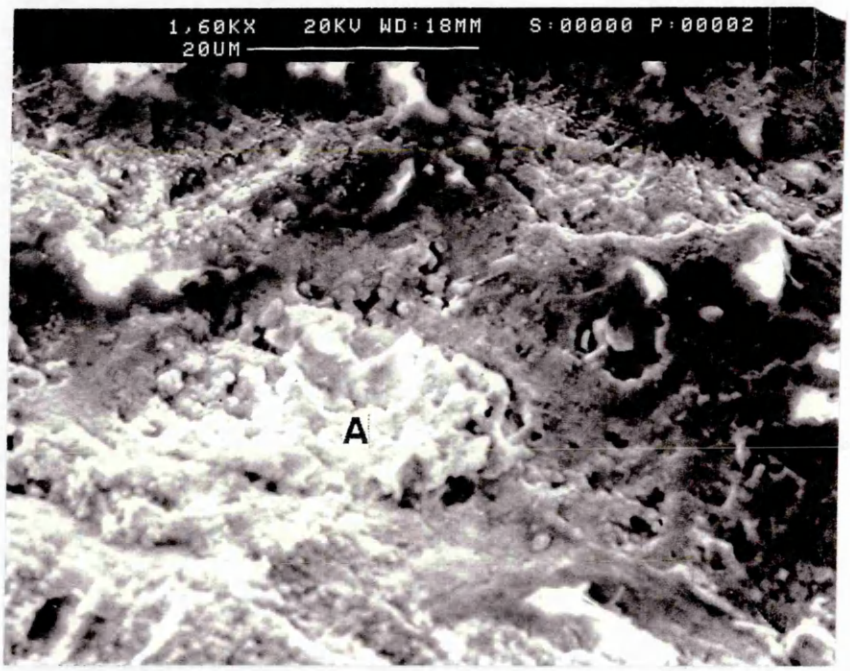


Figure 7.13- $H_2$-10%$H_2O$ pre-oxidation, gritted, aged for 100h at 1100°C. The chromia is marked (A)

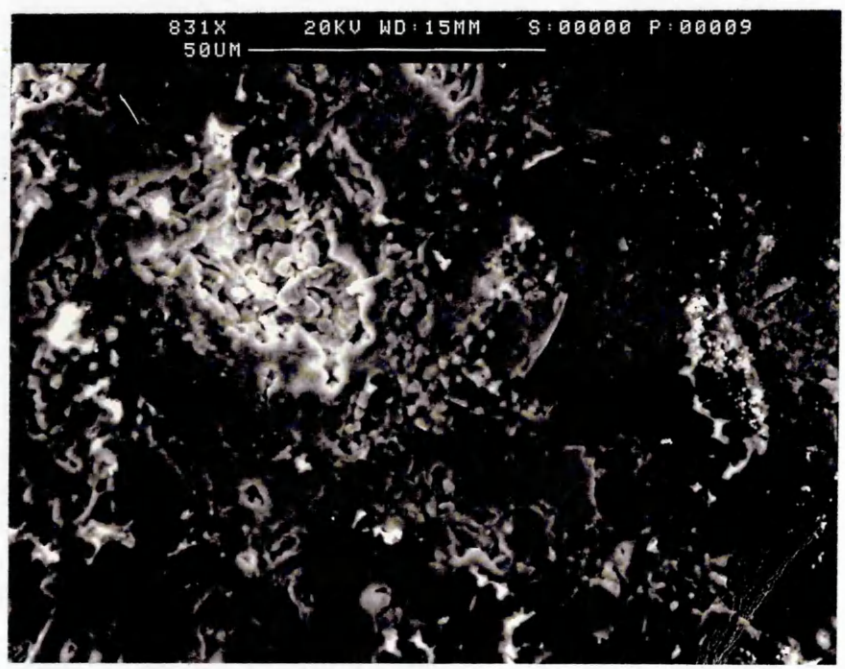


Figure 7.14- Ar-20%$O_2$ pre-oxidation, ungritted, aged for 100h at 1100°C

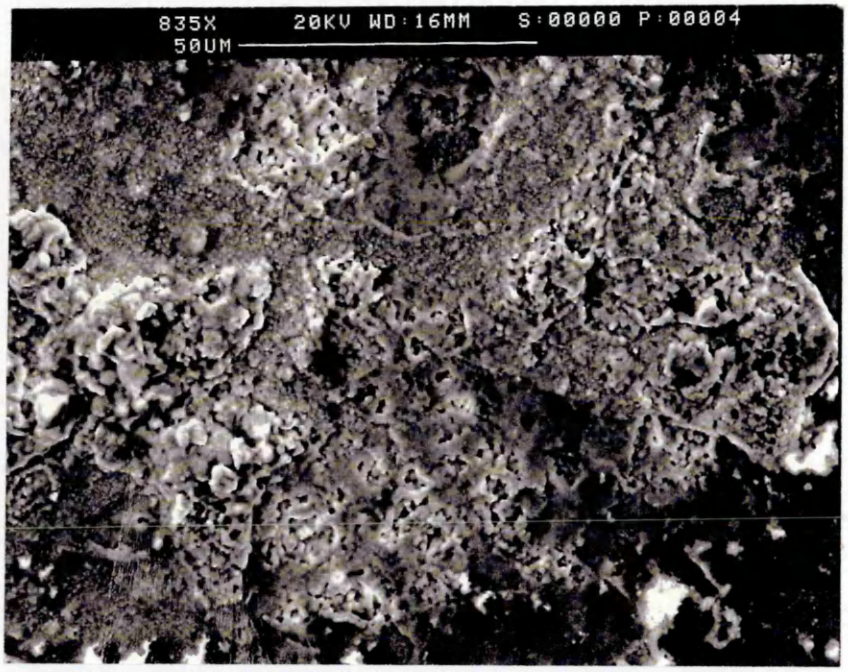


Figure 7.15- Ar-20%$O_2$ pre-oxidation, ungritted, aged for 100h at 1100°C

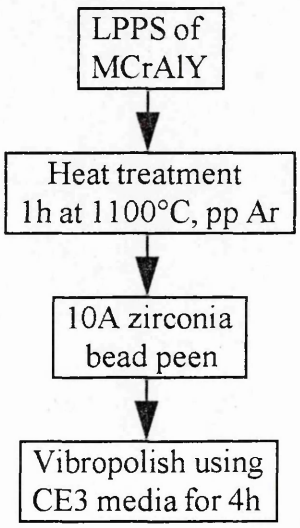


Figure 7.16- Production route for the RT122 bondcoat

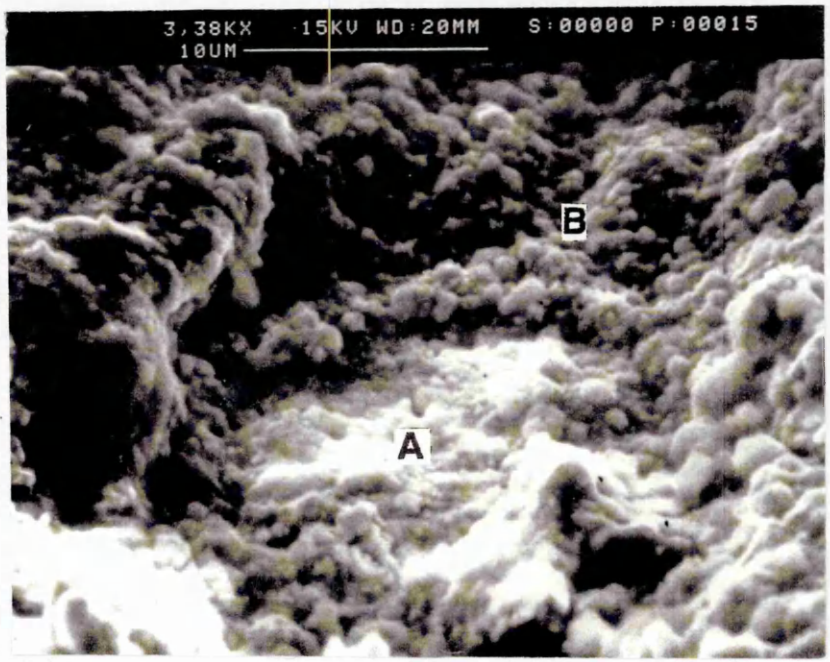


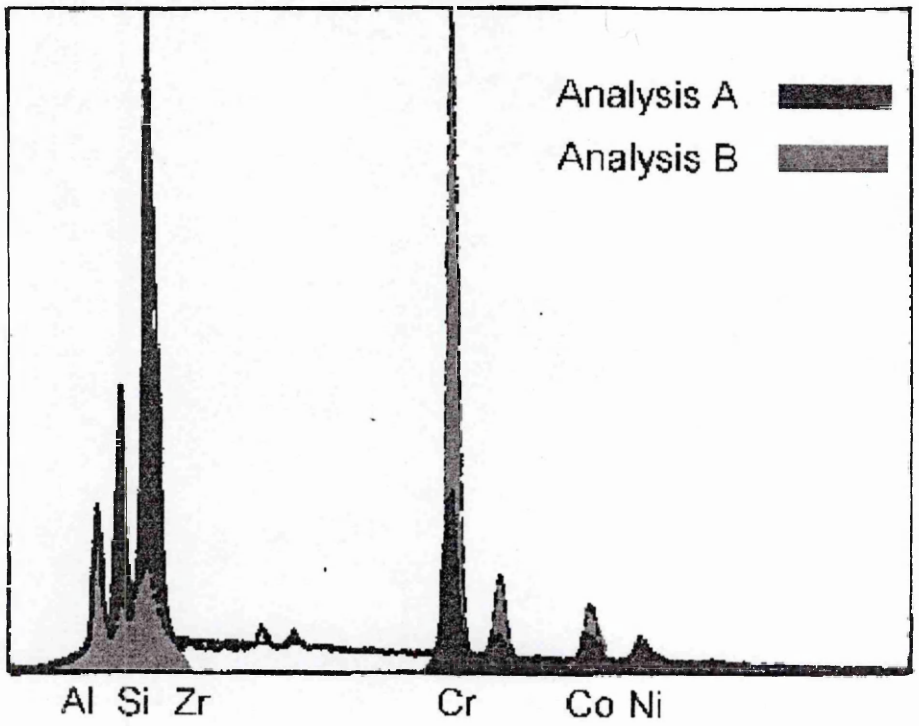


Figure 7.17- Zirconia debris at the oxide/metal interface. $H_2$-10%$H_2O$ pre-oxidation, ungritted, aged for 100h at 1150°C

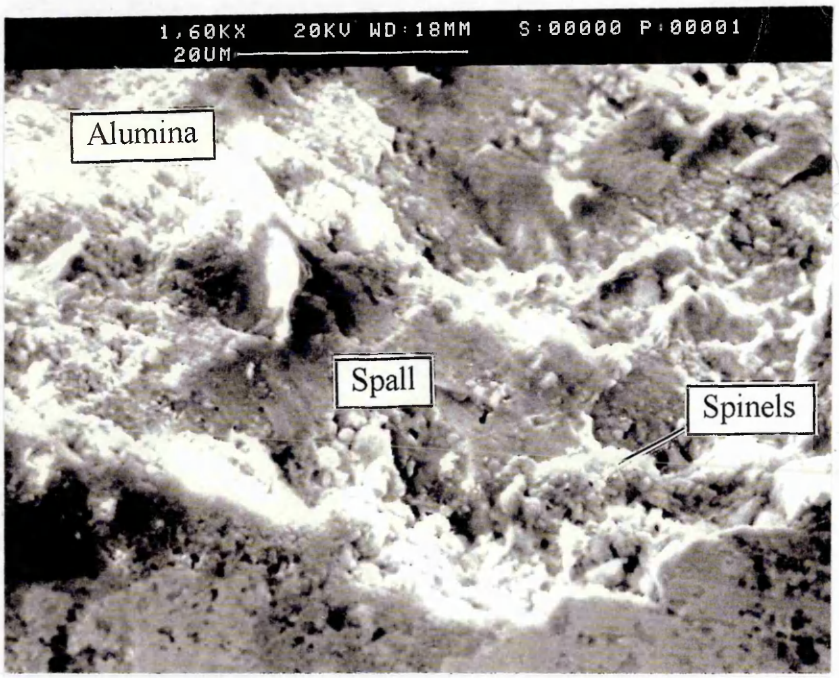


Figure 7.18- $H_2$-10%$H_2O$ pre-oxidation, gritted, aged for 100h at 1100°C. Spallation associated with Cr-based oxide.

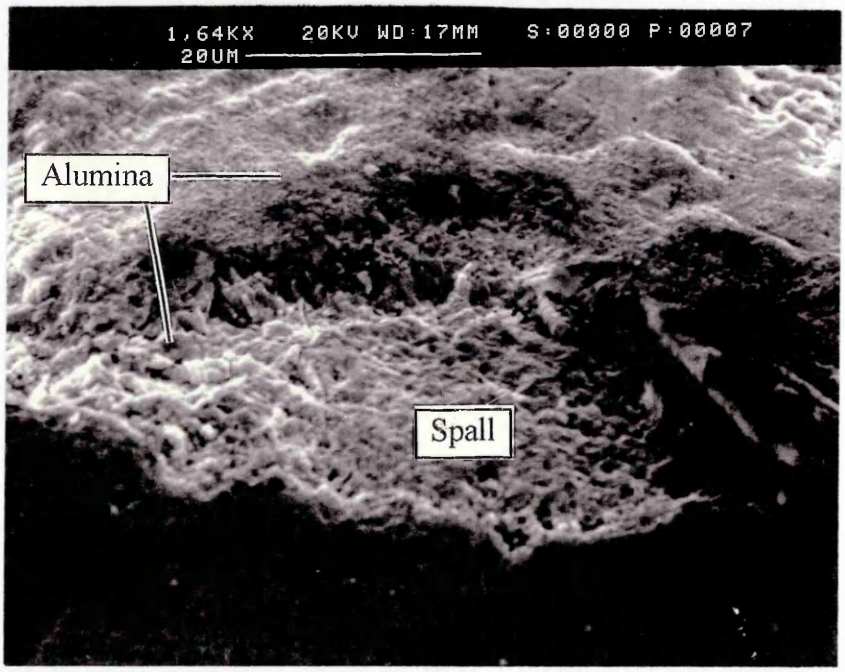


Figure 7.19- Ar-20%$O_2$ pre-oxidation, ungritted, aged for 100h at 1100°C

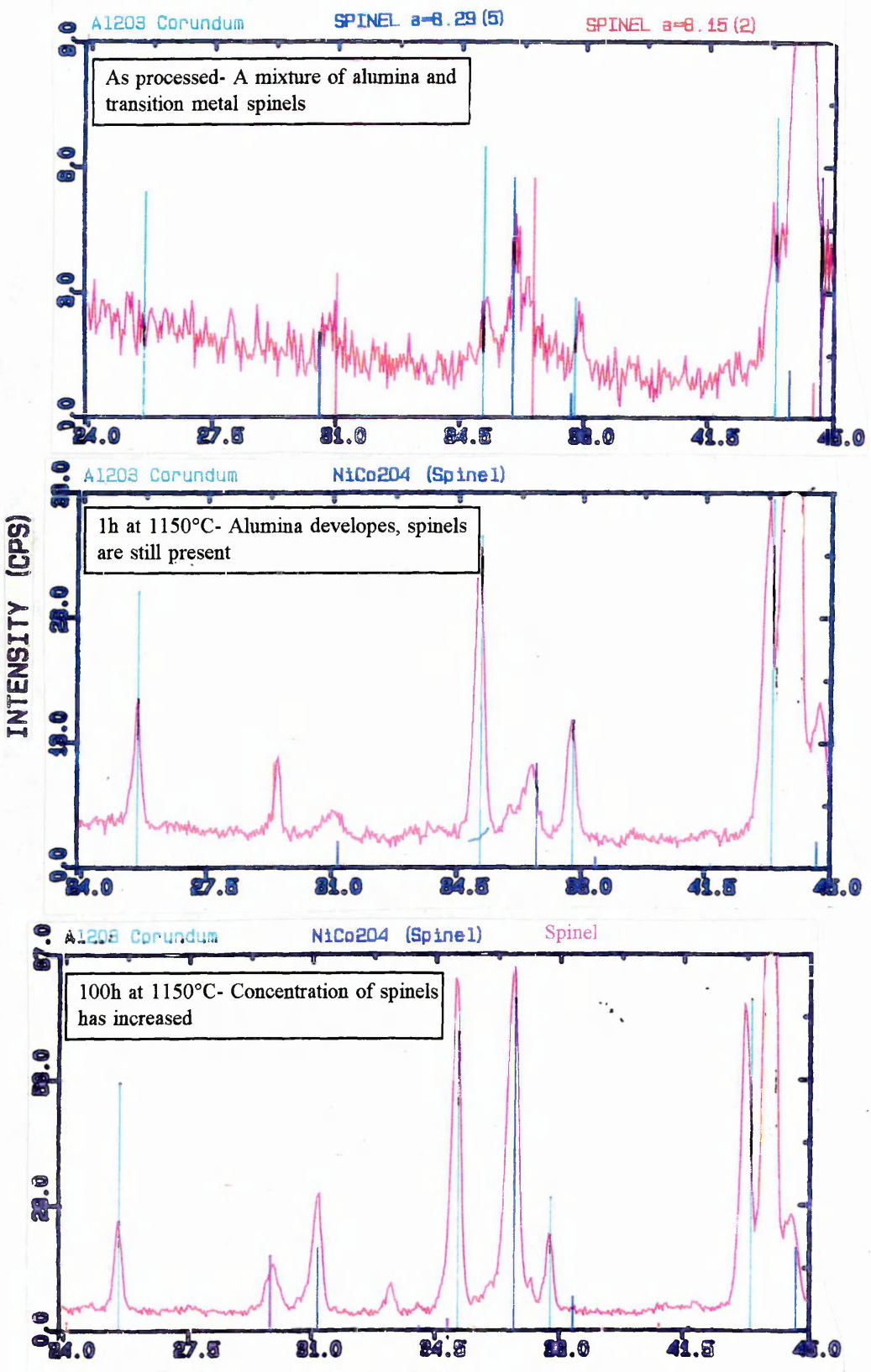


Figure 7.20- XRD traces Ar-20%$O_2$, gritted RT122

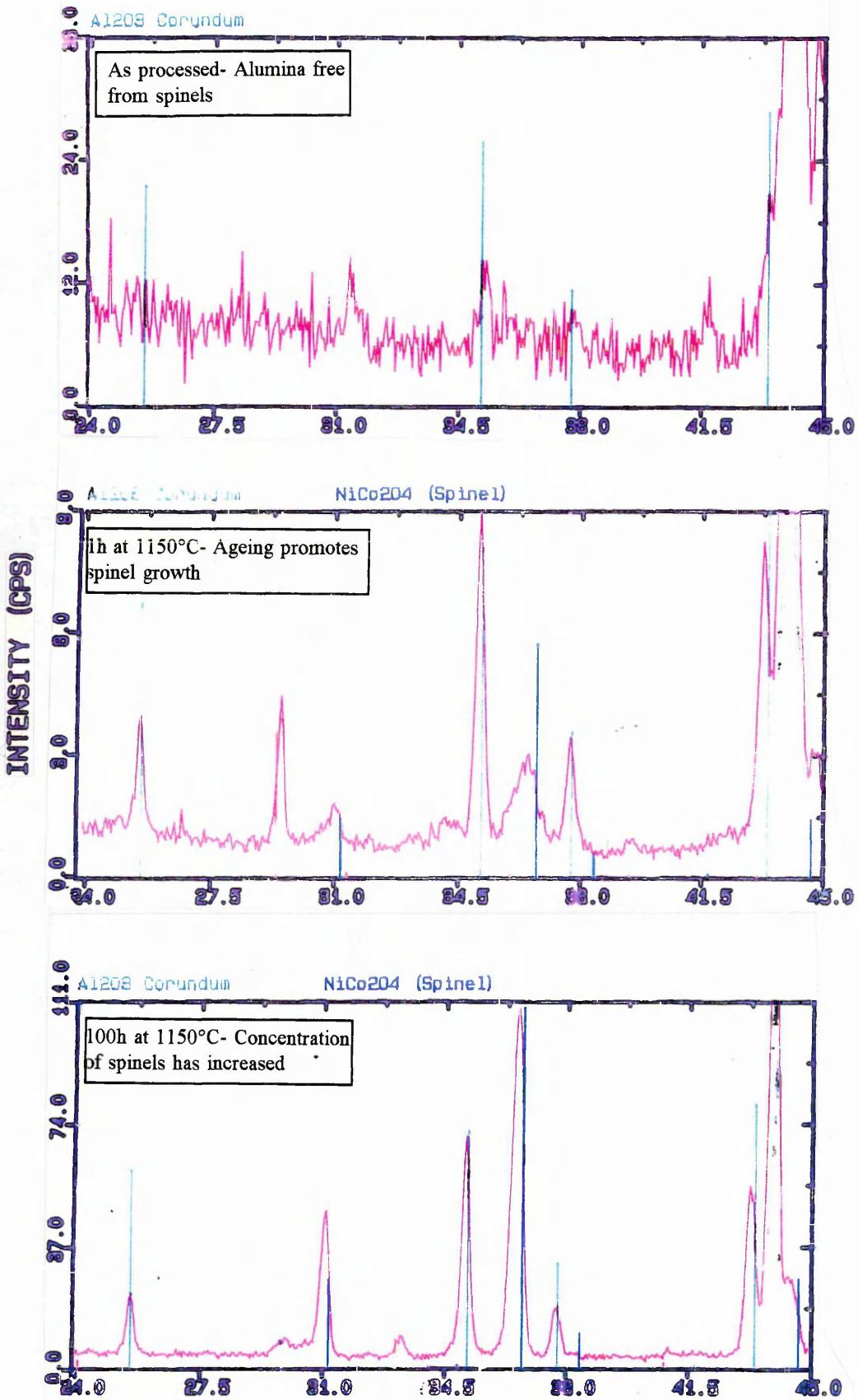


Figure 7.21- XRD traces for $H_2$-10%$H_2O$ pre-oxidation, gritted RT122

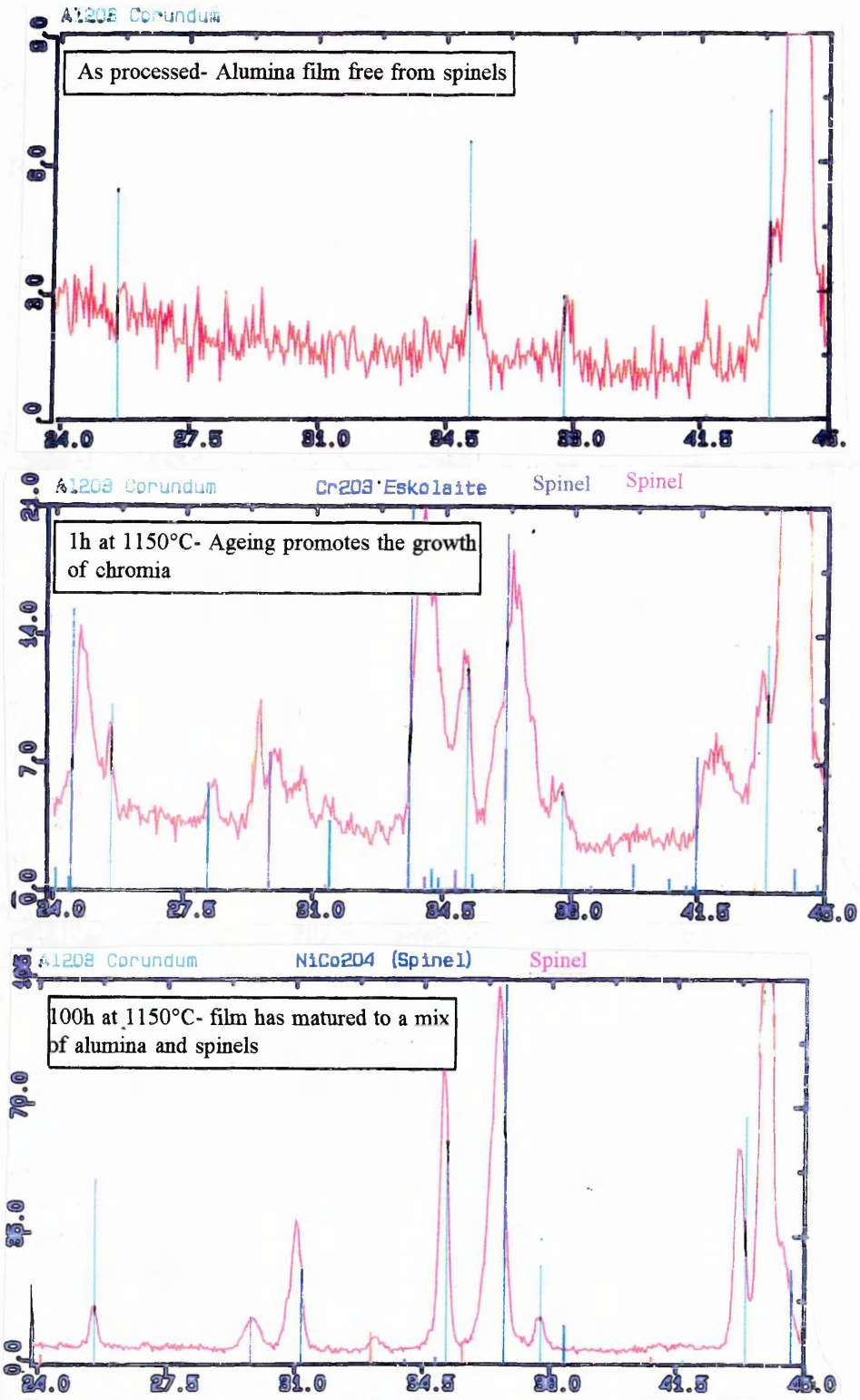


Figure 7.22- XRD traces for $H_2$-10%$H_2O$ pre-oxidation, ungritted RT122

Chapter 8- Results

## The effect of bondcoat composition on the chemistry of the oxide scale

### 8.1 Introduction

TBCs deposited using EB-PVD are chemically bonded to the surface of a bondcoat. It has been established that the optimum adhesion can be achieved by the growth of a complete and compact α-alumina scale at the ceramic/bondcoat interface. The quality of this bond decreases once substrate elements diffuse to the interface, where they either lower the scales cohesion/adhesion or increase the growth rate of the oxide. By tailoring the bondcoat chemistry, it should be possible to produce the desired α-alumina, whilst delaying the growth of the damaging spinels.

The aim of this chapter was to establish the role of bondcoat chemistry in the degradation of a TBC system. The main questions to be addressed were the effects of aluminium, platinum and hafnium content, and to determine whether the oxide grown on an exposed bondcoat was identical to one grown at the interface with a PSYZ ceramic topcoat.

### 8.2 Research Plan

The work plan for this section is illustrated in Figure 8.1. A range of bondcoat systems were chosen to show how coating type and composition can influence adhesion, these were:

- RPS320- High aluminium activity aluminide

- RT22LT- High aluminium activity platinum aluminide

- Coating A- High aluminium content MCrAlX.

- Coating B- High aluminium content MCrAlX + Hf and Si

- RT122- Low aluminium content MCrAlX

Their compositions have been given in Table 6.2

The samples were gritted with 220 mesh alumina at 2.04 bar and pre-oxidised in either an Ar-20%$O_2$ or $H_2$-10%$H_2O$ atmosphere. So it would be possible to assess the affect of a ceramic layer, the sample pins were sputter coated on one side with two microns of zirconia. This was carried out at Cranfield University. The samples were isothermally aged in air for 100h at 1050 and 1100°C and for 1, 10 and 100h at 1150°C. The analysis, following the results from chapter 7, concentrated on the $H_2$-10%$H_2O$ pre-oxidised systems and involved optical, SEM, EDX and XRD techniques. As with chapter 7, the conventional scratch test was used to induce spallation in the thermally grown oxide.

## 8.3 Analysis

### 8.3.1 *The effect of aluminium content.*

The effect of aluminium activity was assessed by comparing RT122 ( a low aluminium content MCrAlX coating) with Coating A (a high aluminium content MCrAlX coating

- *Optical examination in section*

In the as-processed condition, Coating A contained a relatively higher concentration of β NiAl within the coating and no β depletion was observed. In contrast, the RT122 had undergone a β depletion of approximately 7μm. After an isothermal age of 100h at 1050°C, the β phase within both coatings had coarsened. Coating A still had a higher proportion of β, whilst RT122 had suffered a greater β depletion (~25μm as opposed to ~12μm in Coating A). Micrographs of the sections are shown in Figures 8.2 to 8.5.

- *SEM/EDX examination of the surface*

SEM and EDX techniques were employed to characterise the oxide and determine the degradation modes from spallations induced by the conventional scratch test. It was determined that after isothermal ageing, both bondcoats had developed similar oxides. EDX analysis of spallation sites indicated that failure had occurred at the substrate/TGO interface (Figure 8.6). It was observed that on the zirconia coated side of the oxide, far more of the ceramic had spalled from the Coating A than the RT122 (Figures 8.7 and 8.8).

-*XRD analysis*

XRD analysis demonstrated that, once aged, both of the coatings developed a mixed oxide containing both alumina and substrate elements, at similar proportions (Figure 8.9).

*-Summary*

These analyses indicate that aluminium activity plays little part in determining the composition of the oxide. Both EDX and XRD analyses show that, after exposure, mixed oxides of qualitatively similar compositions were produced by both bondcoats. However the amount of β depletion does depend on the aluminium content of the coating.

8.3.2 *The effect of platinum.*

The effect of platinum was assessed by comparing the aluminide RPS320 with the platinum aluminide RT22LT.

*-Examination in section.*

Micrographs of the two coatings in the as processed condition and isothermally aged for 100h at 1050°C are shown in Figures 8.10 to 8.13. The micrograph of the as processed RPS320 shows the two distinct layers of the coating; The outer β-NiAl layer and the inner interdiffusion zone. After ageing, the thickness of the interdiffusion zone had increased from 8μm to 11μm and the precipitates within this zone had coarsened. The overall thickness of the coating had however remained approximately constant. Small white precipitates were observed in the outer β layer. EDX analysis identified these as W and Ta containing particles that were formed by outward diffusion of these elements from the interdiffusion zone. The micrograph of the RT22LT shows the basic three layer structure of the coating. The outer layer consists of β(Ni,Pt)Al and/or $PtAl_2$, depending on the concentration of platinum. The centre layer consisted of a β(Ni,Pt)Al , whilst the inner layer was

the interdiffusion zone. After ageing, the apparent coating thickness had increased from 28μm to 35μm and is due to the growth of the interdiffusion zone. Precipitates, as a result of diffusion of elements from the interdifffusion zone, were distinct in the centre layer, however, they could not be formed in the outer layer of the coating.

*-SEM/EDX analysis of the surface*

After isothermal ageing, RPS320 had grown a mixed oxide containing both alumina and substrate elements, including tungsten and titanium. Areas of spallation were observed within the scale (Figure 8.14) and catastrophic failures had occurred at the tracks produced by the scratch test. Spalled areas were found to contain concentrations of both tungsten and titanium. However it is not known whether these elements were present as a metal or an oxide (Figure 8.15). Conversely, RT22LT produced a complete and compact alumina film, with only slight spallation occurring at the scratch tracks.

*-XRD analysis of the scale*

In the as-processed condition, RPS320 had grown a mixed oxide containing both α-alumina and tungsten. Upon ageing, the concentration of tungsten had significantly increased and hafnium had diffused outwards from the MarM002 substrate to the scale (Figure 8.16). The as processed RT22LT was shown to have produced a pure α-alumina scale. After ageing, hafnium had diffused to the oxide scale, although not in as great a quantity as with RPS320 (Figure 8.17).

*-Summary*

In the as processed condition, RPS320 had grown a mixed oxide scale. Both α-alumina and tungsten(it is not known whether the tungsten was as a metal or an intermetallic) were identified in the oxide or at the oxide/metal interface. Upon ageing, the concentration of tungsten within the scale increased as the metal diffused outwards from the interdiffusion zone. This contamination of the scale led to the degradation of the oxide/substrate bond. The literature relating to failure modes for diffusion coatings are reviewed in chapter 4 and will be discussed further, in light of these results, in chapter 12. The presence of platinum within the RT22LT coating encouraged the growth of an α-alumina film. This agrees with the consensus of opinion, that platinum aluminides will out perform standard aluminide coatings. The methods in which platinum achieves this is also discussed in chapter 12.

Upon ageing, hafnium (an alloy addition within MarM002, which acts as a grain boundary strengthener), diffused from the substrate to the TGO interface. It. has been reported that the beneficial effects of platinum are heightened with the presence of hafnium [106]. This may be due to the benefits provided by the active element effects, such as pegging and sulphur gettering, with hafnium behaving as an active element. The potential advantages of active element additions will be discussed in chapter 14.

8.3.3 *The effect of hafnium and silicon additions.*

The MCrAlX coating Coating B contains additions of both hafnium and silicon. To ascertain their beneficial effects, Coating B was compared to Coating A.

*-Optical examination in section.*

In the as processed condition, both Coating B and Coating A contained a similar proportion of β–NiAl. Neither coatings had undergone any β depletion during fabrication. A micrograph of the as-processed Coating B is shown in Figure 8.18. After ageing, the coatings were again very similar The β phase of the coatings had coarsened and Coating A had become depleted by ~12μm, compared to Coating B being depleted to ~10μm.

*-SEM/EDX examination of the surface.*

EDX analysis could not detect any significant differences between the scales produced by either of the coatings. Both coatings, upon ageing, produced a mixed oxide containing both α-alumina and transition metal spinels.

*-Summary*

These analyses show that there was no significant difference between the scales grown by either the Coating A or Coating B bondcoats. The addition of hafnium and silicon to a MCrAlX coating did no appear to alter the chemistry of the oxide scale or the rate of aluminium consumption significantly

8.3.4 *The effect of a ceramic topcoat*

To assess the effect of a ceramic layer on the oxide chemistry of the scale, XRD analysis was carried out on the PYSZ coated side of the samples. This revealed that, compared to the exposed bondcoats, the presense of the PYSZ layer had inhibited the formation of spinels and therefore, promoted a more desirable α-

alumina scale. No differences were noted between the behaviour of high or low activity bondcoats, as both showed a reduction in the amount of spinel detected (Figures 8.19 and 8.20). This effect has been reported in the literature [29], where it was proposed that the ceramic layer lowered the partial pressure of oxygen at the ceramic/bondcoat interface and so inhibited the growth of spinels.

8.3.5 *Overall Summary*

- Variation in the aluminium activity of the bondcoat between 6 and 12at% appears to have no noticeable effect in determining the chemistry of the oxide scale. Varying the aluminium content does not prevent the growth the growth of spinels, but it does affect the rates of β depletion, and therfore the avaliable aluminium reservoir.

- The addition of platinum to a bondcoat promotes the selective oxidation of aluminium to form a more slowly grown alumina film. Platinum act to block the outward diffusion of damaging substrate elements, such as Ti, W etc, and so appears to prolong the life of the coating.

-Hafnium plus silicon additions to a MCrAlX bondcoat do not appear to alter either the chemistry nor the adhesion of the oxide scale significantly.

- A ceramic topcoat appears to lower the partial pressure of oxygen at the ceramic/bondcoat interface, thereby inhibiting the growth of transition metal spinels.

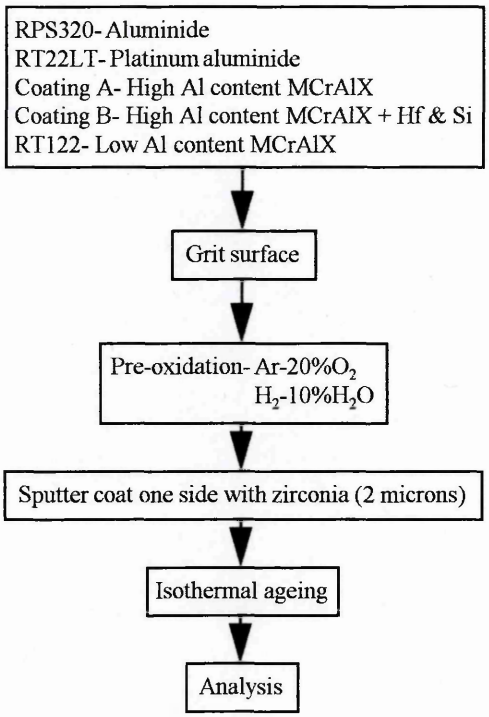


Figure 8.1- Research plan

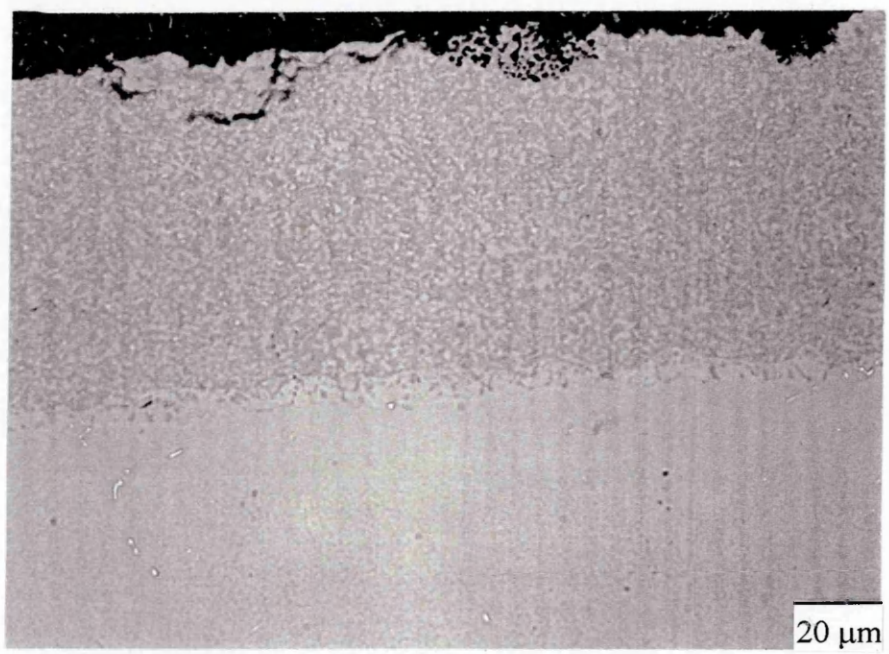


Figure 8.2- Coating A, as-processed

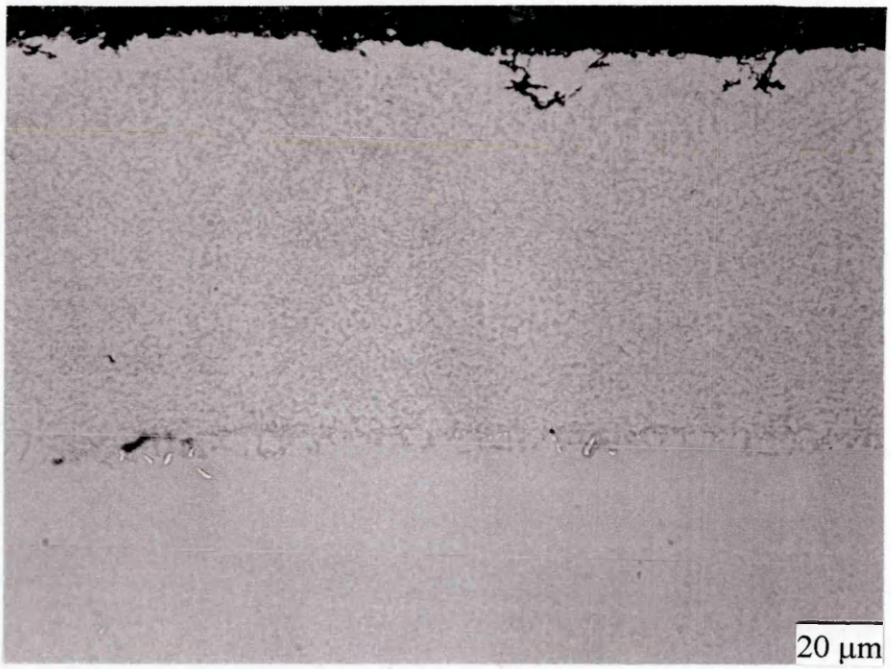


Figure 8.3- Micrograph of RT122, as-processed

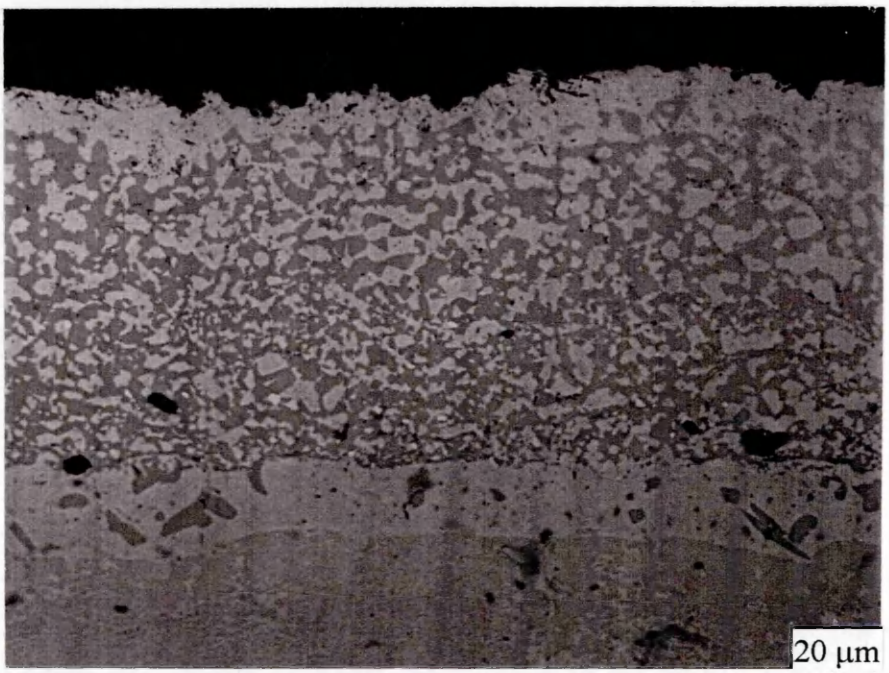


Figure 8.4- Micrograph of Coating A, aged for 100h at 1050°C

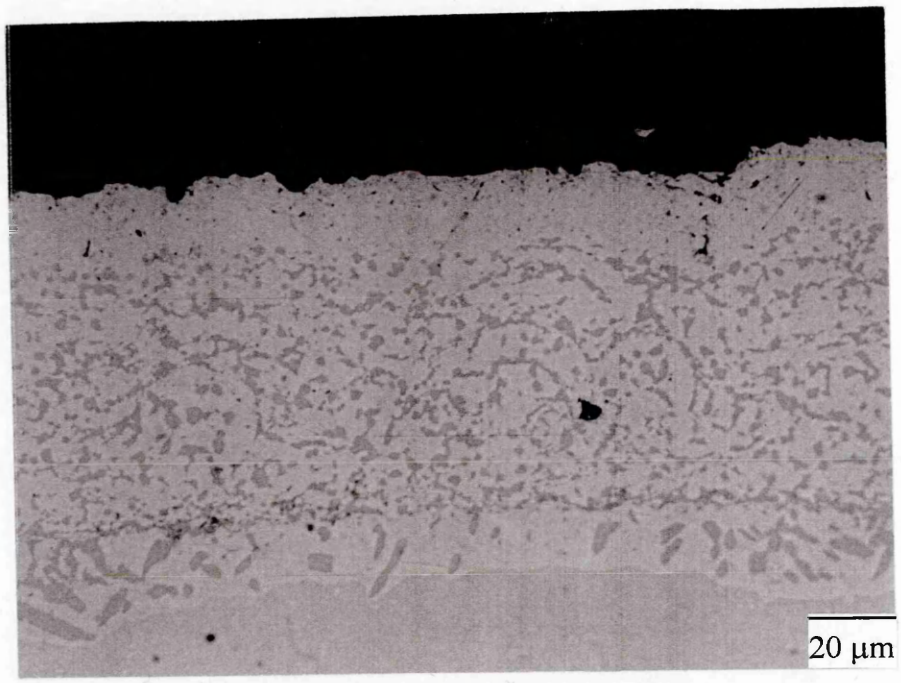


Figure 8.5- Micrograph of RT122, aged for 100h at 1050°C

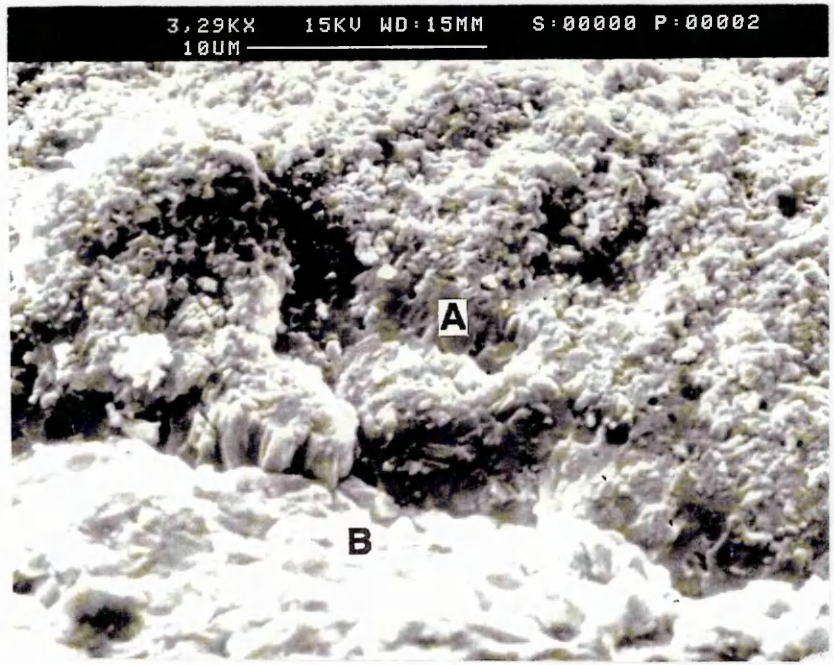


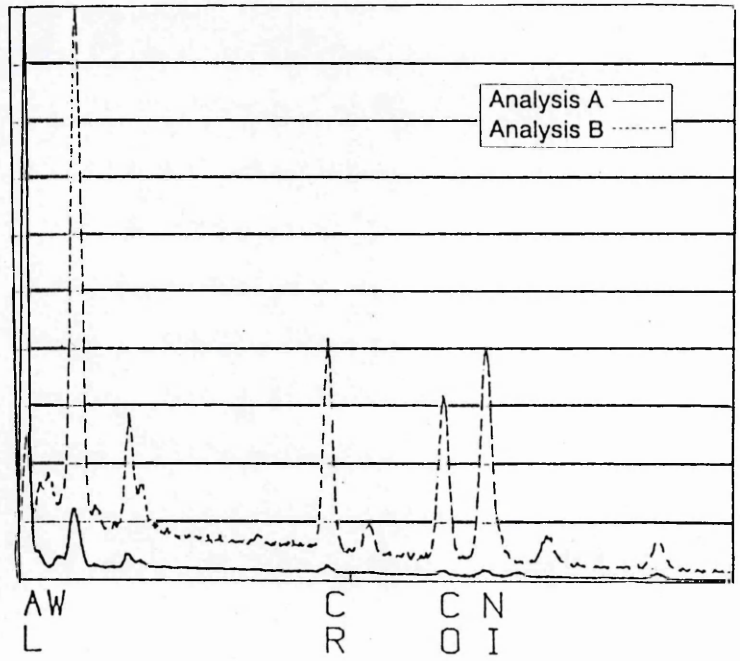


Figure 8.6- Spallation of the oxide formed on RT122, aged for 100h at 1150°C

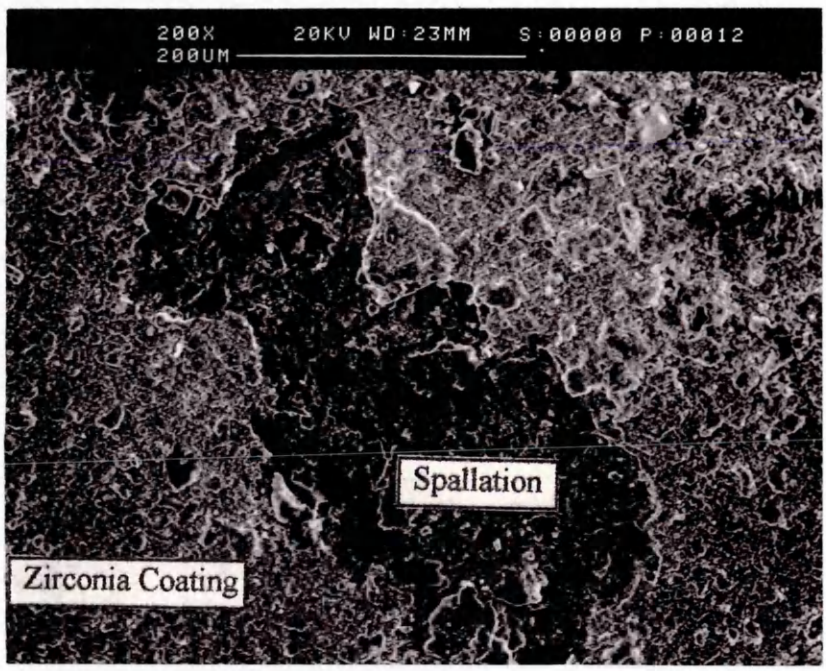


Figure 8.7- Micrograph of the surface of RT122, aged for 100h at 1050°C

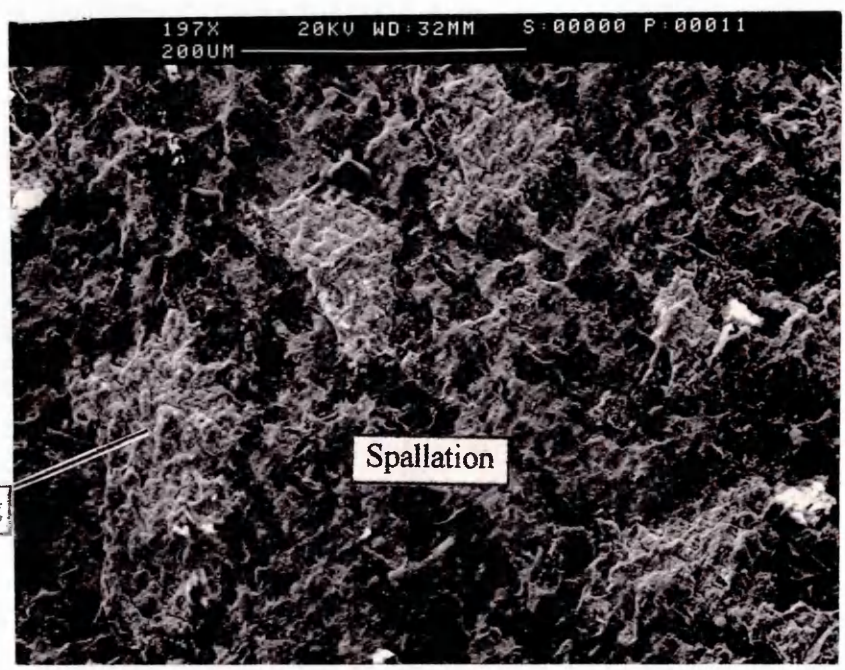


Figure 8.8- Micrograph of the surface of Coating A, aged for 100h at 1050°C

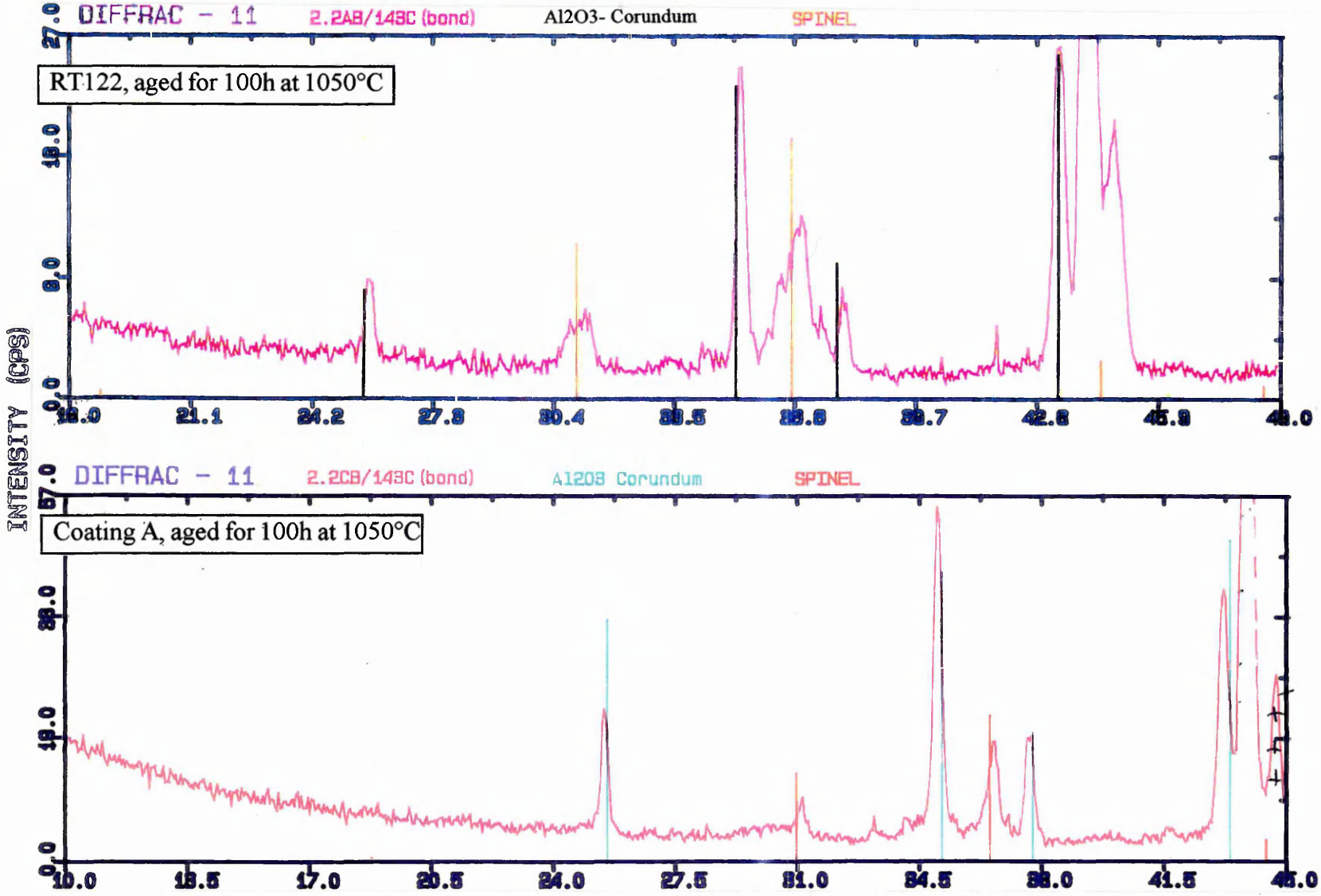


Figure 8.9- XRD analysis of RT122 and Coating A

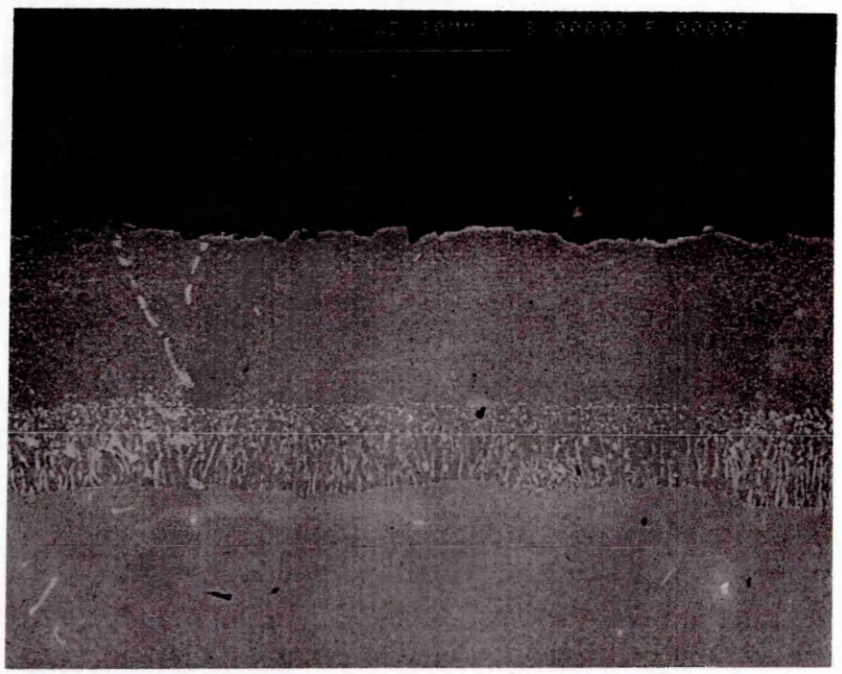

Figure 8.10- Micrograph of RPS320, as-processed

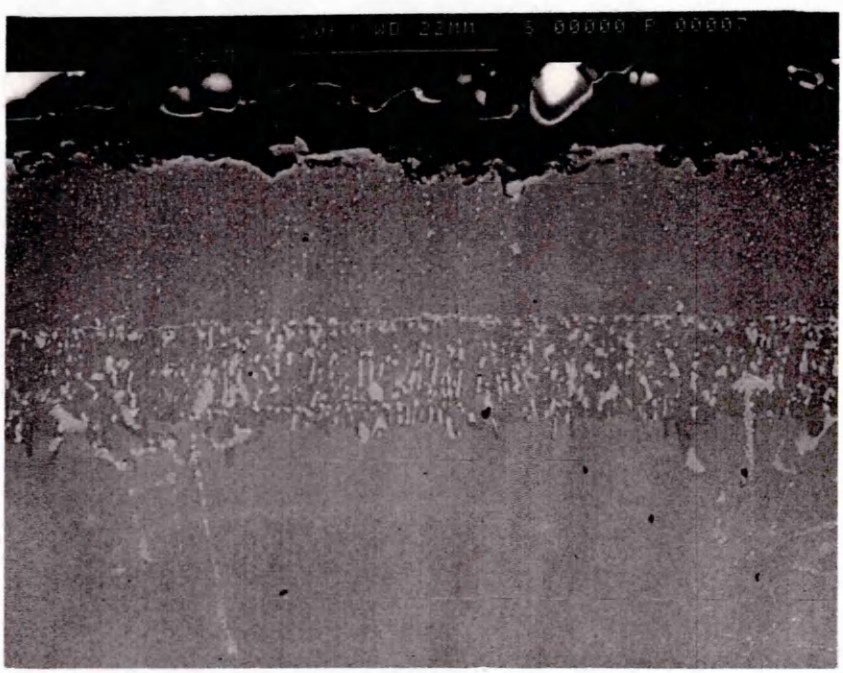

Figure 8.11- Micrograph of RPS320, aged for 100h at 1050°C

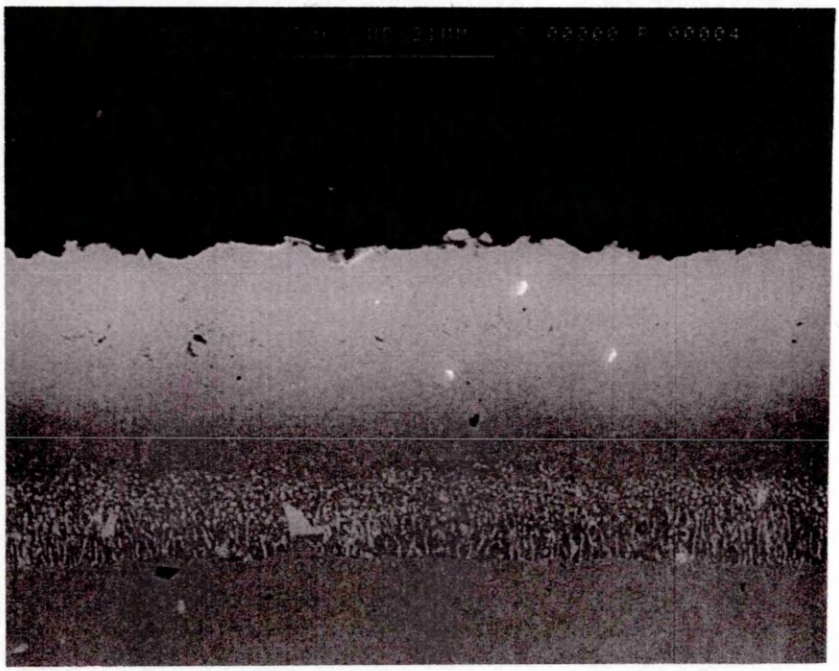

Figure 8.12- Micrograph of RT22LT, as-processed

Figure 8.13- Micrograph of RT22LT, aged for 100h at 1050°C

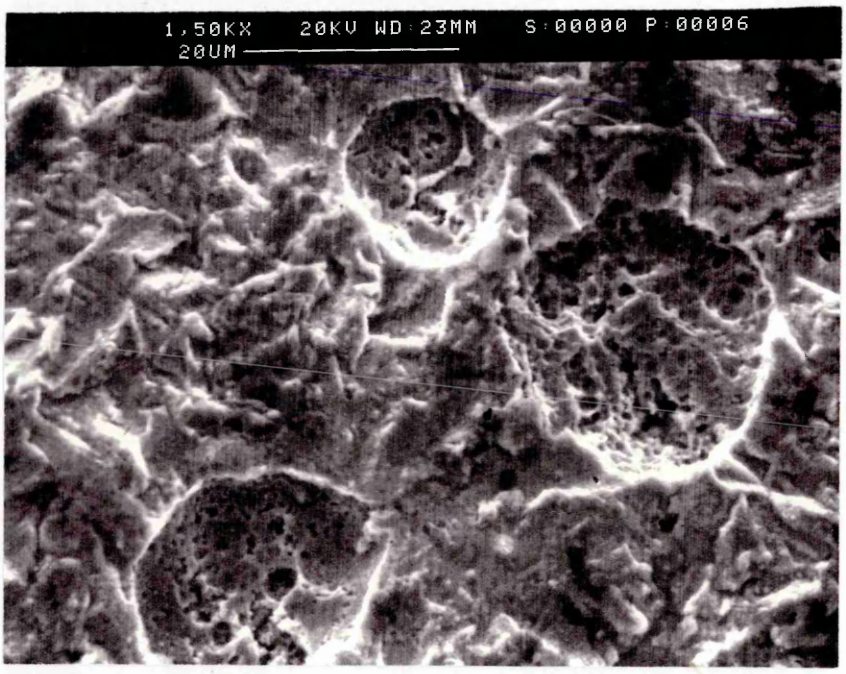


Figure 8.14- Micrograph of RPS320, aged for 10h at 1150°C. Spallation of the oxide scale

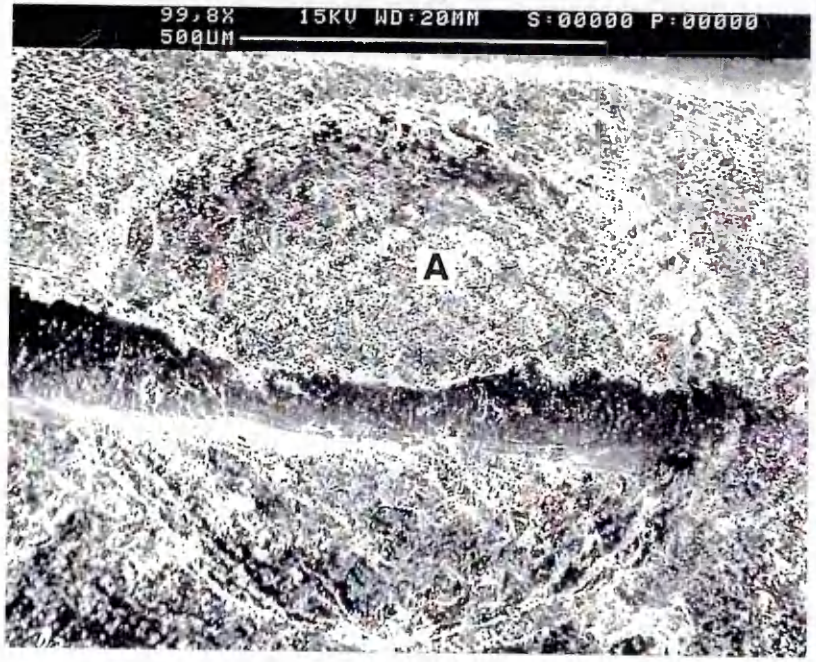


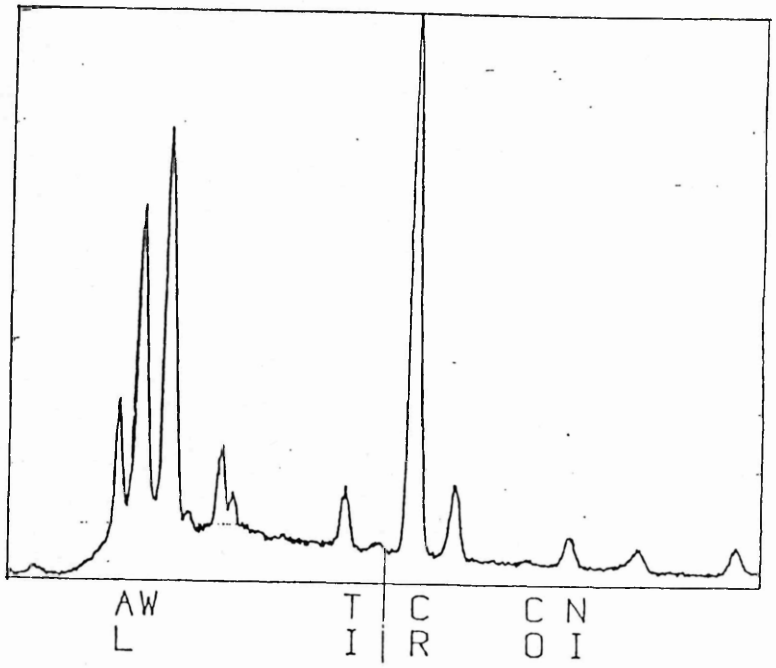


Figure 8.15- Catastrophic failure of the oxide. RPS320, aged for 100h at 1150°C

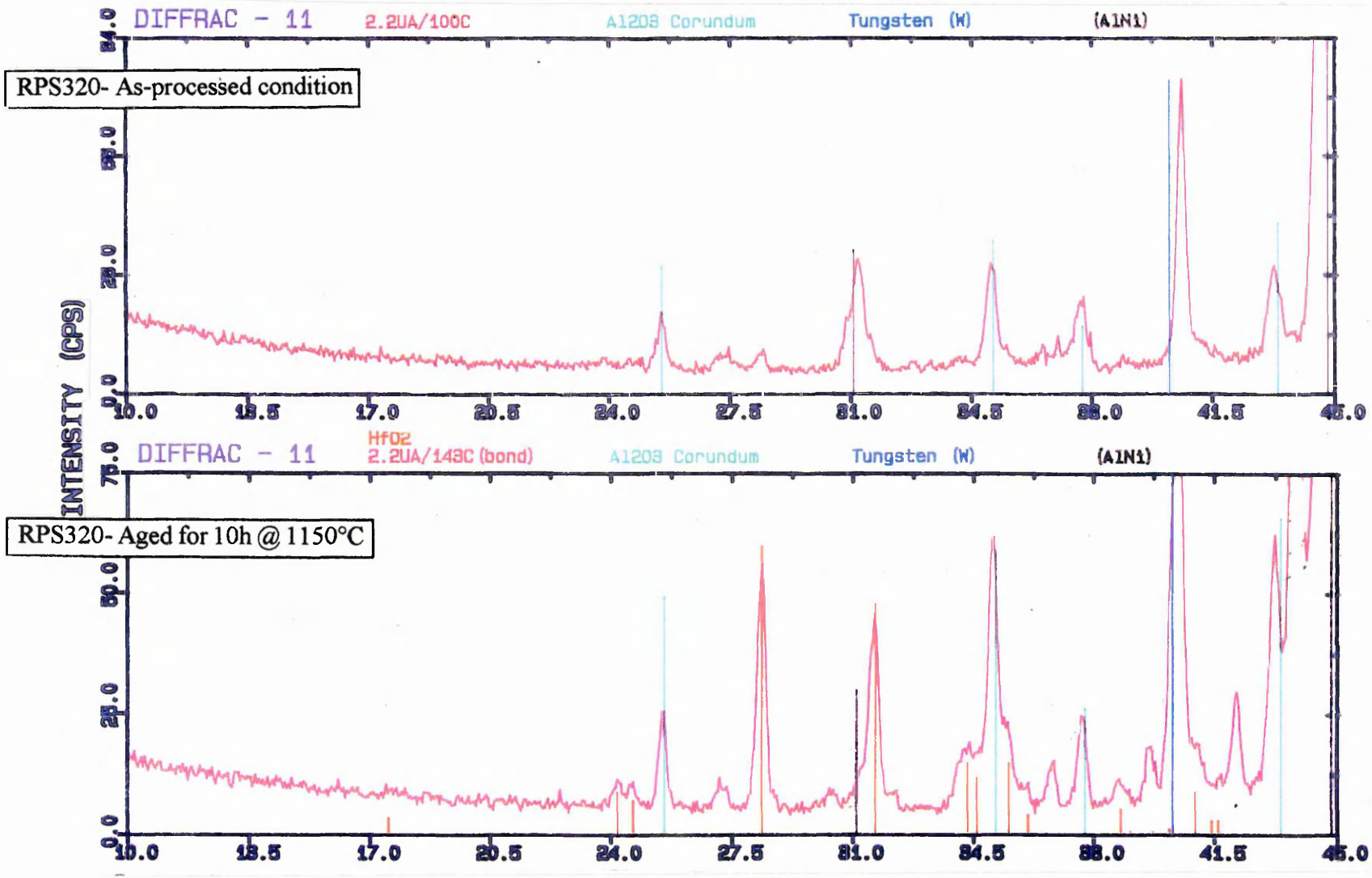


Figure 8.16- XRD analysis of RPS320

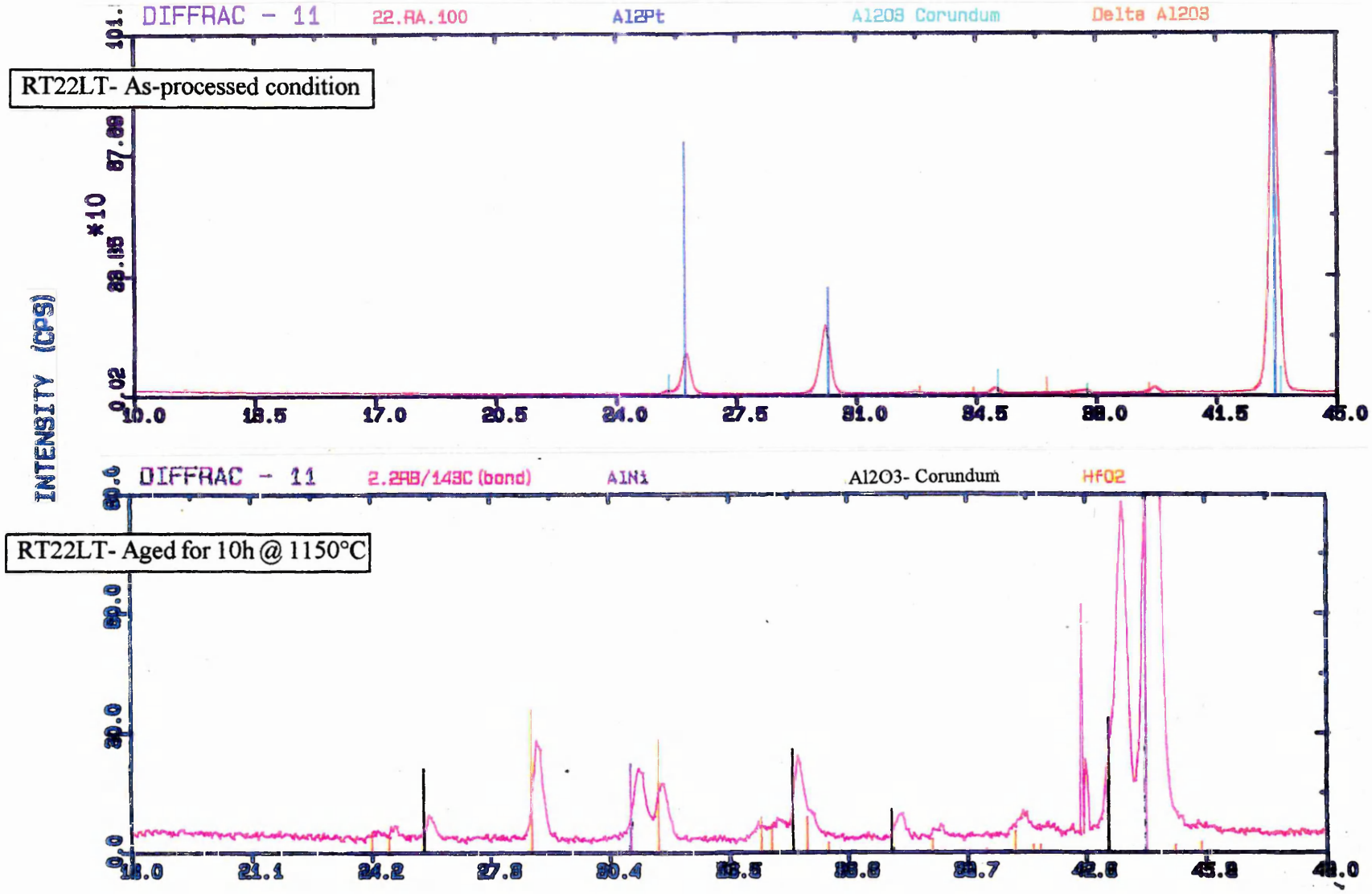


Figure 8.17- XRD analysis of RT22LT

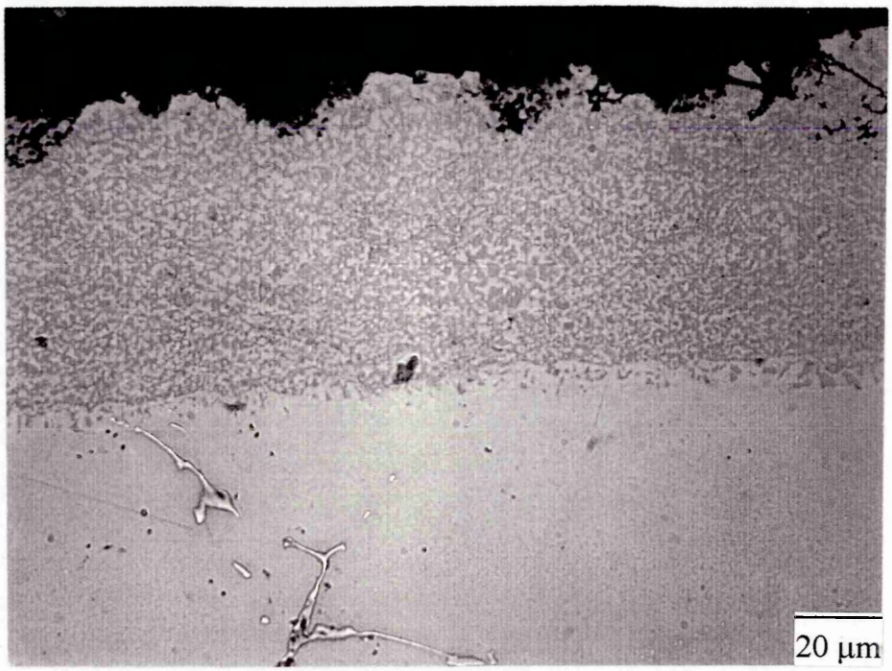


Figure 8.18- Micrograph of Coating B, as-processed

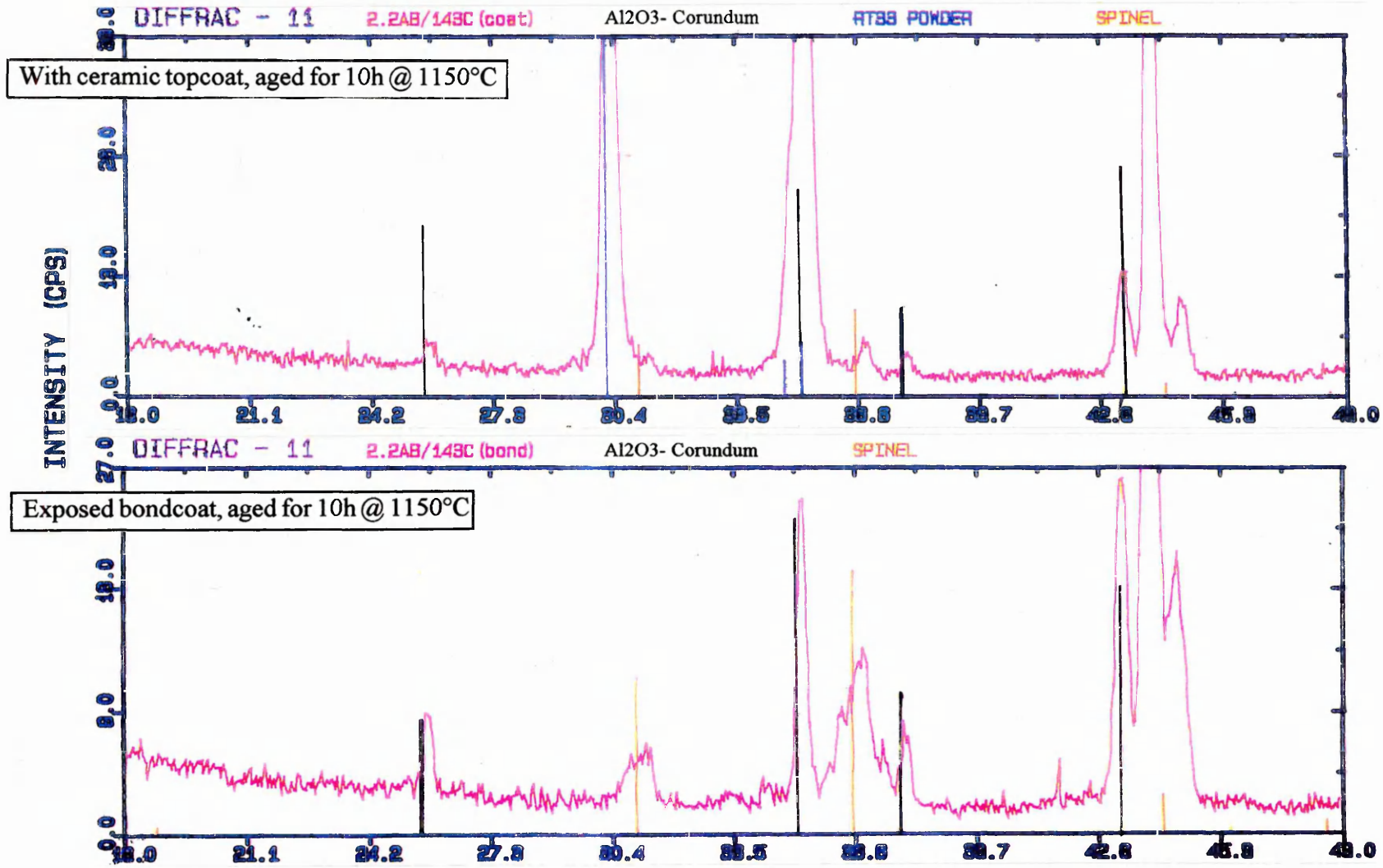


Figure 8.19- XRD analysis of RT122 to determine the effect of a ceramic topcoat

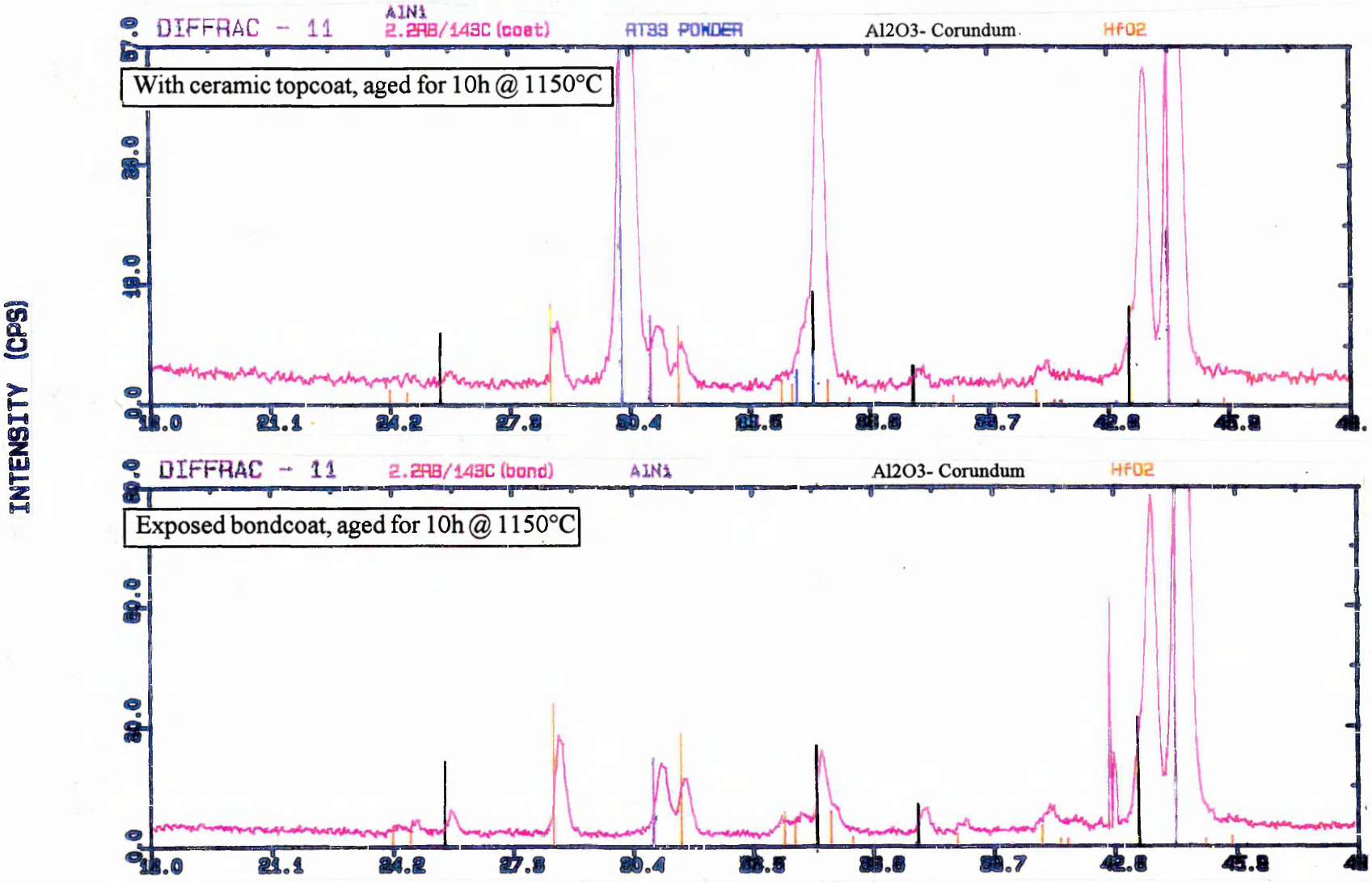


Figure 8.20- XRD analysis of RT22LT to determine the effect of a ceramic topcoat

Chapter 9- Results

## Assessment of in-situ and ex-situ pre-oxidation treatments

### 9.1 Introduction

If pre-oxidation treatments were to be incorporated within the production process for TBC's, the treatment would either be carried out ex-situ, prior to ceramic deposition, or in-situ, within the PVD coater.

This section of work assessed the applicability of both ex-situ and in-situ pre-oxidation treatments to a range of bondcoats, to see if the potential benefits justified the inclusion of the pre-treatment in the production process.

### 9.2- Research Plan

#### *9.2.1- Ex-situ Pre-oxidation.*

A wide range of bondcoats were chosen for this analysis to give a broad understanding of the effects of the pre-treatment on bondcoat behaviour. The bondcoats that were assessed were;

RT22LT-Platinum aluminide

RPS320-High aluminium activity aluminide

RT69- Low activity aluminide

RT31- MCrAlX coating, deposited by EB-PVD

Coating B-MCrAlX coating with Hf and Si additions, deposited by LPPS

RT122-MCrAlX coating, deposited by LPPS

Coating B + RT22LT- Duplex MCrAlX/ platinum aluminide coating

RT122 + Pt- Platinum modified MCrAlX coating

The bondcoats were supplied on MarMOO2 substrates. One pin of each type was assessed. The samples were grit blasted with 120 grit alumina at 2.04 bar and then pre-oxidised in a $H_2$-10%$H_2O$ atmosphere. The ceramic topcoat was then deposited using EB-PVD.

The modified scratch test was used to assess the adherence of the TBC systems in the as-processed condition and aged for 100h at 1100°C. The results were compared to those from untreated specimens.

*9.2.2- In-situ Pre-oxidation*

These pre-treatments were assessed using the MCrAlX bondcoat RT122 on a MarMOO2 substrate. The samples were gritted with 120 grit alumina at 2.04 bar and then underwent in-situ pre-oxidation in a range of atmospheres

Atmosphere A= 10%$O_2$/Ar for 1h (biased ~2.5kV)

Atmosphere B= 90%$O_2$/Ar for 1h (biased ~2.5kV)

Atmosphere C= 1%$O_2$/Ar for 1h (biased~2.5kV)

Atmosphere D= 10%$H_2$/Ar for 1h (biased~2.5kV)

Atmosphere E= 10%$H_2$/Ar for 1h, and then 1%$O_2$/Ar for 1h (biased~2.5 kV)

Atmosphere F= 10%$O_2$/Ar for 1h (unbiased)

Atmosphere G= Reference sample (no pre-treatment)

The atmospheres A, B and C were designed to sputter clean the surface of the coating and then establish an oxide scale. Atmospheres D and E would clean the

surface by $H_2$ reduction, whilst atmosphere E would then re-establish the oxide. Lastly, atmosphere F, being unbiased, would not clean the surface but merely encourage oxide growth.

After pre-oxidation, a ceramic topcoat was applied to the bondcoats using EB-PVD. The adherence of the various systems was assessed in the as-processed condition and aged for 100h at 1100°C condition using the modified scratch test.

## 9.3 Results

### *9.3.1 Ex-situ pre-oxidation*

*- Optical Examination*

The RT122 and RT22LT pre-oxidised systems (being representative of both MCrAlX and diffusion coatings respectfully), were examined in section to determine any differences from untreated systems.

Micrographs of the RT122 system are shown in Figure 9.1. The coating appears to be similar to its untreated counterpart (Figure 9.2). The aged pre-oxidised coating had grown an oxide ~4μm thick and had suffered complete β depletion (Figure 9.3), where as the oxide of the untreated bondcoat was ~4.5μm and after ageing the coating had undergone complete β depletion.

The pre-oxidised RT22LT was, again, similar to the untreated coating (Figures 9.4 and 9.5). Upon ageing, the thickness of the treated coating increased from 54μm to 62μm (due to the growth of the interdiffusion zone) and had grown an oxide ~ 5μm thick (Figure 9.6). This is comparable to an untreated coating.

*-Modified Scratch Test Results*

The results from the scratch test are shown in Figure 9.7. By comparing the pre-oxidised systems to their untreated counterparts, it was revealed that pre-oxidation provides no benefit and is possibly detrimental to the adhesion or life spans of these TBC systems.

*-Summary*

Examination of the systems in section revealed that pre-oxidation did not alter either the chemistry nor the rate of oxidation of the bondcoats. For both diffusion and MCrAlX bondcoats (ie. RT22LT and RT122 respectfully), upon ageing, the treated systems underwent similar composition changes and grew oxides of comparable thicknesses to that of untreated systems. The results of the modified scratch test show that the adherence these bondcoat systems in the as-processed and aged conditions was, in general, less than that of the untreated systems. This indicates that the ex-situ pre-oxidation of these bondcoat systems in a $H_2/10\%H_2O$ atmosphere does not increase the lifetime of the coating and may merely have acted to accelerate the oxidation process.

*9.3.2 In-situ pre-oxidation*

*-Optical Examination*

The pre-oxidation treatments did not appear to alter the chemistry nor the oxidation rate of the bondcoat, as both the β depletion and oxide thickness were similar for both the treated and untreated systems. For example, after ageing, both

the coating treated in atmosphere A and the untreted coating had grown oxide scales ~ 4 μm thick and the β phases were completely depleted

*-Modified Scratch Test*

In the as-processed condition, the pre-oxidation atmospheres D and F appear to have partially degraded the adhesion of the coating system. After an age of 100h at 1100°C all of the pre-treatments and the untreated (reference) sample had failed (Figure 9.8). Thus, the in-situ pre-oxidation treatments did not increase the adherence of the TBC system.

## 9.4 Overall summary of the assessment of pre-oxidation treatments

It was established in chapter 7 that the $H_2/10\%H_2O$ pre-oxidation atmosphere produced some intial benefits to the growth of an alumina film. Once aged however, these benefits were lost as the scale became contaminated with other elements, making the samples indistingushable from those oxidised in the $Ar/20\%O_2$ atmosphere.

These results were confirmed by the ranking of the ex-situ and in-situ pre-oxidation treated samples against there untreated counterparts. Neither pre-treatment process appeared to affect the adhesion at the ceramic/bondcoat interface and no increase in the life span of a TBC system was observed.

It appears that the establishment of an intial alumina film does not guarantee high adhesive properties. Of greater importence is the control of the outward diffusion of elements to the ceramic/bondcoat interface. Chapter 8 detailed how the contamination of the oxide by either spinels or substrate elements, such as tungsten, can lead to the spallation of the scale. This is a residual feature of the fact that the

bondcoats under investigation were originally designed for environmental protection. In ths role, as corrosion resistant coatings, the prevention of scale spallation is not as vital as the ability of the protective film to be self-healed. However, for TBC systems, spallation will lead to the loss of the ceramic layer and the catastrophic failure of the coating.

By tailoring the composition of the bondcoat, it should be possible to hamper the outward diffusion of the damaging elements and so extend the life of a TBC system. The potential benefits of this were shown in chapter 8, with the comparison of RPS320 and RT22LT. The platinum within the RT22LT coating promoted a more pure alumina scale, whilst delaying the outward diffusion of other elements through the coating towards the metal/oxide interface. This produced a far more adherent scale. Due to these reasons, it was decided to harness the properties of platinum and design a range of diffusion bondcoats specifically for TBC systems.

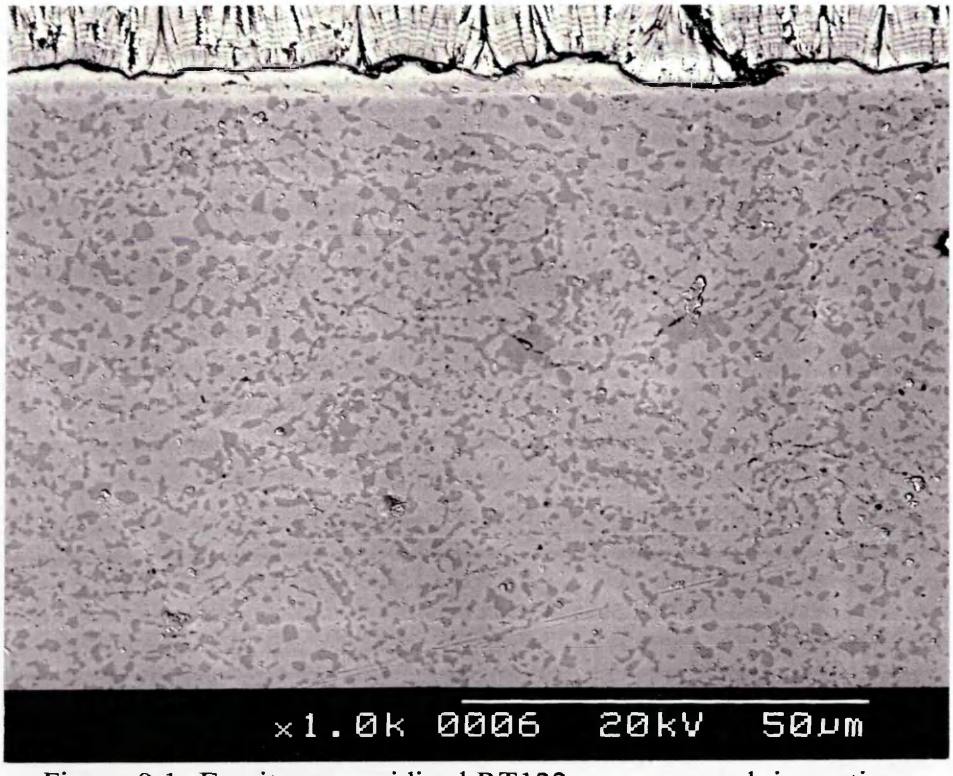


Figure 9.1- Ex-situ pre-oxidised RT122, as-processed, in section

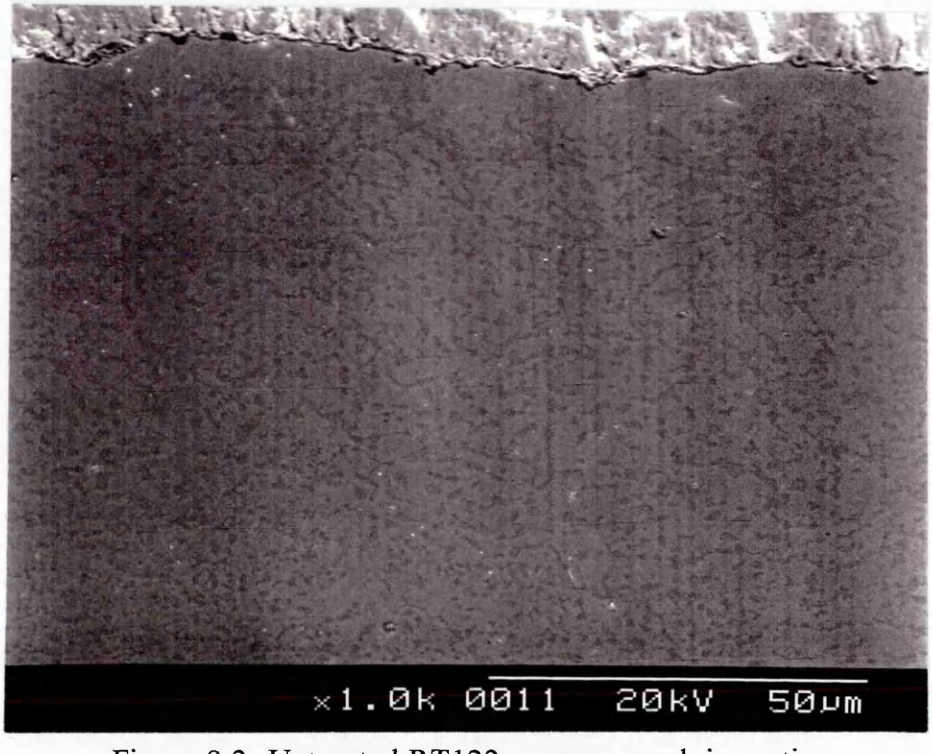


Figure 9.2- Untreated RT122, as-processed, in section

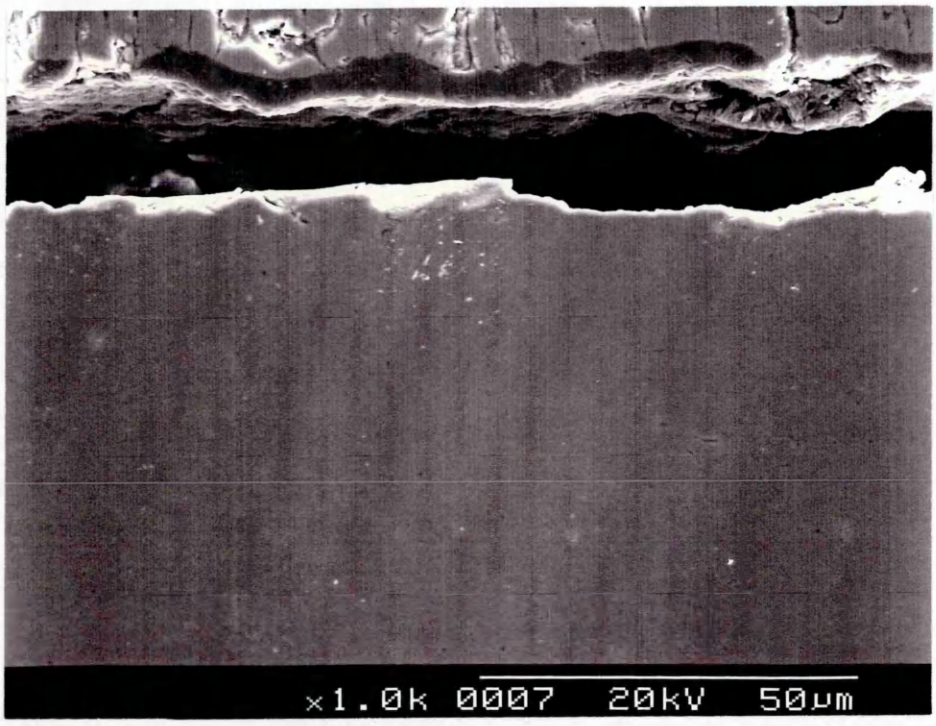


Figure 9.3- Ex-situ pre-oxidised RT122, aged for 100h at 1100°C, in section

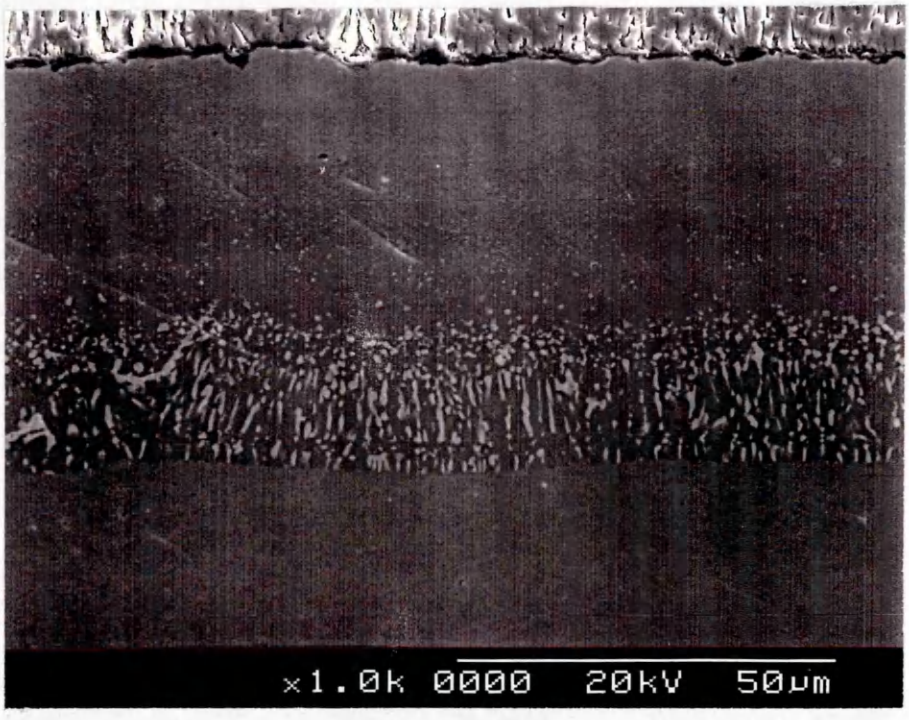


Figure 9.4- Ex-situ pre-oxidised RT22LT, as-processed, in section

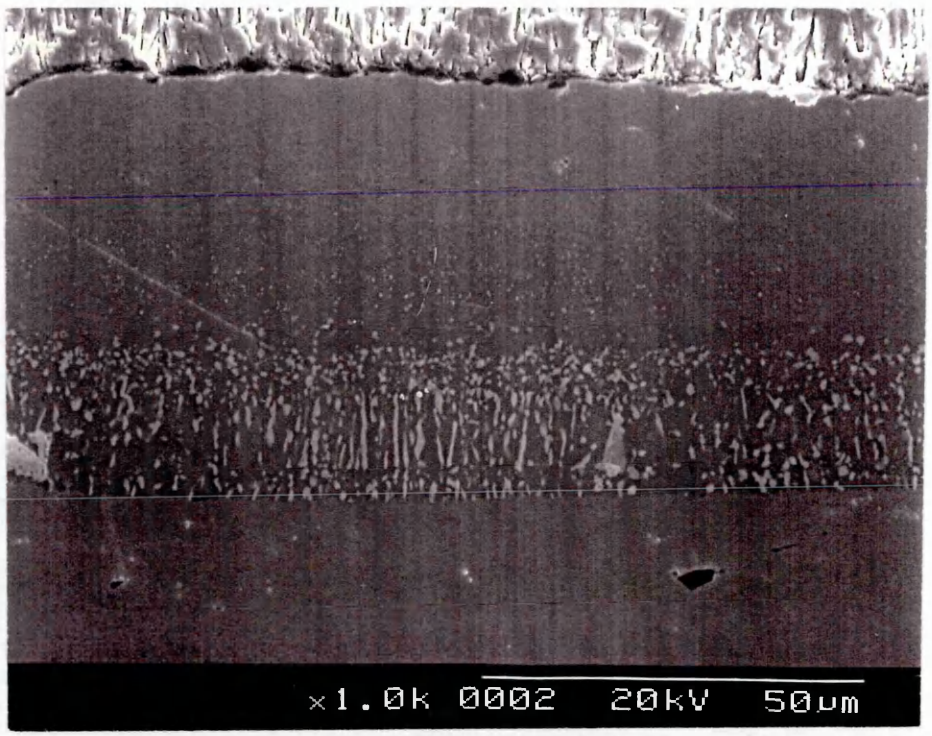


Figure 9.5- Untreated RT22LT, as-processed, in section

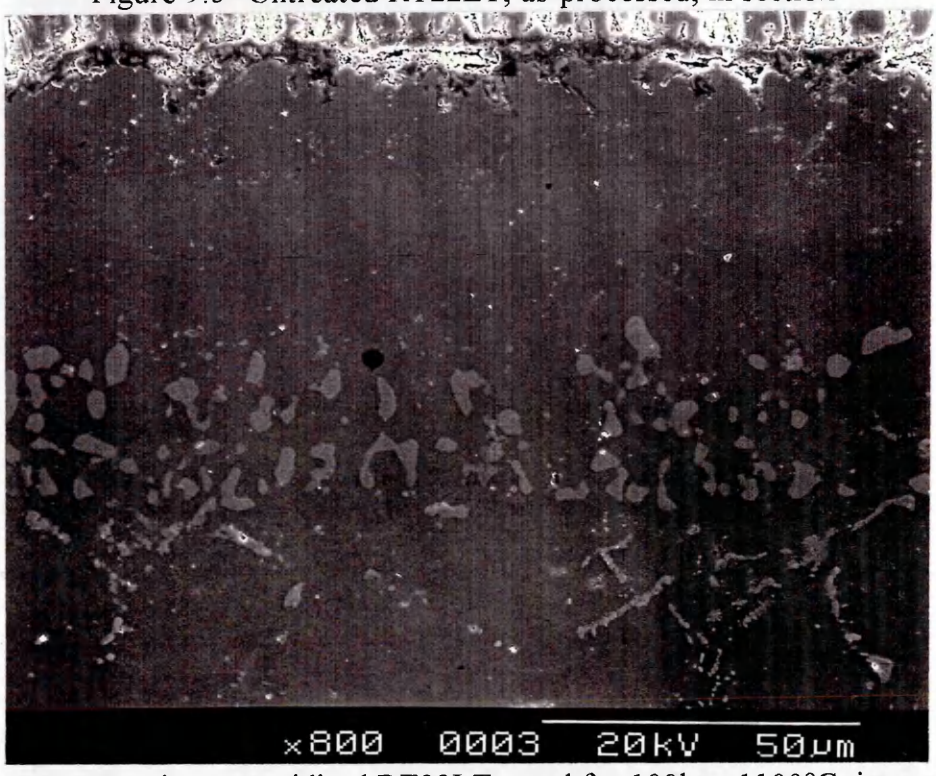


Figure 9.6- Ex-situ pre-oxidised RT22LT, aged for 100h at 1100°C, in section

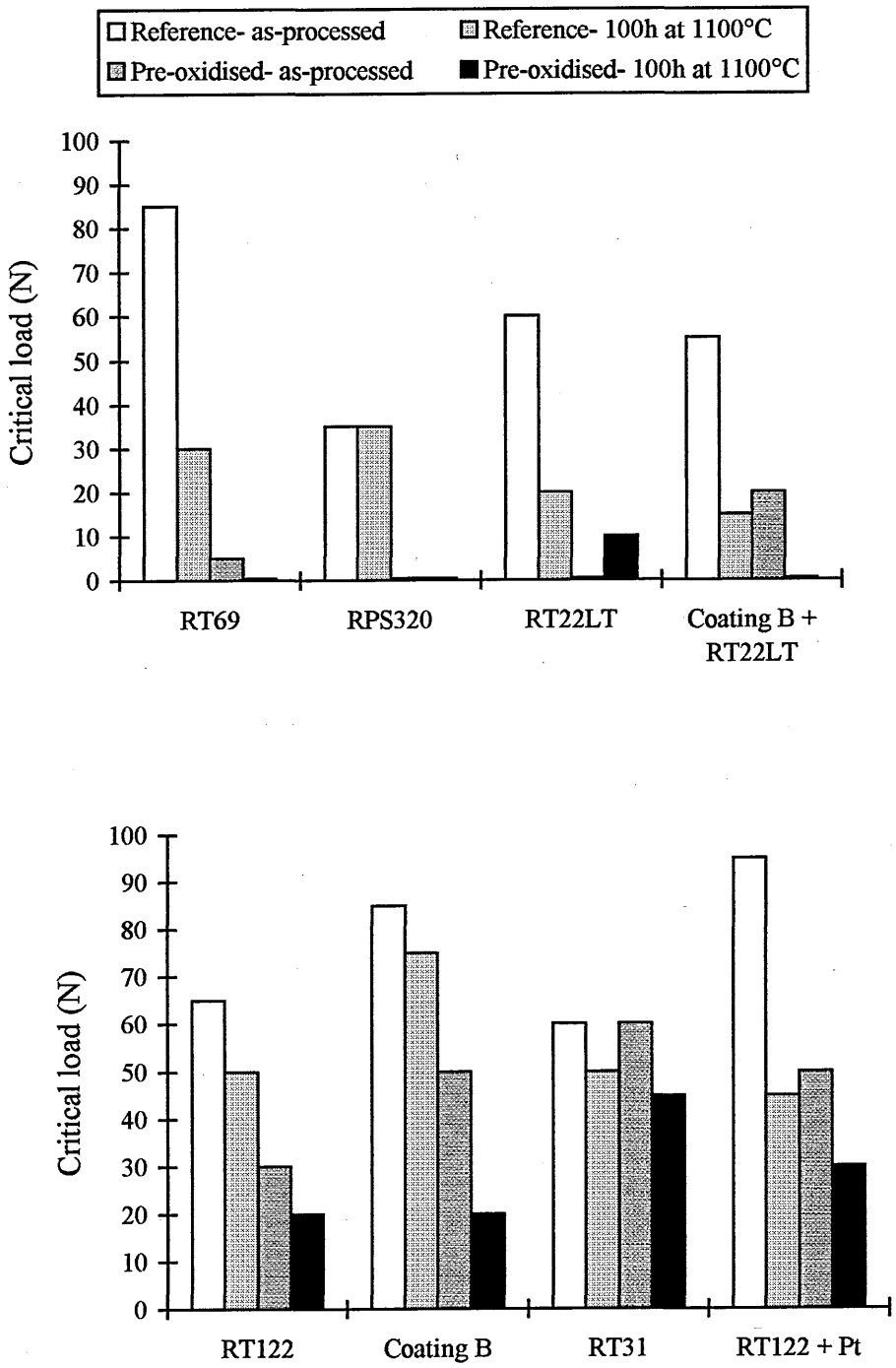


Figure 9.7- Modified scratch test results for the ex-situ pre-oxidised systems

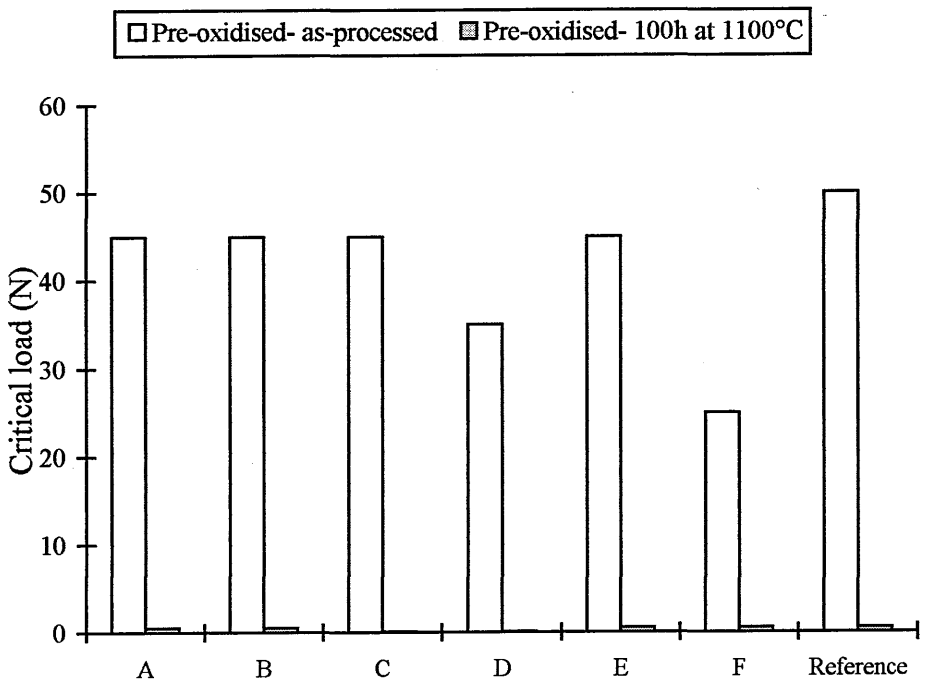


Figure 9.8- Modified scratch test results for the in-situ pre-oxidised systems

Chapter 10- Results

# The Optimisation of an Out-of-Pack Platinum Aluminide for Thermal Barrier Coating Systems

## 10.1 Introduction

Platinum aluminide bondcoats act as an effective remedy against the aggressive environments in which turbine components operate, providing protection against both oxidation and corrosion. However, the effectiveness of diffusion coatings produced by high activity processes, such as RT22LT, can be undermined by contamination from damaging substrate elements. As coatings produced by low activity processes are less susceptible to these problems [26], this section of work examines the optimisation of an out-of-pack platinum aluminide bondcoat for use in TBC systems.

## 10.2 Research plan

A range of nine diffusion coatings were produced by varying the platinum diffusion temperature, the aluminising temperature and the final heat treatment (Table 10.1). The coatings were deposited on CMSX-4 pins and coded C through Z depending on the treatment. The samples were manufactured by Chromalloy UK Ltd.

The coatings were isothermally aged for 25h at 1100, 1150, 1170, 1190 and 1210°C and for 100h at 1100°C. The coatings were analyses using a variety of techniques, including SEM, XPS and XRD, whilst the adhesion of the coating systems was assessed using the modified scratch tester.

## 10.3 Analysis

### *10.3.1- Modified scratch test*

The coatings were ranked, in the both the as-processed and aged conditions using the modified scratch test. A wide range of results were achieved, with coatings C, E, M, O and T (see Table 10.1 for nomenclature) outperforming RT22LT (Figures 10.1 to 10.3)

### *10.3.2 XRD analysis*

A number of these diffusion coatings were analysed using XRD. The structure of the platinum aluminide layer was determined to be a β-(Ni,Pt)Al phase. An example of the XRD traces is given in Figure 10.4. The results were consistent with analyses of low activity platinum aluminides in the published literature [26]. This analysis was carried out at AEA Technology, Harwell.

### *10.3.3 Optical examination in section*

The diffusion coatings were prepared in section and assessed optically to determine both their grain size and the oxide thickness as the aluminides were progressively aged (Figures 10.5 and 10.6).

The average grain size of the coatings in the as-processed condition are shown in Figure 10.7. All of the coatings are consistent , in that they produced a grain size of less than 5 μm. This is far smaller than the average grain size of RT22LT (~ 20 μm).

The thickness of the oxide scale grown during isothermal exposure was measured in the coatings aged for 25h at various temperatures (Figures 10.8 and

10.9). It was shown that over the range of soaking temperatures, all platinum aluminides grew oxides of similar thickness.

*10.3.4 XPS analysis*

XPS analysis was carried out on a selection of samples chosen to show the breadth of performance achieved by the coatings, as indicated by the scratch test data. Analysis was undertaken on samples that, on cooling after an isothermal soak, had failed due to the spallation of the ceramic topcoat at the TGO/substrate interface. This allowed the analysis of both the surface of the sample and the underside of the ceramic/TGO.

No distinction could be made between the coatings, as the oxide scales were shown to be of similar compositions, consisting of an alumina based scale with hafnium at or near the TGO/ bondcoat interface. Examples of the traces are shown in Figures 10.10 and 10.11.

*10.3.5 SEM examination of the surface*

The substrates of the samples that had failed due to ceramic spallation were examined using SEM and EDS techniques. The surfaces of all such pins were found to feature an alumina based scale with areas of smooth faceted pitting, as illustrated in Figure 10.12.

*10.3.6 Image analysis*

To determine whether the size/number of pits correlated with the adhesive strength of the coating (as determined by the modified scratch test), image analysis

was used to ascertain the relative amount of pitting on the coatings C and Z. The inferior coating, Z, was shown to have a far higher proportion of pits than coating C, i.e. 11% for coating C compared to 37% for coating Z.

*10.3.7 SEM analysis in section*

The aged coatings were prepared in section and given a bromine etch. The most prominent feature observed was that the grain boundaries of the coatings were 'decorated' with elements such as Ti, Ta and W. These elements had diffused outwards from the interdiffusion zone (Figures 10.13 and 10.14). Smaller quantities of these refractory elements were also observed within the grains themselves.

## 10.5 Summary

In the as-processed condition, XRD analysis revealed that the diffusion coatings had a β-(Ni,Pt)Al structure. This was the expected result, being consistent with the published literature [26, 81]. All of the development coatings had a similar grain size after isothermal ageing, produced scales that had similar compositions at the spalled interface (re. XPS analysis).

The modified scratch test however, demonstrated that the adhesion of the aluminides varied from very poor (e.g. coating Z), to values that were superior to RT22LT (e.g. coating C). Optical examination of the coatings in section showed that both RT22LT and the development coatings all promoted scales of similar thickness. SEM analysis of the coatings in section revealed that the outward diffusion of Ti, Ta and W from the interdiffusion zone to the oxide occurred via, preferentially, the grain boundaries with some transport through the grains

themselves. Examination of the surface of the spalled samples showed the formation of smooth faceted pits. Although these pits were observed on all of the coatings, image analysis of the surfaces revealed that the relative amount of pit formation was greater on coating Z than on coating C, thus the poor adhesion was consistent with an increased number of interfacial voids.

The varied performances of the coatings suggests that the adherence of the oxide does not only depend on the scale growing to a critical thickness, as suggested in literature [29], but on other factors such as the integrity and composition of the oxide, as evident by the incorporation of transition metal elements within the oxide and the associated appearance of voids at the TGO/bondcoat interface. These must contribute to determine the lifetime of the coating. Both the results and a proposed failure mechanism are discussed in chapter 12.

| Coating Code | Pt Diffusion Temperature (°C), Treatment for 1h | Aluminising Temperature (°C) Treatment for 6h | Heat Treatment (°C) Treatment for 1h |
|---|---|---|---|
| C | 1100 | 1080 | 1100 |
| E | 1000 | 1080 | 1100 |
| M | 1000 | 1080 | 1150 |
| O | 1000 | 1120 | 1100 |
| S | 1000 | 1120 | 1150 |
| T | 1120 | 1080 | 1100 |
| U | 1120 | 1080 | 1150 |
| X | 1120 | 1120 | 1100 |
| Z | 1120 | 1120 | 1150 |

Table 10.1- Matrix of the development coatings

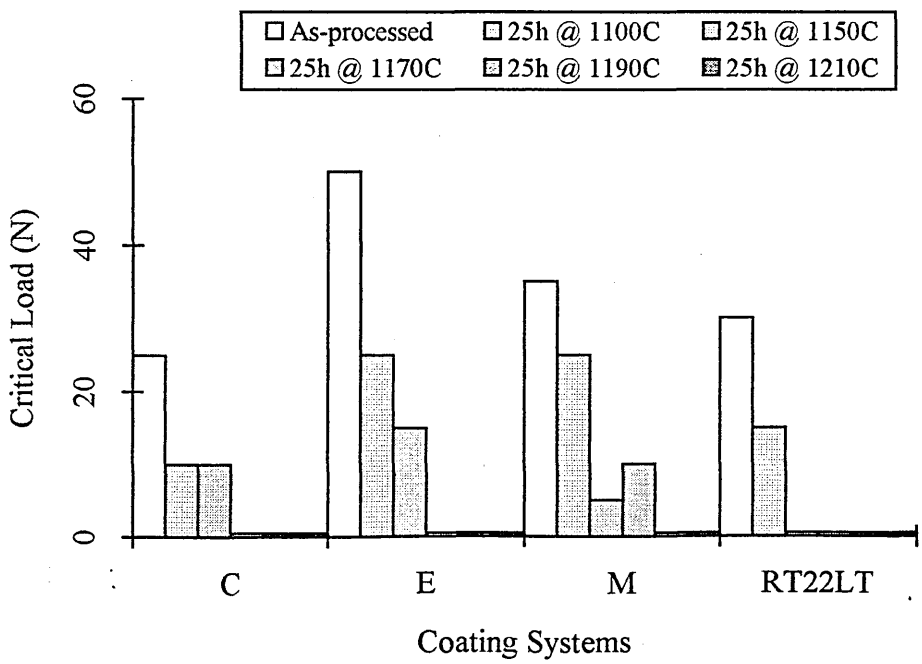


Figure 10.1- Modified scratch test results

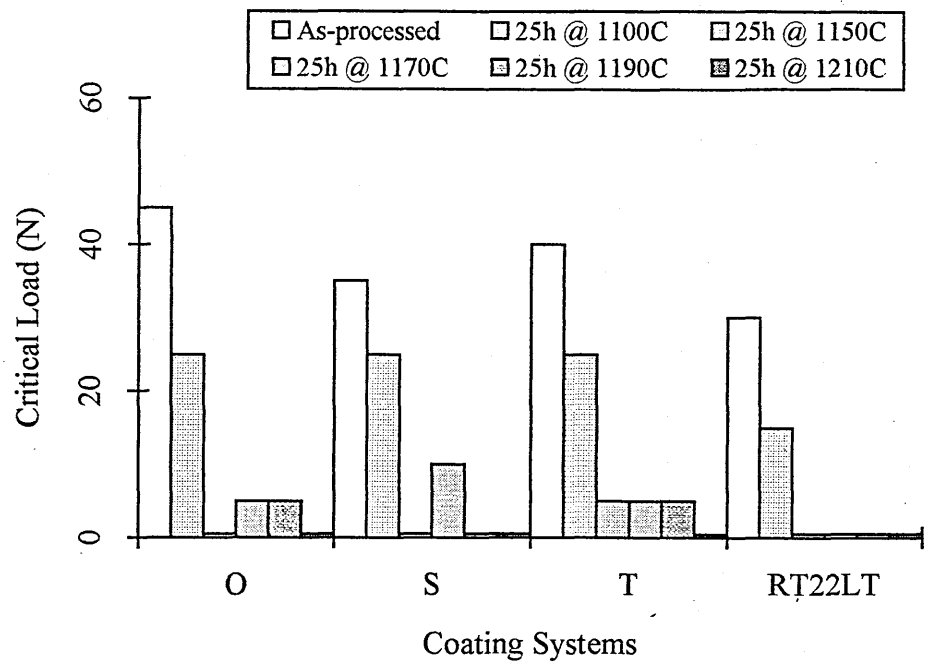


Figure 10.2- Modified scratch test results

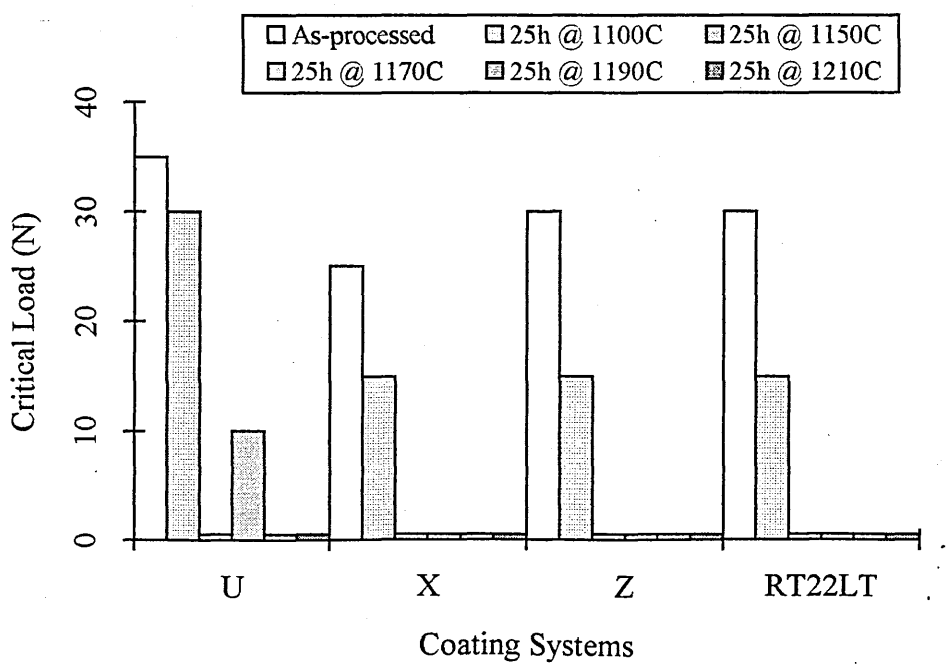


Figure 10.3- Modified scratch test results

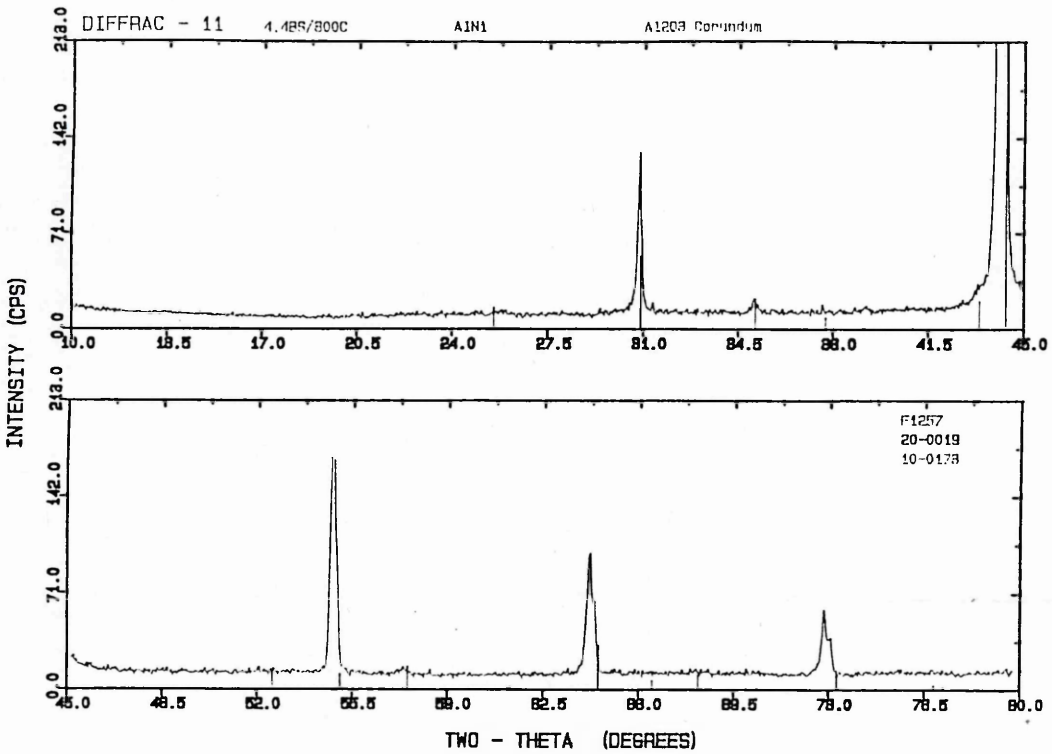


Figure 10.4- XRD analysis of coating C, as-processed

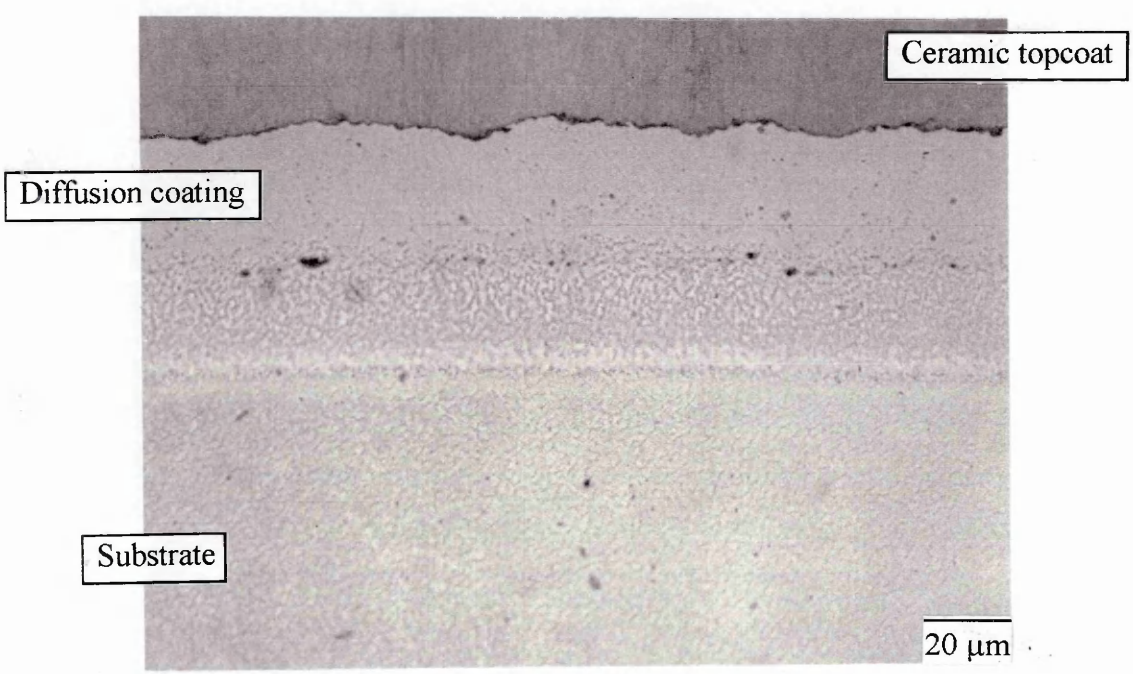


Figure 10.5- Coating C, as-processed, in section

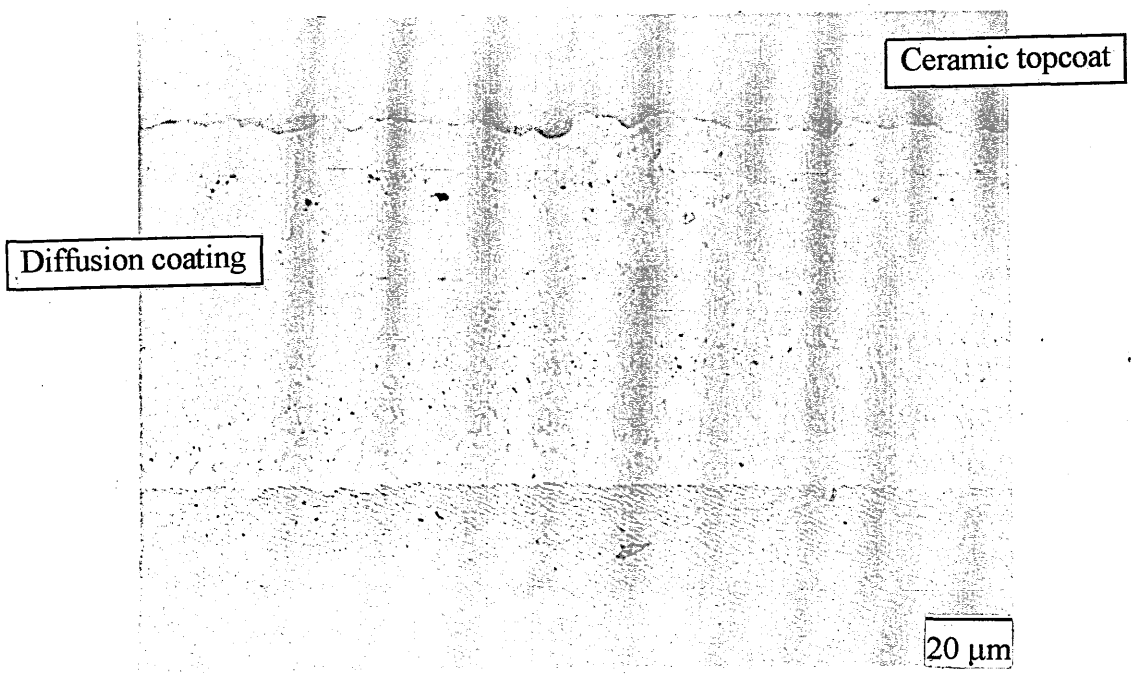


Figure 10.6- Coating C, aged for 25h at 1210°C, in section

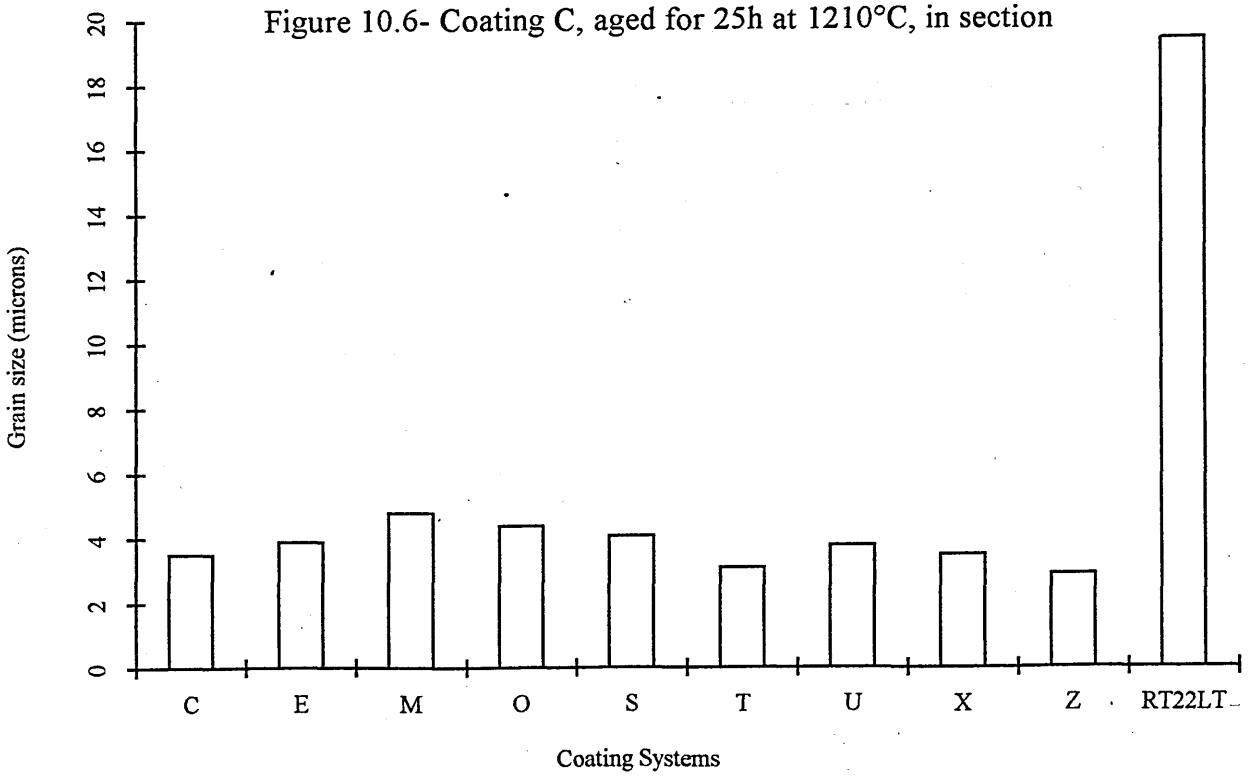


Figure 10.7- Grain size measurments of the development coatings, as-processed

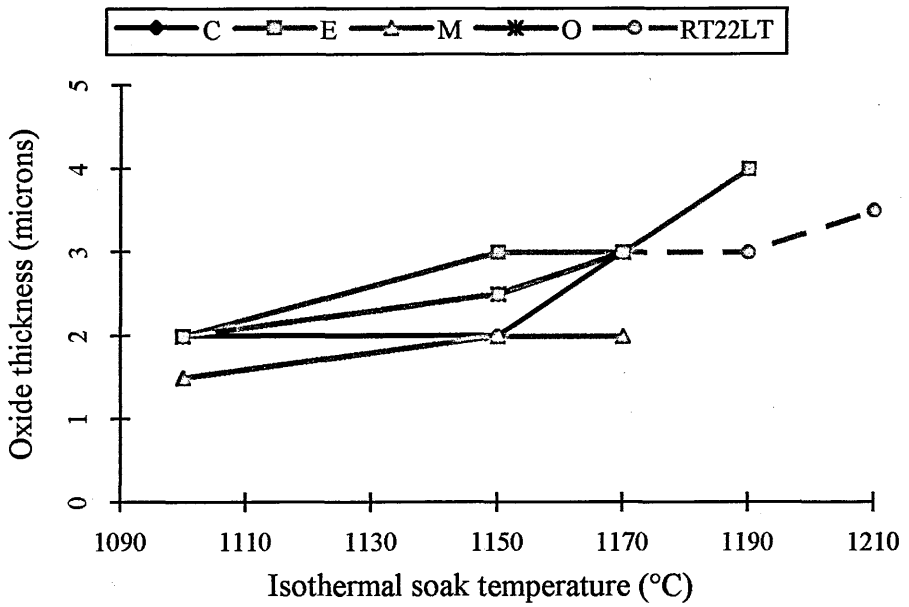


Figure 10.8- Oxide thickness measurments

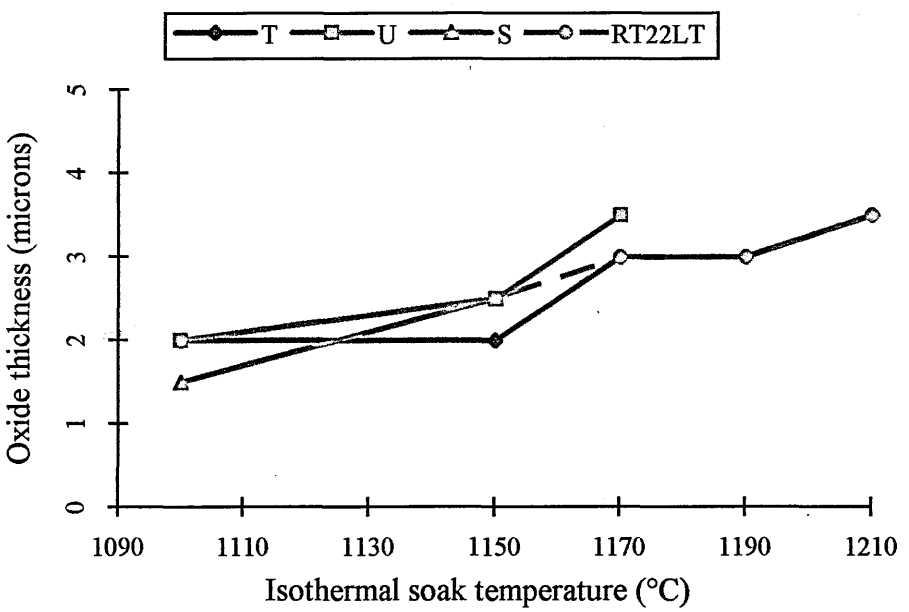


Figure 10.9- Oxide thickness measurments

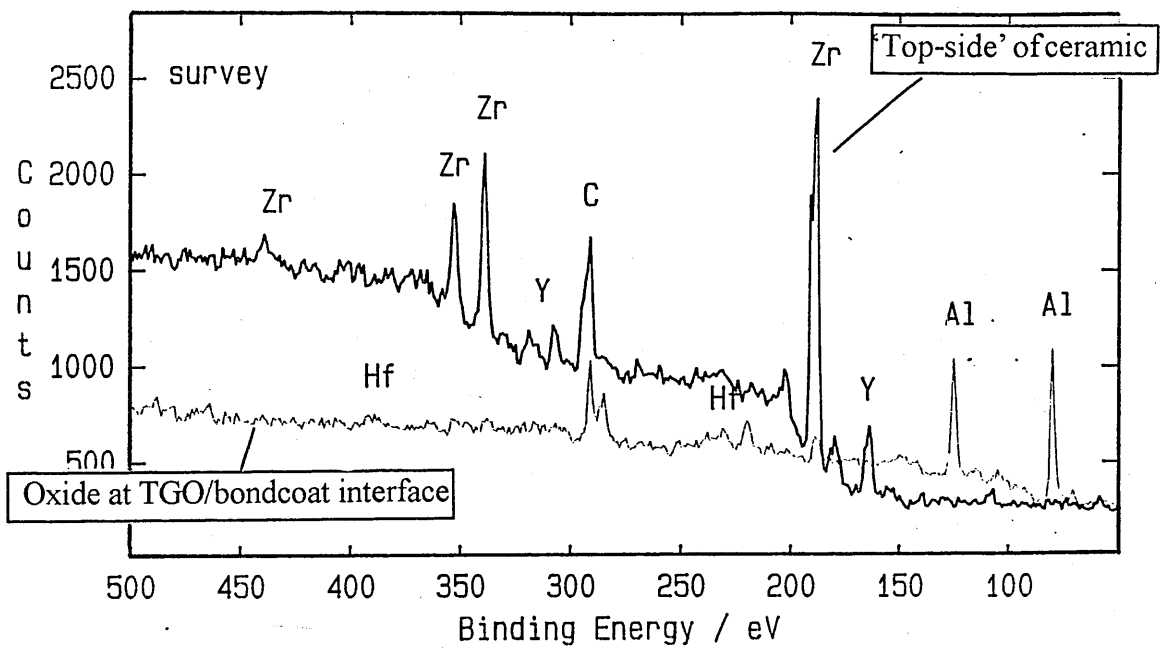


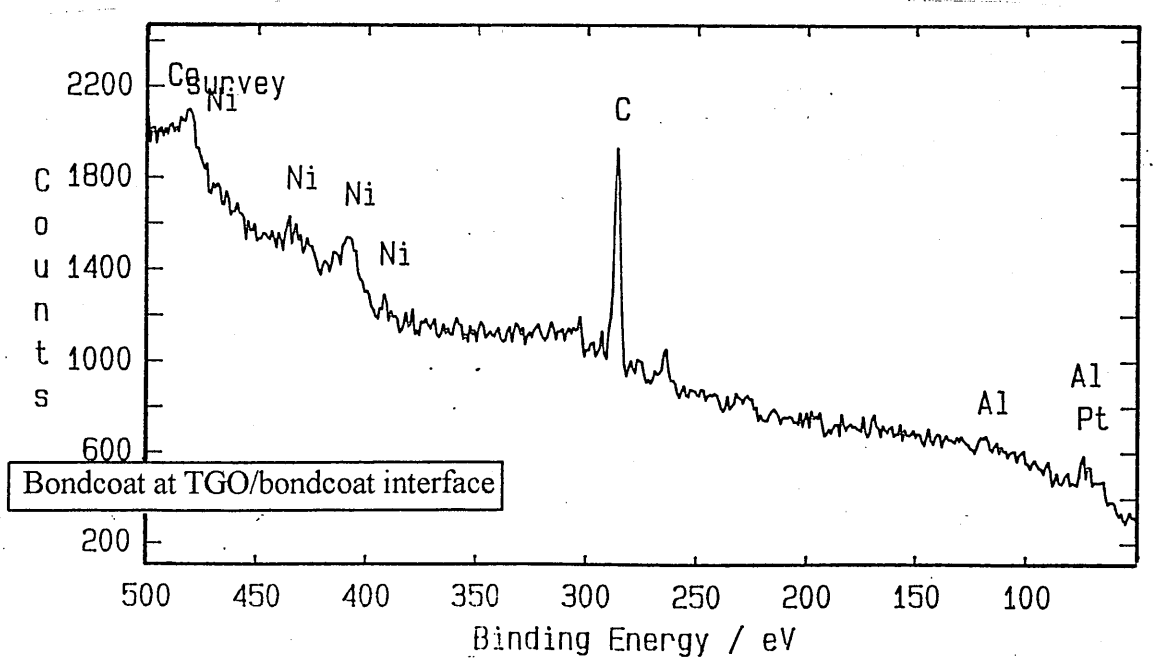


Figure 10.10- XPS analysis of coating C, isothermally soaked for 25h at 1190°C

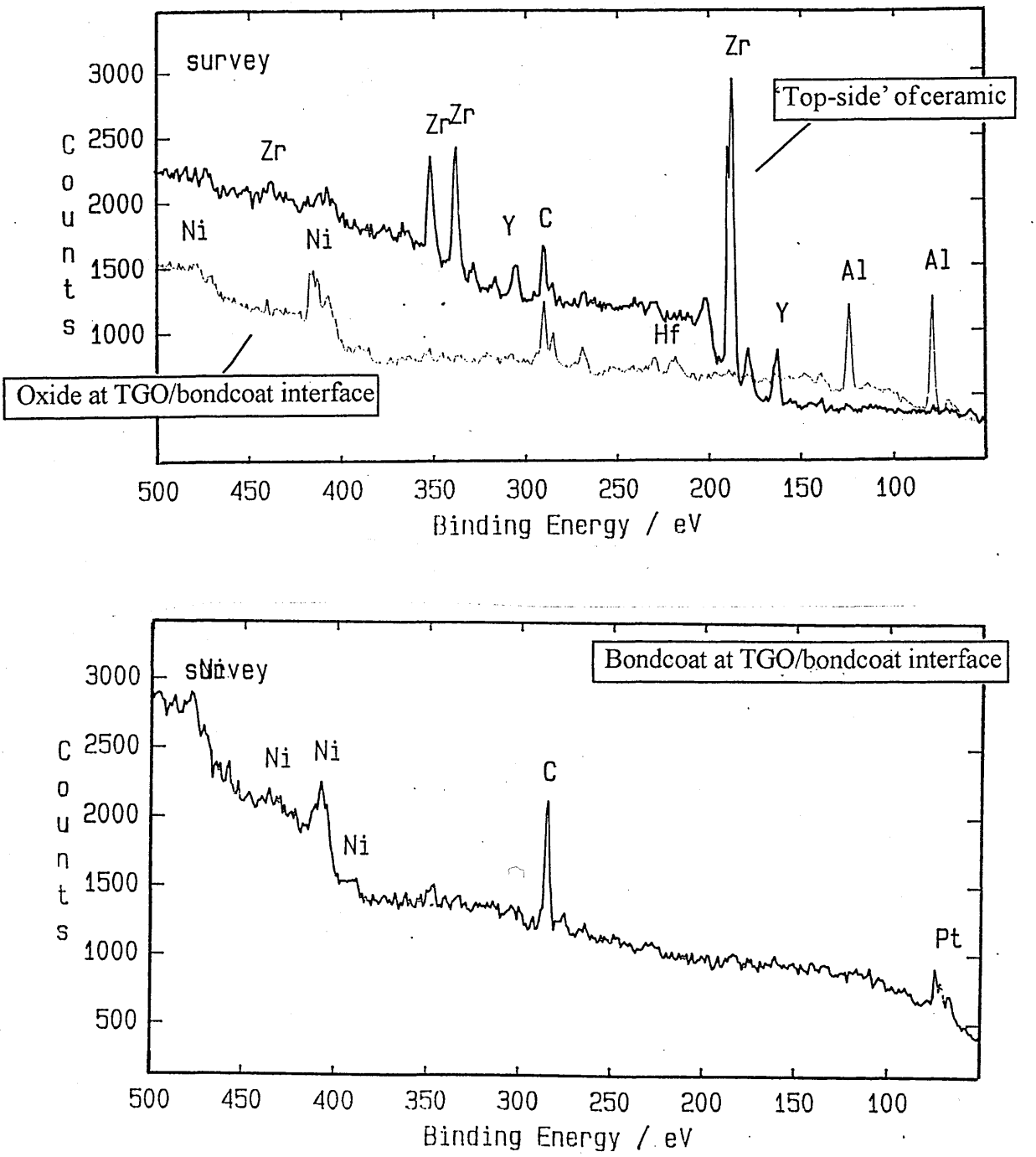


Figure 10.11- XPS analysis of coating Z, isothermally soaked for 25h at 1190°C

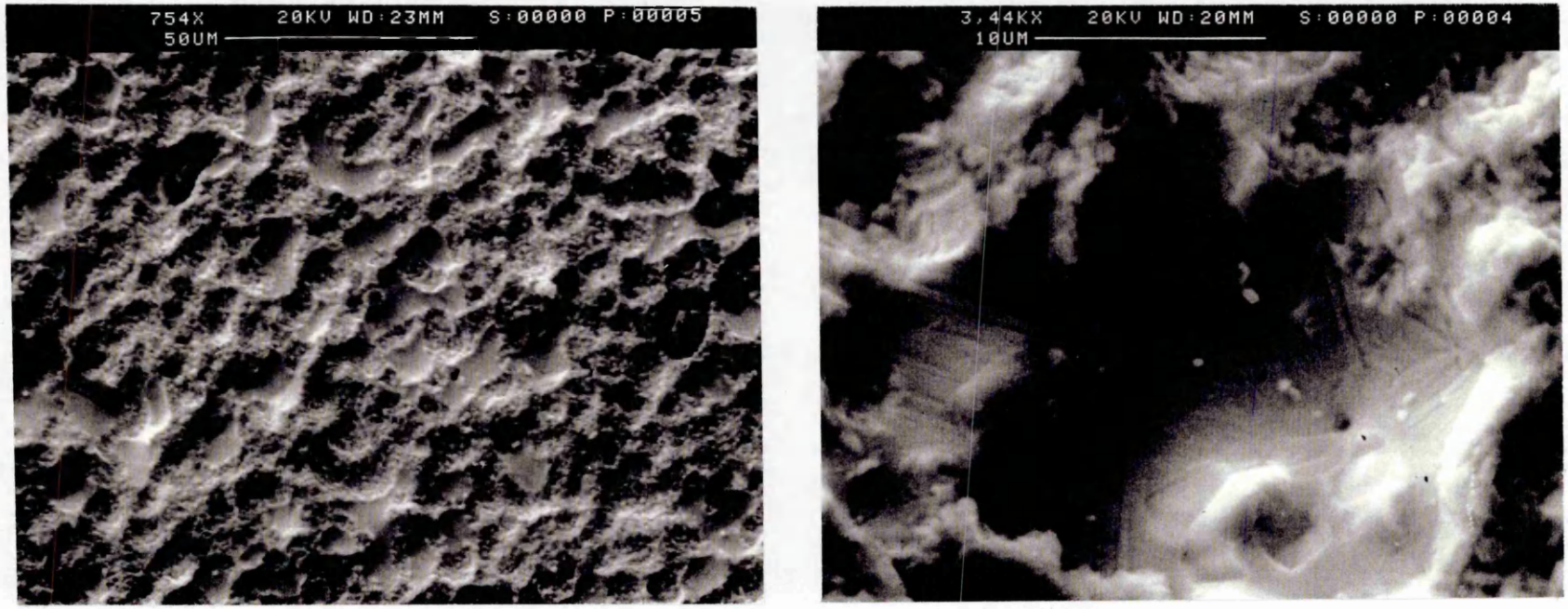


Figure 10.12- Coating E, aged for 25h at 1170°C. Micrographs show the formation of pits at the oxide/metal interface

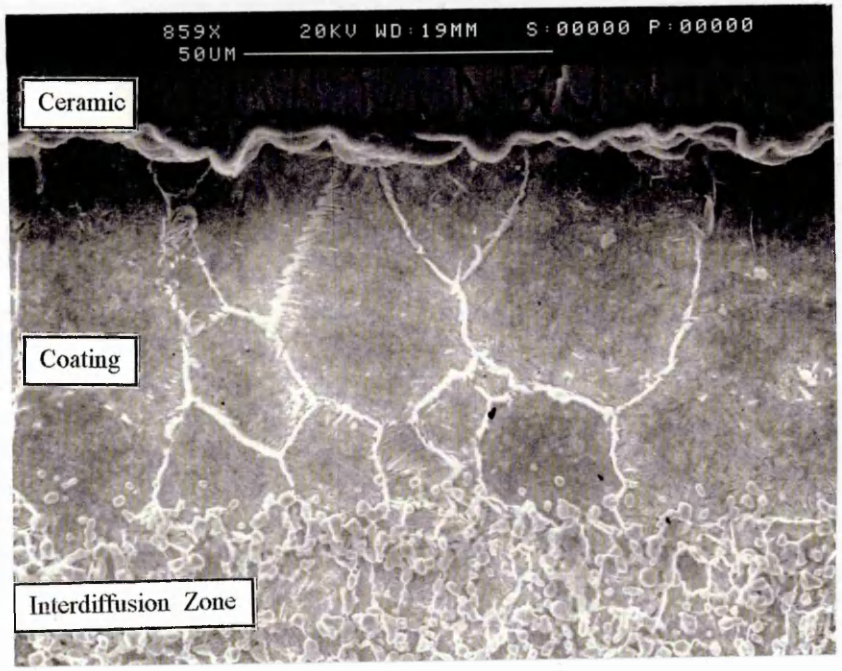


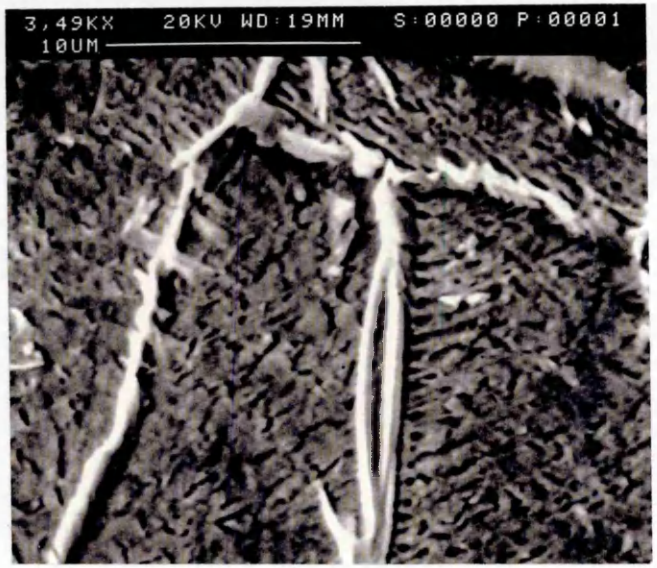


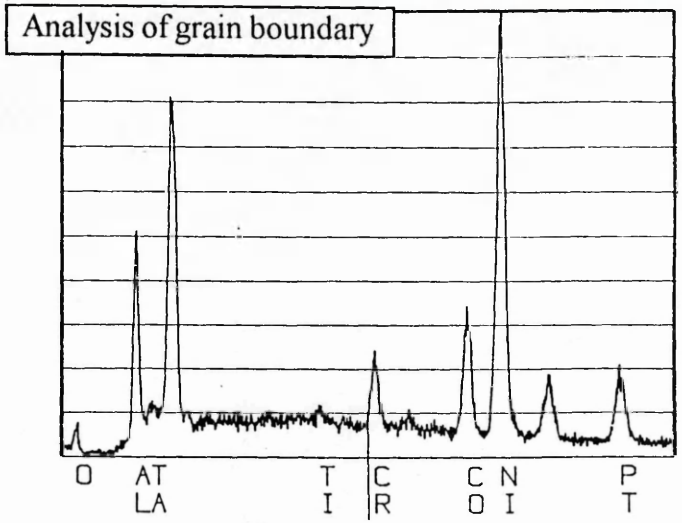


Figure 10.13- Coating C, aged for 25h at 1170°C, deep etched. Micrographs show the outward diffusion along grain boundaries

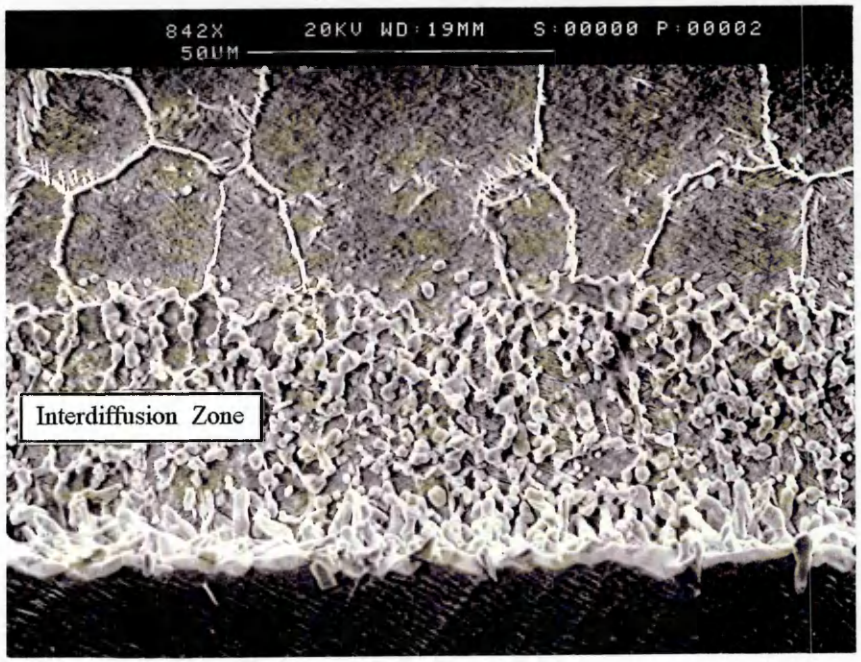


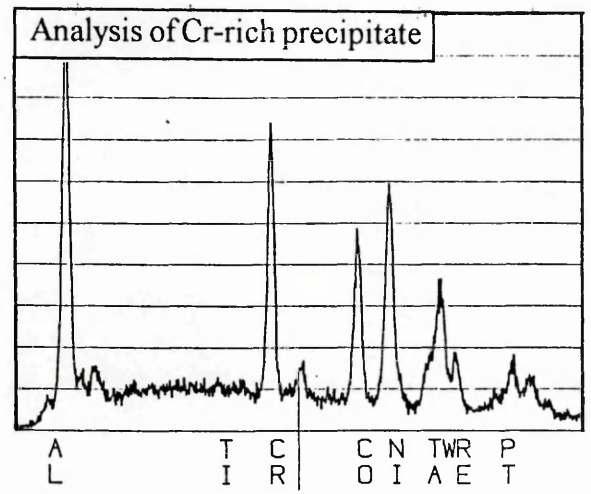


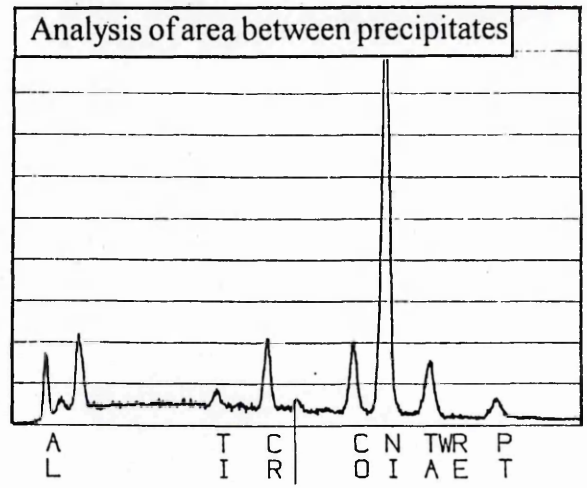


Figure 10.14- Coating C, aged for 25h at 1170°C. Micrographs of the interdiffusion zone.

Chapter 11- Results

# The Design and Optimisation of a Platinum enriched CMSX-4 bondcoat for TBC systems

## 11.1 Introduction

The future demands of TBC systems for turbine blades in aero-gas turbines may not be met by the use of traditional diffusion and MCrAlX bondcoats. Considerations, such as coating thickness, weight and cost, mean that there is a need for the development of novel bondcoat systems. These requirements may be met by utilising the beneficial properties of platinum. The benefits of platinum in an aluminide system are well known, with the improvement of the coatings adhesive properties due to the selective oxidation of aluminium and the blocking of the outward diffusion of damaging elements. This study, however, assessed the potential benefits of a bondcoat system formed simply by the diffusion of platinum into a CMSX-4 substrate.

## 11.2 Experimental

Initially, to assess the effects of substrate composition on the adhesion of a TBC, a ceramic topcoat was deposited by EB-PVD onto C1023, MarM002, CMSX-4 and Alloy RR superalloy sample pins. The samples were manufactured at Chromalloy UK Ltd. To assess their adhesion, the systems were thermally cycled to failure at 1135°C.

A range of platinum/CMSX-4 systems were produced by varying both the as-plated platinum thickness and the diffusion temperatures (Table 11.1). A PSYZ

ceramic layer was then deposited using EB-PVD. The samples were manufactured at Chromalloy UK Ltd.

The coatings were assessed by isothermal soaks for 25 hours at 1100, 1150, 1170, 1190 and 1210°C and thermal cycling at 1135°C. The systems adhesion was ranked using the modified scratch test and they were analysed using XRD, SEM and optical techniques.

## 11.3 Analysis

### *11.3.1 Thermal cycling of the superalloy/ceramic systems*

To assess the effects of superalloy composition on the adherence of the ceramic topcoat, the systems were thermally cycled to failure at 1135°C. The results are shown in Figure 11.1.

### *11.3.2- Optical analysis of the platinum/CMSX-4 systems*

The as-processed coatings were prepared in section and optically assessed. This revealed that the coatings had a two phased structure, the light phase coarsening at the interface with the substrate. The average thickness of the coatings varied with processing conditions, between 7 - 24 μm, as shown in Table 11.2.

### *11.3.3 Probe analysis*

The coatings, in the as-processed condition , were prepared in section and analysed using quantitative micro-probe analysis. Examples of the samples are shown in SEM micrographs, Figures 11.2 to 11.5. No distinction could be made between the two phases formed in coating A; the level of Ni ranged between 44 to

45 wt%, Pt between 26 to 29 wt% and Al between 4.0 to 4.6 wt%. However, as the contrast of the backscattered image relates to the atomic number of the elements present, this may imply that the 'light' phase contained a higher level of Pt compared to the 'dark' phase. Analysis of coatings D, E and F revealed that the 'dark' phase near the ceramic interface had a relatively high concentration of Pt and a low concentration of Ni (Table 11.3- composition (1)). For coatings B and C, the outer 'dark' phase contained a relatively higher concentration of Ni and low concentration of both Pt and Al (Table 11.3- composition (2)). In general, the 'light' phase, compared to composition (2), contained lower levels of Cr, W, Mo, Re and Ta, and higher levels of Al and Ti (Table 11.3- composition (3)).

*11.4 XRD analysis*

A selection of the coatings in the as-processed condition were analysed using XRD. Analysis of coating C revealed that the system had a $\gamma/\gamma'$ structure (Figure 11.6). From the SEM analysis (Table11.3), the phases can be further identified due to the preferential partitioning of elements. The 'light' phase (composition 3) contained relatively higher concentrations of Al and Ti, which would indicate a $\gamma'$ phase. The dark phase contained higher levels of Cr, W, Mo, Ta and Re, indicating a $\gamma$ phase. Analysis of coatings D, E, and F showed that the systems contained a phase not previously reported in the literature. This new phase, given the nomenclature 'O', was found to be isostructural with the orthorhombic phase $NiGePt_2$. (Figure 11.7). The significance of the 'O' phase will be discussed in detail in chapter 12. A schematic of these coating structures is presented in Figure 11.8.

*11.3.5 Modified Scratch Test*

The adhesion of the coating systems in the as-processed and aged conditions was assessed using the modified scratch test. These results are shown in Figure 11.9 and indicate that coatings B, C and D outperform RT22LT. In light of these results and the XRD data, further analysis concentrated on these more diffuse coatings and in particular coating C.

*11.3.6 Analysis of the isothermally aged samples*

SEM examination of the aged coatings in section revealed that the coating thickness did not increase after thermal exposure, however the $\Upsilon'$ phase was observed to have coarsened (Figure 11.10). Thickness measurements of the oxide formed by the aged coating C are shown in Figure 11.11.

Quantitative micro-probe analysis was undertaken on various samples of coating C, which had been aged for 25h at 1100, 1150, 1170 and 1190°C. The areas from which data was collected are shown in Figure 11.12. The results are displayed in Table 11.4. Trends in the diffusion behaviour of the coating were that, with thermal exposure, the level of Ti, Ta and Al increased in the $\gamma$ phase, but only slightly increased in the $\gamma'$ phase. The level of Pt was found to decrease in both the $\gamma'$ and $\gamma$ phases, indicating the inward diffusion of this element.

*11.3.7 Thermal cycling*

Three samples of coating C were cycled to failure at 1135°C. The results are shown in Figure 11.13 and indicated a consistent improvement over RT22LT. SEM analysis of the samples in section revealed similar characteristics to those that had

been isothermally aged, with the coarsening of the $\gamma'$ phase and little increase in the coating thickness (Figure 11.14). Similarly, quantitative probe analysis demonstrated that outward diffusion of Ti and Ta occured and inward diffusion of Pt as a result of the thermal exposure (Table 6.5.5). SEM analysis of the exposed coating interface after failure indicated how failure had occurred. This was at the oxide/coating interface. The majority of the oxide had spalled off with the ceramic, leaving only isolated islands of alumina, and occasionally, the PYSZ ceramic attached to the bondcoat surface. The smooth faceted pits previously observed on diffusion coatings (chapter 10), were not found on the surface of this coating. This suggests that the outward diffusion of Ti and Ta had been impeded by the coating, lessening their damaging effect on scale adherence.

After ceramic failure, the bondcoat should still be capable of affording a turbine blade a degree of environmental protection. To determine the effectiveness of the development coating system in this scenario, a sample pin of coating C was continued to be thermal cycled after ceramic spallation. After 586 cycles, these samples were prepared in section (Figures 11.15 and 11.16) and analysed using quantitative micro-probe analysis. There was little compositional change or further degradation noted and there were no noticeable differences between the spalled areas and those where the ceramic was still attached. This highlighted the overall stability of the coating and its potential for use as an environmental coating as well as a bondcoat.

11.4 Assessment of double-layer platinum systems

The effectiveness of the single layer platinum systems appeared to be due to the 'tieing-up' of damaging elements, such as Ti, in the coatings γ/γ′ structure and so preventing their diffusion to the oxide interface. The aim of the double layer system was to form a stable γ/γ′ diffusion barrier and then produce an outer layer containing a lower concentration of these damaging elements. Three systems were investigated. For each of the systems the initial layer was formed by a 7μm Pt layer , diffused for 1h at 1150°C in an attempt to form the γ/γ′. The second layer was a 5μm Pt layer diffused for 1h at either 900, 1000 or 1100°C. The systems were analysed using XRD in the as-processed condition, This revealed that the coatings diffused at 900 and 1000°C had an outer layer comprising of 'O' and γ phases, whilst the coating diffused at 1100°C had a γ/γ′. This was to be expected due to the greater inward diffusion of Pt.

The coating systems were isothermally aged for 25h at 1100, 1150, 1175, 1190, and 1210°C. The modified scratch test was used to gauge the adherence of both the as-processed and the aged coatings. The results are shown in Figure 11.17 and demonstrate that the double-layer systems did not perform as well as the single-layer coatings. This may have been due to the benefits of the single Pt layer system being lost due to an 'over diffused' composition for the double Pt layer systems or a too high concentration of Pt in the outer surface from the double deposition. Therefore, further work on these systems was curtailed.

## 11.5 Summary

The enrichment of the surface of CMSX-4 with platinum has produced an effective bondcoat. The more diffuse of these coatings have a $\gamma/\gamma'$ structure. The thicker, less diffuse coatings also contain a previously unreported 'O' phase, which is isomorphous with the phase $NiGePt_2$. The coating system appears to lessen the detrimental effects of elements such as Ti by minimising the diffusion of refractory metals to the bondcoat/oxide interface. The superior performance of these coatings was demonstrated using the modified scratch test and by thermal cycling at 1135°C. The attempt to further improve on this diffusion barrier effect by depositing the platinum in two subsequent layers was found to be ineffective. An in-depth analysis and assessment of the coating system follows in chapter 12.

| Pt thickness (microns) | Diffusion Temperature (°C) | | | |
|---|---|---|---|---|
| | 1000 | 1100 | 1150 | 1190 |
| 3 | Coating F | Coating G | Coating A | Coating H |
| 7 | | | Coating B | |
| 10 | | | Coating C | |
| 12 | | | Coating D | |
| 17 | | | Coating E | |

Table 11.1- Matrix of coating systems

| Coating System | Average thickness (microns) |
|---|---|
| A | 7 |
| B | 16 |
| C | 20 |
| D | 20 |
| E | 24 |
| F | 22 |
| G | 24 |
| H | 23 |

Table 11.2- Coating thickness, in the as-processed condition

| Elements | Weight % | | |
|---|---|---|---|
| | Composition (1) | Composition (2) | Composition (3) |
| Pt | 79 | 48.6 | 53.7 |
| Ni | 12.6 | 29.7 | 29.5 |
| Al | 3 | 0.8 | 2.5 |
| Ti | 0.11 | 0.3 | 1 |
| Co | 2.3 | 2.75 | 4.8 |
| Cr | 2.7 | 1.2 | 0.35 |
| Re | Trace | 2.6 | 1.6 |
| W | Trace | 0.5 | 0.2 |
| Mo | Trace | 6.7 | 3.6 |
| Ta | Trace | 6.9 | 3 |

Table 11.3- Representative compositions of the phases present in the coating, in the as-processed condition

| Element | Weight % | | | | | | | |
|---|---|---|---|---|---|---|---|---|
| | 25h @1100°C | | 25h @1150°C | | 25h @1170°C | | 25h @1190°C | |
| | Dark phase | Light phase | Dark phase | Light phase | Dark phase | Light phase | Dark phase | Light phase |
| Cr | 8.69 | 2.1 | 8.53 | 2.09 | 8.14 | 2.05 | 8.57 | 2.21 |
| Co | 8 | 3.29 | 8.06 | 3.62 | 7.77 | 3.88 | 8.68 | 4.45 |
| Mo | 0.69 | 0.06 | 0.62 | 0.08 | 0.62 | 0.1 | 0.72 | 0.05 |
| W | 4.69 | 1.97 | 5.38 | 2.08 | 5.92 | 2.15 | 6.66 | 2.43 |
| Re | 1.83 | 0.24 | 2.88 | 0.34 | 3.13 | 0.25 | 3.43 | 0.46 |
| Al | 2.32 | 4.84 | 2.59 | 4.98 | 2.73 | 4.94 | 3.07 | 5.53 |
| Ti | 0.5 | 1.48 | 0.58 | 1.61 | 0.62 | 1.67 | 0.7 | 1.73 |
| Ta | 2.29 | 6.74 | 3.04 | 7.63 | 3.16 | 7.88 | 3.6 | 8.31 |
| Ni | 39.1 | 35.29 | 39.7 | 36.4 | 39.29 | 36.54 | 42.64 | 42.09 |
| Pt | 32.35 | 43.98 | 28.47 | 42.4 | 25.9 | 39.59 | 20.56 | 32.65 |

Table 11.4- Phase compositions of coating C, after isothermal soaks

| Element | Weight % | | | | | |
|---|---|---|---|---|---|---|
| | 156 Cycles @ 11358C | | 236 Cycles @ 1135°C | | 342 Cycles @ 1135°C | |
| | Near surface | Inner Coating | Near surface | Inner Coating | Near surface | Inner Coating |
| Cr | 4.82 | 2.25 | 10.3 | 2.23 | 10.55 | 2.3 |
| Co | 7.34 | 4.75 | 10.12 | 4.7 | 10.55 | 5.1 |
| Mo | 0.53 | 0.14 | 0.85 | 0.12 | 0.83 | 0.17 |
| W | 5.14 | 3.09 | 6.5 | 2.7 | 7.02 | 3.1 |
| Re | 2.05 | 0.51 | 4.5 | 0.41 | 5.01 | 0.56 |
| Al | 5.13 | 5.97 | 2.66 | 5.62 | 2.89 | 5.76 |
| Ti | 0.96 | 1.32 | 0.58 | 1.67 | 0.54 | 1.58 |
| Ta | 6.82 | 8.35 | 2.41 | 8.02 | 2.56 | 8.28 |
| Ni | 50.61 | 44.07 | 52.39 | 44.42 | 44.82 | 46.5 |
| Pt | 18.09 | 28.38 | 7.29 | 31.49 | 16.4 | 26.79 |

Table 11.5- Phase compositions of coating C, after thermal cycling at 1135°C

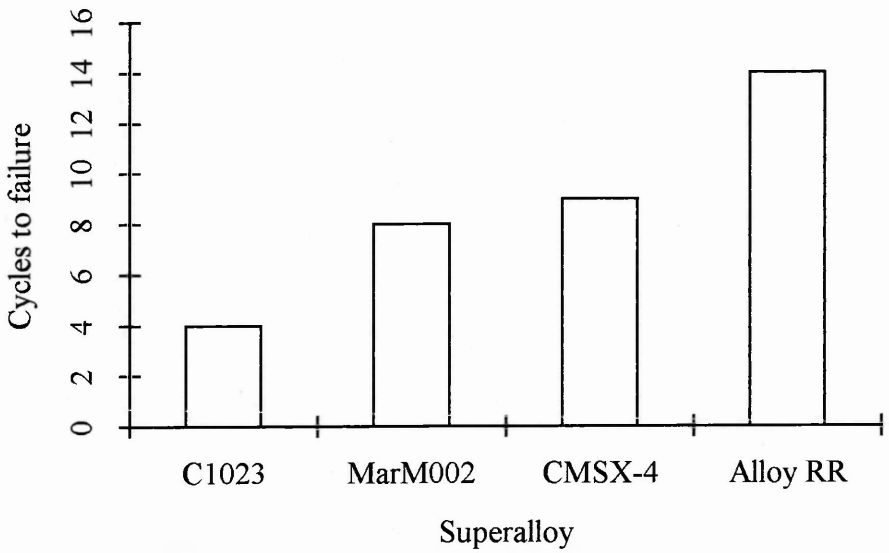


Figure 11.1- Cyclic life of the superalloy/ceramic systems at 1135°C

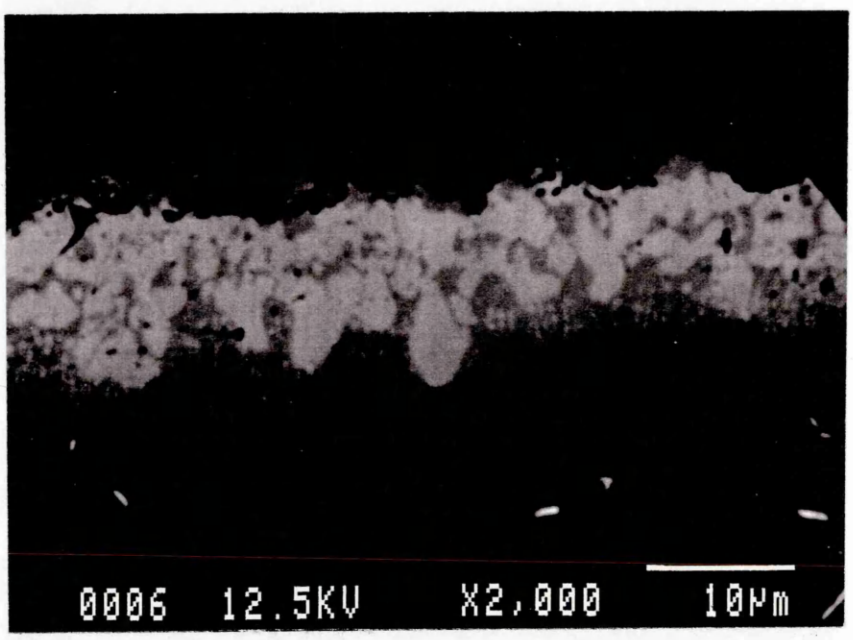


Figure 11.2- Coating A, as-processed, in section

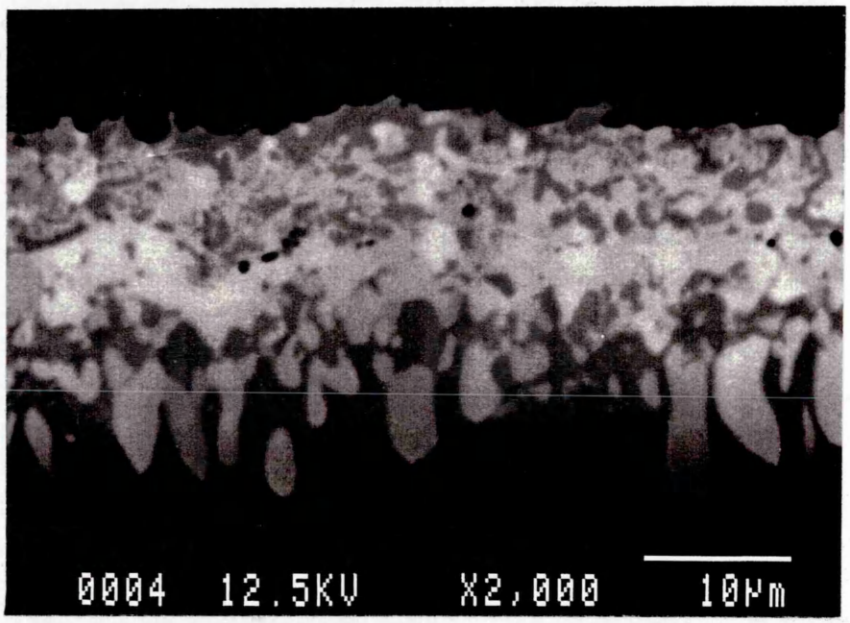


Figure 11.3- Coating B, as-processed, in section

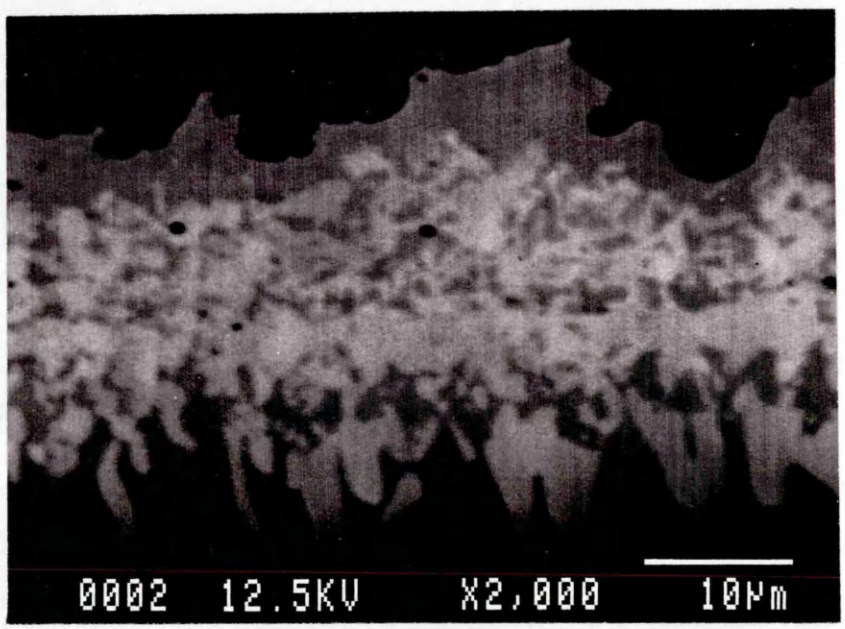


Figure 11.4- Coating C, as-processed, in section

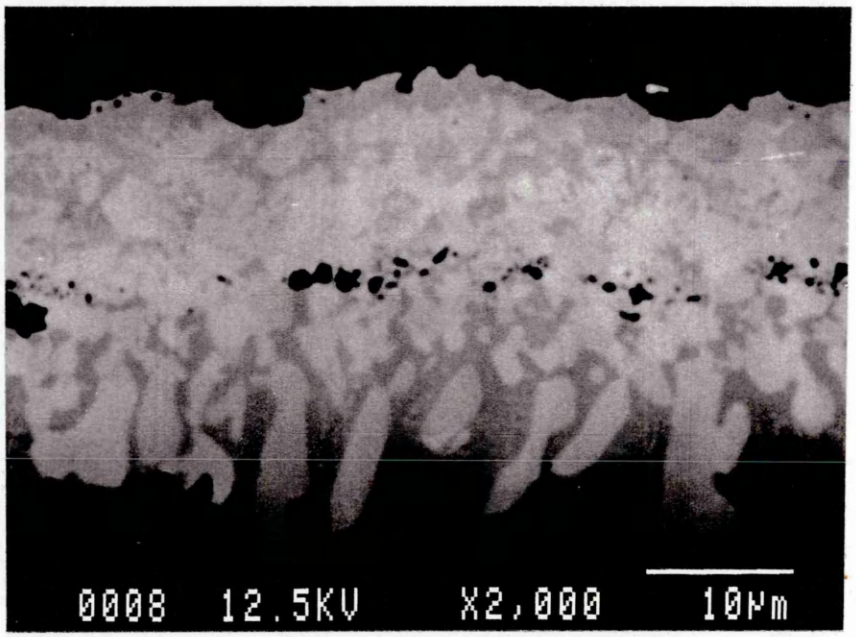


Figure 11.5- Coating D, as-processed, in section

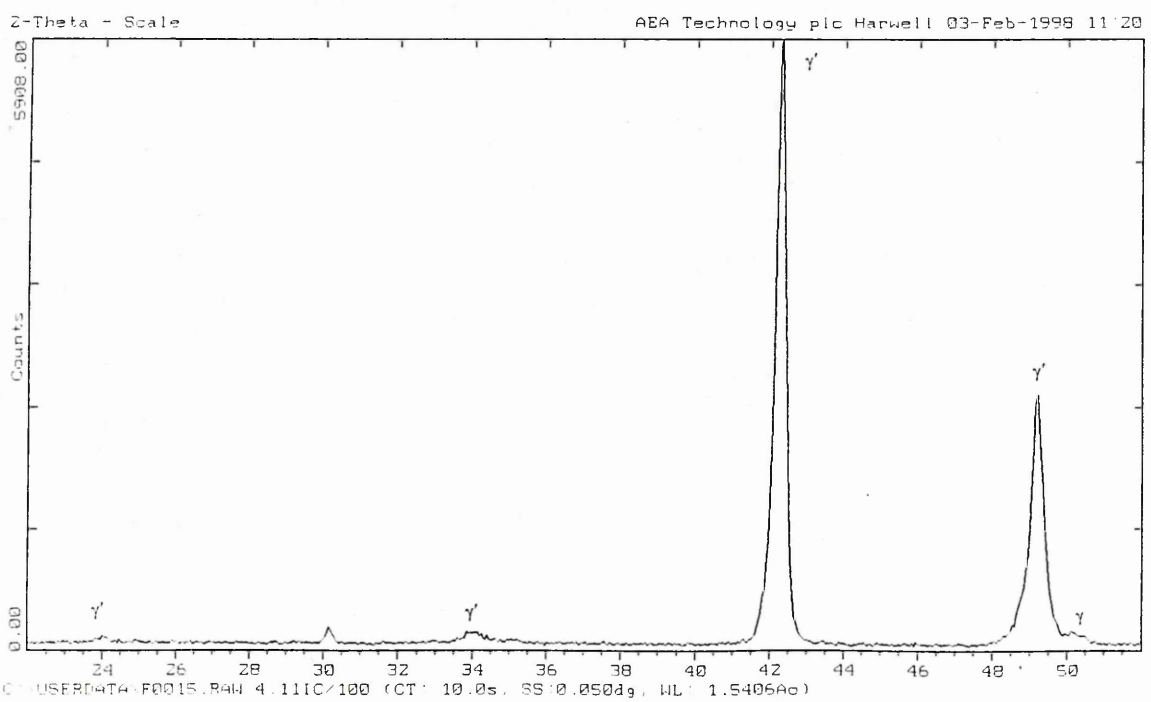


Figure 11.6- XRD analysis of coating C, as-processed

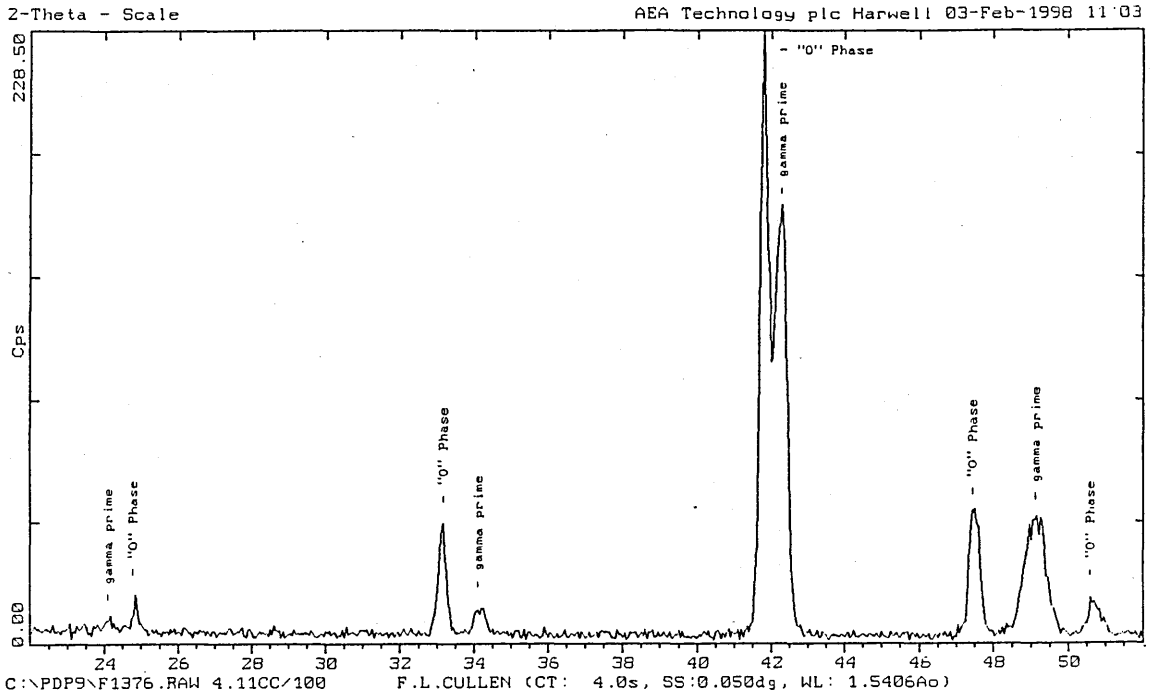


Figure 11.7- XRD analysis of coating D, as-processed

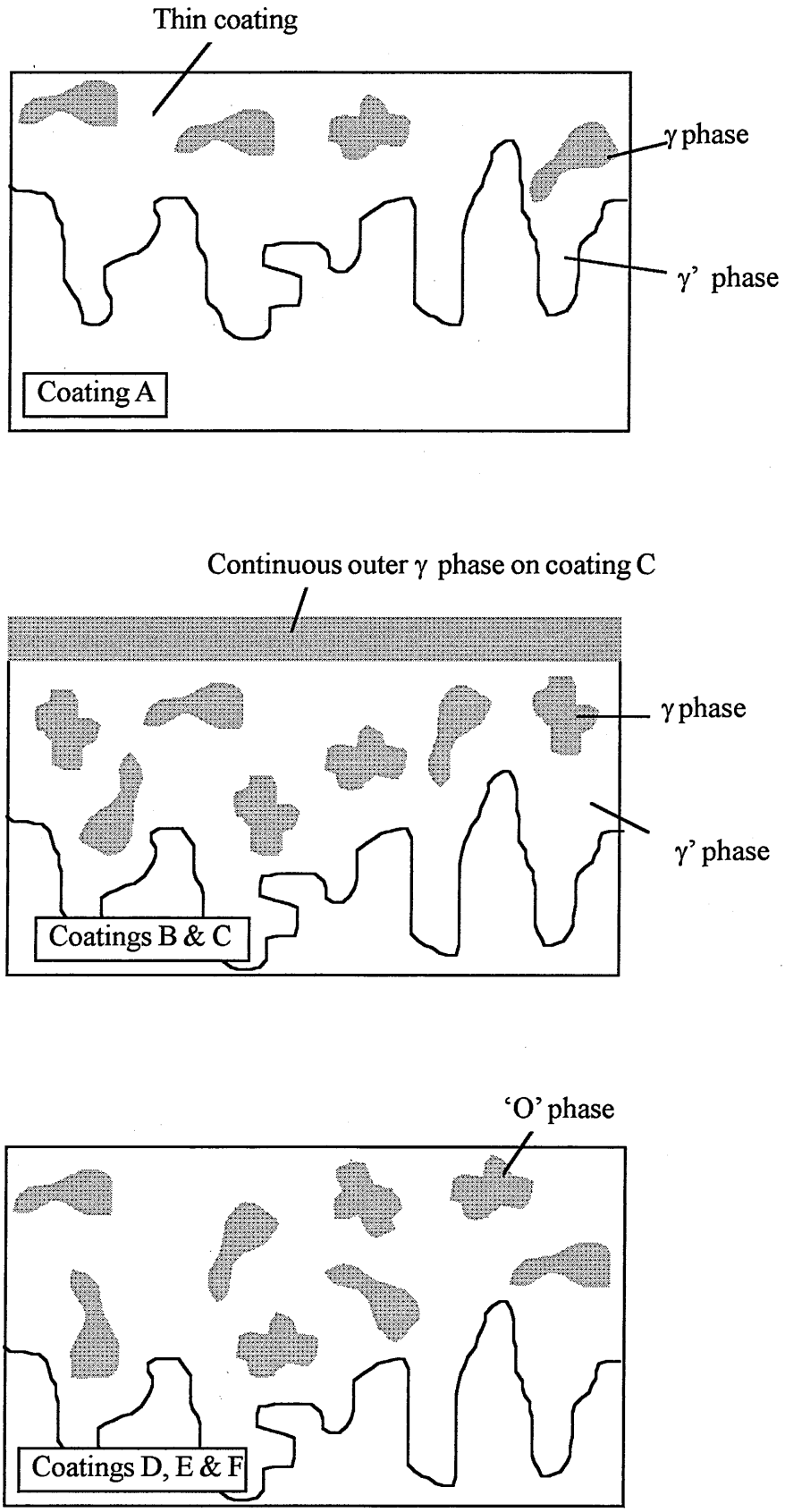


Figure 11.8- Schematic diagram of the coating structures

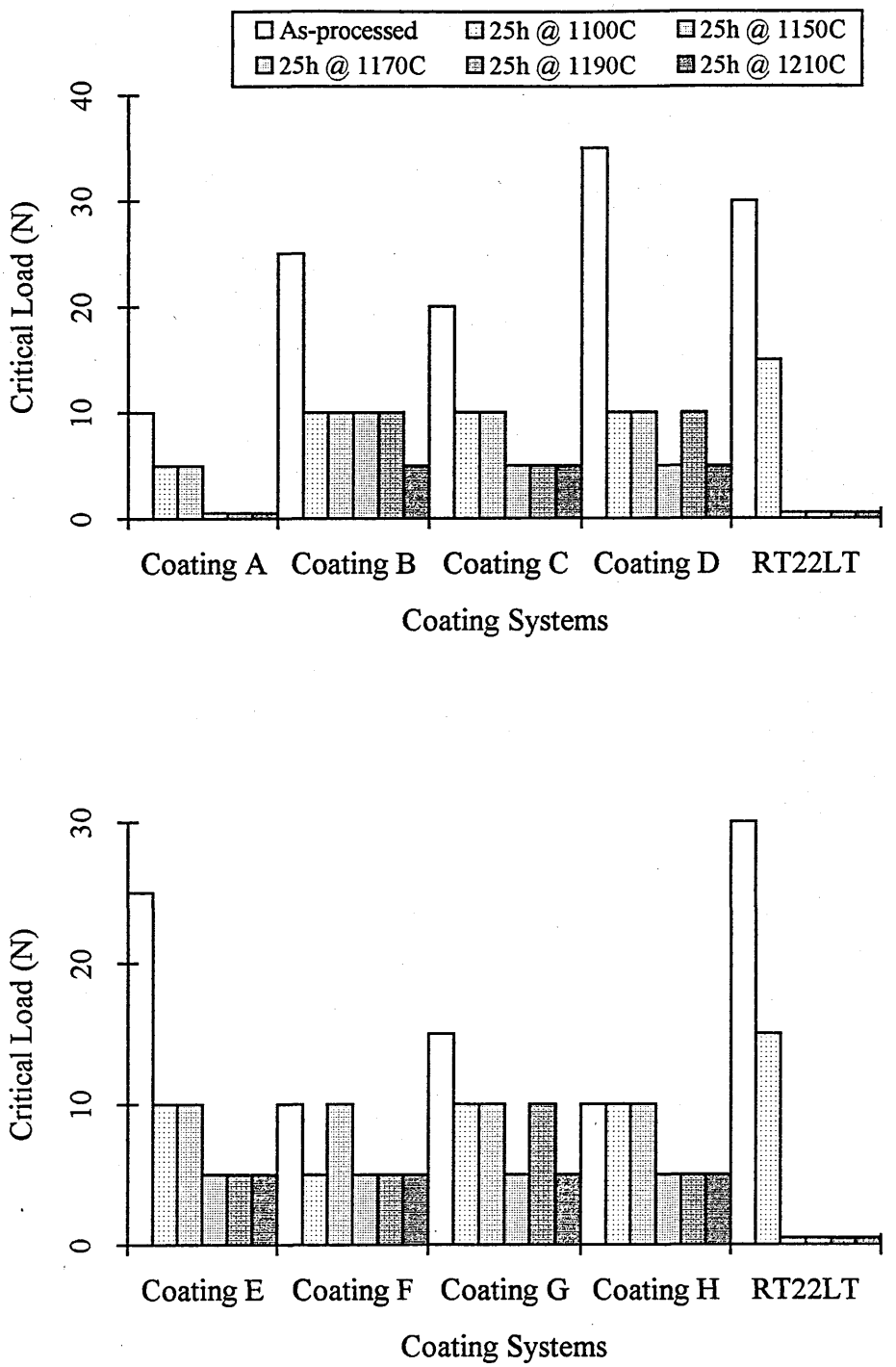


Figure 11.9- Modified scratch test results

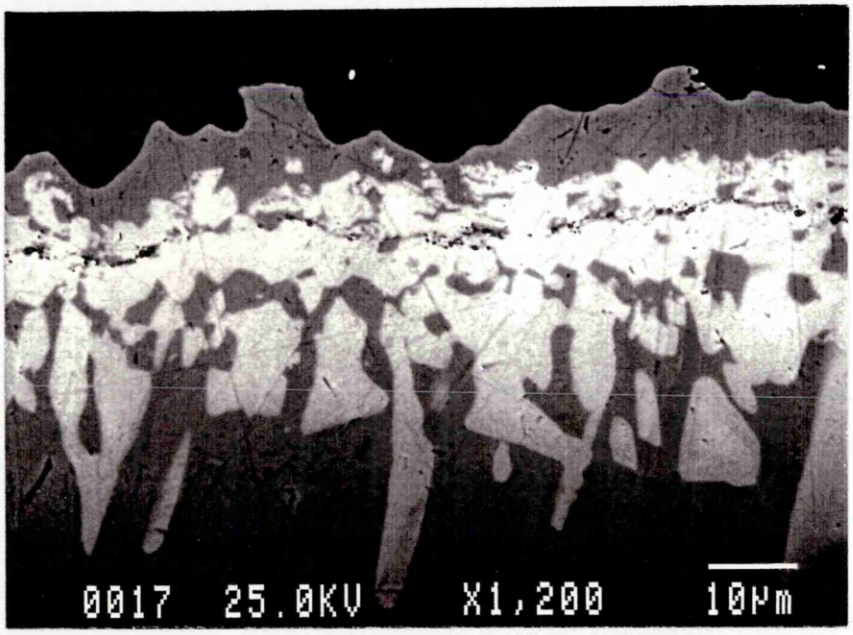


Figure 11.10- Coating C, aged for 25h at 1150 ° C

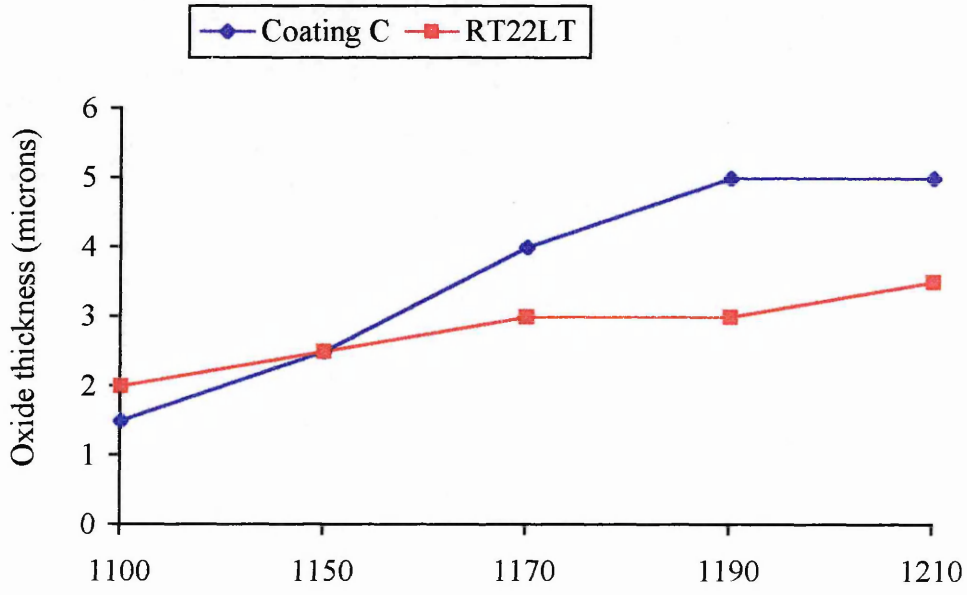


Figure 11.11- Oxide thickness measurments

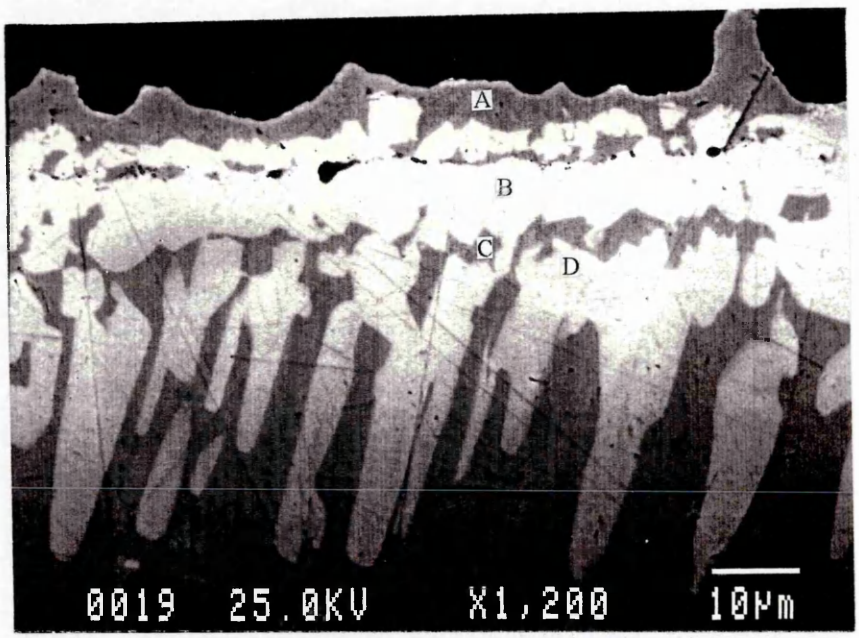


Figure 11.12- Coating C, aged for 25h at 1190 ° C, in section. Areas of analysis are marked A to D

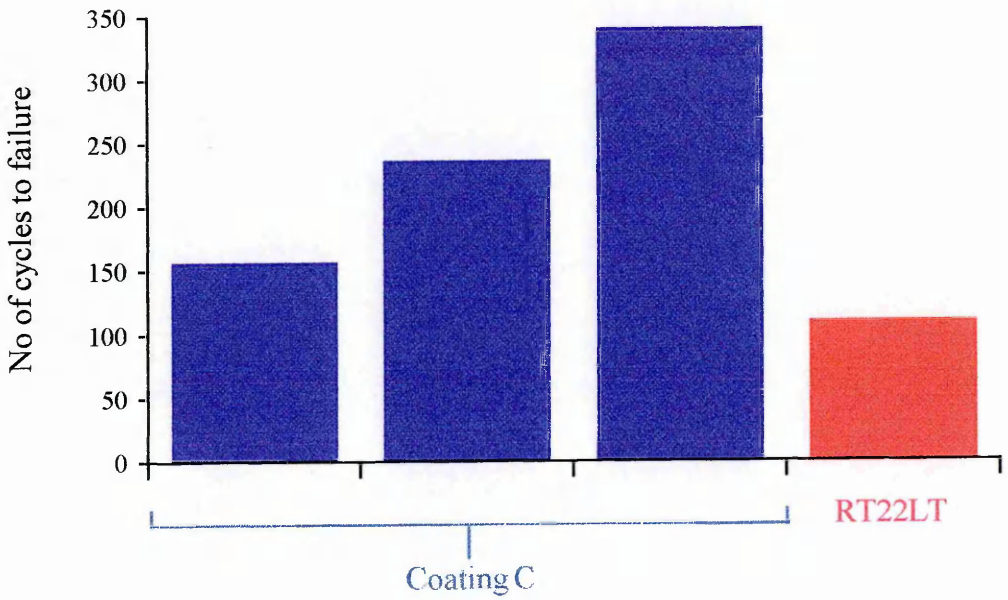


Figure 11.13- Cyclic life of coating C at 1135 ° C

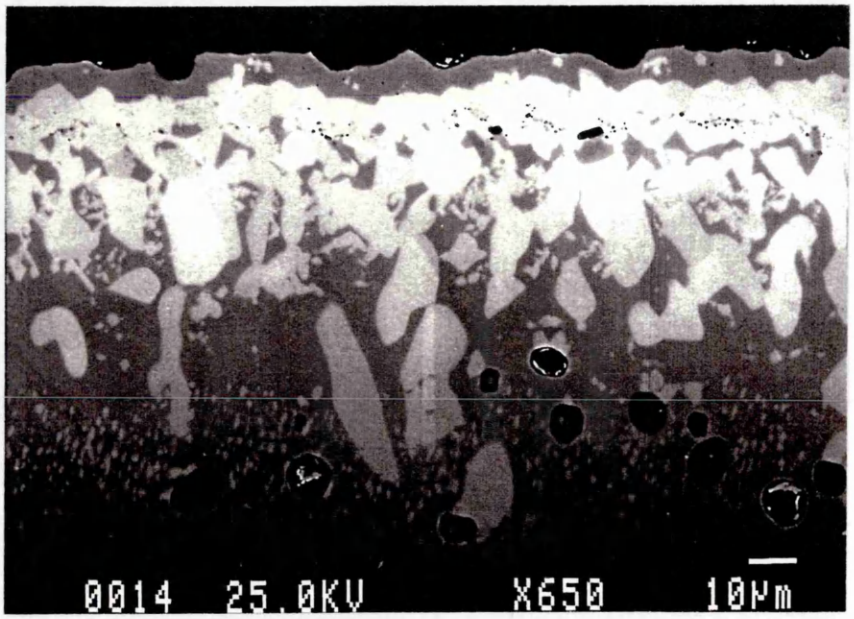


Figure 11.14- Coating C, 236 cycles at 1135°C

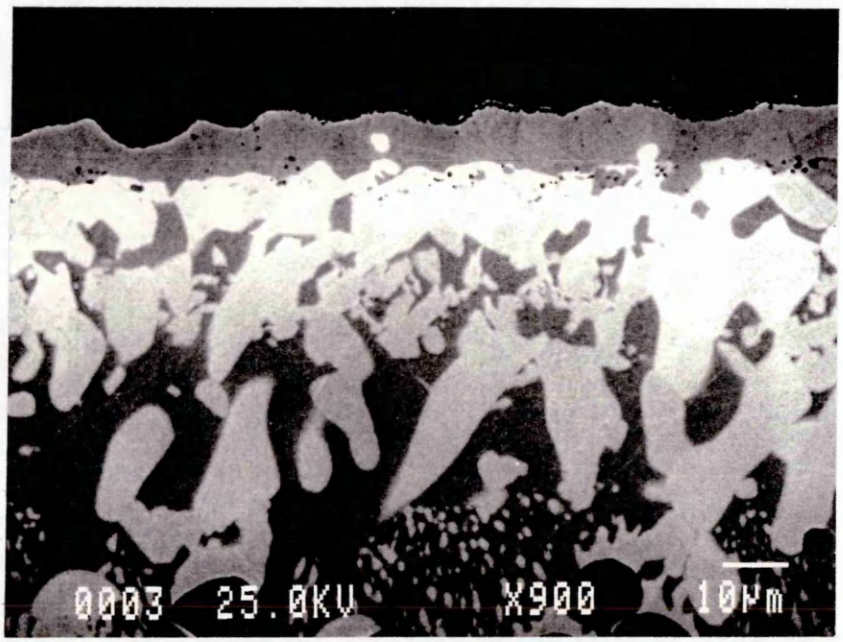


Figure 11.15- Coating C, 586 cycles, spalled area

Figure 11.16- Coating C, 586 cycles, ceramic attached

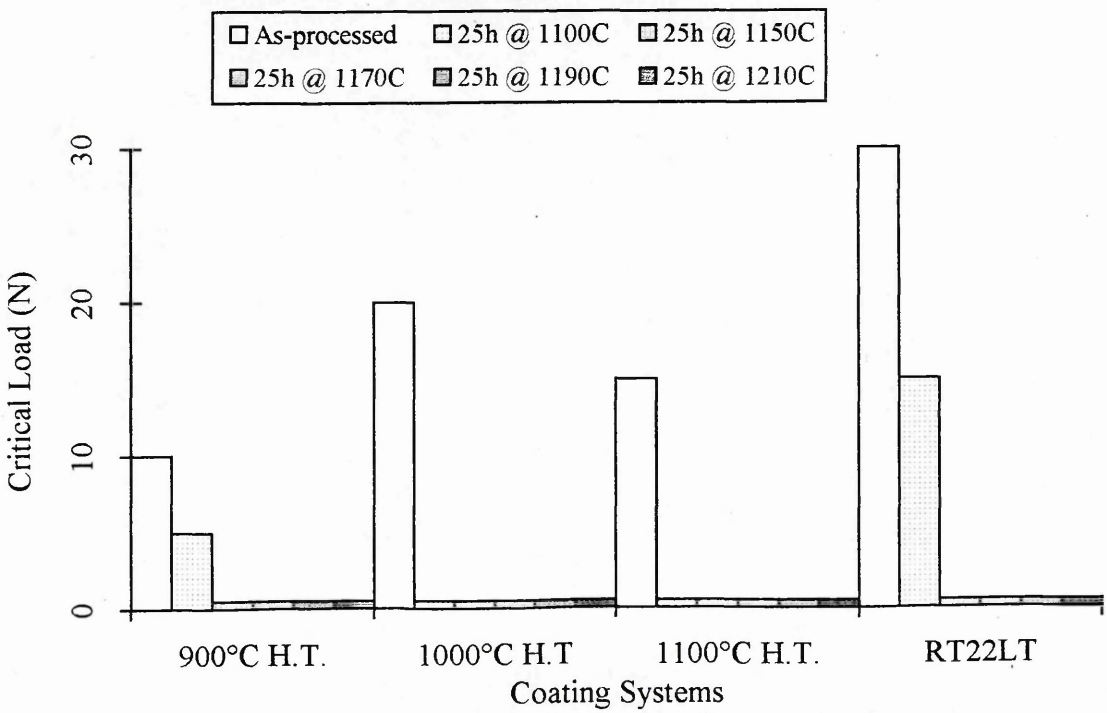


Figure 11.17- Modified scratch test results for the double layer systems

# DISCUSSION

Chapter 12

# Discussion

## 12.1 Introduction

Various research programmes were undertaken to optimise the stability of the bondcoat oxide, first by the use of pre-treatments then through optimising the design of the bondcoat. This chapter will review the results achieved, discuss them with respect to current thinking as reported in the literature and hence, determine the effectiveness of the various approaches.

## 12.2 The Effects of Pre-oxidation

A programme of work was undertaken to assess the claims in published literature [72 → 76] that pre-oxidation treatments were beneficial , extending the life of a TBC system. In chapter 7, the effects of two pre-oxidation atmospheres were gauged by pre-oxidising a RT122/MarM002 system in an Ar-20%$O_2$ or a $H_2$-10%$H_2O$ atmosphere. The effects of the pre-treatments were assessed using the techniques described in chapter 6.

The β-depletion measurements of the aged pre-treated systems failed to show any differences between the two pre-oxidation atmospheres. This indicates that both the $H_2$-10%$H_2O$ and the Ar-20%$O_2$ treated samples consume aluminium at similar rates to produce a protective oxide.

Both SEM and XRD analysis of the surfaces of the samples in the as-processed condition confirmed that the coating pre-oxidised in the Ar-20%$O_2$ atmosphere had produced a mixed oxide containing both alumina and Ni, Co and Cr

rich spinels. Whether the spinels were concentrated at either of the scale interfaces or were distributed through out the oxide however, was not determined. The coating pre-oxidised in the $H_2$-10%$H_2O$ atmosphere had grown the desired α-alumina based oxide. SEM analysis revealed the presence of transitional aluminas within the oxide (identified by their morphology and EDX analysis). However XRD analysis could not identify their phase composition.

Upon ageing, the concentration of spinels in the oxide for the Ar-20%$O_2$ treated samples was found to have increased. Similarly, the oxide formed by the $H_2$-10%$H_2O$ treated sample became contaminated with transition metal spinels, the concentration of which increased with time at temperature. Thus, although initially forming a continuous alumina scale and offering the potential of improved protection, the formation of these transition metal spinels means that the protection offered by this $H_2$-10%$H_2O$ also eventually breaks down. The transitional aluminas observed on the as-processed surface were not found within the scale formed on the aged samples. This is due to the transformation of the outwardly grown aluminas to α-alumina. as expected from reports in the literature [36]. Cracking of the oxide, due to the volume changes induced by the transformation were not observed and it is assumed that they had been 'self-healed' by the coating.

By using the conventional scratch test, spallation was induced in the oxide formed on these aged samples. Analysis of the damaged areas has shown that failures were either associated with the presence of transition metal oxides or were cohesive failures within the alumina. No differences were noted between the type or quantity of damage induced on either of the pre-treated samples. However, SEM analysis of the oxides formed after 100h at 1100°C, (when the β phase within the

coatings was completely depleted), showed that the Ar-20%$O_2$ treated sample suffered a higher level of spallation than the equivalently exposed $H_2$-10%$H_2O$ treated sample. The lower adherence of the scale formed by the Ar-20%$O_2$ treated coatings is thought to be due to the higher concentration of transition metal spinels, that formed within the oxide in an Ar-20%$O_2$ environment. This supports the commonly reported belief that the incorporation of spinels within an alumina scale is detrimental, as they act to lower the adhesion of the scale and foreshortening the life of the coating [64 → 66] (chapter 3). Thus, it has been demonstrated that the Ar-20%$O_2$ pre-oxidation atmosphere is not successful in promoting a more adherent oxide scale and so was considered an ineffective pre-treatment for the RT122/MarM002 system, contrary to reports in the literature [72].

The $H_2$-10%$H_2O$ pre-oxidation atmosphere however, displayed some initial potential benefits by promoting an α-alumina based oxide. Even though, after isothermal exposure, the scale became contaminated with undesirable spinels, the oxide still appeared to be more adherent than that formed by the Ar-20%$O_2$ atmosphere and so was considered the more effective of the two pre-treatments.

The possible benefits from pre-oxidation were further investigated in chapter 9. This programme assessed the merits of either ex-situ pre-oxidation in a $H_2$-10%$H_2O$ atmosphere or in-situ pre-oxidation using a variety of Ar-based atmospheres, on increasing the adherence of a TBC system.

In this part of the study, a wide range of diffusion and MCrAlX bondcoats were examined using an ex-situ pre-oxidation treatment, prior to the deposition of a ceramic topcoat. The RT122 and RT22LT systems (being representative of both MCrAlX and diffusion coatings respectfully) were examined in section in the as-

processed and aged conditions. Both the compositional changes in the coatings and the thickness of the oxide scales were comparable to untreated systems. This indicated that the pre-treatment had neither altered the oxide growth mechanism nor the rate of scale formation.

The modified scratch test was employed to gauge the adhesion of the treated systems in the as-processed and aged conditions (Figure 9.7). The results revealed that the ex-situ pre-oxidation treatment provided no measurable benefit and infact may have been detrimental to the adhesion of the TBC for some systems. Therefore, the initial benefits observed for the $H_2$-10%$H_2O$ atmosphere in chapter 7 were not realised for fully processed TBC systems and this has demonstrated that the pre-treatment in Ar-20%$O_2$ and $H_2$-10%$H_2O$ environments are ineffective as methods of improving TBC adhesion.

The use of in-situ pre-oxidation treatments were assessed using an MCrAlX bondcoat, RT122, on a MarM002 substrate. The range of atmospheres used were designed to either clean the surface of the coating and then establish an oxide, or to simply establish an initial oxide layer. After being processed, the TBC systems were aged for 100h at 1100°C. The examination of the coatings in section revealed that there was little to differentiate between the pre-treated and untreated coatings, both having comparable rates of β depletion and producing oxides of similar thickness. This indicated that the in-situ pre-oxidation treatments had not altered the rate of aluminium consumption to form an oxide. Again the modified scratch test was used to assess the adherence of the ceramic top coat to these coatings (see Figure 9.8. The more effective of the pre-treatments appeared to be those that both cleaned the surface and promoted an oxide to grow. As atmospheres D and F, which only either

cleaned the surface (D) or only promoted an oxide to grow (F), were both shown to have lower adhesive values. However, as both the pre-treated and the untreated systems had failed after 100h at 1100°C, it was concluded that the in-situ pre-oxidation treatments provided insufficient improvment to the adhesion of the TBC systems.

The results achieved in this research programme differ from those reported in the literature (section 4.2). Lih et al [72] reported a two fold increase in the performance of a pre-oxidised (in air) NiCrAlY bondcoat, claiming this was due to the establishment of an α-alumina film and the subsequent decrease in the oxidation rate of the bondcoat. However, neither the air equivalent atmosphere (Ar-20%$O_2$) or the $H_2$-10%$H_2O$ atmosphere affected the performance of the RT122 bondcoat, neither were found to alter the oxidation rate of the coating. This difference in performance may be due to a number of reasons. Firstly, the TBC system pre-oxidised by Lih et al was produced by depositing the ceramic layer by APS, where as the systems evaluated by this programme comprised of ceramics deposited by EB-PVD. The differing morphology and adherence modes produced by the two deposition techniques, (see chapter 3), may have affected the relative performance of the various pre-oxidised treatments studied. Secondly, Lih et al assessed the oxidation resistance of their system at 1050°C whereas in this study, the Ar-20%$O_2$ and $H_2$-10%$H_2O$ atmospheres were evaluated at temperatures up to 1150°C. It is possible that any benefits endowed by the pre-oxidation treatment were rendered ineffective by exposure to these more severe conditions. Lastly, Lih et al deposited their bondcoat onto a MarM247 substrate, as opposed to MarM002. However, it is unlikely that the use of MarM002 had a life-limiting effect on the performance of the

bondcoat when compared to MarM247 and it is the authors opinion that the most probable cause for these observed differences reflects the difference in oxidation kinetics at 1050 compared with 1150°C and the differing natures of the ceramic layers.

Lih et al [76] also reported a six to eight fold increase in performance due to the pre-oxidation and aluminising of the bondcoat. However, in chapter 9, the pre-oxidation of a Coating B/RT22LT system was assessed and found not to have had a significant effect on the lifetime of the TBC. Again, this may be due to the harsher test conditions used in this study, coupled with the use of an EB-PVD ceramic layer.

To summarise, an extensive programme was undertaken to assesses the performance benefits of an Ar-20%$O_2$ and a $H_2$-10%$H_2O$ pre-oxidation atmosphere. By testing both in- and ex-situ treatments on a wide range of MCrAlX and diffusion coatings, it was revealed that, although the formation of an initial $\alpha$-alumina film could be achieved, after prolonged isothermal soaks, neither pre-treatment was found to have extended the life time of the TBC systems when exposed at temperatures of 1050°C and above. These results differ from those previously reported in literature due to the harsher test conditions used in this study. The ceramic deposition conditions may have a secondary effect as the ceramic was applied by EB-PVD in this study, as opposed to APS. Also, the results demonstrate that the key to prolonging the life of a TBC does not wholly rely on the initial formation of an $\alpha$-alumina scale but equally, if not more important, is the maintenance of the integrity of the scale through the exclusion of such elements as Ni, Co and Cr. This will be discussed further in section 13.4.

13.3 The Effect of Gritting as a Surface Preparation

It is standard industrial practice to grit blast the surface of a bondcoat prior to ceramic deposition. This is carried out both to clean the surface and to provide a rough interface to aid the adhesion of the ceramic layer (especially ceramics applied by APS). The coldworking of the surface of chromia-forming alloys has been found to increase the number of fast diffusion paths (e.g. dislocations and grain boundaries) in the near surface of the alloy, so aiding outward diffusion of the scale forming elements [58, 77]. The transitional aluminas are formed onalumina forming coatings grow by the outward diffusion of aluminium. At temperatures greater than 1000°C these transitional aluminas transform to α-alumina. Therefore if the coldworking of the surface increased the formation of transitional aluminas and so aid the growth of a stable α-alumina film, gritting would be considered an effective pre-treatment.

The effect of gritting was assessed in chapter 7. Samples of a RT122/MarM002 system, were either gritted with 220 mesh alumina at 2.04 bar or left ungritted. The coatings were pre-oxidised and then isothermally soaked. β depletion measurements of the aged coatings could not discern any difference between the gritted and ungritted systems (Figure 7.2). This indicated that gritting of the surface had not significantly altered the rate of aluminium consumption or scale growth. Similarly, SEM and XRD analysis revealed there was little difference in either composition or adherence of the oxide produced by either gritted or ungritted coatings. For example, the gritted and ungritted coatings pre-oxidised in the $H_2$-10%$H_2O$ atmosphere were found to both have promoted an α-alumina scale in the as-processed condition, which, upon ageing, degraded in a similar manner, due to the growth of damaging spinels. Therefore, gritting must be considered a benign

pre-treatment, as the process of coldworking and cleaning the substrate did not have a significant effect on the composition of the oxide. As a ceramic layer was not deposited on top of these treated bondcoats, it is unclear whether the rougher interface produced by the pre-treatment would increase the adherence of the TBC. However, since the ceramic would have been deposited using EB-PVD (which results in the ceramic being chemically bonded to the bondcoat and not relying on a mechanical bond as with APS deposition), it is presumed that again, the pre-treatment would have acted in a benign manner.

## 13.4 The Effect of Bondcoat Composition on the Chemistry of an Oxide Scale

The optimum adhesion for an EB-PVD TBC system can be achieved by the promotion of a complete and slow growing α-alumina film. However, as demonstrated in section 13.2, the adherence of the oxide will decrease once substrate elements have diffused to the interface. Chapter 8 aimed to establish the role played by the oxide for TBC systems. Questions that were addressed were the effects of aluminium, platinum and hafnium contents and whether the oxide grown on an exposed bondcoat was identical to one grown at the interface with a PSYZ ceramic layer. These topics will be discussed in turn.

### 13.4.1 *The Effect of Aluminium Content*

The role of aluminium content was assessed by comparing the oxidation performance of RT122 (a low aluminium content MCrAlX coating) with Coating A (a high aluminium content MCrAlX coating). β depletion measurements revealed that in the as-processed condition. Coating A had a higher proportion of β phase and

unlike RT122, had not undergone any depletion. Similarly, after isothermal exposure, the Coating A suffered less β depletion than the RT122 coating. However, considering that Coating A contains a higher concentration of aluminium (and therefore β phase), these results were not unexpected.

The characterisation of the oxides produced by both coatings was carried out using SEM and XRD techniques. This revealed that after isothermal exposure, both of the coatings had produced α-alumina based scales that were contaminated with spinels. However, it was observed that the level of zirconia spallation was greater on Coating A than on RT122. These β depletion results are consistent with the expected behaviour that with a higher concentration of aluminium within the coating, Coating A should, potentially, have maintained an alumina scale for a longer period. However, after the exposures used in this study, the composition of the oxide was found to be similar to that of RT122 and from the level of spallation, it would appear, the adherence of the oxide on Coating A may have been lower. Therefore, the ability to maintain the integrity of an alumina scale does not rely on the aluminium activity of the coating, but is due to the diffusional processes during oxidation, even if the coating contains a relatively high concentration of aluminium, contamination of the oxide can still occur, which will act to affect the oxides adhesion.

### 13.4.2 *The Effect of Platinum*

The effect of the platinum content of the coating on oxide chemistry was assessed by comparing the performance of the basic aluminide RPS320 with the platinum aluminide RT22LT.

XRD analysis of the coatings in the as-processed condition revealed the presence of W within the alumina scale formed on the RPS320 coating (however, it was not determined whether the W was present as a metal, an intermetallic or oxide). The RT22LT coating was found to have promoted a pure α-alumina scale (Figure 8.9). Examination of the aged RPS320 coating in section revealed that elements, such as W and Ta, had diffused outwards from the interdiffusion zone to the oxide/coating interface. This outward diffusion was not as prevalent in the RT22LT coating, as evidenced by the lack of precipitates in the outer platinum rich phases. Analysis of the oxide scales confirmed that both W, Hf and Ta had become incorporated within the oxide grown on RPS320 and as indicated by the catastrophic failures induced by the scratch tester, the adhesion of the scale to this coating appeared to be weak. After exposure the oxide promoted by the RT22LT coating was found to be free from W, however XRD analysis identified the presence of Hf, although not in as great a quantity as with RPS320. The adhesion of the scale appeared to be higher on RT22LT, as only slight spallation was induced by the scratch test.

These results confirmed both the consensus of opinion, that platinum aluminides out perform basic aluminides (see chapter 4) and the assertion that the adherence of the oxide can be maintained by the exclusion of damaging elements. The superior performance attributed to platinum is due to a number of effects (see section 4.3).

1) The affinity of aluminium for platinum creates an aluminium reservoir in the outer portion of the coating [85]

2) Platinum promotes the selective oxidation of the aluminium, as aluminium is very mobile in the platinum aluminide phases, whilst other elements have to competitively diffuse relatively slowly to the oxide interface. Therefore, the platinum phases act as a barrier, impeding the diffusion of damaging elements.

The oxide produced by the basic aluminide, RPS320, was heavily contaminated with W which resulted in the poor adherence of the scale. The platinum rich phases within RT22LT were able to hinder the outward diffusion of such damaging elements and so maintain a more adherent scale. The degradation of diffusion coatings is discussed further in section 12.5.

After ageing, Hf was identified within the scale of both coatings. At an optimum level, Hf is thought to be beneficial, due to such active element effects as pegging, slowing short circuit diffusion etc, and it has been shown that the beneficial effects of platinum are heightened in the presence of Hf [106]. However, it has been observed in this study that extensive peg growth at the oxide interface can act to degrade the coating. As reported in Fisher et al [107], it was found that, during the oxidation of a RT22LT/MarM002 system at 1100°C hafnia-rich pegs were enveloped with alumina formed at the oxide interface. As oxidation progressed, the pegs grew outwards into the oxide and depleted the local area of aluminium. This induced stresses within the oxide and led to local spallation. The RT22LT coating was not as susceptible to Hf contamination as RPS320, however the platinum rich layers still did not effectively block the outward diffusion of this element. As Hf will preferentially diffuse along grain boundaries this acts to highlight the importance of coating morphology on coating performance, which is discussed at greater length in section 13.5.

13.4.3 *The Effect of Hf and Si additions.*

To assess the benefits of Hf and Si additions to a MCrAlX coating the oxidation performance of Coating B was compared to Coating A. Examination of the coatings in the as-processed condition in section revealed that both coatings had a similar proportion of β phase and neither coating had undergone any depletion. After ageing, both coatings underwent similar levels of β depletion. This indicated that the Hf and Si additions together do not alter the rate of aluminium consumption. Analysis of the oxides could not discern any significant differences between the scales promoted by either coating, as they both produced α-alumina based scales contaminated with transition metals. Therefore, the additions of Hf and Si to a MCrAlX coating were not considered to be beneficial in slowing the rate of aluminium consumption nor in helping maintain a stable alumina scale.

13.4.4 *The Effect of a Ceramic Topcoat*

It is common for investigations of oxide chemistry in TBC systems to be undertaken on exposed bondcoats, without the presence of a ceramic topcoat. To determine the effect of the ceramic on the chemistry of the scale, bondcoats investigated in chapter 8 were sputter coated with 2μm of zirconia. After isothermal ageing, the oxides formed were analysed using XRD. This revealed that the oxides formed beneath a ceramic layer were less contaminated with spinels, consistant with the topcoat acting to lower the partial pressure of oxygen at the ceramic/bondcoat interface, inhibiting spinel formation [29]. No differences were noted between high and low aluminium activity coatings, as both showed a reduction in the amount of spinel present. Therefore, studies of oxide chemistry conducted on exposed

bondcoats without a ceramic topcoat will give a harsher impression than would actually occur in a TBC system. This is not necessarily a bad situation, as it provides a conservative view of bondcoat behaviour, thus if a given 'exposed' bondcoat system is found to have particular benefits, those advantages could be excentuated with the application of a ceramic topcoat.

## 13.5 Summary of the Pre-treatment Studies

The investigations of pre-oxidation treatments showed that at best that they could be used to establish an initial α-alumina scale. Any advantages were short lived as, upon isothermal ageing, the scale soon became contaminated with spinels. This coupled with the investigation of bondcoat/oxide chemistry (section 13.4), signified that the ability to grow a pure alumina film did not nescessarily guarantee an adherent TBC system. As shown, through the comparison between RT22LT and RPS320 (section 13.4.2), of greater importance is the maintenance of the integrity of the scale by the exclusion of damaging elements. However, as highlighted by the presence of Hf within the oxide formed by RT22LT, to improve the adhesion of the scale, the composition and morphology of the bondcoats needed to be optimised. This results from the fact that the bondcoats under investigation were originally designed as environmental coatings and as such occasional scale spallation was not considered to be a significant damaging feature as any failures that may occur could be self-healed. Within TBC systems however, the initial spallation of the oxide will lead to ceramic loss and the failure of the component. Therefore, by designing the composition of the bondcoat with the intention of impeding the outward diffusion of damaging elements, it was thought possible to extend the life of a TBC system. Due

to the performance of RT22LT, as compared to RPS320, it was decided to utilise the benefits of platinum and design a number of diffusion bondcoats for TBC systems based on modified platinum additions.

## 13.6 The Optimisation of an Out-of-Pack Platinum Aluminide Bondcoat

The analysis of the oxidation performance of the high activity coating RT22LT demonstrated how the adherence of an alumina scale could be undermined by the diffusion of damaging elements to the oxide interface. As low activity coatings are thought to be less susceptible to this problem, it was decided to optimise a low activity , out-of-pack platinum aluminide for TBC systems.

A range of nine platinum aluminide/CMSX-4 systems were produced by varying the platinum diffusion temperature, the aluminising temperature and the final heat treatment (Table 10.1). Once fully processed the coatings underwent a series of isothermal soaks to assess their adhesion.

XRD analysis of the systems in the as-processed condition revealed that the coatings had a β phase structure. This was the expected composition, being consistent with similar analyses published in the open literature [26]. In effect, the coatings had a two layered structure, the outer layer being the β phase, the inner, an interdiffusion zone. Optical examination of the as-processed coatings in section showed that the grain size of the development coatings was relatively low compared to RT22LT (Figure 10.3). The significance of this will be discussed later.

The modified scratch test was used to gauge the adherence of the development systems. Using the performance of RT22LT as a base reference, it was revealed that coatings C, E, M, O and T had relatively superior adhesion. With

reference to Table 10.1, it can be seen that these coatings had been processed at, overall, lower temperatures than those with inferior adhesion. This implies that the final composition of the coating affects its adhesive properties. Those processed at an overall lower temperature range (and therefore least diffuse systems), were shown to be superior.

Examination of the aged coatings in section revealed that the oxide thickness produced during isothermal exposure were similar for all of the development coatings and for RT22LT. With reference to the modified scratch test results, this implied that the thickness of the oxide scale is not the only factor governing adhesion/spallation. Of equal importance is the change in oxide composition and for these coatings, this appears to dominate oxide adhesion, and therefore, the performance of the bondcoat. The theory suggested in the literature, that failure occurs when the oxide reaches a critical thickness [29] is therefore not strictly true, as other factors, such as the composition of the oxide may play a more important role in determining the onset of scale failure and thus modify this critical thickness concept.

An important feature revealed by the examination of the samples prepared with a bromine deep etch, was that outward transport of elements such as Ti, Ta and W occured by diffusion both along grain boundaries and within the grains of the coating. In section 7.4, it was demonstrated that the presence of W within the oxide lowered the scales adherence. The large number of grain boundaries (which act as high diffusion paths) within these developmental coatings must therefore be considered detrimental as they allow for the fast diffusion of damaging elements to the interface. Unlike for both RT22LT and RPS320, the presence of Hf was not

noted at the oxide interface. This reflects the lower level of Hf within CMSX-4 (0.1wt%), as opposed to MarM002 (1.5wt%). Therefore, failure due to the extensive growth of pegs across the oxide bondcoat interface was not observed and was not a degradation mode for these modified diffusion coatings on CMSX-4.

SEM examination of the oxide surfaces after ceramic spallation revealed the presence of smooth faceted pits. As reported in chapter 4, similar features have been reported on other superalloys [58], for intermetallics [90, 91], aluminides [41] and FeCrAl/FeCrAlY alloys [93]. There are two main schools of thought as to the reason for the formation of these pits. Either they are attributed to the Kirkendall Effect, due to preferential consumption of aluminium at high diffusion paths, or they are formed due to the contamination of the oxide with elements such as Ti. These elements act to dope the oxide growth, resulting in increased aluminium consumption.

With reference to the observations made of the coatings in section in this study, the formation of the faceted pits on the development coatings may be a combination of both of these reasons. It was observed that Ti, Ta and W were preferentially diffusing along grain boundaries to the oxide interface. Once incorporated within the scale, the elements act to locally increase the oxide growth. In the case of Ti, as α-alumina acts as a p-type semiconductor [108], the inclusion of $Ti^{4+}$ ions within the scale will increase the rate of aluminium consumption due to the Wagner-Hauffe doping effect [109]. The substitution of $Ti^{4+}$ ions for $Al^{3+}$ ions will lead to the creation of aluminium vacancies within the scale and so increase the rate of oxide growth. It has also been reported that the inclusion of $Ti^{3+}$ ions will increase aluminium consumption. However, as vacancies are not being created by

the incorporation of these ions, it maybe a result of the further oxidation of $Ti^{3+}$ to $Ti^{4+}$ that produced the observed results [103].

The localised increase in scale thickness will result in the formation of Kirkendall-type voids beneath the scale and buckling within the oxide. This decohesion will result in the failure of the TBC. It is assumed that Ta and W will act in a similar manner to Ti. However, due to the relative diffusion rates of W and Ti (in γ-Fe W diffuses at 456 x $10^{-12}$ $cm^2s^{-1}$ whilst Ti diffuses at 8420 x $10^{-12}$ $cm^2s^{-1}$ respectfully)[110], it is expected that Ti would be more prevalent at the interface than W. A schematic disgram of this failure mode is illustrated in Figure 13.1.

Image analysis of the oxide surfaces after ceramic failure revealed that coating C (with good adhesion) had fewer pits than coating Z (with poor adhesion). Therefore the large formation of pits and subsequent detachment of the oxide had caused the relatively premature failure of coating Z. The higher proportion of pits on the surface of the poorer performing coatings revealed that the coatings were more susceptible to oxide doping, indicating that the level of oxide doping was higher. This higher level of doping must be due to the higher processing temperatures used in their production which may have overly diffused the platinum (and so decreasing any blocking capability) or introduced damaging elements from the interdiffusion zone to the β phase layer (decreasing the distance required for further diffusion to reach the interface).

In the literature Auger analysis of the oxides containing voids had either found that S was present within the voids [94, 104] or both in the voids and within the scale [95]. The effect of S in relation to void formation therefore, still remains unclear. In this work, XPS analysis of the oxide interfaces formed through oxidation

of the development coatings did not show the presence of sulphur at detecable levels for either good or poor performance coatings. The S level must have been below the level of detection of the XPS and so was not considered a factor in their degradation of these coatings.

From the results presented in section 10, it can be determined that the factors affecting the lifetime of a diffusion bondcoat are;

1) The number of grain boundaries,
2) The rate of diffusion within the lattice, and
3) The composition of the coating.

Grain boundaries act as short circuit diffusion paths. Atchinson [30] determined that the rate of diffusion along grain boundaries within NiO was a factor of 100 greater than within the lattice. Although relatively slower, the rate of diffusion within the lattice is still an important feature. The diffusion rates of Ti, Ta and W within β–(Pt, Ni)Al are not available in the open literature. However an important property would be to have a sufficient level of Pt so as hinder the diffusion of these elements to the oxide interface. If the composition of the coating is such that it contains damaging elements in the outer layer(s), the distance required to diffuse to the oxide interface is decreased. High activity coatings, being inwardly formed, will be particularly susceptible to this problem. Low activity coatings however, being outward formed should be relatively free from contamination, rejecting the damaging elements to the interdiffusion zone.

To optimise the performance of a platinum aluminide bondcoat, the design of the coating should ensure a large grain size, have sufficient platinum within the

coating to impede lattice diffusion and be free from damaging elements, restricting them to the interdiffusion zone (i.e. coatings formed by the low activity process).

To summerise, this research programme has shown that by varying the conditions of a low activity production process, the performance of a platinum aluminide can be improved to meet the standard required as a bondcoat for TBC systems. The coatings produced at the lower tempratures (e.g. coating C), were shown to have superior oxidation resistance to RT22LT, inspite of having a smaller grain size. This indicated the importance of coating composition and the rate of diffusion within the lattice in determining the lifetime of a TBC. The low activity production route (e.g. Pt diffused for 1h at 1100°C, aluminised for 6h at 1080° and heat treated for 1h at 1100°C) had resulted in a composition that more effectively excluded the damaging elements from the coating and impeded their diffusion to the coating/scale interface. The higher temperatures used for the production of , for example, coating Z, may have resulted in the increased outward diffusion of damaging elements and so increased their concentration within the scale. This, therefore, led to greater contamination at the oxide/coating interface and the lower lifetime of the TBC.

## 13.7 The Development and Optimisation of a Platinum/CMSX-4 Bondcoat System

The demands of TBC systems require that such factors as coating thickness, weight and cost be decreased. Due to the limitations of traditional bondcoats, it was decided to research and hence design a noval bondcoat system to met these criteria.

Two important results discussed in chapter 10 were;

1. The importent beneficial properties of platinum, acting to both impede the outward diffusion of damaging elements and to promote the selective oxidation of aluminium.

2. That aluminium enrichment of the substrate did no necessarily guarentee an adherent scale.

Therefore it was thought possible to utilise the properties of platinum to promote an adherent alumina scale formed from the aluminium inherent within the single crystal superalloy, CMSX-4.

Initially, a number of 'bondcoatless' TBC systems were produced on a range of superalloys to assess the effects of alloy composition. The systems were assessed by being thermally cycled at 1135°C and showed that the adherence of the systems improved with the decreasing Ti content of the superalloy (i.e. the superalloy C1023, the least adherent system contains 3.6 wt% Ti, whilst Alloy RR, the most adherent contains 0.23 wt% Ti). This highlighted the detrimental effects of Ti (section 13.6) and reinforced the view that improving the adherence of the bondcoat oxide could be achieved by the impedence of the outward diffusion of these damaging elements to the oxide interface.

A range of platinum/CMSX-4 systems were produced by varying the platinum thickness and diffusion temperatures. The coatings were assessed by isothermal soaks over a range of temperatures and by thermal cycling at 1135°C.

Optical analysis of the coatings revealed that they had a two phased structure. The average thickness of the coatings (Table 11.2) show that, compared with platinum aluminides (e.g. average thickness of RT22LT~60μm), they were approximately one third thinner (7 to 24 μm). XRD analysis of the coatings in the

as-processed condition revealed that the systems could be divided into two groups. The thicker initial Pt layers, and so the least diffused coatings (systems D, E and F), were shown to contain a phase not previously reported in the open literature. The phase was given the nomenclature 'O' and was found to be isostructural with the orthorhombic $NiGePt_2$ phase. Probe analysis of these systems revealed that the 'O' phase contained a relatively high level of platinum and low level of nickel (Table 11.3). XRD analysis of the other systems revealed that they had a $\gamma/\gamma'$ structure. Probe analysis demonstrated that, preferential partitioning of the elements occured between the two phases, the compositions of which were reported in Table 11.3.

The modified scratch test results (section 11.3.4) demonstrated that, apart from coating A, the development systems all outperformed the platinum aluminide RT22LT. The poor performance of coating A was due to the low level of platinum, not allowing the system to operate at the same performance level as the other coatings. The coatings that contained the 'O' phase were found to perform at a similar level to the $\gamma/\gamma'$ systems. However due to the extra thickness of platinum used (therefore a more expensive coating without reciprocal benefits) and the possibility that any structural changes due to exposure could be detrimental, further analysis of the 'O' phase containing systems was curtailed. Similarly, the coating diffused at 1190°C did not show any benefits due to the higher diffusion temperature and so analysis concentrated on the remaining systems.

Samples of coating C were thermally cycled at 1135°C. The results demonstrated how the development coating had a far superior performance compared to contempory platinum aluminides. Analysis of both the isothermally soaked and thermally cycled samples revealed that during exposure the level of Ta

and Ti had increased in the γ phase whilst remaining constant in the γ′ phase and that Pt had diffused further into the substrate. SEM analysis of the bondcoat interface after ceramic failure did not show the smooth pits, common to the platinum aluminides discussed in section 13.5 and EDS analysis could not identify the presence of Ta and Ti at the bondcoat interface. This, coupled with the oxide thickness measurments (Figure 11.7) suggested that the coatings had not failed due to the contamination and doping of the oxide, as with other diffusion coatings. The platinum rich layer had successfully impeded the outward diffusion of the damaging elements, primarily by the γ′ phase and then the γ phase, allowing the controlled production of an adherent scale. This scale continued to grow until, as suggested in the literature [29], a critical thickness was reached where the stresses within the oxide could not be compensated for and failure occurred. Samples that were thermally cycled after failure demonstrated the stability of the coating, as after the initial oxide failure the platinum layer still acted in a beneficial manner and so the system would perform as an effective environmental coating aswell.

The poor performance of the double layer systems suggested that the production process had affected the ability of the Pt rich layers to promote the formation of a complete alumina film and/or block the damaging elements.

In summary, the diffusion of platinum into a CMSX-4 substrate has been shown to act as an effective bondcoat. The systems fulfill the considerations required for future TBC systems, i.e. the coatings are thinner, weigh less and due to their simple processing, are cheaper than conventional diffusion bondcoats. With reference to the criteria for an effective diffusion coating (section 13.6), the development systems outperform contempory aluminides due to the ability of the

platinum-rich $\gamma/\gamma'$ structure to impede the outward diffusion of damaging elements such as Ti. This is due to both the properties of platinum and the phase structure of the coating. Ti can form very stable phases with Pt, as compared to Ni (as an indication, the melting point of PtTi is 1830°C [111], whilst the melting point of NiTi is between 1240 and 1310°C [112]) and the solubility of Ti is higher in a $\gamma'$ phase than in a $\beta$ phase (i.e. the phase usually present within a diffusion coating) [103]. Therefore, the $\gamma/\gamma'$ structure of the coating facilitates the formation of stable Ti-containing phases. This effectively, decreases the outward diffusion of Ti, both along grain boundaries and through the lattice, by 'tieing' the elements up away from the oxide interface.

The optimisation programme has defined a production window having determined an effective range of platinum thickness and the required diffusion treatment (i.e. depositng between 7 and 10μm of platinum and diffusing at 1150 °C for 1 hour). Overall, it has been shown that by appreciating the degradation modes of a bondcoat, it has been possible to design an effective bondcoat system for thermal barrier coatings.

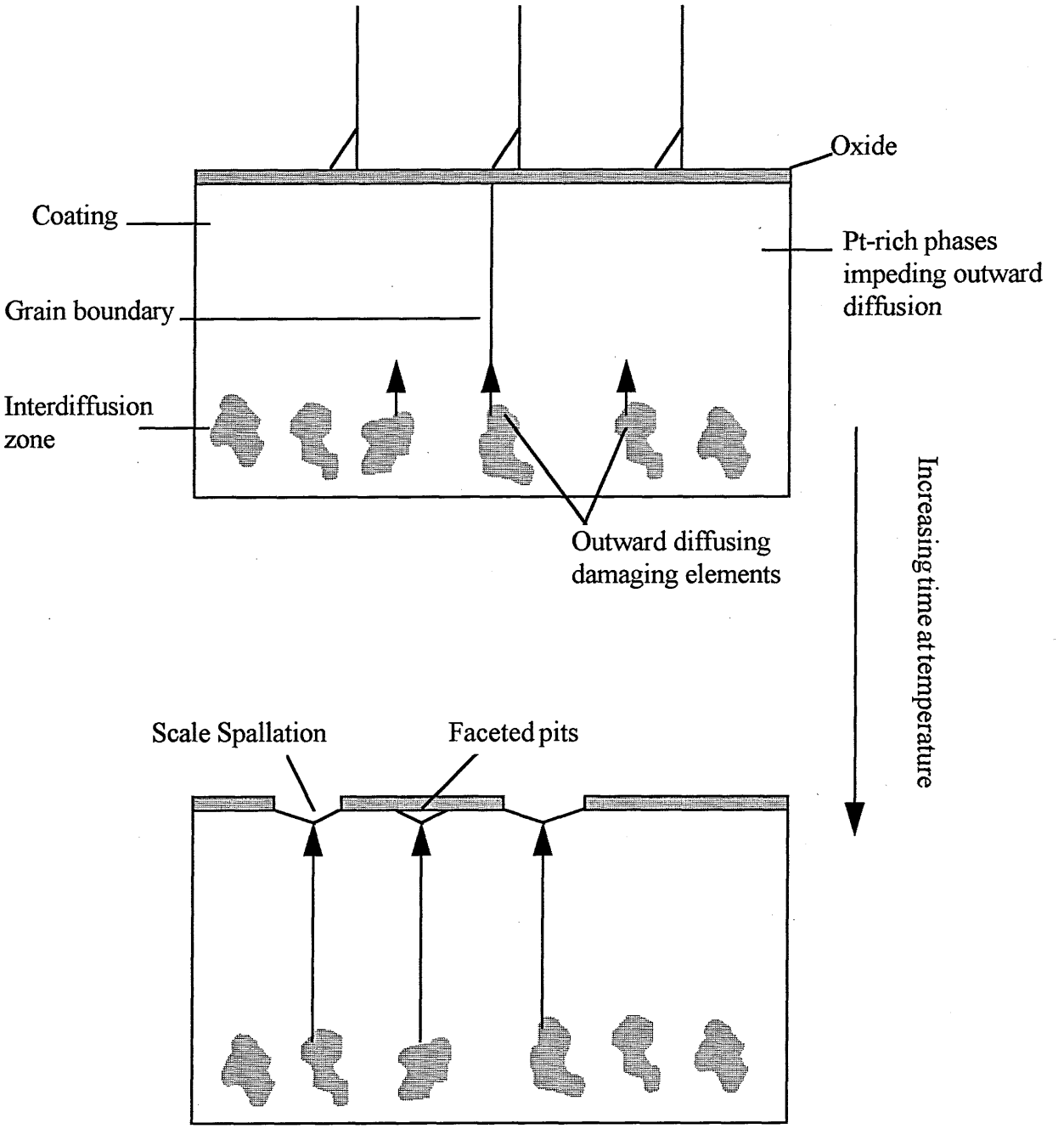


Figure 12.1- Schematic diagram of the failure mechanism for the platinum aluminide/TBC systems

# CONCLUSIONS

Chapter 13

# Conclusions

## 13.1 The effects of pre-oxidation on the oxide chemistry

**1.** In the as-processed condition, the samples pre-treated in the Ar-20%$O_2$ atmosphere were found to promote a mixed oxide containing both alumina and transition metal spinels. After isothermal exposure, the concentration of spinels increased. Therefore, the pre-oxidation of RT122 in an Ar-20%$O_2$ atmosphere was not an effective pre-treatment.

**2.** In the as-processed condition, the samples pre-oxidised in the $H_2$-10%$H_2O$ atmosphere formed an alumina based oxide. After isothermal exposure, the scale became contaminated with transition metal spinels. Therefore, the initial potential benefits of this pre-treatment were not realised.

**3.** Spallation of the oxide scales were either associated with transition metal spinels or were cohesive failures within the alumina. The higher level of spallation on the Ar-20%$O_2$ pre-treated samples was thought to be due to the greater concentration of spinels within the scale.

**4.** As the oxides formed by the $H_2$-10%$H_2O$ pre-treated samples appeared to be more adherent than those formed by the Ar-20%$O_2$ pre-oxidised coatings, it was considered that the $H_2$-10%$H_2O$ pre-treatment was the more effective of the two atmospheres.

13.2 The effect of gritting as a surface preparation

**5.** As the gritting pre-treatment did not alter either the rate of aluminium consumption, or the composition of the scale and its degradation, the process was considered a benign treatment as far as bondcoat oxidation is concerned.

13.3 The effect of bondcoat composition on the chemistry of the oxide scale

*13.3.1 The effect of aluminium content*

**6.** Similar compositions of oxides were produced by the Coating A ('high' aluminium content) and the RT122 coating ('low' aluminium content), with the adherence of the oxide on Coating A somewhat lower. It is proposed that the aluminium content of the coating is not a major factor which determines the adherence of the scale.

*13.3.2 The effect of platinum*

**7.** Platinum aluminide coatings have a higher oxidation resistance than basic aluminides. The Pt-rich phases act to promote the selective oxidation of aluminium, whilst impeding the outward diffusion of damaging elements.

*13.3.3 The effect of Hf and Si additions*

**8.** The addition of both Hf and Si to a MCrAlX coating was determined to be ineffective in improving scale performance, as they did not alter either the composition nor the adherence of the scale.

*13.3.4 The effect of a ceramic topcoat*

**9.** The presence of a ceramic topcoat was found to decrease the concentration of spinels within the oxide scale.

13.4 Assessment of in-situ and ex-situ pre-oxidation treatments

**10.** The ex-situ pre-oxidation of diffusion and MCrAlX bondcoats in a $H_2$-10%$H_2O$ atmosphere did not improve the adherence of the TBC systems and may have been detrimental. Therefore, the pre-treatment was shown to be ineffective.

**11.** The in-situ pre-oxidation of the RT122 bondcoats was found to have no significant influence on the adherence of the TBC systems and so it was considered to be an ineffective pre-treatment.

13.5 The optimisation of an out-of-pack platinum aluminide bondcoat

**12.** The thickness of the oxide scale was a less critical factor in determining the lifetime of the TBC systems, than the composition of the scale.

**13.** Bondcoats fail due to the outward diffusion of elements, such as Ti, from the substrate. These elements acted to dope the alumina, increasing the growth rate and aluminium consumption. This resulted in the formation of faceted pits at the metal/oxide interface, decreasing in the adhesion between the bondcoat and the oxide resulting in TBC failure.

**14.** The main factors that affect the lifetime of a diffusion bondcoat are the number of grain boundaries within the coating, the rate of diffusion within the lattice and the consumption of aluminium from the coating.

**15.** By using a low aluminium activity, out-of-pack process and by optimising the production temperatures, a range of platinum aluminide bondcoats were produced that were superior to the high aluminium activity RT22LT coating.

13.6 The design and optimisation of a platinum enriched CMSX-4 bondcoat for TBC systems

**16.** An effective diffusion bondcoat that had a higher oxidation resistance than conventional diffusion coatings has been produced. This coating is cheaper to produce, thinner and of less weight than conventional platinum aluminides.

**17.** The coatings achieved this high performance due to the Pt-rich phases blocking the outward diffusion of damaging elements to the oxide interface.

**18.** Due to the effective impedance of damaging elements, the coatings failed due to the oxide growing to a critical thickness, as opposed to the formation of faceted pits ( see conclusion ~ 13)

13.7 Overall conclusions

**19.** The studies of bondcoat pre-treatments revealed that although an initial $\alpha$-alumina layer maybe promoted, the subsequent contamination of the scale upon exposure by

transitional metal elements resulted in no long term benefits. This indicated that, to improve the adherence of the scale, the composition of the bondcoats needed to be optimised. By exploiting the beneficial properties of platinum to limit the damaging effects of the transition metals, it was possible to design and develop a range of diffusion bondcoats that were able to met the needs of a modern Thermal Barrier Coating system.

# FUTURE WORK

Chapter 14

# Future Work

## 14.1 Introduction

This study has demonstrated the importance of bondcoat chemistry and composition in providing the optimum adhesion for a TBC, and has developed two effective bondcoat systems. This chapter describes how further testing of the development bondcoats is required to give a fuller simulation of the conditions in an aero-gas turbine ( i.e. hot corrosion testing), and how the coatings could be further developed with, for example, active element additions.

## 14.2 Hot corrosion testing

Chapters 10 and 11 demonstrated the excellent performance of both the low activity platinum aluminides and the platinum/CMSX-4 systems under high temperature oxidation conditions. However, to fully simulate the environment that would be experienced within the modern aero-gas turbine, the diffusion bondcoats should be tested in regimes where both Type I and Type II hot corrosion occur. The author suggests that this could be achieved using either a 'sea-salt spray' test, the Dean test or burner rig tests.

## 14.3 The addition of active elements

The benefits of active element additions to MCrAlX coatings are well documented in the literature. The inclusion of elements such as Y or Hf will have a number of beneficial results, such as decreasing the oxide growth rate, increasing the mechanical properties of the oxide and acting as S getters [58, 114]. Similarly,

investigations of the addition of active elements to β-NiAl intermetallics have revealed similar benefits [115, 116, 117]. However, the effects of Y additions to a diffusion coating appear to be unclear, as both beneficial [26] and detrimental [118] results have been reported. It is suggested that the potential benefits of additions of either Y or Hf to both the platinum aluminides and the platinum/CMSX-4 systems should be investigated. The possible methods for deposition that could be used include either ion implantation, sputter coating or co-deposition during the aluminising process.

## 14.4 Noble metal aluminide bondcoats

This study has demonstrated the benefits of platinum in a bondcoat system . However, due to the relatively high cost of platinum, it is suggested that aluminide systems containing other noble metals (e.g. Ir, Ru or Rh) are investigated to determine whether they can similarly improve the life of a TBC.

## 8.5 Co-Pt/CMSX-4 bondcoat systems

The investigations of pre-treatments undertaken by Lih and co-workers [72, 74] highlighted the superior oxidation performance of CoCrAlY coatings compared with NiCrAlY bondcoats (Figure 14.1). A 'scoping' programme was undertaken to determine whether similar benefits could be achieved by the addition of Co to a Pt/CMSX-4 system. The systems that were assessed are shown in Figure 14.2. The coatings were isothermally aged for 25h at 1100, 1150, 1170, 1190 and 1210°C and their adhesion assessed using the modified scratch test (Figure 14.3).

The results show how the coatings provided excellent oxidation resistance. However, due to time constraints, it was not possible to further investigate the benefits

of the coatings nor gain a fuller understanding of their chemistry and composition. It is recommended that further studies are undertaken to determine the benefits of this system and to assess the effects of Co additions to platinum aluminide coatings.

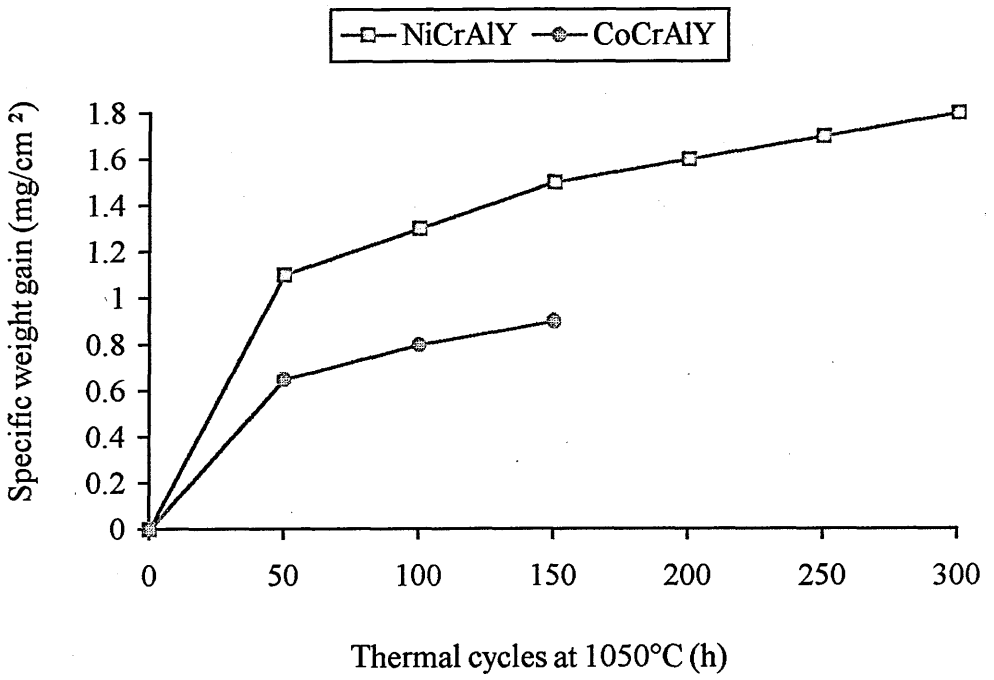


Figure 14.1- Specific weight gains of NiCrAlY and CoCrAlY coatings , thermally cycled at 1050 °C [72, 74].

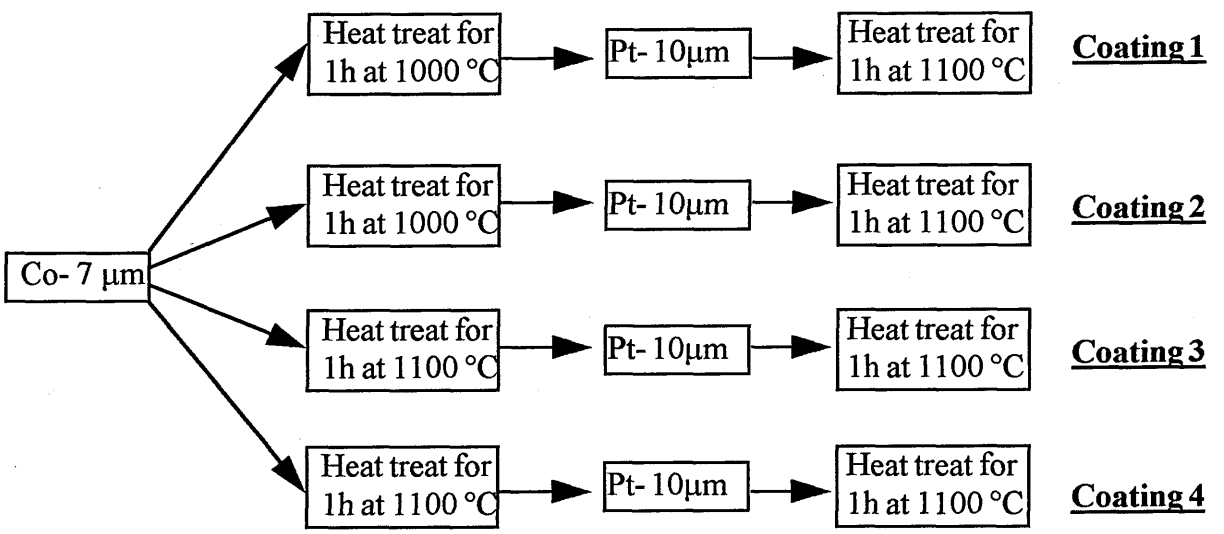


Figure 14.2- Processing route for Co-Pt/CMSX-4 coatings

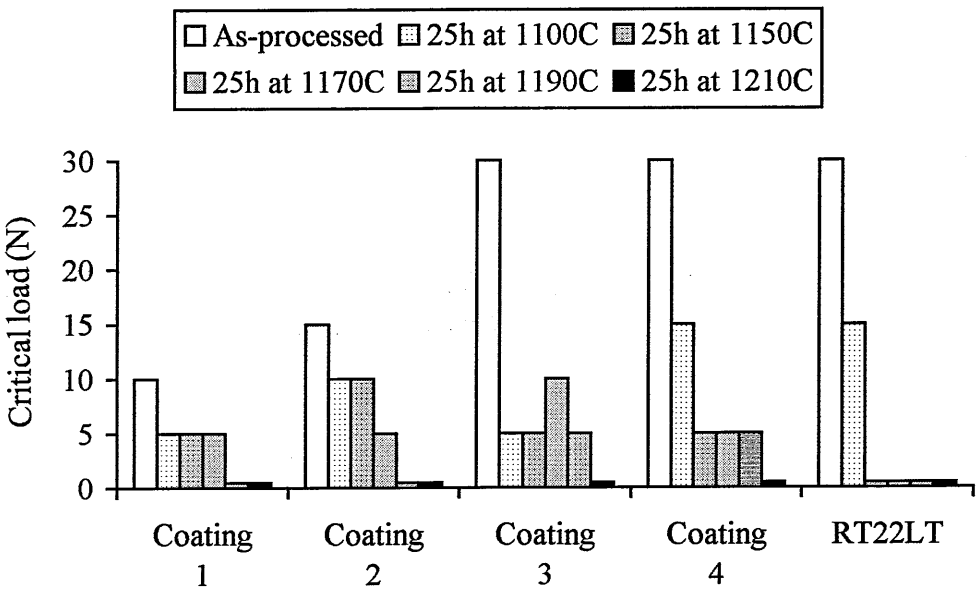


Figure 14.3- Scratch test results for the Co-Pt/CMSX-4 systems

# REFERENCES

References


1. D. J. Wortman, E. C. Duderstadt, W. A. Nelson, Jn of Engineering for Gas Turbines and Power, **112**, 1990, p527

2. F. S. Pettit, G. W. Goward, Coatings for High Temperature Applications, Applied Science Pub., 1983, p341

3. R. G. Wing, I. R. McGill, Platinum Metals Review, **25**, 3, 1981, p94

4. S. M. Meier, D. K. Gupta, ASME Report 92/GT/203, 1992

5. S. M. Meier, D. K. Gupta, K. D. Sheffler, JoM, march, 1991, p50

6. J. R. Nicholls, D. J. Stephenson, Metals and Materials, march, 1991, p156

7. K. D. Sheffler, D. K. Gupta, Jn of Engineering for Gas Turbines and Power, **110**, 1988, p605

8. W. J. Brindley, R. A. Miller, Advanced Materials & Processes, **8**, 1989, p29

9. D.S. Rickerby, P. Morrell, Design and Development of EB-PVD Thermal Barrier Coatings for Gas Turbines, High Temperature Surface Engineering, Edingburgh 1997, Institute of Materials, submitted for publication

10. A. Bennett, F. C. Toriz, A. B. Thakker, Surface & Coatings Technology, **32** 1987, p359

11. D. L. Anton, Intermetallic Compounds v2, Ed. J. H. Westbrook, R. L. Fleischer, John Wiley & Son Ltd, 1994, p3

12. J. K. Tien, S. Purushothaman, Properties of High Temperature Alloys, Ed. Z. A. Foroulis, F. S. Pettit, 1976, p3

13. G. W. Meetham, Metals Technology, **11**, 1984, p414

14. H. T. Michels, W. Z. Friend, Corrosion of Nickel & Nickel-based Alloys, Ed. W. Z. Friend, Electrochemical Soc. Inc, 1980, p435

15. A. K. Jena, M. C. Chaturvedi, J of Materials Science, **19**, 1984, p3121

16. G. P. Sabol, R. Stickler, Phys. Stat. Sol, **35**, 11, 1969, p11

17. C. T. Sims, A history of superalloy metallurgy for superalloy metallurgists, Proc. Int Symp. Superalloys, AIME, 1984, Ed M. Gell, p399

18. E. W. Ross, C. T. Sims, Superalloys II, Ed. C.T. Sims, N. S. Stoloff, W.C. Hagel John Wiley & Son Ltd, 1987, p97

**19.** G. W. Meetham, Materials & Design, **10**, 2, 1989, p77

**20.** G. H. Gessinger, R. F. Singer, Superalloys: Principles & applications, 4th Riso Int. Sym. Metallurgy & Materials Science, Ed. J. B. Bilde-Sorensen, 1983

**21.** R. J. E. Glenny, J. E. Northwood, A. Burwood-Smith, International Metal Review **20**, 1975, p1

**22.** G. W. Meetham, Materials & Design, **9**, 4, 1988, p213

**23.** G. Lehnert, H. Meinhardt, Electrodeposition & Surface Treatment, **1**, 1972/1973, p71

**24.** P. C. Patnaik, Materials & Manufacturing Processes, **4**, 1, 1989, p133

**25.** R. Mevrel, Research & Development of High Temperature Materials for Industry, ONERA, 1989, p145

**26.** R. Strieff, Jn de Physique IV, Colloque C9, supplement au Jn de Physique III **3**, 1993, p17

**27.** B. M. Warnes, D. C. Punola, Power Generation Technology. Int. Review of Primary Power Production, Ed. R. Knox, Sterling, 1995

**28.** T. N. Rhys-Jones, Corrosion Science, **29**, 6, 1989, p623

**29.** A. Bennett, Materials Science & Technology, **12**, 1986, p257

**30.** A. Atkinson, Materials Science & Technology, **4**, 1988, p1046

**31.** J. L. Smialek, G. H. Meier, Superalloys II, Ed. C. T. Sims, N. S. Stoloff W. C. Hagel, John Wiley & Son, 1987, p293

**32.** A. Atkinson, Reviews of Modern Physics, **57**, 2, 1985, p437

**33.** J-G. Li, Jn American Ceramic Society, **75**, 11, p3118

**34.** B. Derby, Joining of Ceramics, Ed. M. G. Nicholls, Chapman & Hall 1990, p94

**35.** R. Prescott, M. J. Graham, Oxidation of Metals, **38**, 3/4, 1992, p233

**36.** J. Doychak, J.L. Smialek & C. A. Barrett, Oxidation of high temperature Intermetallics, Ed. T. Grobstien & J. Doychak, Minerals, Metals & Materials Soc, 1989, p41

**37.** H. Hindman, D. P. Whittle, Oxidation of Metals, **18**, 5/6, 1982, p245

**38.** J Jedlinski, S. Mrowec, Materials Science & Engineering, **87**, 1987, p281

**39.** J. l. Smialek, Metallurgical Transactions A, **9A**, 1978, p309

**40.** H. Hindman, W. W. Smeltzer, Oxidation of Metals, **14**, 4, 1980, p337

**41.** R. Prescott, D. F. Mitchell, M. J. Graham, Corrosion Science, **50**, 1, 1994, p64

**42.** A. M. Huntz, Materials Science & Engineering, **87**, 1987, p251

**43.** G. C. Rybicki, J. L. Smialek, Oxidation of Metals, **31**, 3/4, 1989, p275

**44.** J Jedlinski, G. Borchardt, Oxidation of Metals, **36**, 3/4, 1991, p317

**45.** H. M. Hindman, W. W. Smeltzer, Jn Electrochemical Society, **127**, 7, 1980, p1630

**46.** E. W. A. Young, J. H. W. de Wit, Solid State Ionics, **16**, 1985, p39

**47.** T. T. Huang, R. Richer, Y. L. Chang, E. Pfender, Metallurgical Transactions, **16A**, 1985, p2051

**48.** F. H. Stott & G. C. Wood, Materials Science & Engineering, **87**, 1987, p267

**49.** C. Duret-Thual, R. Morbioli, P. Steinmetz, Commission of the European Communities, report EUR10682, 1986

**50.** N. S. Bernstien, M. A. DesCresante, H. A. Roth, Deposition & Corrosion of Gas Turbines, Ed. A. B. Hart, A. J. B. Cutler, 1973, p70

**51.** R. A. Rapp, Y. S. Zhang, JoM, december, 1994, p47

**52.** K. R. Tretheway, J. Chambers, Corrosion, Longman, 1988, p352

**53.**. A. S. Grot & J. K. Martyn, Ceramic Bulletin, **60**, 8, 1981, p807

**54.** R. Stevens, Zirconia & zirconia ceramics, Magnesium Elektron, 1986, p38

**55.** D. G. Lees, Oxidation of Metals, **27**, 1/2, 1987, p75

**56.** G. Moulin, G. Abderrazik, J. M. Rousselet, Materials Science & Technology **4**, 1988, p479

**57.** C. Forest, J. H. Davidson, Oxidation of Metals, **43**, 5/6, 1995, p479

**58.** N. Birks, G. H. Meier, F. S. Pettit, JoM, december, 1994, p42

**59.** J. L. Smialek, The effect of sulphur content on $Al_2O_3$ scale adhesion, Microscopy of Oxidation, Conference Proceedings, 26-28/3/90, Ed. M. J. Bennett, G. W. Lorimer, Institute of Materials, 1991

**60.** H. J. Grabke, G. Kurbatov, H. J. Schmutzler, Oxidation of Metals, **43**, 1/2, 1995, p97

**61.** K. L. Luthra, C. L. Briant, Oxidation of Metals, **26**, 5/6, 1986 p397

**62.** F. H. Stott, The role of active elements in the oxidation behaviour of high temperature metals and alloys, Ed. E. Lang, Elsevier Applied Science, 1991, p3

**63.** W. J. Quadakkers, H. Holzbrecher, K. G. Briefs, H. Beske, The role of active elements in the oxidation behaviour of high temperature metals and alloys, Ed. E. Lang, Elsevier Applied Science, 1991, p72

**64.** S. Sacre, U. Wienstroth, H-G. Feller, L. K. Thomas, Jn of Materials Science, **28**, 1993, p1843

**65.** E. Y. Lee, R. R. Biederman, R. D. Sisson Jr, Surface Modification Technology IV, Ed. T. S. Sudarshan, D. G. Bhat, M. Jeandin, Minerals Metals & Materials Soc, 1991, p15

**66.** L. Lelait, S. Alperine & R. Mevrel: Microscopy of Oxidation, Ed M. J. Bennett & G. W. Lorimer, Institute of Materials, 1991, p161

**67.** B-C Wu, E. Chang, S-F Chang & D. Tu: Jn of the American Ceramics Society, **72**, 2, 1989, p212

**68.** B-C, Wu, E. Chang, S-F Chang & C. H. Chao: Thin Solid Films, **172**, 1989, p185

**69.** H. M. Tawancy, N. Sridhar,B. S. Tawabin & N. M. Abbas: Jn of Materials Science, **27**, 1992, p6463

**70.** M. Gobel, A. Rahme, M. Schutze, M. Schorr & W. T. Wu: Materials at High Temperature, **00**, 0, 1993, p1

**71.** H. M. Tawancy, N. M. Abbas & T. N. Rhys-Jones: Surface &Coatings Technology **54/55**, 1992, p1

**72.** W. Lih, E. Chang, B. C. Wu & C. H. Chao, Oxidation of Metals, **36**, 1991, p221

**73.** B. C. Wu, C. H. Chao, E. Chang & T. C. Chang, Materials Science & Engineering, **A124**, 1990, p215

**74.** W. Lih, E. Chang, B. C. H. Chao & M. L. Tsai, Oxidation of Metals, **38**, 1992, p99

**75.** J. H. Sun, E. Chang, B. C. Wu & C. H. Tsai, Surface Coatings & Technology, **58**, 1993, p93

**76.** W. Lih, E. Chang, B. C. Wu, C. H. Chao & A. Peng, Oxidation of Metals,**40**, 1993, p229

**77.** S. Bull, Materials at High Temperatures, **13**, 4, 1995, p169

**78.** J. Schaffer, G. M. Kim, G. H. Meier & F. S. Pettit: The role of active elements in the oxidation behaviour of high temperature metals and alloys, Ed. E. Lang, Elsevier Applied Science, 1991, p231

**79.** G. W. Goward & L. W. Cannon: Transactions of ASME, **110**, 1988, p150

**80.** C. Duret & R. Pichoir: Coatings for High Temperatures Application, Ed. E. Lang, Applied Science Publishers, 1984, p33

**81.** G. W. Goward & D. H. Boone: Oxidation of Metals, **3**, 5, 1971 p475

**82.** J. G. Fountain, F. A. Golightly, F. H. Stott & G. C. Wood: Oxidation of Metals, **10**, 5, 1976, p341

**83.** G. J. Tatlock & T. J. Hurd: Oxidation of Metals, **22**, 5/6, 1984, p201

**84.** D. H. Boone & J. S. Smith: International Symposium: High Temperature Corrosion Protection. June 26-30, 1990, Shenyang, China,

**85.** G. H. Meier & F. S. Pettit: Surface & Coatings Technology, **39/40**, 1989, p1

**86.** H. Jehn, Jn of Less Common Metals, **100**, 1984, p321

**87.** H. M. Tawancy, N. M. Abbas & T. N. Rhys-Jones: Surface & Coatings Technology, **49**, 1991, p1

**88.** R. Strieff & D. H. Boone: Jn of Materials Engineering, **10**, 1988, p15

**89.** D. F. Bettridge & R. G. Wing: ASME International Gas Turbine Conference, Dusseldorf, June 1986

**90.** S. C. Choi, H. J. Cho & D. B. Lee: Oxidation of Metals, **46**, 1/2, 1996, p109

**91.** J. L. Smialek: Metallurgical Transactions A, **9A**, 1978, p309

**92.** B. A. Pint, J. R. Martin & L. W. Hobbs,Oxidation of Metals, **39**, 3/4, 1993, p167

**93.** T. T. Huang, R. Richter, Y. L. Chang & E. Pfender: Metallurgical Transactions A, **16A**, 1985, p2051

**94.** H. J. Grabke, G. Kurbatov & H. J. Schmutzler: Oxidation of Metals, **43**, 1/2, 1993 p97

**95.** P. Y. Hou & J. Stringer: Oxidation of Metals: **38**, 5/6, 1992, p323

**96.** V. K. Tolpygo & H. J. Grabke: Oxidation of Metals, **41**, 5/6, 1994, p343

**97.** H. M. Tawancy, N. Sridhar, B. S. Tawabini, N. M. Abbas & T. N. Rhys-Jones: Jn of Materials Science, **27**, 1992, p6463

**98.** B. M. Warnes & D. C. Punola: Power Generation Technology. International Review of Primary Power Production, Ed. R. Knox, Sterling Publishing Ltd, 1995, p207

**99.** S. Yang: Oxidation of Metals, **15**, 5/6, 1981, p375

**100.** A. M. Huntz, A. Baumaza & G. Moulin: Oxiation of Metals, **30**, 3/4, 1988, p141

**101.** W. D. Kingery: Introduction to Ceramics, Wiley & Sons, 1976, p479

**102.** R. D. Bagley, I. B. Cutler & D. L. Johnson, Jn of the American Ceramic Society **53**, 3, 1970, p136

**103.** P. Fox & G. J. Tatlock: Materials Science & Technology, **5**, 1989, p816

**104.** B. A. Pint: Oxidation of Metals, **45**, 1/2, 1996, p1

**105.** H. M. Tawancy, N. Sridhar, B. S. Tawabin & N. M. Abbas: Jn of Materials Science, **27**, 1992, p6463

**106.** I.M. Allam, H. C. Akuezue, D. P. Whittle, Oxidation of Metals, **14**, 6, 1980, p517

**107.** G. Fisher, P. K. Datta, J. S. Burnell-Gray & W. Y. Chan, An investigation of the oxidation resistance of platinum alumnide coatings produced by either high or low activity processes, High Temperature Surface Engineering, Edinburgh 23-25 september, 1997, Institute of Materials, submited for publication

**108.**. A. Kumar, M. Nasrallah & D. L. Douglas, Oxidation of Metals, **8**, 4, 1974, p227

**109.** P.J.Hunt, The high temperature corrosion of some nickel based alloys in an oxygen/sulphur environment, PhD thesis, Newcastle-upon-Tyne Polytechnic 1978, p33

**110.** J. F. Stringer, AGARD Report No AGARD-AG-200, 1975

**111.** R. P. Elliott, Constitution of Binary Alloys, McGraw-Hill, 1965, p751

**112.** M. Hansen, Constitution of Binary Alloys, McGraw-Hill, 1958, p1050

**113.** M. K. Loudjini, A. M. Huntz & R. Cortes: Jn of Materials Science, **28**, 1993, p6466

**114.** A. M. Huntz: Materials Science & Technology, **87**, 1987, p251

**115.** J. Jedlinski & G. Borchardt: Oxidation of Metals, **36**, 3/4, 1991, p317

**116.** J. Jedlinski & S. Mrowec: Materials Science & Engineering, **87**, 1987, p281

**117.** E. Schumann, J. C. Yang, M. Ruhle & M. J. Graham: Oxidation of Metals, **46**, 1/2, 1996, p37

**118.** L. Peichl & D. F. Bettridge, Materials for Advanced Power Engineering, Kulwer Academic Publishers, 1994, p717